

Spatio-temporal characterization of the surface electrocardiogram for catheter ablation outcome prediction in persistent atrial fibrillation

Marianna Meo

▶ **To cite this version:**

Marianna Meo. Spatio-temporal characterization of the surface electrocardiogram for catheter ablation outcome prediction in persistent atrial fibrillation. Other. Université Nice Sophia Antipolis, 2013. English. NNT : 2013NICE4122 . tel-00940440v3

HAL Id: tel-00940440

https://theses.hal.science/tel-00940440v3

Submitted on 25 Feb 2014

HAL is a multi-disciplinary open access archive for the deposit and dissemination of scientific research documents, whether they are published or not. The documents may come from teaching and research institutions in France or abroad, or from public or private research centers.

L'archive ouverte pluridisciplinaire **HAL**, est destinée au dépôt et à la diffusion de documents scientifiques de niveau recherche, publiés ou non, émanant des établissements d'enseignement et de recherche français ou étrangers, des laboratoires publics ou privés.

UNIVERSITÉ NICE SOPHIA ANTIPOLIS

ÉCOLE DOCTORALE STIC
SCIENCES ET TECHNOLOGIES DE L'INFORMATION ET DE LA COMMUNICATION

THÈSE

pour l'obtention du grade de:

Docteur en Sciences

Mention: Automatique Traitement du Signal et des Images

de l'Université Nice Sophia Antipolis

Présentée par

Marianna MEO

Caractérisation spatio-temporelle de l'électrocardiogramme de surface pour prédire le résultat de l'ablation par cathéter de la fibrillation atriale persistante

thèse dirigée par
Vicente Zarzoso, Professeur, Université Nice Sophia Antipolis
Olivier Meste, Professeur, Université Nice Sophia Antipolis

Soutenue publiquement le 12 décembre 2013 devant le jury composé de :

Président :	Gérard Favier, Directeur de Recherche, CNRS
Rapporteurs :	Sergio Cerutti, Professeur, Politecnico di Milano, Italie Leïf Sörnmo, Professeur, Lund University, Suéde
Examinateurs :	Pietro Bonizzi, Maître de Conférences, Université de Maastricht, Pays Bas Rémi Dubois, Maître de Conférences, ESPCI - ParisTech Nadir Saoudi, Professeur, Centre Hospitalier Princesse Grace, Monaco Olivier Meste, Professeur, Université Nice Sophia Antipolis Vicente Zarzoso, Professeur, Université Nice Sophia Antipolis

Marianna MEO

CARACTÉRISATION SPATIO-TEMPORELLE DE L'ÉLECTROCARDIOGRAMME DE SURFACE POUR PRÉDIRE LE RÉSULTAT DE L'ABLATION PAR CATHÉTER DE LA FIBRILLATION ATRIALE PERSISTANTE

UNIVERSITY OF NICE SOPHIA ANTIPOLIS

Doctoral School of Information and Communications Technology

THESIS

in fulfillment of the requirements for the degree of

Doctor in Sciences

Specialty: Systems, Signal and Image Processing

at University of Nice Sophia Antipolis

Presented by

Marianna MEO

Spatio-temporal characterization of the surface electrocardiogram for catheter ablation outcome prediction in persistent atrial fibrillation

Thesis supervised by

Vicente Zarzoso, Professor, University of Nice Sophia Antipolis

Olivier Meste, Professor, University of Nice Sophia Antipolis

Presented on the 12th December 2013 to the jury committee composed by :

President :	Gérard Favier, Research director, CNRS
Reviewers :	Sergio Cerutti, Professor, Politecnico di Milano, Italy Leïf Sörnmo, Professor, Lund University, Sweden
Jury committee:	Pietro Bonizzi, Assistant Professor, Maastricht University, The Netherlands Rémi Dubois, Associate Professor, ESPCI - ParisTech Nadir Saoudi, Professor, Princesse Grâce Hospital, Monaco Olivier Meste, Professor, University of Nice Sophia Antipolis Vicente Zarzoso, Professor, University of Nice Sophia Antipolis

Marianna MEO

SPATIO-TEMPORAL CHARACTERIZATION OF THE SURFACE ELECTROCARDIOGRAM FOR CATHETER ABLATION OUTCOME PREDICTION IN PERSISTENT ATRIAL FIBRILLATION

Abstract

Atrial fibrillation (AF) is the most common sustained cardiac arrhythmia encountered in clinical practice, and one of the main causes of ictus and strokes. Despite the advances in the comprehension of its mechanisms, its thorough characterization and the quantification of its effects on the human heart are still an open issue. In particular, the choice of the most appropriate therapy is frequently a hard task. Radiofrequency catheter ablation (CA) is becoming one of the most popular solutions for the treatment of the disease. Yet, very little is known about its impact on heart substrate during AF, thus leading to an inaccurate selection of positive responders to therapy and a low success rate; hence, the need for advanced signal processing tools able to quantify AF impact on heart substrate and assess the effectiveness of the CA therapy in an objective and quantitative manner. This approach would help understand which patients could effectively benefit from ablation, thus avoiding unnecessary and expensive procedures, and helping in the selection of a patient-tailored therapy.

Valuable information about AF can be provided by multilead electrocardiogram (ECG) recordings of heart electrical activity in a noninvasive and cost-effective manner. However, most of standard ECG processing techniques are affected by several shortcomings. First, some CA outcome predictors are manually determined on surface ECG, thus affected by low repetitiveness. In addition, several parameters are merely computed in one ECG lead, therefore neglecting potential information about AF and its spatial distribution coming from the other leads.

This doctoral thesis aims at exploiting the multi-lead character of the standard ECG to enhance CA outcome prediction accuracy and the ability of the extracted features to characterize CA. Application of multivariate signal decomposition techniques, such as principal component analysis (PCA), weighted PCA (WPCA) and nonnegative matrix factorization (NMF), allow enhancing the most discriminant components of ECG content. Features determined in this multivariate framework will act as classifiers for distinguishing between successful and failing CA procedures prior to their performance.

Spatial variability of the standard ECG can be exploited to highlight some properties of the ECG signal typically observed during AF. In particular, the role of fibrillatory wave (f-wave) amplitude as a predictor of AF termination by CA is effectively enhanced in a multilead framework based on the PCA of the observed data matrix. Higher amplitude values prove to be correlated with CA success, and drawbacks of traditional methods, such as manual computation and single-lead analysis, are overcome. Variations in this parameter measured between the beginning and the end of the procedure are also able to quantify CA effects on AF dynamics, related to ablation outcome.

Similarly, some multivariate signal decomposition techniques are employed to assess the predictive power of AF spatio-temporal variability (STV) on the 12-lead ECG. Previous studies have demonstrated the correlation between single-lead STV measures and AF organization. The present study exploits the multivariate character of standard ECG enhanced by WPCA and underlines the ability of multilead STV descriptors to predict long-term CA outcome in persistent AF: the more irregular and dispersive the AF pattern, the less likely AF termination by CA. To the same extent, the NMF method proves to be an effective tool for processing STV variability content of the ECG.

The aforementioned ECG properties can be also exploited for a combined analysis of AF content by means of the logistic regression (LR) technique. This model condenses in a

unique index the most relevant contributions provided by surface recordings by selectively enhancing the most content-bearing ECG leads, while reducing the influence of the other electrodes. LR measures can effectively assess AF termination by CA at several follow-up periods.

Further contributions to AF analysis are provided by information theory, which actually helps exploring surface ECG spatial variability by assessing the degree of similarity between AF patterns observed on different leads. These regularity measures also prove to quantify CA effectiveness, and a link between the degree of interlead correlation and the procedural success is demonstrated.

Another line of investigation focuses on the analysis of the ventricular response, as changes in atrioventricular (AV) node function and its refractoriness during AF are reflected on the irregularity of the RR interval (RRI) distribution. Heartbeat occurrences are modeled as a point process, and effects of sino-atrial (SA) node response to sympathetic and parasympathetic inputs from the autonomous nervous system are taken into account in this probabilistic framework. Such a method allows for the extraction of heart rate variability (HRV) indexes which effectively highlight asymmetry and dispersion characteristics of the RRI distribution in presence of AF.

Résumé

La fibrillation auriculaire (FA) est la trouble cardiaque la plus courante, ainsi que une des causes principales des accidents vasculaires cérébraux. Malgré le progrès dans la compréhension de cette pathologie, les mécanismes à la base de la FA ses effets sur le coeur humain ne sont pas encore très clairs. D'où il vient le problème du choix de la stratégie de traitement la plus appropriée. La thérapie d'ablation par cathéter (CA) est de plus en plus utilisée pour traiter la FA, mais ses effets sur le substrat cardiaque ne sont pas suffisamment compris, d'où un taux de réussite très variable et le besoin d'outils du traitement des signaux capables de quantifier cette action. Cette approche permétttrait de traiter par CA seulement les sujets qui peuvent béneficier de cette thérapie.

L'électrocardiogramme (ECG) à 12 voies représente un outil non invasif peu coûteux pour caractériser la FA à partir de l'activité électrique du coeur. Cependant, les prédicteurs classiques de l'issue de la CA présentent plusieurs inconvénients, notamment leur calcul manuel sur une seule voie de l'ECG, qu'amène à négliger l'information sur la FA présente sur les autres dérivations.

Cette thèse exploite explicitement le caractère multi-capteur de l'ECG au moyen de techniques de décomposition multivariées, par exemple, l'analyse en composantes principales (PCA), la PCA pondérée (WPCA), la factorisation en matrices non négatives (NMF), démontrant qu'elles peuvent améliorer la puissance prédictive de certaines propriétés de l'ECG dans le cadre de la CA.

La variabilité spatiale de l'ECG standard peut être exploitée pour souligner certaines proprietés du signal ECG qui sont typiquement observées en présence de la FA. En particulier, l'amplitude des ondes fibrillatoires est corrélée avec le résultat de la CA, et traitée par une méthode multi-capteur basée sur la PCA. Valeurs plus élévées de ce paramètre prédisent la réussite de l'ablation, et les inconvenients des méthodes classiques (en particulier, le calcule manuel sur une seule dérivation) sont eliminés. Les variations de ce déscripteur mésurée entre le début et la fin de l'ablation sont également capables de quantifier les effets de la CA sur la dynamique de la FA, en rélation avec le résultat de l'ablation.

D'autres techniques comme la WPCA et la NMF peuvent aussi quantifier la variabilité spatio-temporelle (STV) de la FA sur l'ECG. Des études précedents ont démontré une corrélation entre des mésures de la STV sur une seule voie et la complexité de la FA. Cette thèse souligne la valeur prédictive de cette mésure obténue dans un cadre multicapteur au moyen de la WPCA. Formes d'onde plus varaibles et irrégulieres sont associées à l'échec de la CA. Résultats similaires sont obténus en utilisant la NMF. Ces propriétés de l'ECG peuvent aussi être combinées par la régression logistique (LR), qui mets en valeur les contributions les plus significatives pour la caractérisation du résultat de l'ablation.

La théorie de l'information permet également d'estimer le niveau de corrélation entre les voies de l'ECG, mis en relation avec le résultat de la CA grâce à des approches multi-capteurs.

Enfin, une dernière ligne de recherche concerne la réponse ventriculaire manifestée sur la variabilité cardiaque. L'approche paramétrique de processus ponctuel est capable de quantifier les effets de la réponse vagale sur le noeud sino-atriale, et souligner certaines propriétés de cette variabilité, améliorant ainsi la caractérisation de la FA.

Contents

Acronyms **3**

1 Introduction **5**
1.1 Background and motivation 5
1.2 Objectives 6
1.3 Thesis overview and summary of contributions 6
1.4 Publications issued from this work 9

I Background **11**

2 Electrophysiology of the heart and electrocardiography **13**
2.1 Introduction 13
2.2 Anatomy of the heart 13
2.3 The electrical conduction system 16
2.4 The standard 12-lead ECG 17
2.5 Summary and conclusions 27

3 Atrial fibrillation **29**
3.1 Introduction 29
3.2 Definition of atrial arrhythmias 29
3.3 Atrial fibrillation 30
3.4 Overview of the main AF therapies 35
3.5 Ablation therapy for AF treatment 38
3.6 Predicting CA outcome from ECG analysis 45
3.7 Summary and conclusions 46

II Contributions **47**

4 F-wave amplitude multivariate assessment **49**
4.1 Introduction 49
4.2 Clinical assessment of f-wave amplitude 50
4.3 Multilead characterization of f-wave amplitude by means of principal component analysis 52
4.4 Prediction of acute AF termination by CA 58
4.5 Measures of central tendency for long-term CA outcome prediction 64
4.6 Assessment of therapy effects on AF dynamics during CA 66
4.7 Summary and conclusions 72

5 AF STV multivariate assessment for CA outcome prediction 75
5.1 Introduction . . . 75
5.2 Motivation and links with AF organization . . . 76
5.3 Multilead STV predictors in the PCA framework . . . 78
5.4 Moving to the weighting perspective in the WPCA framework: weighted principal component analysis for STV quantification . . . 84
5.5 Multilead STV measures on standard ECG in the nonnegative matrix factorization framework . . . 94
5.6 STV predictors of CA outcome: extension to long-term CA outcome prediction and classification test on a larger ECG database . . . 99
5.7 Summary and conclusions . . . 100

6 Combination of multiple features assessed on standard ECG 103
6.1 Introduction . . . 103
6.2 Definition of the logistic regression model . . . 103
6.3 LR modeling of multivariate f-wave amplitude . . . 104
6.4 LR modeling of AF STV multilead measures . . . 108
6.5 LR modeling of combined measures of f-wave amplitude and STV content . 109
6.6 Summary and conclusions . . . 114

7 Contributions from information theory to CA outcome prediction 117
7.1 Introduction . . . 117
7.2 Basic theoretic definitions . . . 118
7.3 Single-lead assessment of AF regularity on surface ECG for CA analysis . . 120
7.4 Multilead assessment of AF regularity on surface ECG for CA analysis . . 123
7.5 Summary and conclusions . . . 131

8 Point process characterization of ventricular response during AF 133
8.1 Introduction . . . 133
8.2 Point process modeling of RRI distribution . . . 134
8.3 Point process analysis of heart rate and heart rate variability in CA outcome prediction . . . 139
8.4 Point process application to AF pattern recognition . . . 145
8.5 Summary and conclusions . . . 155

III Summary and conclusions 157

9 Conclusions and future work 159
9.1 Summary and conclusions . . . 159
9.2 Future work . . . 162

Bibliography 165
Appendixes179
A.1 Derivation of the least squares estimates . . . 181
A.2 WPCA algorithm . . . 181
A.3 NMF: ALS algorithm . . . 182
A.4 Chain rule in information theory . . . 183

A.5 IT entropy extension to multiple variables 183

List of Figures

1.1 Thesis structure graphical representation. 7

2.1 Anatomy of the heart 14
2.2 Section of the heart wall layers. 15
2.3 Pulmonary and the systemic circuits. 15
2.4 Sequence of the instantaneous heart wavefront vectors at each step of the cardiac cycle [96]. 19
2.5 ECG signal, its fiducial points and the corresponding phases in the cardiac cycle [68]. 20
2.6 The heart conduction system with its main components, their typical potential waveforms and the corresponding points on surface ECG [96]. . . . 20
2.7 Frontal ECG leads. 22
2.8 Precordial ECG leads [96]. 23
2.9 The projections of the lead vectors of the standard ECG system in 3 orthogonal planes. 23
2.10 Examples of IEGM. 24
2.11 Example of electroanatomic voltage map. 25
2.12 BSPM system. 26

3.1 Differences in ECG pattern between AF and SR. 31
3.2 Models of AF mechanisms. 32
3.3 Wells' criterion for AF classification. 35
3.4 CEE procedure for conversion of AF to normal SR [148]. 37
3.5 Maze lesion. 38
3.6 ECG database diagram. 42

4.1 Example of ECG recording during AF. 49
4.2 Single-lead atrial waveform interpolation algorithm. 53
4.3 The multilead AA signal $\mathbf{Y}_{\mathrm{AA}}$ (continuous line) and its rank-1 estimation by PCA (dashed line). Top: lead II. Middle: lead V_1. Bottom: lead V_3. . 57
4.4 $\widetilde{D}_L$ prediction performance as a function of the size L. 60
4.5 AUC of $\widetilde{D}_8$ as a function of R. 62
4.6 Example of a scatter plot of random data, the regression line $y = Sx + I$ and discrepancies d_i between estimated and real data 67
4.7 Scatter plot of $\overline{(D_L)}_{\mathrm{END}}$ as a function of $\overline{(D_L)}_{\mathrm{START}}$. 69
4.8 regression analysis of $(\widetilde{D}_8)_{\mathrm{START,PCHIP}}$ as a function of $(\widetilde{D}_8)_{\mathrm{END,PCHIP}}$. . . . 72

5.1 Repartition of the multilead AA signal in segments for STV content extraction. 78
5.2 Diagram of the main steps of the algorithm for AF STV multivariate assessment. 80

5.3 Evolution of the inverse-variance weighted mean $\widetilde{\mu}_{\mathrm{PCA}_8}$ as a function of NMSE tuning parameters. . . . 81
5.4 Single-lead NMSE spatial distribution and AUC assessment. . . . 82
5.5 AUC values describing $\widetilde{\mu}_{\mathrm{PCA}_8}$ prediction performance as a function of the rank n of the WPCA decomposition. . . . 83
5.6 Evolution of $\widetilde{\mu}_{\mathrm{WPCA}_8}$ as a function of the number of segments S. . . . 86
5.7 Evolution of $\widetilde{\mu}_{\mathrm{WPCA}_8}$ as a function of the number of samples per segment N_S. . . . 87
5.8 AUC values related to the multilead AF STV descriptor as a function of the number of leads L: PCA vs WPCA. . . . 89
5.9 Effects of the multilead weighting scheme on AA reconstruction. σ^2_{AA}: variance of the input AA signal per lead; σ^2_{PCA}: variance per lead of the rank-1 AA signal approximation by PCA; σ^2_{WPCA}: variance per lead of the rank-1 AA signal approximation by WPCA. . . . 90
5.10 Assessment of CA outcome prediction performance of single-lead energy descriptors. σ^2_{AA}: energy per lead of the original AA signal; σ^2_{PCA}: energy per lead of the rank-1 AA signal approximation by PCA; σ^2_{WPCA}: energy per lead of the rank-1 AA signal approximation by WPCA. . . . 91
5.11 AUC values describing $\widetilde{\mu}_{\mathrm{WPCA}_8}$ prediction performance as a function of the rank n of the WPCA decomposition. . . . 92
5.12 AUC dependence on the NMF approximation rank R in CA outcome prediction. . . . 98

6.1 Amplitude LR score: AUC evolution as a function of L in long-term prediction of CA outcome. . . . 105
6.2 Spatial distribution of the AUC index in the LR framework. . . . 112
6.3 LR regression coefficients of ECG multivariate features, both in separate and combined analysis. . . . 113

7.1 Graphical representation of the relationships between the IT parameters defined in Sec. 7.2. . . . 119
7.2 Box-and-whisker plot of the single-lead entropy $H(X)$ in the long-term CA outcome prediction. . . . 121
7.3 AUC index related to $H(X)$ long-term CA outcome prediction quality on each ECG lead. . . . 122
7.4 Spatial distribution of the negentropy index determined on each ECG lead of the AA signal before and after variance normalization. . . . 122

8.1 Some representative examples of HDIG PDF. . . . 136
8.2 RRI histogram: Left: AF, subject 7; Right: SR, subject 8. . . . 137
8.3 RRI time series as a function of R wave time instants: Left. AF, subject 7; Right. SR, subject 8. . . . 138
8.4 Representative examples of KS plots for testing HDIG model goodness-of-fit. Top: an example of accurate fit (patient 2). Bottom: an example of poor fit (patient 22). . . . 141

8.5 Representative examples of autocorrelation function of the rescaled RRIs and their related bounds of confidence. Top: good agreement with uncorrelation hypothesis (patient 5). Bottom: an example of low consistency with uncorrelation hypothesis (patient 31). 142
8.6 Box-and-whiskers plots of HR and RRI variability indices in AF pattern recognition. 150
8.7 Autocorrelation function of the rescaled RRIs computed in AF patient 8 for 2 distinct regression order values q. Left: $q = 2$. Right: $q = 5$. 152
8.8 Two examples of KS plots for HRV characterization in AF patients and healthy subjects. Left: High modeling accuracy (AF, subject 39). Right: Low modeling accuracy (SR, subject 62). 154

List of Tables

4.1 Interclass statistical analysis for AF procedural acute termination assessment. 58
4.2 CA outcome prediction performance for AF procedural acute termination assessment. . . . 59
4.3 ECG lead subsets with optimal prediction performance based on parameter $\widetilde{D}_L$ . . . 61
4.4 Interclass statistical analysis: extension of amplitude measures to the long-term follow-up. . . . 65
4.5 CA outcome prediction performance: extension of amplitude measures to the long-term assessment of AF termination by CA. . . . 65
4.6 Regression analysis of the parameters $\overline{D}_L$, $D(V_1)$, $\widetilde{D}_L$ (mV) and NMSE (n.u.: normalized units). . . . 68
4.7 F-wave amplitude linear regression in the long-term follow-up. . . . 71

5.1 PCA characterization of STV content for long-term CA outcome prediction. 81
5.2 WPCA convergence. . . . 88
5.3 Long-term CA outcome prediction through the WPCA decomposition . . . 88
5.4 ECG lead subsets with optimal prediction performance of $\widetilde{\mu}_{\mathrm{PCA_8}}$ and $\widetilde{\mu}_{\mathrm{WPCA_8}}$. 88
5.5 Short-term CA outcome assessment: interclass statistical analysis. . . . 97
5.6 ROC analysis of the NMF decomposition for short-term CA outcome prediction . . . 97
5.7 AF STV indices: extension to the 36-patient database in the long-term follow-up. . . . 100

6.1 Statistical analysis of the LR modeling of f-wave amplitude in long-term CA outcome prediction. . . . 105
6.2 ROC analysis of the LR modeling of f-wave amplitude in long-term CA outcome prediction. . . . 106
6.3 ECG lead subsets with optimal prediction performance based on the LR score LR_A . . . 106
6.4 LR analysis of combined ECG features for selection of CEE candidates: unpaired statistical test and ROC analysis. . . . 116

7.1 ROC analysis of the short-term CA outcome of the JE index directly computed on the AA signal. . . . 124
7.2 ROC analysis of the long-term CA outcome of the JE index directly computed on the AA signal. . . . 125
7.3 AUC criterion assessment of long-term AF termination prediction performance of the MMI index directly computed on the AA signal . . . 126
7.4 ROC analysis of the long-term CA outcome of the JE index computed on the PCA low-rank approximation to AA signal. . . . 128

7.5 ROC analysis of the short-term CA outcome of the JE index computed on the PCA low-rank approximation to AA signal. 129
7.6 Unpaired statistical analysis and long-term CA outcome prediction performance of MMI measures. 130

8.1 Number of subjects n_s for whom regression order q is optimal according to the AIC criterion. 143
8.2 Long-term CA outcome prediction: HR and RRI variability parameters under the RRI independence assumption (non-parametric approach) 144
8.3 Long-term CA outcome prediction: HR and RRI variability parameters; RRI time series is considered stationary and obeys a HDIG model, and its first moment is approximated to mean RRI. 144
8.4 Long-term CA outcome prediction: HR and RRI variability parameters; RRI time series is considered stationary and obeys a HDIG model, without first moment approximations. 144
8.5 Long-term CA outcome prediction: HR and RRI variability parameters; RRI time series is assumed non-stationary and obeys a HDIG model. . . . 145
8.6 Goodness-of-fit of the HDIG model in CA outcome prediction 145
8.7 KS test of transformed RRIs: point process vs the KDE method. 147
8.8 Analysis of the skewness index computed on RRI data modeled by the KDE method. 147
8.9 Number of subjects n_s with optimal regression order q according to the AIC criterion in AF pattern recognition. 149
8.10 LDA classification of HRV features determined on raw RRI series data. . . 151
8.11 LDA classification of HRV features under the point process modeling. . . . 151

Contents

Acronyms

AA	atrial activity
AF	atrial fibrillation
AEG	atrial electrograms
AFCL	atrial fibrillation cycle length
AFL	atrial flutter
AIC	Akaike information criterion
ALS	alternating least squares
AR	autoregressive
AT	atrial tachycardia
AUC	area under curve
AV	atrioventricular
AVNRT	AV nodal re-entrant tachycardia
bpm	beats per minute
BSPM	body surface potential mapping
CA	catheter ablation
CDF	cumulative distribution function
CEE	electrical cardioversion
CFAE	complex fractionated electrograms
CS	coronary sinus
ECG	electrocardiogram
EEG	electroencephalogram
EVD	eigenvalue decomposition
FN	false negative
FP	false positive
f-wave	fibrillatory wave
HDG	history-dependent Gaussian
HDIG	history-dependent inverse Gaussian
HIS d	distal HIS-bundle
HIS p	proximal HIS-bundle
HOSVD	high order singular value decomposition
HR	heart rate
HRA	high right atrial
HRV	heart rate variability
IEGM	intracardiac electrogram
IG	IG inverse Gaussian
IT	information theory
IVC	inferior vena cava
JE	joint entropy
KDE	kernel density estimation
KS	Kolmogorov-Smirnov
LA	left atrium
LAA	left atrial appendage
LDA	linear discriminant analysis

LIPV	left inferior pulmonary vein
LOOCV	leave-one-out cross validation
LR	logistic regression
LS	least squares
LV	left ventricle
MI	mutual information
ML	maximum likelihood
MLL	maximum log-likelihood
MMI	multivariate mutual information
MPCA	multilinear principal component analysis
MSV	mean square value
MV	mitral valve
NMSE	normalized mean square error
NMF	nonnegative matrix factorization
n.u.	normalized units
PAC	premature atrial contraction
PARAFAC	parallel factor analysis
PC	principal component
PCA	principal component analysis
PCHIP	paroxysmal supraventricular tachycardia
PSVT	pulmonary vein
PV	pulmonary vein
QSE	squared sample entropy
RA	right atrium
RAA	right atrial appendage
RIPV	right inferior pulmonary vein
RMS	root mean square
ROC	receiver-operating curve
RRI	RR interval
RSPV	right superior pulmonary vein
RV	right ventricle
r.v.	random variable
RVA	right ventricular apex
SA	sinoatrial
STV	spatio-temporal variability
SVA	supraventricular arrhythmia
SVC	superior vena cava
SVD	singular value decomposition
TN	true negative
TP	true positive
TV	tricuspid valve
VC	venae cavae
WPCA	weighted principal component analysis
WPW	Wolff-Parkinson-White

1 Introduction

1.1 Background and motivation

Atrial fibrillation (AF) is currently the most common sustained cardiac arrhythmia, responsible for serious long-term issues, such as ictus and stroke. Unlike other cardiac diseases, despite advances in its understanding, AF mechanisms are not clear yet, and still need to be elucidated. Accordingly, several theories about its generation and maintenance have been put forward. Such a variety of hypotheses have given rise to several therapeutic approaches, mainly dependent on AF chronicity, as well as patient's clinical background. One of the most recurrent strategies in persistent AF treatment is represented by radiofrequency catheter ablation (CA), aiming at cauterizing abnormal rhythm sources in the atrial myocardium.

Despite its increasing employment and the higher efficacy with respect to traditional cardioversion therapies, results obtained in clinical centers are still quite disparate and hardly comparable, due to the multiplicity of modalities and methodologies applied for ablation performance. Indeed, as AF causes are not known yet, it is equally hard to establish an effective protocol, applicable under any circumstances. By contrast, in medical centers CA performance is mainly guided by clinician's considerations, related to the pratictioner's experience and subjectivity. One of the main AF management lines consists in identifying potential positive responders to CA therapy, so as to exclusively treat patients who will benefit from CA and avoid unnecessary and potentially harmful procedures. Nevertheless, also in this case most of patient's evaluation is frequently biased by clinician's subjectivity, with no assessment of AF condition by means of quantitative and measurable parameters.

To this extent, some efforts have been made so as to search for any potential descriptors of heart electrical activity during AF, which can shed some light on CA effectiveness, thus revealing which patients can be treated by CA without risk of AF recurrence in the follow-up. Standard electrocardiogram (ECG) is widely employed in medical centers for recording heart electrical activity by means of some electrodes positioned on patient's body and monitoring his conditions. It is characterized by several advantages: it is noninvasive, rapid, cost-effective, easy to acquire and provides potential diagnostic information about a wide variety of cardiac diseases. This tool is suitable for AF analysis, whose presence can be even visually detected on standard ECG, for instance, through the absence of P waves, replaced by irregular fibrillatory waves (f-waves), and the more irregular RR interval (RRI) distribution. Accordingly, several attempts have been made in order to define novel ECG-based features to be combined with patient's clinical characteristics and quantify CA effects on heart substrate in the presence of AF. Nevertheless, most

of these parameters present several drawbacks. In particular, some of them are manually obtained on the standard ECG, thus affecting repeatability of the measure, which is operator-dependent, and increasing error probability. In addition, such indices are usually computed in only one ECG lead, thus discarding the remaining ones. However, such an approach lacks robustness to lead selection, as spatial variability of surface ECG is not taken into account. ECG content can considerably change with respect to the heart plane and orientation considered, and so can the parameters measured at that specific location. Most of the traditional techniques are not able to process ECG content from all ECG leads at the same time, and they are therefore subject to the lead choice constraint.

1.2 Objectives

The present thesis takes a step from these preliminary considerations, and it is motivated by the research for novel multilead measures extracted from the 12-lead ECG which can predict AF termination by CA. Our investigation aims at yielding ECG-based parameters which take into account contributions from all ECG leads, and which are herein compared with classical methods for AF analysis and CA outcome assessment. To this end, standard ECG content is properly processed by multivariate techniques that are able to enhance the most content-bearing components while reducing the influence of polluting and/or redundant elements. This strategy presents the potential of examining the whole multilead recording at once, with no need for an a priori selection of the ECG leads to be analyzed, since the most significant contributions are automatically emphasized.

One of the main goals of this work is characterizing some classical indices determined on the standard ECG in a multilead framework, and corroborating the correlation with CA clinical outcome. These objectives motivate the multivariate description of f-wave amplitude, widely regarded as a predictor of AF termination by CA. To the same extent, information about spatio-temporal variability (STV) of AF coming from surface ECG, which is usually exploited for rendering AF complexity, is herein applied to distinguish between successful and failing CA procedures. Combination of these heterogeneous features is also applied to prediction of AF recurrence after CA at several follow-ups. Another line of research investigates the predictive accuracy of other features, based on information theory (IT). These measures render the degree of AF regularity in terms of spatial correlation between ECG leads. Finally, AF analysis and CA outcome prediction are envisaged from another perspective, based on the analysis of the ventricular response. Changes in RRI variability due to AF impact are characterized in a parametric probabilistic scenario, modeling as well the dependence of RRI length on dynamic vagal inputs to the sinoatrial (SA) node is modeled as well.

1.3 Thesis overview and summary of contributions

The remaining of this thesis consists of 8 chapters (Chapters 2 - 9) divided in 3 main parts. In the first part, a general overview about the main themes envisaged in this dissertation is provided. In particular, in **Chapter 2** we focus on some *basic clinical concepts*, which help understanding the *anatomy* and the *electrophysiology of the heart*, with particular attention to the conduction system, responsible for heart electrical activity

propagation. The informative content of the *standard ECG* and its clinical application are then illustrated, after indicating its main characteristics, both in healthy and pathologic conditions, and the processing modalities prior to information extraction.

Then, **Chapter 3** introduces the *AF* problem. AF *pathophysiology* is herein defined, and the main theories about its *generation and maintenance* are summarized, as well as the criteria for *classifying its complexity*, which are crucial for therapeutic choices. Particular attention is paid to AF chronicity effects, altering atria structure and function through electromechanical remodeling. The most current *AF therapies* are then described in our dissertation. *Pharmacological and electrical cardioversion* are illustrated, and their advantages and drawbacks are reviewed. The final part of this chapter focuses on *radiofrequency CA*, regarded as a new frontier in persistent AF treatment; its performance modalities, as well as some of the *protocols* adopted, are explained. Issues derived from this therapy prompts the search for criteria allowing the selection of the most suitable candidates to be treated by CA. Hence, it motivates the analysis of standard ECG and the extraction of some measures conventionally regarded as predictors of procedural AF termination, yet affected by some critical drawbacks, such as their manual computation in a single lead.

The central part of this thesis concerns the contributions and the methods developed to fulfill the objectives highlighted in the previous section. The principal lines of investigation of this thesis can be graphically summarized in Fig. 1.1. The main goals of this

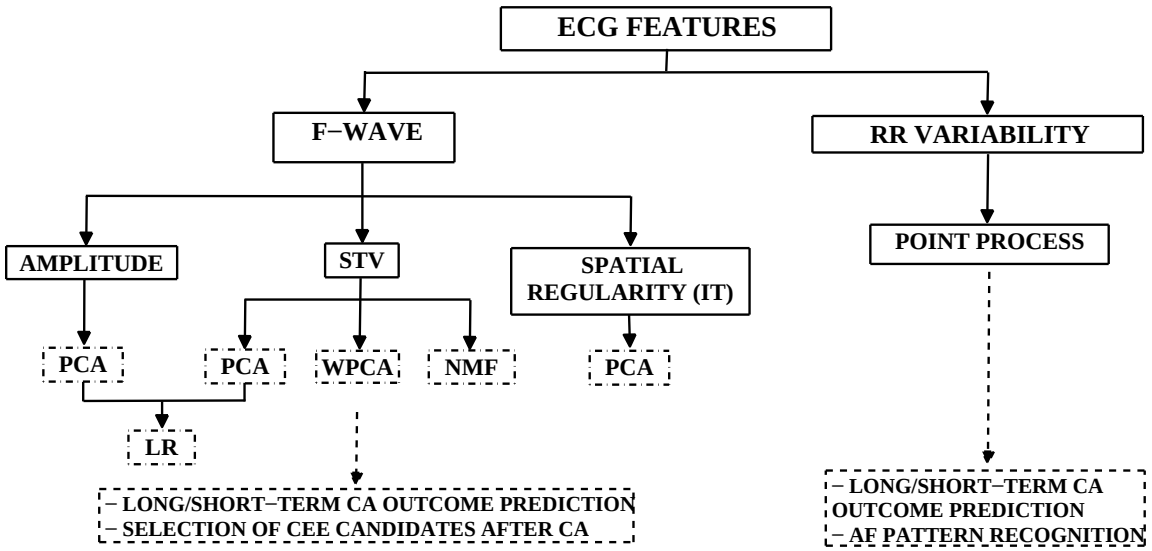


Figure 1.1: Explicative diagram of the main parts composing the thesis study. Sections referring to ECG features are contained in solid-line boxes. The multivariate techniques employed are included in dash-dot boxes. Clinical applications tested are marked in dashed boxes. Meaning of acronyms: AF: atrial fibrillation; CA: catheter ablation; CEE: electrical cardioversion; ECG: electrocardiogram; f-wave: fibrillatory wave; IT: information theory; LR: logistic regression; NMF: nonnegative matrix factorization; PCA: principal component analysis; STV: spatio-temporal variability; WPCA: weighted PCA.

work are the multilead assessment and enhancement of ECG features having remarkable

predictive properties for CA outcome definition. Accordingly, we mainly focused on 2 ECG characteristics, namely, fibrillatory waves **(f-wave)** and **RR variability**. First, in **Chapter 4** *the predictive role of f-wave amplitude in CA of persistent AF, traditionally assessed in only one lead on surface ECG, is herein automatically computed and extended to multiple ECG leads.* This is achieved by means of reduced-rank approximations to the AA signal determined by principal component analysis (PCA), which enhance the maximum-variance components of the AA signal, and show to improve CA outcome prediction. This is demonstrated at different follow-up lengths, by properly combining contributions from all ECG leads through suitable statistical descriptors (e.g., the median amplitude).

Then, in **Chapter 5** we investigate another ECG feature, depicting the *spatio-temporal variability (STV) of the AF pattern.* Some single-lead measures of this AF property recently proposed are correlated with AF complexity, traditionally assessed on endocardial recordings, for instance, by means of Wells' and Konings' criteria. *In this thesis we provide a multilead characterization of such indices, thus assessing not only the extent of temporal repetitiveness of the atrial pattern, but also its spatial distribution over ECG leads.* To this extent, several multivariate signal processing techniques, such as PCA, weighted PCA (WPCA), nonnegative matrix factorization (NMF), have been tested for AA signal processing. *The measures output by the algorithms developed are able to discriminate between effective and failing CA procedures at several follow-up periods.*

In **Chapter 6** we *combine heterogeneous ECG features* for assessing AF therapy outcome. Unlike previous chapters, we examine information about *f-wave amplitude and STV* properties presented in Chapter 4 and Chapter 5 coming from all ECG leads at the same time. Multivariate characterization of such measures is performed by the *logistic regression (LR) model*, which properly weights contributions provided by the ECG leads examined. Such selective action allows for enhancing components which are most relevant to *CA outcome prediction*, which has been *effectively performed at different follow-up* moments.

In **Chapter 7** *we explore the potential predictive role of several indices typical of the information theory (IT) domain*, which quantify the level of coupling between leads, and thus the degree of *spatial correlation.* This concepts have been borrowed from the theory of telecommunication systems, whose objective is assessing the amount of information exchanged between transmitter and receiver, and thus the percentage of data loss. To our knowledge, they are applied for the first time to CA outcome prediction in persistent AF and characterized in a multivariate framework. The link of AF regularity as measured by these parameters with clinical outcome of CA therapy is emphasized on multiple ECG leads, thanks to the compressing properties of PCA, enhancing the most relevant components of AA signal. Regularity assessment is first carried out on 2 ECG leads, and a multilead extension is provided as well.

In **Chapter 8** we approach another perspective for AF analysis, based on the *characterization of the ventricular response. RRI distribution is modeled in a parametric probabilistic framework, not yet applied in the framework of AF, which takes into account the effects of the dynamic vagal inputs to the SA node on the RRI length.* Features describing the RRI variability in terms of distribution dispersion and asymmetry depend on model

characteristics and *their predictive power in CA outcome assessment is investigated*. Such indices are subsequently exploited in AF pattern recognition, and differences between AF and SR conditions are explored.

The final part of the manuscript includes **Chapter 9**, which summarizes the main results presented in this thesis and sheds some light on potential new perspectives for AF investigation and CA outcome prediction.

1.4 Publications issued from this work

1.4.1 International journals

M. Meo, V. Zarzoso, O. Meste, D. G. Latcu and N. Saoudi, Catheter Ablation Outcome Prediction in Persistent Atrial Fibrillation Using Weighted Principal Component Analysis, *Biomedical Signal Processing and Control*, special issue on atrial arrhythmias, 2013, in press.

M. Meo, V. Zarzoso, O. Meste, D. G. Latcu and N. Saoudi, Spatial Variability of the 12-Lead Surface ECG as a Tool for Noninvasive Prediction of Catheter Ablation Outcome in Persistent Atrial Fibrillation, *IEEE Transactions on Biomedical Engineering*, Vol. 60, no. 1, pages 20-27, Jan. 2013.

1.4.2 International conferences

M. Meo, V. Zarzoso, O. Meste, D. G. Latcu, N. Saoudi and R. Barbieri, Point Process Modeling of R-R Interval Dynamics during Atrial Fibrillation, *Computing in Cardiology*, Sept. 22-25, 2013, Zaragoza, Spain, accepted.

V. Zarzoso, M. Meo and O. Meste, Low-rank Signal Approximations with Reduced Error Dispersion, *in: Proc. 21st European Signal Processing Conference (EUSIPCO)*, Marrakech, Morocco, September 9 - 13, 2013, accepted.

M. Meo, V. Zarzoso, O. Meste, D. G. Latcu and N. Saoudi, Noninvasive Prediction of Catheter Ablation Acute Outcome in Persistent Atrial Fibrillation Based on Logistic Regression of ECG Fibrillatory Wave Amplitude and Spatio-temporal Variability, *in: Proc. 35th Annual International IEEE Engineering in Medicine and Biology Society Conference (EMBC)*, Osaka, Japan, July 3-7, 2013, pages 5821-5824.

M. Meo, D.G. Latcu, V. Zarzoso, O. Meste, M. Garibaldi, I. Popescu, N. Saoudi, Automatic Multilead Characterization of F-wave Amplitude Enhances Prediction of Catheter Ablation Outcome in Persistent Atrial Fibrillation, abstract presented at *EHRA EUROPACE 2013*, Athens, Greece, June 23-26 2013.

M. Meo, V. Zarzoso, O. Meste, D. G. Latcu and N. Saoudi, Multidimensional Characterization of Fibrillatory Wave Amplitude on Surface ECG to Describe Catheter Ablation

Impact on Persistent Atrial Fibrillation, in: Proc. 34th Annual International IEEE Engineering in Medicine and Biology Society Conference (EMBC), San Diego, MA, Aug. 28 - Sep. 1, 2012, pages 617-620.

G. Laouini, O. Meste and M. Meo, Analysis of Heart Rate Variability Using Time-Varying Filtering of Heart Transplanted Patients, *in: Proc. 34th Annual International IEEE Engineering in Medicine and Biology Society Conference (EMBC)*, San Diego, MA, Aug. 28- Sep. 1, 2012, pages 3436-3439.

M. Meo, D.G. Latcu, V. Zarzoso, O. Meste, M. Garibaldi, I. Popescu, N. Saoudi, Mathematical Analysis of Atrial Spatiotemporal Complexity on Standard ECG for Catheter Ablation Outcome Prediction in Persistent Atrial Fibrillation, abstract presented at *European Society of Cardiology Congress*, Munich, Germany, Aug. 25-29, 2012.

M. Meo, D.G. Latcu, V. Zarzoso, O. Meste, M. Garibaldi, I. Popescu, N. Saoudi, ECG Spatiotemporal Complexity Predicts Catheter Ablation Outcome in Persistent Afib, abstract presented at *CARDIOSTIM 2012*, Nice, France, June 13-16, 2012.

M. Garibaldi, V. Zarzoso, D.G. Latcu, M. Meo, O. Meste, I. Popescu, N. Saoudi, Persistent Atrial Fibrillation Dominant Frequency on Standard ECG Predicts Catheter Ablation Outcome, abstract presented at *CARDIOSTIM 2012*, Nice, France, June 13-16, 2012.

M. Meo, V. Zarzoso, O. Meste, D. G. Latcu and N. Saoudi, Nonnegative Matrix Factorization for Noninvasive Prediction of Catheter Ablation Outcome in Persistent Atrial Fibrillation, *in: Proc. IEEE International Conference on Acoustics, Speech, and Signal Processing (ICASSP)*, Kyoto, Japan, March 25-30, 2012, pages 601-604.

M. Meo, V. Zarzoso, O. Meste, D. G. Latcu and N. Saoudi, Catheter Ablation Outcome Prediction in Persistent Atrial Fibrillation Based on Spatio-Temporal Complexity Measures of the Surface ECG, *in: Proc. Computing in Cardiology*, Hangzhou, China , vol. 38, Sept. 18-21, 2011, pages 261-265.

M. Meo, V. Zarzoso, O. Meste, D. G. Latcu and N. Saoudi, Non-invasive Prediction of Catheter Ablation Outcome in Persistent Atrial Fibrillation by Exploiting the Spatial Diversity of Surface ECG, *in: Proc. 33rd Annual International IEEE Engineering in Medicine and Biology Society Conference (EMBC)*, Boston, MA, Aug. 30-Sep. 3, 2011, pages 5531-5534.

Part I

Background

2 Electrophysiology of the heart and electrocardiography

2.1 Introduction

The first part of this doctoral thesis aims at providing a general description of heart anatomy, its structure and leading steps of the cardiac cycle, responsible for distribution of oxygen to all parts of the human body. The main goal of this section is helping comprehension of heart activity in healthy conditions so as to better understand alterations and complications deriving from cardiac diseases. Particular attention is paid to the electrical conduction system, enabling the propagation of electrical potentials throughout the cardiac tissue, and thus the blood pumping action intrinsic to the electromechanical coupling function. Recording heart electrical activity is essential for a rapid diagnosis of certain cardiac diseases, as well as a deeper understanding of their triggering causes. To this goal, the 12-lead ECG represents a noninvasive and cost-effective tool increasingly employed in clinical centers; hence, the increasing interest in developing sophisticated signal processing techniques able to extract valuable clinical information, especially under pathological conditions. Accordingly, after introducing the clinical background around the heart and its main functions, we give a general description of the standard ECG and its main characteristics. More precisely, in Sec. 2.2 we provide a general overview of heart anatomy. Subsequently, we focus on the electrical conduction system in Sec. 2.3. Standard ECG is then introduced in Sec. 2.4. Finally, an overall summary of our description is reported in Sec. 2.5.

2.2 Anatomy of the heart

Most of this chapter refers to [55, 96, 114, 143]. The human heart is an organ that pumps blood throughout the body via the circulatory system. It is located under the ribcage in the center of body chest between right and left lungs. It is widely known that the heart can be regarded as a pump propelling blood throughout the body and consisting of 4 chambers, made entirely of muscle. The upper chambers are referred to as atria, whereas the lower ones are named ventricles (see Fig. 2.1). These hollow compartments are delimited by heart walls, composed of cardiac muscle, called myocardium. A wall of muscle named the septum separates the right and the left side of the heart[1].

[1] http://www.texasheartinstitute.org/HIC/Anatomy/anatomy2.cfm

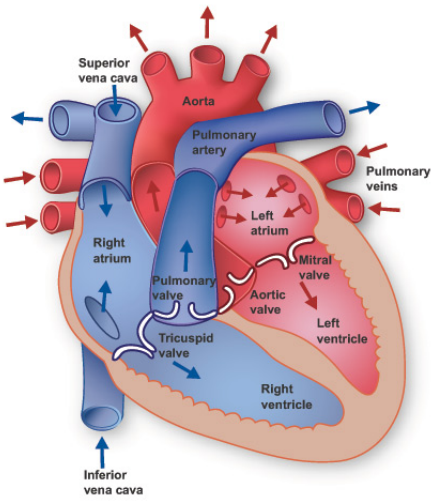


Figure 2.1: Anatomy of the heart [2].

Moving from the outermost heart tissue layers, a double-walled sac called the pericardium encases the heart, so as to protect and anchor it inside the chest. It is formed by 3 layers, as shown in Fig. 2.2, and between them some pericardial fluid flows so as to lubricate the heart during contractions and movements of the lungs and diaphragm. The innermost pericardium component is referred to as the epicardium, which represents the external membrane enclosing the heart. Then we meet the myocardium, the thickest layer, consisting of cardiac muscle inducing contraction. Finally, the innermost layer, or endocardium, is the epithelial tissue lining in contact with the blood.

The heart can be regarded as an ensemble of 2 pumps connected in series. Indeed, it pumps blood through 2 circuits: the pulmonary circuit and the systemic circuit. The first one, the right ventricle (RV), receives blood from the right atrium (RA), after coming from superior and inferior venous cavae (SVC and IVC, respectively), and propels deoxygenated blood via the pulmonary artery. Blood reaches the lungs, absorbs oxygen and goes back to the left atrium (LA) and then to the left ventricle (LV) through the pulmonary veins (PVs). This pathway represents the pulmonary circuit. In the second pathway, the systemic circuit, oxygenated blood leaves the body via the aortic valve to the aorta, and from there enters the arteries and capillaries of the systemic circulation, where it supplies the body's tissues with oxygen. Deoxygenated blood returns via the veins to the venae cavae (VC), re-entering the heart's RA, so that the cycle can start again. Blood flow through the heart is unidirectional, thanks to the cardiac valves, whose opening and closure are enabled by proper pressure gradients. Between the RA and RV lies the tricuspid valve (TV), and between the LA and LV there is the mitral valve (MV). The pulmonary valve separates RV and the pulmonary artery, while the aortic valve lies in the outflow tract of the LV, and separates the RV from the aorta. All the aforementioned components of the heart are displayed in Fig. 2.1. A graphical representation of the blood circuits is provided in Fig. 2.3.

[2] http://histologyolm.stevegallik.org/node/347

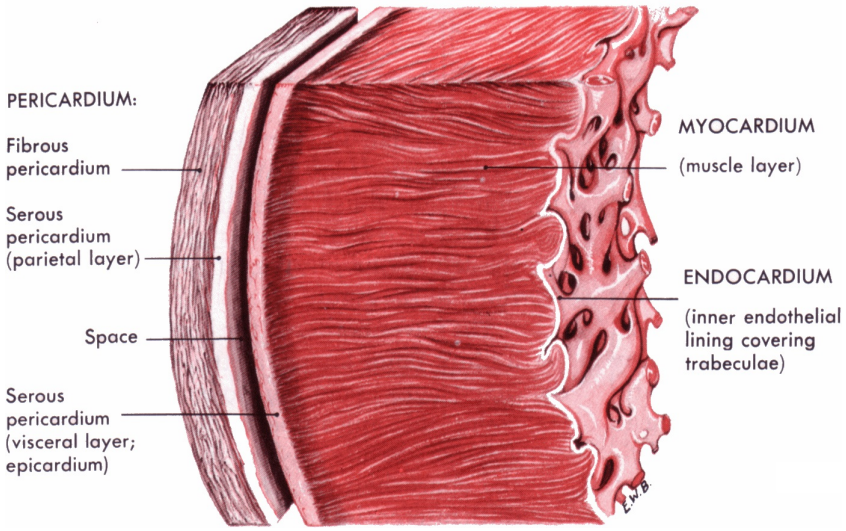


Figure 2.2: Section of the heart wall showing the components of the outer pericardium (heart sac), muscle layer (myocardium), and inner lining (endocardium)[2].

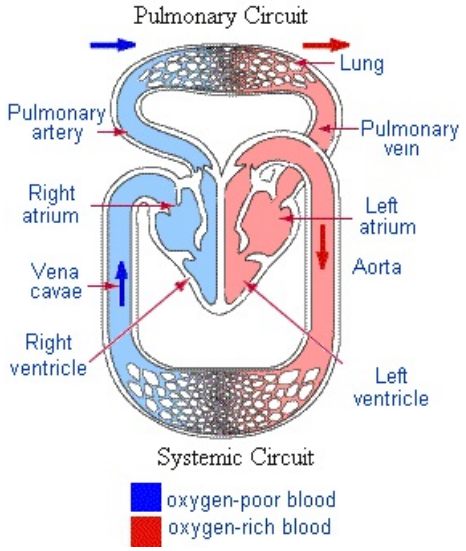


Figure 2.3: Schematic representation of the pulmonary and the systemic circuits with their main components [81].

2.3 The electrical conduction system and the electromechanical coupling

The electrical conduction system of the heart, shown in Fig. 2.6, allows for the generation and propagation of impulses via a specialized conduction pathway, which stimulate the heart to contract and pump blood. In contrast with other kinds of muscles, heart muscle fibers are self-excitatory. It turns out that potential generation can occur without any nerve signal triggers. The anatomy of cardiac muscle is such that the initiation of an action potential in a fiber would result in the action potential excitation of all the muscle fibers. Even though any part of the heart can generate impulses, the sinoatrial (SA) node serves as a natural pacemaker, since it exhibits the highest intrinsic frequency, thus it sets the activation frequency of the whole heart. It is located in the RA where VC terminates, and its firing rate is usually around 70 bpm. Even though its function is quite autonomous, we must mention that its pacing is also influenced by information sent by the sympathetic and the parasympathetic inputs of the autonomic nervous system. Indeed, the former increases the heart rate (HR), whereas the latter induces the opposite effect.

The cardiac cycle is created when such impulse propagates through the conduction system, so as to trigger the mechanical force. As a consequence, the electrical event always precedes the mechanical action. When RA is triggered to contract, it pumps the blood collected from all the parts of the body into the RV. When it is completely filled, blood is forced into the lungs for oxygenation and then returned to the LA through the PVs. Blood is finally emptied to the LV, so as to be spread throughout the body. As previously stated, all these mechanical events are triggered by electrical stimuli. Each cardiac cycle consists of 2 mechanical phases, contraction and relaxation, whose electrical counterparts are referred to as depolarization and repolarization, respectively. Depolarization is induced by a variation in the resting membrane potential of myocardial cells (from -90 to 20 mV), which rapidly spreads throughout the myocardium. The self-depolarization of the SA node enables a rhythmic series of action potentials, which spread throughout the RA and LA. This induces atria contraction, and blood is pumped into ventricles (diastole). The action potential propagates through the atria at a relatively slow velocity ($0.3 - 0.4\ m/s$). Depolarization wavefront then reaches the atrioventricular (AV) node, which provides atria with a conductive pathway to ventricles. Since its natural frequency is lower than SA firing rate (i.e., about 50 bpm), the AV node spontaneously follows SA frequency. The action potentials propagates from the atrium to the AV node, thus allowing time for the atria to pump blood into the ventricles. The AV node is a pathway of muscle fiber which introduces a short delay of about 11 ms into the impulse propagation to the ventricles, so that atria can effectively contract and completely empty blood into ventricles. Signal transmission from the AV node to the ventricles is ensured by a specialized conduction system. It consists of a bundle, i.e., the bundle of His, which then ramifies into two bundle branches, which in turn divide into Purkinje fibers, directly connected to the inner ventricular walls. Such components are themselves large muscle fibers whose action potentials propagate at a velocity of $1.5 - 2\ m/s$. The depolarization wavefronts then spread through the ventricular wall, from endocardium to epicardium, enabling ventricular contraction. Once each ventricle cell has depolarized, repolarization allows for relaxation of the myocardial muscle, and the cardiac cycle can start again. This slow process gives

rise to a plateau in the cardiac action potential which can be observed in Fig. 2.6, in contrast with nerve and skeletal action potentials. This plateau allows the muscle fibers to contract in synchronism resulting in a forceful pumping action. The ECG signal, picked up by the surface electrode on the body surface is a superposition of these action potentials.

2.4 The standard 12-lead ECG

Due to their conductive nature, heart nerves and cells can be regarded as a source of electrical charges in motion during depolarization and repolarization processes within a volume conductor, i.e., the thorax. Indeed, the sum of cardiac cell potentials can be represented by a unique heart electrical vector in a first-order approximation, whose magnitude and direction change in time according to pulse wavefront propagation and strength. The electrical field generated by these charges can be thus detected on its equipotential lines on thorax surface. This electrical activity signal can be acquired by means of electrodes positioned on the subject's thorax and then amplified and recorded by the electrocardiograph. Electrocardiography is a commonly used, noninvasive procedure for recording heart electrical activity. The signal recorded, named electrocardiogram (ECG or EKG), graphically shows the series of waves associated with electrical phenomena of depolarization and repolarization of the heart during the cardiac cycle, and represents the summation in space of the action potentials generated by the myocadial cells at each time instant. The first practical ECG was invented in 1903 by Einthoven, who was awarded with the Nobel Prize in Medicine in 1924 for it. He refined the string galvanometer used for measuring the heart's rhythms, and he also paid attention to wave terminology definition and examination of some cardiac disorders on ECG [49]. ECG leads thus report the instantaneous difference in potential between electrodes. The signals are detected by means of metal cutaneous electrodes attached to the extremities and chest wall, and they are then amplified and recorded by the electrocardiograph. A difference of voltage can be measured between each pair of electrodes, named lead, whose amplitude and direction depend on electrodes' configuration. ECG signal values are generally quite low, ranging from a few microvolt up to 1 V, therefore acquisition system always includes an amplifier.

As it is a noninvasive, rapid and cost-effective test, ECG is a valuable and highly versatile tool in clinical practice for detecting several heart dysfunctions by inspection of alterations in ECG pattern shape or duration of wave intervals.

Electrocardiography is a starting point for detecting many cardiac problems, such as angina pectoris, ischemic heart disease, arrhythmias, myocardial infarction. In addition, it may reveal other findings related to life-threatening metabolic disturbances (e.g., hyperkalemia) or increased susceptibility to sudden cardiac death (e.g., QT prolongation syndromes). It is routinely employed for monitoring surgeries and exercise tolerance tests (e.g., stress tests), as well as evaluating certain symptoms (for instance, chest pain, shortness of breath, palpitations).

As previously stated, the ECG records the complex spatial and temporal summation of electrical potentials from multiple myocardial fibers conducted to the surface of the body [55]. Each group of cells depolarizing at the same time can be represented as an equivalent current dipole vector. Each vector describes the dipole's time-varying position,

orientation, and magnitude. The vectors related to all these groups can be summed to give a dominant vector which describes the main direction of the electrical impulse throughout the heart. In order to better understand the generation of the ECG signal, Fig. 2.4 displays the sequence of the instantaneous heart wavefront vectors at each step of the cardiac cycle. Each phase of the depolarization and repolarization processes are reflected on ECG by the following characteristic points, also shown in Fig. 2.5:

- **P wave**: it describes simultaneous depolarization of left and right atria. The normal atrial depolarization vector is oriented downward and toward the subject's left, as it reflects the wavefront moving from the SA to the RA and then the LA myocardium.
- **QRS complex**: it represents ventricular depolarization. As ventricles have larger mass compared to the atria, the QRS complex usually has a much larger amplitude than the P wave. The process can be divided into 2 major, sequential phases. The first one concerns the depolarization of the interventricular septum from the left to the right and anteriorly. The second phase includes the simultaneous depolarization of RV and LV. The QRS pattern in the extremity leads may vary considerably from one normal subject to another depending on the electrical axis of the QRS, whose mean orientation is referred to the 6 frontal plane leads. In healthy conditions, the QRS axis ranges between $-30°$ and $+100°$. Any deviation outside the lower (upper) bound is referred as to left (right) axis deviation. It may occur as a normal variant of heart condition, but sometimes it can also be symptom of more serious diseases.
- **T wave**: it is associated with ventricular repolarization, and its representative vector is oriented roughly concordant with the mean QRS vector (within about $45°$ in the frontal plane). The interval from the beginning of the QRS complex to the apex of the T wave is referred to as the absolute refractory period, whereas the terminal part of the T wave reflects the relative refractory period.

Atrial repolarization is usually too low in amplitude to be detected, but it may become apparent in some conditions, e.g., acute pericarditis or atrial infarction. The QRST waveforms of the standard ECG correspond in a general way with the different phases of simultaneously obtained ventricular action potentials, depicting the activity of single myocardial fibers. With reference to Fig. 2.6, the rapid upstroke of the action potential corresponds to the QRS onset. This is followed by the plateau phase, corresponding to the isoelectric ST segment, and then completed by the active repolarization, represented by the inscription of the T wave on ECG.

ECG baseline (the flat horizontal segments) is measured between the end of the T wave and the beginning of the next P wave. It represents the resting potential of the myocardial cells. Also in the PR and ST segments we encounter ECG baseline. In SR conditions, the baseline is equivalent to the isoelectric line (0 mV). By contrast, in presence of certain diseases there could be drifts from zero due to injury currents flowing when the ventricles are at rest.

In clinical practice, some intervals are also studied on ECG, knowing that alterations in their duration can be symptom of certain pathologies. In particular we mention:

- **RR interval**: the mean distance between two consecutive R peaks provides a HR measure, ranging between 60 and 100 bpm at rest.
- **PR interval**: starting at the beginning of the P wave up to the beginning of the QRS complex, it indicates the time of propagation of the potential action from the SA to the AV node, thus rendering a good estimate of AV node function.
- **QT interval**: extending from the beginning of the QRS complex up to the end of

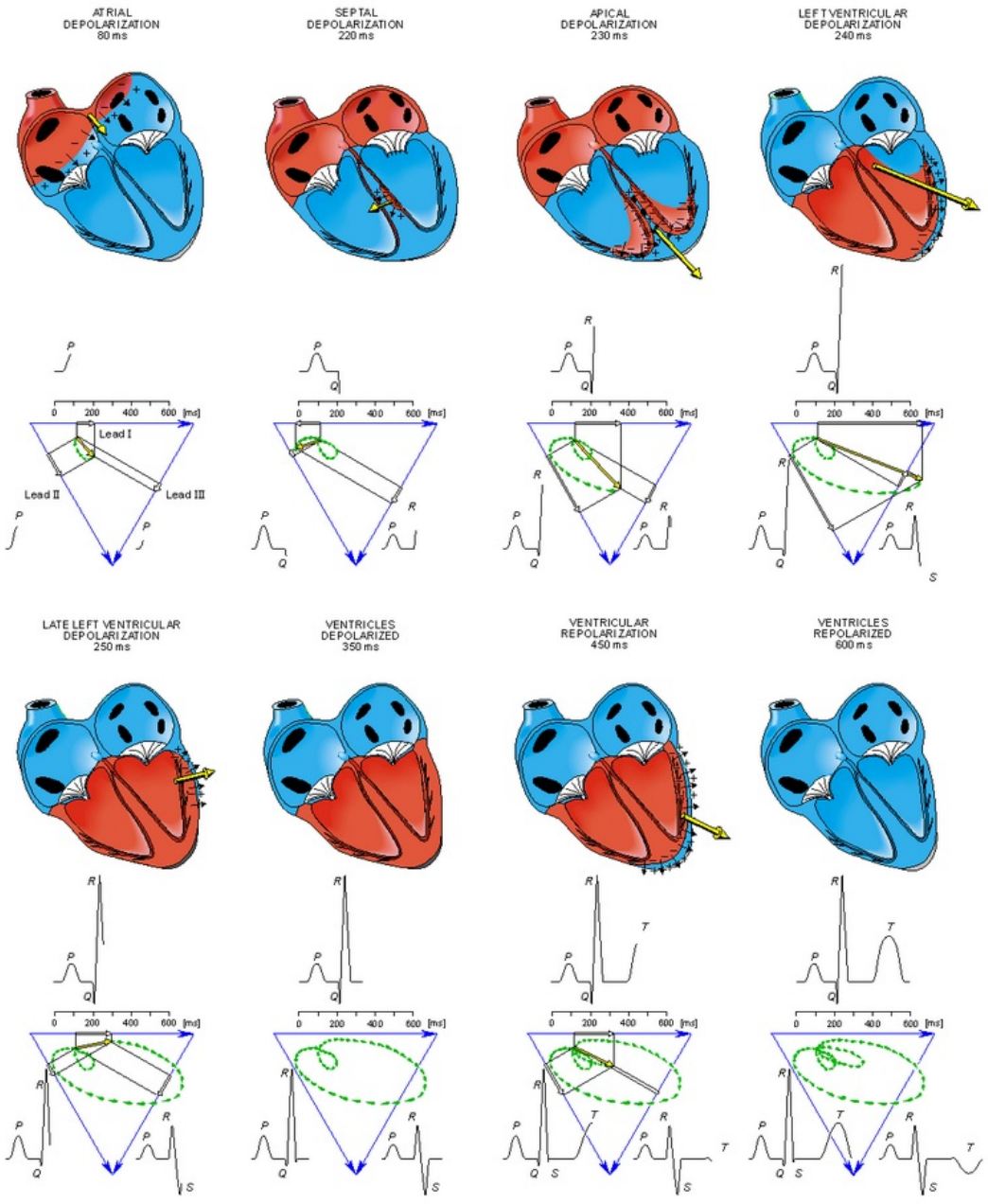


Figure 2.4: Sequence of the instantaneous heart wavefront vectors at each step of the cardiac cycle [96].

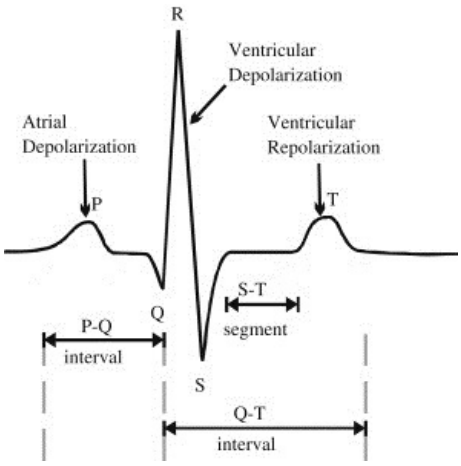


Figure 2.5: ECG signal, its fiducial points and the corresponding phases in the cardiac cycle [68].

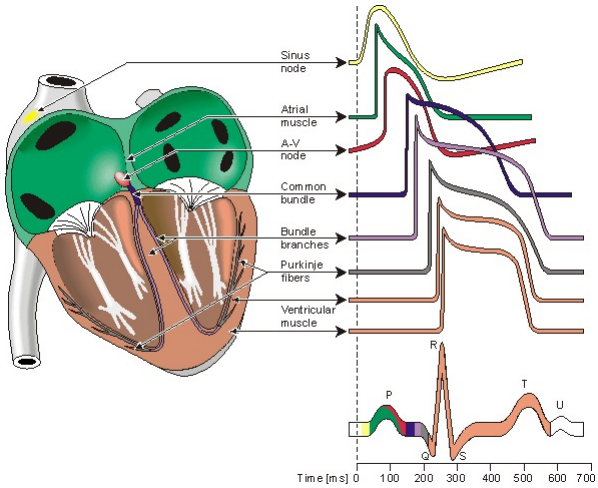


Figure 2.6: The heart conduction system with its main components, their typical potential waveforms and the corresponding points on surface ECG [96].

the T wave. A prolonged duration is predictive of ventricular tachyarrhythmias and sudden death.

The choice of a unique, standard system of lead position for ECG acquisition derives from the need to compare cardiac potentials recorded in different subjects, and examine signals acquired in the same subject, but at different times and places. In the standard ECG 12 leads are employed. More precisely, 10 electrodes are placed at standardized positions of the body surface. As explained later, some potentials are linearly dependent between them. Since the voltages recorded in the leads are regarded as projections of the heart electrical vector on the particular lead, any two of the leads may be used to plot the instantaneous magnitude and direction of the cardiac vector in the plane they form.

The ECG leads can be subdivided into two general types, namely, bipolar leads and unipolar leads [109]. A bipolar lead consists of two electrodes placed at two distinct sites, so as to register the difference in potential between them. The actual absolute potential at either electrode is not known, and only the difference between them is recorded. One electrode is designated as the positive input; the potential at the other, or negative, electrode is subtracted from the potential at the positive electrode to yield the bipolar potential. Unipolar leads, in contrast, measure the absolute electrical potential at one site, with respect to a reference potential, which is deemed to be zero. In clinical electrocardiography, a specially designed electrode configuration is adopted for the 12-lead ECG, detailed in Sec. 2.4.1-2.4.3.

2.4.1 EINTHOVEN'S LEADS

The first 3 leads are defined by Einthoven's triangle. Each lead measures the difference in potential between electrodes at 2 of the 3 extremities (right arm; left arm; left leg), as displayed in Fig. 2.7. Potentials are thus defined as:

$$I = \Phi_{\mathrm{L}} - \Phi_{\mathrm{R}} \tag{2.1}$$

$$II = \Phi_{\mathrm{F}} - \Phi_{\mathrm{R}} \tag{2.2}$$

$$III = \Phi_{\mathrm{F}} - \Phi_{\mathrm{L}} \tag{2.3}$$

where I, II and III stand for potential of lead I, II and III, respectively, Φ_{L}, Φ_{R} and Φ_{F} represent the potentials at the left arm, the right arm and the left foot. As these leads form a closed circuit, each of them can be expressed as a linear combination of the other ones:

$$II = I + III \tag{2.4}$$

What is more, since these 3 electrodes are positioned at the corners of a equilateral triangle, containing the human heart at the center, such a leads' configuration registers heart electrical activity on the frontal plane, and each direction differs from the other one of 60°. Note that the right leg acts as a ground potential.

[7] http://www.nottingham.ac.uk/nursing/practice/resources/cardiology/function/bipolar_leads.php

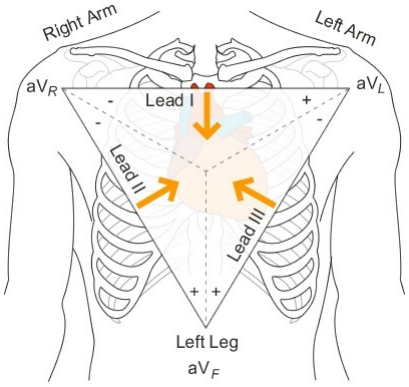


Figure 2.7: Frontal ECG leads: Einthoven's leads, and Goldberger's (augmented) leads[7].

2.4.2 Goldberger's leads

In addition to the bipolar limb leads, there are 3 augmented limb leads, also known as Goldberger's leads. Potential of these leads is measured by assuming the central Wilson's terminal (or indifferent electrode) as a reference. This ground electrode is referenced against a combination of the other limb electrodes, from which they are shifted of 30°. Hence, these potentials aV_R, aV_L and aV_F, are considered unipolar and are electrically augmented by 50% by omitting the resistance from the Wilson central terminal, which is connected to the measurement electrode. Potentials measured are mathematically expressed as:

$$aV_R = \frac{I - II}{2} \tag{2.5}$$

$$aV_L = I - \frac{1}{2}II \tag{2.6}$$

$$aV_F = II - \frac{1}{2}I \tag{2.7}$$

2.4.3 Precordial leads

The limb leads take into account direction of depolarization in the frontal plane. However, as the heart is not parallel to this plane, related leads give information about the inferior and lateral walls but do not distinguish between other areas, in particular septal and anterior and lateral heart walls. The precordial, unipolar leads are positioned in specific sites on the rib cage and record potentials transmitted onto the horizontal plane (see Fig. 2.8). In particular, leads V_1 and V_2 are positioned at the 4th intercostal space, to the right and the left of the sternum, respectively. Lead V_3 is placed midway between V_2 and V_4, which is in turn located on the midclavicular line, at the 5th intercostal space; lead V_5 is on the anterior axillary line, at the same level as V_4. Finally, lead V_6 is positioned on the midaxillary line, at the same level as V_4 and V_5.

2.4.4 Information content of the standard ECG

In this framework, all the aforementioned electrodes provide a three-dimensional representation of heart electrical activity in the cardiac cycle. Most of the heart's electric

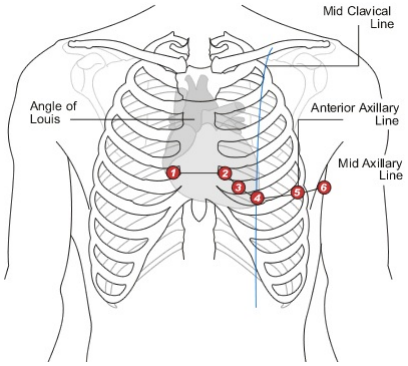


Figure 2.8: Precordial ECG leads [96].

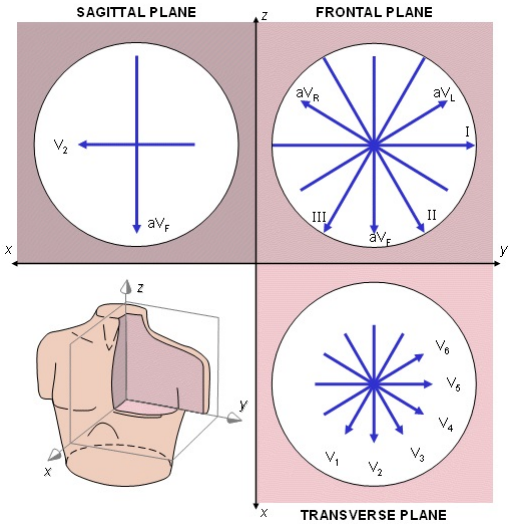


Figure 2.9: The projections of the lead vectors of the standard ECG system in 3 orthogonal planes. The volume conductor is assumed to be spherical homogeneous and the cardiac source centrally located [96].

activity can be characterized with a dipole source model. Under this hypothesis, 3 linearly independent leads (2 limb leads and a precordial one) are sufficient to describe heart electrical activity temporal evolution. Indeed, in the 12-lead system, there is a redundancy of 4 leads. The limb leads and the augmented leads can be expressed as a function of 2 independent potential differences, therefore standard ECG includes 8 independent leads. The interest in considering also the other leads can be explained by the standard ECG ability to detect further nondipolar components, which have diagnostic significance because of their proximity to the frontal part of the heart.

The main reason for recording also redundant leads is that it enhances pattern recognition. Indeed, it allows comparing the projections of the resultant vectors in two orthogonal planes and at different angles. For instance, right precordial leads, V_3R and V_4R, are useful in detecting evidence of acute right ventricular ischemia. In Fig. 2.9, ECG lead projections are displayed in 3 perpendicular planes.



Figure 2.10: Examples of IEGM. HRA: high right atrial IEGM; HIS p and HIS d: proximal and distal HIS-bundle IEGM; CS $1-2$, CS $3-4$, CS $5-6$, CS $7-8$, CS $9-10$: distal bipole $1-2$, bipole $3-4$, bipole $5-6$, bipole $7-8$, proximal bipole $9-10$, respectively; RVa = RV apex IEGM; Stim 2 = stimulus channel. These signals are induced by straight atrial pacing with a drive-cycle length of 340ms and acquired by means of a decapolar catheter in the CS and quadripolar catheters in the high RA, His-bundle region and RV apex, according to the protocol described in [51].

2.4.5 Other forms of heart electrical activity recording

For the sake of completeness, even though our investigation merely focuses on standard ECG, it is worth to provide a few notions about other kinds of signals depicting heart electrical activity, whose description can help comprehension of other sections of this dissertation, in particular those concerning AF organization and type classification.

Intracardiac electrograms

An intracardiac electrogram (IEGM) is a record of timing or sequence of activation of specific cardiac locations (e.g., the distal CS or the left upper PV), as measured with electrodes directly placed within the heart via endocardiac catheters. They are generally employed for recording electric potentials of sites that cannot be assessed by body surface electrodes, for instance, the bundle of His, which is too small to produce sufficiently high voltages to register on the surface ECG [162]. Furthermore, it is widely know how difficult is to correlate heart electrical events recorded at body surface with in-depth activity, therefore knowledge about ECG content needs to be supported by intracardiac signals.

There are two types of IEGMs, namely, bipolar and unipolar signals. Bipolar signals are produced when the voltages on the two recording electrodes both vary with time - as is the case when each is positioned within the heart. By contrast, unipolar signals are produced when one varying signal is compared with a constant (or indifferent) reference placed outside the heart. In general, clinical practice refers to bipolar signals, as they reduce far-field signals and they are less prone to electrical noise [162]. Examination of unipolar signals is motivated by interest in signals from each pole of a catheter separately. In Fig. 2.10 some examples of IEGMs are shown.

This kind of recordings allows electrophysiologists to follow the propagation of electri-

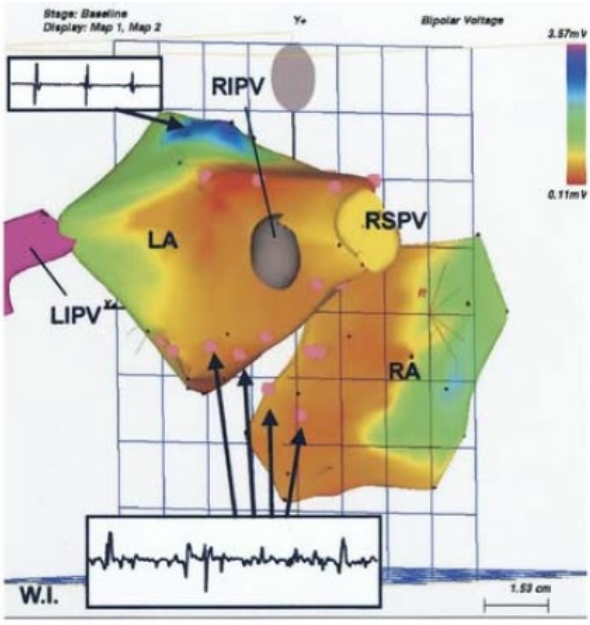


Figure 2.11: Example of electroanatomic voltage map [116]. LIPV: left inferior PV. RIPV: right inferior PV. RSPV right superior PV.

cal activation by noting the order of the signals in time. When an electrical impulse passes the tissue close to an electrode, depolarization of cardiac cells takes place, as reflected by steep deflections, named activations, in the recording. This attention to the activation sequence represents the main difference between IEGM and ECG, which rather focuses on signal morphology.

Such a local approach makes IEGM highly reliable, since it is barely influenced by other biological signals, such as surrounding muscular activity or electrical activity of other tissues and organs. On the other hand, the invasivity of this analysis increases the risks of infections and other side-effects (e.g., thromboembolic accidents), and requires a careful management of signal acquisition.

In AF investigation, these kind of signals are widely employed for understanding the mechanisms of triggering and maintenance of this arrhythmia, for instance, under guided tissue stimulation or by mapping heart electrical activity. Moreover, they are currently used in CA for positioning the ablation catheter in combination with a visual mapping system (e.g. CARTO system, see Fig. 2.11) and then checking whether the arrhythmia has been terminated at the end of the procedure.

Body surface potential mapping

Despite the multiple advantages of the ECG system, the reduced number of recording spots on the chest can sometimes makes it quite hard to detect small variations in heart electrical activity and investigate certain diseases. As a consequence, body surface potential mapping (BSPM) systems are increasingly employed so as to perform a higher resolution analysis of heart electrical activity as seen by a higher number of sites on the entire surface of the chest and the back of patient's body. The number of acquisition leads ranges between 32 and 240. This kind of system enables the generation of a torso map of electrical activity, in which we can follow the flow of electricity related to a heartbeat. An

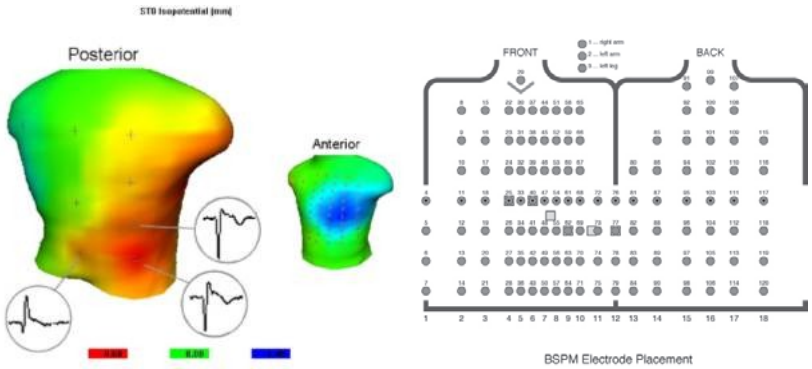


Figure 2.12: BSPM system. Left: An example of map [155]. Right: Position of BSPM leads [93].

example of BSPM map is displayed in Fig. 2.12, besides the a schematic representation of leads' location.

AF comprehension has considerably taken benefit from BSPM analysis. In [57] different patterns of atrial activation have been observed in surface in several subjects by means of this system. In [58], noninvasive localization of AF trigger sites is accomplished by the BSPM system. The study led in [18] demonstrates that it is possible to assess AF spatio-temporal organization on BSPM maps by means of PCA.

Despite its valuable clinical content, BSPM has not been adopted yet as a routine tool for cardiac diagnosis. This can be explained by several factors, such as the longer time of signal acquisition, the more difficult equipment installation and the unsuitability to be used during surgery. Accordingly, standard ECG represent a proper trade-off between invasive recordings and high-resolution surface potential mapping and it is generally preferred for daily clinical practice.

2.4.6 ECG processing

ECG acquisition can be hampered by different types of noise and artifacts which can profoundly alter and/or hide useful information about heart electrical activity. Hence, the importance of an adequate ECG signal processing prior to information extraction and further computational steps. In general, some preprocessing actions are required for noise filtering. Understanding the causes of noise can help choosing the proper filter, and keeping signal properties as most unaltered as possible, since any changes in voltage amplitude, phase, frequency, morphology can notably influence ECG interpretation and alter final diagnosis about the presence/absence of a disease.

Some sources of noise are technical. For instance, potential interference can come from power line interference ($50-60$ Hz), owed to improper grounding of the ECG equipment and interference from other equipment close to the ECG acquisition system. Other types of noise can have a physiological origin. For instance, we mention baseline wander, with spectral content below 1 Hz, which can be caused by respiration or body movements. Another source of interference is the electromyographic noise, due to the electrical activity of skeletal muscles during contraction. Unlike baseline wander, the range of its frequency components is comparable with that of the QRS complex. It turns out that suppressing this kind of noise is not a trivial task, as there is the risk of introducing signal distortion.

Similar issues are encountered when electrodes are not correctly positioned or they get disconnected, as contact impedance of the skin around the electrode is altered.

Another preprocessing task which is particularly useful in cardiac disease diagnosis is the automatic detection of ECG fiducial points and intervals. Such inspection can also help isolating certain components on the ECG (for example, distinguishing ventricular and atrial activity, VA and AA). The interest in developing automatic tools makes ECG processing operator-independent and provides rapid and objective measures of ECG properties.

Preprocessing operations strongly depend on signal properties, as well as the goal of the investigation on ECG. The preprocessing tools employed in this doctoral thesis will be presented in more detail later for AF characterization in the Contributions' part of the manuscript.

2.5 SUMMARY AND CONCLUSIONS

This introductory chapter renders a general overview of cardiac electrophysiology. Basic anatomy and physiology concepts and definitions are provided so as to facilitate comprehension of the main problems around AF, its treatment and the technical tools developed in the Contributions' section. Special attention is paid to the heart conduction system, since the knowledge about its activity and any alterations are fundamental for understanding and tackling the AF problem. We focused on non invasive tools for AF diagnosis and treatment as provided by the ECG analysis, a cost-effective and rapid approach, which is increasingly employed in clinical centers for recording heart electrical signal evolution. All these concepts will help understanding AF pathology and envisaging potential diagnostic and therapeutic strategies.

3 Atrial fibrillation

3.1 Introduction

In Chapter 2 we have described some concepts about heart anatomy and functions, and we have illustrated the role of standard ECG for examining heart electrical activity. In this chapter we introduce the AF problem and we provide some elements which help understanding this arrhythmia. First, in Sec. 3.2 we provide a general definition of atrial arrhythmia, then we move to AF description in Sec. 3.3. Several AF treatment strategies are discussed in Sec. 3.4, with particular attention to the CA therapy in Sec. 3.5, whose outcome prediction techniques are dealt with in Sec. 3.6. Main conclusions are finally summarized in Sec. 3.7.

3.2 Definition of atrial arrhythmias

Arrhythmias are defined as dysfunctions in the normal beating action of the heart, and are generally divided into two categories: ventricular and supraventricular. The irregular beats can either be too slow (bradycardia) or too fast (tachycardia). Ventricular arrhythmias occur in the lower chambers of the heart, namely, the ventricles. Supraventricular arrhythmias (SVA) are heart rhythm disorders affecting the upper part of the heart, i.e., the atria or the atrial conduction pathways [16]. In particular, they generally involve the atria, the AV junction, or vessels directly communicating with the atria, such as the vena cava or PVs. All cardiac arrhythmias are produced by several mechanisms, including disorders of initiation and propagation of potential impulses, respectively defined as automatic and re-entrant. Cardiac cells affected by abnormal automaticity exhibit an increase in firing rate, and they can overdrive the SA node, the natural heart pacemaker, if the rate of the ectopic focus is higher. The most current types of supraventricular arrhythmias include:

- **Premature atrial contractions (PACs)**: occurring when the atria contract too soon, causing the heart to beat out of sequence.
- **Paroxysmal supraventricular tachycardia (PSVT)**: a rapid but regular heart rhythm which originates in the atria and speeds up the heart rate up to $150 - 250$ bpm. The word "paroxysmal" refers to a non-permanent condition, and it means occasional or occurring from time to time.
- **Accessory pathway tachycardias (e.g., Wolff-Parkinson-White, WPW, syndrome)**: a group of abnormalities caused by extra, abnormal muscle pathways between the atria and the ventricles. The pathways cause the electrical signals to

arrive at the ventricles too soon, and the signals are sent back to the atria. The result is a very fast heartbeat. People with WPW may also be more likely to have PSVT episodes.

- **AV nodal re-entrant tachycardia (AVNRT)**: a rapid rhythm caused by multiple pathways passing through the AV node.
- **Atrial tachycardia (AT)**: a rapid heart rhythm coming from the atria.
- **Atrial fibrillation (AF)**: consisting in the chaotic generation of electrical impulses in the atria which propagate through the AV node in a irregular and rapid manner. Further details are provided in the following sections.
- **Atrial flutter (AFL)**: similarly to AF, AFL is induced by one or more rapid circuits in the atria, but it is generally characterized by the presence of a more organized electrical circuit. The activation usually originates within the RA and produces characteristic saw-toothed waves on the ECG.

3.3 Atrial fibrillation

3.3.1 Definition and pathophysiology

It is estimated that 2.2 million adults in the United States have intermittent or chronic AF, making it the most common sustained arrhythmia [133]. It increases in prevalence with age, and affects up to 5% of the population older than 69 years, and 8% of the population older than 80 years. AF is associated with a 5-fold increase in risk of stroke [132].

AF is a supraventricular tachyarrhythmia inducing a disorganized generation of electrical signals in the atria and consequent deterioration of mechanical function [53]. More precisely, the atria beat in a chaotic and irregular manner, out of coordination with the ventricles (see Fig. 3.1). Consequently, the atria risk to empty blood into the ventricles during their contraction in an incomplete manner, thus increasing the probability of pooling or clotting. These clots can break off and travel downstream, and if they lodge in an artery in the brain, this can cause a stroke. In general, AF is associated with increased rates of death, stroke and other thrombo-embolic events, heart failure and hospitalizations, degraded quality of life, reduced exercise capacity, and LV dysfunction [53].

AF is thought to be caused by atrial fibrosis, and lost of atrial muscle mass, due to several factors, such as aging, chamber dilatation, inflammatory processes, and genetic causes. Dilatation of the atria can derive from any structural abnormalities of the heart that cause a rise in the intra-cardiac pressures. This includes valvular heart disease (such as mitral stenosis, mitral and tricuspid regurgitation), hypertension, and congestive heart failure. Atria dilatation activates several molecular pathways, which induce atrial remodeling and fibrosis, with loss of atrial muscle mass, and may also involve the SA node and the AV node, with changes in electrical refractoriness [53].

3.3.2 ECG aspects of AF

Standard ECG is more and more exploited for AF understanding and treatment, for its noninvasivity, cost-effective acquisition and all the other advantages presented in

[3] http://www.saintvincenthealth.com/services/heart/heart-resource-library/atrial-fibrillation/default.aspx

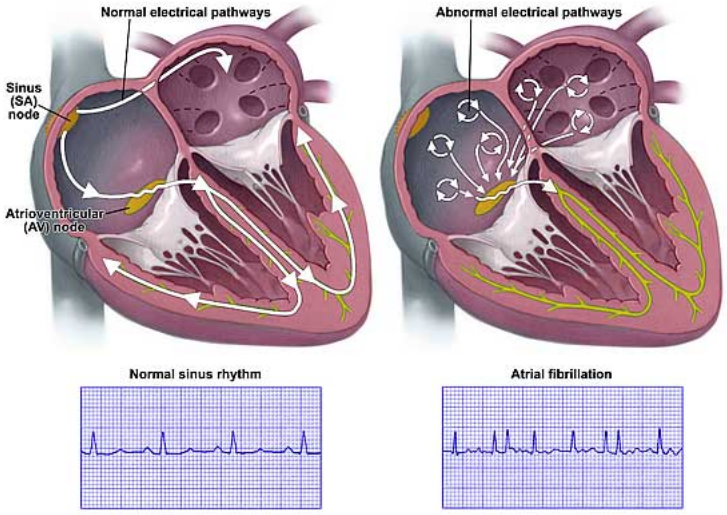


Figure 3.1: Heart electrical wavefront propagation during SR (left) and AF (right) and their effects on ECG pattern [3].

Chapter 2. Indeed, AF impact on heart electrical activity can be even visually detected on ECG recording, as shown in Fig. 3.1. During AF, no regular P waves are identifiable, but thy are replaced by multiple, irregular f-waves firing at rate of 150-300 bpm on the undulating baseline, rendering alterations in the atrial depolarization. Ventricular response variability is also affected by higher dispersion compared with SR, and it is reflected in RR interval distribution on ECG, though the QRS contour is usually normal [96].

3.3.3 Mechanisms of AF triggering and maintenance

Despite advances in the understanding of this disease, very little is known about the mechanisms responsible for AF triggering and maintenance. To this end, several theories about AF initiation and perpetuation have been put forward as to help its monitoring and guide treatment strategies. Indeed, AF triggers may be focal targets for ablative therapy.

AF induction is now thought to involve an interaction between initiating triggers and an abnormal atrial tissue substrate capable of maintaining the arrhythmia. Such triggers are often in the form of rapidly firing ectopic foci located in muscular sleeves extending from the LA into the proximal parts of PVs and overriding the normal impulses generated by the SA node. Although structural heart disease underlies many cases of AF, the pathogenesis of AF in apparently normal hearts is less well understood [97]. According to [54], two major theories have been put forward to explain AF genesis and maintenance (see Fig. 3.2), namely:

1) single or multiple rapidly firing atrial ectopic foci;

2) circuit re-entry and multiple wavelets.

Ectopic foci hypothesis

The ectopic foci hypothesis deals with a single or small number of reentrant source(s) giving rise to fibrillatory conduction. Ectopic foci arise when electrical impulses rapidly

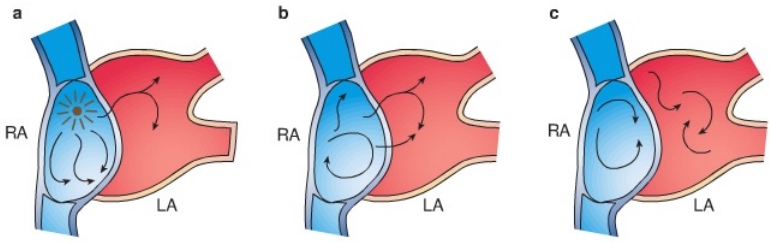


Figure 3.2: Models of AF mechanisms.
Models of AF mechanisms. a. Ectopic foci. b. Single reentry circuit. c. Multiple reentry circuits [119].

discharge in areas outside the SA node, widely known to be the heart natural "pacemaker", as explained in Sec. 2.3. This can come from a steepening of the diastolic phase of the action potential in cells that normally show automaticity, causing them to reach their threshold potential earlier and generate ectopic firing [119]. Alternatively, ectopic foci can sometimes arise just after the main action potential, due to alterations in ionic exchange current flows, which can activate cells again, and induce ectopic firing. More recently, however, in [62, 69] it has been shown that some ectopic foci sources triggering and sustaining AF can be identified around the PVs. This discover opened new therapeutic possibilities aiming at interfering with the ability of the re-entering circuits to perpetuate themselves, for instance the maze operation developed in [38]. Because of shorter refractory periods and the abrupt changes in fiber orientation, PVs are widely known to be potentially responsible for AF uncoordinated activity. Targeted destruction of ectopic foci is usually accomplished by surgery or catheter-based techniques.

Circuit re-entry and multiple wavelet theory

Re-entries occur when a signal loops back and activates cells that has already triggered. Under these circumstances, different areas can continuously reactivate each other, thus giving rise to one or more circuits. One of the first model is referred to as "leading-circle model" in [8] and encompasses re-entry propagation around an anatomical obstacle, such as a vein orifice. One of the basic ideas of this theory is the concept of "wavelength of re-entry". This wavelength represents the distance covered by the electrical impulse in one refractory period, and it is equal to the product of the refractory period and the conduction velocity. According to this theory, if the pathway of the potential circuit is shorter than this characteristic wavelength, the impulse will traverse the circuit and return to its starting point in a time shorter than the refractory period, thus it will encounter refractory cells and will be extinguished. Therefore, the wavelength is the shortest electrical pathway able to sustain re-entry. The other impulses will have longer revolution times, and will therefore be dominated by the faster activity of the "leading circle". As a result, this model assumes that the number of circuits that can be maintained depends on atrial size and the refractory wavelength. The lower the conduction wavelength, the lower the minimum circuit size, the higher the number of circuits that can be accommodated for perpetuating AF. The number of wavelets depends on the refractory period, conduction velocity, and mass of atrial tissue. Increased atrial mass, shortened atrial refractory period, and delayed intra-atrial conduction increase the number

of wavelets and promote sustained AF [53, 97]. Re-entry within the atrial myocardium is facilitated by conduction slowing and shortening of the refractory period, with increased dispersion of refractoriness further contributing to arrhythmogenesis. The role of other functional regions, for instance, the LA posterior free wall, superior and inferior vena cava, coronary sinus (CS), and interatrial septum, has also been taken into account in AF pathogenesis. Even though the distinction described is not strict, it is hypothesized that PV sources may play a dominant role in younger patients with short paroxysms of AF, whereas an abnormal atrial tissue substrate may play a more important role in patients with structural heart disease and persistent or permanent AF. The so-called "multiple wavelet hypothesis", assessed for the first time in [110], can also be ascribed to this group of theory concerning AF maintenance and generation. This recent model rather involves multiple randomly propagating wavelets instead of closed loop re-entry. This process is thought to maintain AF regardless of its triggering source, as perpetuated by continuous conduction of several independent wavelets of excitation [30], varying in size and velocity, irregularly wandering through atria, which collide, mutually annihilate, coalesce, or give rise to new wavelets in a self-sustaining turbulent process [159].
Before concluding this section, it is worth noting some more recent hypotheses, which represent a basis for some of the most employed AF therapeutic strategies, in particular in relation with ablation. The study led in [116] points to the role of complex fractionated atrial electrograms (CFAE) as the substrate responsible for AF maintenance. In [147] the potential application of CFAE analysis to AF ablation is investigated. In [118] it is stated that AF may be sustained by localized electrical rotors and focal impulses. Wavelets and multiple re-entry circuits can be suppressed by drugs that prolong the refractory period and inhibit re-entry, and by ablating areas of the re-entrant pathway.

3.3.4 Atrial electrical remodeling

AF can produce changes in atrial function and structure, which explain the gradual worsening with time of this arrhythmia [7]. Atrial remodeling consists in any persistent change in atrial structure or function, increasing the tendency to triggering or sustaining AF [120], either through rapid ectopic firing or reentry mechanisms. It has been shown that long-term rapid atrial pacing or maintenance of AF led to a progressive increase in the susceptibility to AF: "AF begets AF" [119]). This phenomenon was explained by a shortening in atrial impulse wavelength. When the wavelength is short, small areas of intra-atria conduction block may already serve as a site for initiation of reentry, thus increasing the vulnerability to AF. This condition is also expected to increase the tendency to AF maintenance, since it allows more reentering wavelets to coexist in the available atrial surface. Clinical evidence shows that patients with more prolonged AF may develop increasing problems with time and are less likely to experience SR restoration and maintenance [7]. Several mechanisms and effects are implied in the atrial remodeling. First, ionic exchanges are profoundly altered by this phenomenon, in particular a gradual inactivation of the calcium current subsequent to intracellular overload [120]. In turn, this action reduces the action potential duration and atrial refractory period, responsible for sustaining AF. Such phenomena cause atrial contractility loss, since calcium current abnormalities induce atrial dilation, which further promotes reentry, and facilitates atrial fibrosis occurrence. Assessment of remodeling effects has a fundamental clinical value for AF treatment and its successful outcome [7]. Hence, the importance of a deep under-

standing of AF mechanisms.

3.3.5 AF classification

Several criteria are adopted for AF study and management. Clinical guidelines illustrated in [28] ascribes AF cases to 5 categories according to the presentation and duration of the arrhythmia:

- **First-diagnosed AF**: it concerns every subject presenting an AF episode for the first time, regardless of its duration or the presence and severity of other symptoms.
- **Paroxysmal**: it is a self-terminating AF form, usually within a 48 hour temporal window. Below this limit, spontaneous AF termination is more likely. In this type of AF, triggered activity seems to be the dominant factor, therefore suppressing the firing source should terminate the arrhythmia.
- **Persistent**: it is either characterized by recurrent AF episodes or longer than 7 days, and must be treated by cardioversion, either pharmacological or electrical. Such advanced forms of AF exhibit a certain degree of electrical remodeling, proportional to arrhythmia progress.
- **Long-standing persistent**: AF episodes last longer than 1 year, and a rhythm control strategy is required.
- **Permanent**: patients are affected by ongoing long-term episodes, with failed or no attempt at cardioversion.

An alternative criterion leading AF classification takes into account the degree of its organization, traditionally assessed on invasive cardiac signal recording, dependent on the number of fibrillating wavelets and the chronification of the disease. This concept will be explained in detail in Sec. 5.2. In the literature, we can find two reference systems for AF classification from invasive recordings. The Wells' system put forward in [161] takes into account the morphology of single bipolar atrial electrograms. Four distinct AF types are encompassed by this criterion:

- **Type I, AF1**: characterized by discrete beat-to-beat atrial electrogram complexes of variable morphology and cycle-length, alternating to isoelectric baseline segments free from perturbation.
- **Type II, AF2**: beat-to-beat complexes are similar to those typical of Type I. By contrast, the baseline is not isoelectric and it is affected by multiple perturbations.
- **Type III, AF3**: AF pattern presents a higher degree of disorganization, with no clear isoelectric intervals.
- **Type IV, AF4**: resulting from the alternation between the Type II and Type III patterns.

For the sake of clarity, some representative pattern examples are displayed in Fig. 3.3 for the first three types.

The second paradigm is the Konings' system [78], aiming at classifying patterns of human RA activation during electrically induced AF. According to the number of wavelets activating the atrial wall and mapped by high-density epicardial recordings, we can encounter three different types of AF.

- **Type I**: single broad wave fronts propagate uniformly across the RA.
- **Type II**: presenting 1-2 nonuniformly conducting wavelets
- **Type III**: RA activation is highly fragmented and exhibits 3 or more wavelets with variable direction of propagation.

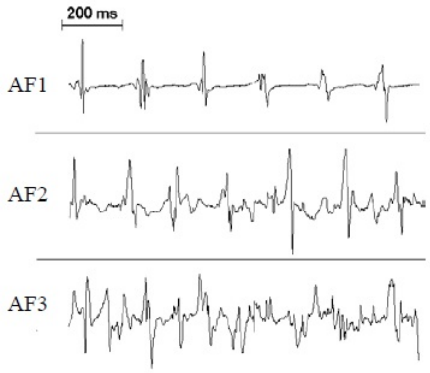


Figure 3.3: Classification of bipolar atrial recordings during AF according to Wells' criterion: Type I (AF1), Type II (AF2) and Type III (AF3) [10].

In general, Wells' classification is more frequently adopted, since it can be acquired more easily during clinical electrophysiological studies.

3.4 Overview of the main AF therapies

AF management strategies aim at relief of symptoms and prevention of severe complications associated with AF at the same time [28]. For this purpose, antithrombotic therapy, control of ventricular rate, and treatment of concomitant cardiac pathologies are generally performed.

In patients with short paroxysms of AF, curative strategies should generally concentrate on providing control of the arrhythmia itself. By contrast, in patients with persistent AF, it is not trivial to decide whether to try to restore and then maintain SR (rhythm control), or to accept the arrhythmia and control the ventricular rate (rate control) [97]. In rate control strategies, the arrhythmia is allowed to continue. Even though the control of ventricular rate allows for improving symptoms, the risk of thromboembolism persists and ventricles are passively filled, without any active atrial contraction, since atria are still in fibrillation. On the other hand, rhythm control aims at SR restoration and AF suppression, but the pharmacological treatment adopted is prone to provoke serious thromboembolic complications. Therefore, regardless of the arrhythmia pattern, and in the absence of contraindications, such a therapy should be combined with anticoagulation. The choice of one of these approaches strongly depends on several factors, such as AF history and severity of additional disturbances.

3.4.1 Cardioversion of persistent AF

In the rhythm control therapies' scenario, cardioversion procedure refers to the process of SR restoration in the presence of an abnormal rhythm. Indeed, the objective of this kind of therapies is "resetting" AF irregular fibrillatory rate and restore the physiological SR, either by pharmacological or electrical means. Cardioversion is used most frequently for those who are symptomatic or newly diagnosed. Broadly speaking, cardioversion is generally applied to two patients' categories: those who are affected by AF symptoms and those who present with AF for the first time [138]. Symptoms can be quite different in

terms of severity, such as hypotension, uncontrolled ischemia, or angina, or palpitations, fatigue. However, any AF symptoms caused by atrial fibrillation warrant consideration of cardioversion as a management option. Also patients exhibiting AF for the first time are generally treated by cardioversion, so as to slow disease progression. Another group of patients who may benefit from cardioversion are those who have postoperative AF. Indeed, it can occur in the first days after surgery, when anticoagulation may be undesirable. Many episodes of postoperative AF resolve spontaneously. Patients who do not experience spontaneous AF termination may undergo cardioversion before an AF duration of 48 hours in order to avoid coagulation. It is important to remember that all types of cardioversion can present some side-effects related to embolic risks. Thromboembolism (blood clot traveling through the bloodstream) can occur after cardioversion if a thrombus (blood clot) becomes dislodged from the atria as the heart begins to beat normally. Blood clots can form within the atria during AF since blood flow is slowed. Accordingly, patients are usually given an anticoagulant and their monitoring during and after the procedure is strongly recommended.

3.4.2 Pharmacological treatment

Several pharmacological agents may be used for acute cardioversion in AF patients with AF, including oral and intravenous medications [42]. Pharmacological cardioversion is generally employed in subjects affected by short AF episodes with little or no structural heart disease. Indeed, it can be suitable for the treatment of AF of recent onset, but efficacy is dramatically reduced in patients with AF persisting for more than 48 hours [97]. It also serves as a complementary therapy in combination with electrical cardioversion either after the procedure (to stabilize SR restoration effects) or prior to its performance (in order to increase its success probability). Several drug categories are generally administered to AF patients, including oral and intravenous medications.

SR conversion rate of chemical cardioversion is generally lower than with electrical cardioversion, but it does not require conscious sedation or anasthesia, and may facilitate the selection of proper antiarrhythmic drug therapies to prevent AF recurrence [53].

3.4.3 Electrical cardioversion

Because of the relative simplicity and high efficacy, electrical cardioversion (CEE) is more frequently performed than its chemical counterpart [42]. This therapy consists in applying a synchronized, low-voltage electric current to convert AF rhythm back to normal SR [138]. The electric current enters the body through metal paddles or patches applied to the skin of the chest, either in anteroposterior or anterolateral configuration, as in Fig. 3.4. A cable connects the pads to an external defibrillator, which allows for monitoring patient's heart rhythm and applying the necessary energy to restore SR. CEE is usually accompanied by sedation or total anesthesia, as the shock may be uncomfortable. The delivered shock causes all the heart cells to contract simultaneously, thereby interrupting and terminating the abnormal electrical rhythm. If initial shocks do not succeed in restoring SR, cardioversion is repeated after changing paddle position, and/or delivering higher energy. Then, according to the protocol adopted, procedure can be repeated until AF termination or is interrupted. It is important to avoid rupture of blood clots which may become dislodged from the heart and cause a stroke. Therefore, during

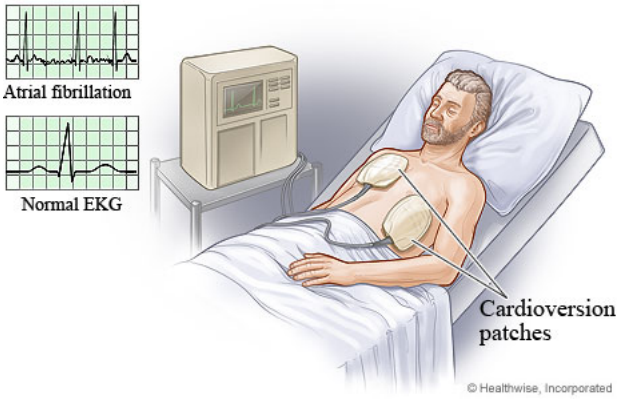


Figure 3.4: CEE procedure for conversion of AF to normal SR [148].

the procedure, anticoagulants are usually given to the patient prior to its performance. It is generally preferred to chemical cardioversion not only for the higher success rate, but also for the shorter duration of the procedure and the reduced risk of causing other arrhythmia. Success probability is inversely related to the AF duration and LA size [89]. Furthermore, since adequate current delivery determines its successful accomplishment, it is essential to ensure an effective contact of paddles to patient's body, so as to reduce electrical impedance and facilitate energy delivering.

3.4.4 Some considerations about cardioversion limitations

Even though more than 90% of cardioversion interventions prove to be effective, they can be affected by several drawbacks occurring in the postoperative phase. Success probability increases if electrical and pharmacological cardioversion are combined, which prevents reverting back to AF. Indeed, cardioversion can sometimes be responsible for other arrhythmias or problems of impulse conduction.

As stated above, since quivering atria do not contract vigorously in AF patients, blood clots can form and can be dislodged from the heart when applying CEE, thus increasing the risk of a heart attack or a stroke [138]. Fortunately, most blood clots can be prevented by previous anticoagulation therapy, thus thinning the blood before cardioversion. Furthermore, concerning CEE, some precautions must be adopted when setting energy of electrical shocks and the number of their attempts so as to avoid tissue damage.

In general, cardioversion effectiveness depends on several factors, such as patient's AF history, episode duration, presence and severity of additional symptoms. If disease chronification is quite advanced, both types of cardioversion can fail restoring SR. As a consequence, persistent and chronic forms of AF are more likely to be successfully cured by other kinds of strategies, in particular ablative therapies.

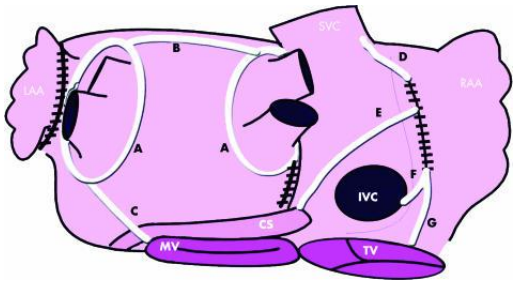


Figure 3.5: An example of a Maze lesion in the atria from a posterior perspective. The 4 PVs are visible on the LA. The black hatched lines are incisions and the white lines ablation lesions [45].

3.5 Ablation therapy for AF treatment

3.5.1 Introduction

In AF treatment framework, ablation is an invasive technique aiming at destroying the sources of abnormal rhythm and modifying atrial conduction properties so that AF cannot be maintained even when triggered. First ablation attempts were made by James Cox in 1987, who introduced a surgical intervention (the Maze procedure) aiming at preventing AF propagation by means of strategic incisions in the atria [39]. Hereinafter, procedure noninvasivity became one of the main clinical goals, thus incisions were not performed anymore during an open-heart surgery, but catheters delivering energy were introduces so as to burn fibrillatory targets. The key to the success of any catheter or surgical ablation of AF is the correct choice of lesions and the production of adequate transmural lesions, which can even yield more effective results than those obtained with electrical and/or pharmacological cardioversion. A 5-year study has demonstrated that after a single procedure more than half of patients experience SR restoration [125].

3.5.2 Maze ablation

Maze ablation is a procedure accomplished during an open-heart surgery in which several incisions are performed in several atria critical locations by means of a scalpel, such that a maze is created and AF wavefronts cannot propagate [26]. This surgical strategy assumed that reentry mechanisms illustrated in Sec. 3.3.3 are the main cause of AF triggering and maintenance. The atrial incisions, shown in Fig. 3.5, act as anatomic barriers which prevent atrial reentry and allow sinus impulses to activate the entire atrial myocardium, thereby preserving atrial transport function postoperatively [39]. Irrigated radiofrequency ablation can be sent through a bipolar clamp or endocardially using a monopolar pen. Since its introduction, the procedure has gone through three iterations (Maze I, II, and III) based on cut-and-sew techniques that ensure transmural lesions to isolate the PVs, connect these dividing lines to the mitral valve annulus, and create electrical barriers in the RA that prevent macroentrant rhythms.

In order to reduce intervention invasivity, as well as its duration, a tendency to decrease the number of lesions has been pursued, by keeping the same mechanistic goals aforementioned. In some studies it was remarked that LA is usually the source of AF wavefronts, whereas RA acts as a bystander. Accordingly, Cox introduced the so-called

Minimaze procedure. Indeed, he discovered that in most subjects AF conduction can be prevented by a lesion set isolating all PVs, a line between the isolated PV line to the mitral valve annulus (which ideally encircles the CS at that point) and a right atrial line across the TV-IVC.

Secondly, new energy sources for ablation have been developed so as to replace cut-and-sew techniques. Cryoablation and radiofrequency ablation are the most common methods, which use hand-held probes applied endocardially by direct vision. Alternatively, clamp devices hold the atrial wall between 2 jaws, and send radiofrequency energy to produce a complete lesion. Newer energy sources (e.g., laser, microwave, and ultrasound) have the advantage of generating transmural lesions even when applied epicardially. A further development of this technique is the use of a limited thoracic incision and thorascopically guided procedure.

Despite the quite high long-term success rate, Maze ablation is not considered as a first-line strategy in AF treatment, since it requires a cardiopulmonary bypass in a open-heart surgery. Several severe side-effects can occur in the postoperative phase, including stroke, pneumonia, myocardial infarction or other arrhythmias. Accordingly, it is usually performed subsequently to other therapies' failure (both cardioversion and/or catheter-ablation treatment) or during other urgent heart surgery, for instance, coronary artery bypass surgery or heart valve repair. Some people could need a pacemaker implanted after the procedure.

3.5.3 Radiofrequency catheter ablation

In this paragraph, most of the description of CA procedure refers to [92]. Radiofrequency CA is a nonsurgical procedure for treating AF aiming at the electrical isolation of abnormal AF sources so as to avoid irregular rhythm conduction throughout heart tissue [44]. Nowadays, CA is regarded as a first-line therapy, as it can directly eliminate the abnormal sources responsible for AF and offers the possibility of a lasting cure [157]. Early radiofrequency CA techniques take a step from the Maze procedure by performing linear lesions in the atrial endocardium. In this procedure thin, flexible catheters are inserted into the femoral vein in the groin and threaded up through the vena cava (VC) and into the heart. An electrode at the tip of the wires delivers radiofrequency energy to the fibrillating heart tissue. Once the catheter is positioned, some small electrodes are inserted in different areas of the heart. They allow for the detection of heart areas altering physiological electrical activity. Once the source of the problem has been found, one of the catheter lines is used to send electrical energy to the selected area. Subsequently, a small scar is created, thus electrically "disconnecting" fibrillating sources from healthy heart regions and stopping abnormal rhythm conduction. Catheter positioning, as well as the anatomy of the PVs and LA, are confirmed by fluoroscopy, pulmonary venography, 3-dimensional electroanatomical mapping, intracardiac echocardiography, computed tomography, remote guidance using magnetic resonance imaging, or combinations of these techniques. An injury is likely to be induced to the myocardium by the application of thermal energy - most commonly by radiofrequency or cryothermy.

Some initial successful attempts to stop AF have been obtained by creating linear incisions in the atria, as in the surgical Cox-Maze procedure, and replicating these lesions with radiofrequency CA. Electrical isolation of PVs from the rest of the atrium, performed around the origin of the veins, is the cornerstone of most CA procedures [69], based on

the ectopic foci hypothesis explained in Sec. 3.3.3. Furthermore, vagal inputs may also influence mechanisms of AF triggering and maintenance, and many of them are located close to the PV-LA junction [27]. The study in [116] introduces the concept of CFAEs, which are signals with rapid deflections and short cycle lengths corresponding to areas of wavebreak, vagal innervation, slow conduction, or re-entry. They were originally defined as either atrial electrograms that have fractionated electrograms composed of two or more deflections, and/or perturbation of the baseline with continuous deflection of a prolonged activation complex, or atrial electrograms with a very short cycle length ($<$ 120 ms). In [99] CFAEs in RA and LA have been regarded as an ablation target, hence the interest in their role in AF management. According to [117], ablation of such sources could restore SR definitively with no risk of AF recurrence. By ablating these areas the propagating random wavefronts are progressively restricted until the atria can no longer support AF. In [115] freedom from AF following a single has been reported in 70% of permanent AF patients.

By contrast, more recent studies claim that other sites can trigger the arrhythmia, such as LA posterior wall, SVC, CS. Moreover, further modifications of the procedures have incorporated linear LA ablation, or mitral isthmus ablation, or both for certain patients. Accordingly, initial approaches aiming at eliminating isolated foci in the PVs has progressively evolved to circumferential electrical isolation of the entire PVs' tissue.

CA seems to be more effective in restoring SR than conventional anti-arrhythmic drugs, by reporting a success rate of 85% of cases at 1 year and 52% at 5 years [50]. Unlike other therapies, if the patient proves to be a positive responder to CA therapy, procedural SR restoration is durable and the subject can be considered completely free from the arrhythmia.

3.5.4 Objectives and protocols

Due to uncertainty about its outcome, criteria defining the main CA steps as well as its endpoint are not strictly systematic, thus leading to different medical protocols. The ideal approach depends on individual patient characteristics and AF chronicity, and may require a combination of strategies.

The limited available studies suggest that catheter-based ablation offers benefit to selected patients with AF, but these studies do not provide convincing evidence of absolute rates of therapy effectiveness. Heterogeneity in the methods of published trials limits the ability to compare different techniques. Outcomes may have been influenced by the different patient populations studied, ablative techniques and end points utilized, and number of repeat ablations. Other confounding factors are prevalence of structural heart disease, the length of follow up, the use of antiarrhythmic drugs, SR restoration modalities [45]. More specifically, one of the main issues in CA characterization is the definition of procedural success itself, varying among groups practicing this therapy.

All therapeutic strategies generally aim at either SR restoration or AF conversion to an intermediate arrhythmia, such as AFL. While conversion to SR during ablation of persistent AF has been often associated with excellent outcomes, it is not clear whether this endpoint is a sufficient condition for long-term freedom from AF recurrence [46, 85], since acute AF termination does not necessarily imply durable therapeutic success. Using similar stepwise ablation protocols, results have varied for termination of persistent AF during ablation from 48% to 85% despite similar long-term outcomes. This implies

either that AF termination is not necessary for good long-term outcomes or that, if all drivers/sources were not terminated at the first session, they can be addressed during another session. In other words, the cumulative effect of multiple ablation procedures may be equivalent to AF termination during the first session. At a follow-up of 1-2 years, approximately 85% of patients undergoing one or more CA procedures were reported to be arrhythmia-free without antiarrhythmic medications.

Different contrasting theories about therapy combination have been put forward. In some centers ablation target is SR restoration immediately after the procedure as well as in the follow-up. Other groups do not necessarily aim at arrhythmia termination within the procedure, but they also exploit complementary therapies (i.e., cardioversion) to achieve long-term AF freedom and stabilize CA effects. The study carried out in [61] shows that most patients undergoing CEE after CA experience AF recurrences. Conversely, in [46] it is stated that acute AF termination by CA has no influence over the long-term outcome, thus justifying the use of complementary curative strategies. The main procedural endpoints may depend on the type of AF and include completion of a predetermined lesion set, depending on technical choices. Some groups aim at AF termination during ablation [63], while other rather address noninducibility of AF after CA [70]. In any case, there is still debate surrounding the predictive value of such endpoints, and various approaches are currently adopted in medical practice.

In addition, follow-up length is highly variable as well, as AF can be observed in several moments of the postoperative phase, especially when treating a persistent form. At follow-up visits, a 12-lead ECG should be recorded to document the rhythm and rate, and to investigate disease progression. The assessment of clinical intermediate and long-term outcome after CA is still a subject of discussion. Symptom-based follow-up may be sufficient, as symptom relief is the main aim of AF ablation [28]. The most recent HRS Expert Consensus Statement guidelines for CA trials in [27] recommend that, immediately after CA performance, there be a 3-month "blanking period" during which any fibrillatory episodes are seen as a physiological reaction during recovery from CA, and not as AF recurrence episodes. After this blanking period, if the patient remains free of arrhythmia recurrences, CA can be considered effectively accomplished. Expert consensus recommends an initial follow-up visit at 3 months, with 6 monthly intervals thereafter for at least 2 years.

3.5.5 Introduction to the clinical protocols and the ECG databases employed in the study experimental setup

As evinced in previous sections, multiple paradigms can be used for assessing CA procedural success. According to the procedural success criterion examined, ECG parameters proposed in this doctoral thesis have been examined and validated on different ECG databases. In each chapter, we examine one-minute 12-lead surface ECG signals recorded at a sampling rate of 1 kHz. Standard ECG is acquired in each patient undergoing CA at the beginning of the procedure. We generally refer to such signals when dealing with prediction tasks. In other experimental parts, for instance, in Sec. 4.6, we will examine the same kind of recordings acquired in other moments of the procedure, in particular close to the end of ablation.

One on the main difficulties encountered throughout our work has been the management of a database whose size has changed in time, as patients involved in our study did

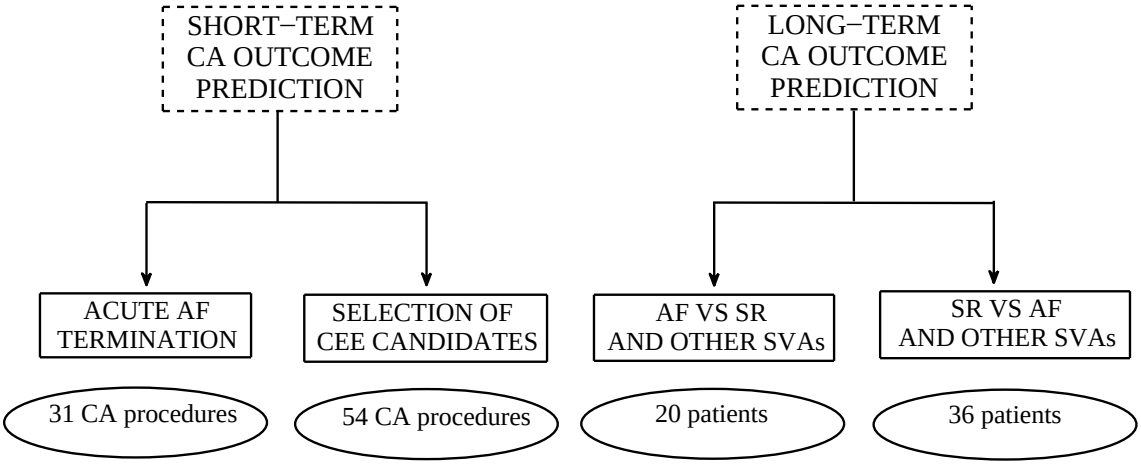


Figure 3.6: Schematic diagram of the ECG databases employed for the experimental validation of our methods. Each dataset refers to a different clinical criterion for CA outcome assessment and its size is also reported. Meaning of acronyms: AF: atrial fibrillation; CA: catheter ablation; CEE: electrical cardioversion; SR: sinus rhythm; SVA: supraventricular arrhythmia.

not undergo CA all at the same time. As a consequence, clinical conditions of some subjects have been evaluated later in time. This explains the employment of different datasets throughout the dissertation; they are graphically represented in the diagram in Fig. 3.6. The subjects involved in our study undergo stepwise CA [25], starting with circumferential PV ablation with LASSO-guided disconnection, followed by fragmented potentials, non-PV triggers, roof line and mitral isthmus line right atrial ablation. Some patients received a pharmacological treatment subsequent to CA procedure, mainly amiodarone (for some patients, solatol and flecaine). Some of them underwent a second ablation. In this case, only ECG signals related to the first procedure are taken into account in our study.

We globally deal with two main criteria for CA outcome prediction, which differ for the length of the follow-up length, when postoperative AF screening is carried out. Indeed, looking at the short-term outcome means evaluating CA procedure effectiveness, whereas in longer follow-ups clinicians more generally focus on patient's conditions and take AF history into account. As a result, the **short-term** ECG dataset is related to a certain number of **CA procedures**, whereas the **long-term** database concern a group of distinct AF **patients**. If we look at the diagram in Fig. 3.6 from left to right, we can summarize such datasets according to the clinical task of interest as follows:

1) **Acute AF termination** by CA: The dataset includes 28 patients, whose procedural outcome is considered in a very short-term temporal window within the blanking period. During this period, no clinical evaluation about definitive freedom from AF can be put forward, since any kind of fibrillatory activity within this temporal window is generally part of the postoperative reaction, in combination with other phenomena, such as edemas and inflammations. As a consequence, examining ablation outcome in this time interval exclusively provides a preliminary perspective of immediate CA effectiveness right after the procedure. Acute AF procedural termination was

defined as the conversion either directly to SR or intermediate SVAs, either directly by ablation or by CA followed by CEE. Three patients who did not experience AF termination after a first procedure underwent a second ablation, making a total of $n_P = 31$ procedures. Accordingly, $n_S = 26$ procedures are considered successful, whereas $n_F = 5$ procedures failed.

2) **Selection of CEE candidates**: In line the CA procedural protocol adopted in this study, cardiologists perform a certain number of steps during the procedure aiming at AF termination. However, if they are not able to effectively stop fibrillatory activity at the end of the intervention, they usually perform CEE so as to restore SR and stabilize ablation effects. In the light of these considerations, cardioversion performance in the short-term postoperative phase can be regarded as a criterion of ablation procedural failure, hence the importance of properly choose positive responders to CEE. Accordingly, 54 ECG recordings have been included in our analysis (3 subjects out of 51 experienced a double procedure). In 37 procedures, AF was not terminated by CA only, and CEE was applied immediately after ablation. In the remaining cases, AF was terminated either by CA exclusively or accompanied by pharmacological treatment in the follow-up.

3) **AF vs SR and other SVAs**: We move now to a longer follow-up interval, beginning after the aforementioned blanking period, whose duration must be at least about 6 months. As we said before, this retrospective analysis of patient's clinical conditions must take into account a multiplicity of factors which can influence the final procedural outcome, with particular attention to complementary CEE therapies or additional ablations. If multiple procedures are performed, signals acquired during the first intervention are examined. The main endpoint is AF termination in the long-term follow-up; the arrhythmia can be converted either directly to SR or to intermediate arrhythmias. In this framework, supraventricular arrhythmias (SVAs) are considered as an evolution of AF uncoordinated electrical activity to more organized and regular waveforms, which are likely to be more easily treated by other therapies. Twenty patients (19 males, 60 ± 11 years) with a median persistent AF episode duration of 4.5 months (2 to 84) form this ECG dataset. After a median follow-up of 9.5 months, CA was successfully accomplished in $n_S = 13$ out of $n_P = 20$ patients (65%), whereas $n_F = 7$ procedures were not effective.

4) **SR vs AF and other SVAs**: The ECG recordings forming this set have been acquired in 36 patients. More precisely, $n_S = 29$ subjects experienced AF termination by CA and durable SR restoration in the long-term follow-up (8 ± 4 months), whereas the remaining ones ($n_F = 7$) did not. In case of repeat ablations, ECG recordings related to the first CA procedure are included into the analysis. Unlike the previous therapy success definition, despite the same temporal follow-up window, a stricter criterion for assessing AF termination is imposed. Indeed, long-term CA success is defined as freedom from ECG/Holter-documented sustained AF recurrence (> 30 s) at follow-up after at least 6 months subsequent to the blanking period. Therefore, at a certain moment of the long-term follow-up clinicians verify whether durable SR restoration has been achieved. Accordingly, any SVA form is regarded as a procedural failure. As opposed to previous studies [17, 121], termination of AF during CA was generally not achieved in all patients. Nevertheless, this is not detrimental to

our study, since AF termination by CA is not predictive of long-term outcome [46], which is the event with clinical interest.

Assessment of CA procedural outcome has been carried out according to criteria 1 and 4 throughout the Contributions' parts (Chapters 4-6). ECG features' ability to generalize prediction results at each follow-up is attempted, and significant results are commented and explained. Despite the clinical interest of criterion 3, the gold standard [25] seems to privilege definitive freedom from every kind of arrhythmia as a clinical endpoint (as in Criterion 4), so as to guarantee durable SR and healthier conditions to the patient and make him free from AF therapy. Concerning the selection of CEE candidates according to criterion 2, its performance has not only a therapeutic value, but it also represents an important technical contribution of this thesis, since in Chapter 6 we will merge some of the ECG features of interest and test such combined measures for this therapeutic task. However, as we deal with persistent form of AF, CEE is not generally able to restore SR permanently, and usually plays the role as a complementary therapy.

3.5.6 Risks and limitations

It is important to remember that treating AF by ablation implies some potential risks. The main clinical goals are abolishing or reducing symptoms, improving LV function by restoring both electrical and mechanical atrial systole, and finally reducing the risk of stroke [45].

CA risks in persistent AF are somewhat higher than with ablation for other cardiac arrhythmias [50]. This is due to several factors, such as the longer duration of the procedure, the greater extent of the scars, as well as their location (e.g., near the PVs). Post-procedural stroke can occur in up to 2% of the treated patients. PV damage (which can produce lung problems leading to severe shortness of breath, cough, and recurrent pneumonia) occurs in up to 3%. Damage to other blood vessels (in particular, those through which the catheters are inserted) affect $1-2\%$ of ablated patients. Also bleeding from the cauterized sites must be taken into account. In general, both the success of the procedure and the risk of complications improve when the ablation is conducted by an electrophysiologist with extensive experience in ablating AF.

Recently, new and very advanced 3-D mapping systems have been developed for use in ablation procedures, and allow cardiologists to create ablation scars with a high level of precision. In spite of these advances, CA is still a lengthy (4 or more hours) and difficult procedure, and its success rate is quite uncertain. Even with modern mapping systems, ablation procedures work best in patients who have relatively brief AF episodes, which is the case of paroxysmal AF. Success rate is lower in patients affected by chronic or persistent AF forms, or by critical underlying cardiac disease, such as heart failure, or heart valve disease. Initial reports described success rates between 22% and 85%, with better results observed for patients with paroxysmal rather than persistent or permanent AF. Long term results are limited by follow-up of generally no more than 1 year in most trials [92]. The arrhythmia recurs in at least $15-20\%$ within 1 year, and in $25-50\%$ within 3 to 5 years. Furthermore, it is important to continue with anticoagulant therapy to prevent strokes, whose risk remains elevated even after CA.

As pointed out in Sec. 3.5.4, the lack of a unique technical protocol and differences in procedural endpoints makes it hard results' comparison. The existence of such a wide variety of techniques is due to the inability to generalize procedure results: the same

method can lead to different procedural outcomes in more patients. Since very little is known about AF generation, it is equally difficult to clearly assess CA mechanisms and quantify its effects on heart substrate. CA effectiveness still strongly relies on operator's experience, and evaluation of patient's conditions before and during CA. Since not all subjects seem to positively respond to ablation therapy, one of the main current tendencies is attempting to select patients who are more likely to experience AF termination by CA, thus allowing an improved patient-tailored management of AF. In such a manner, the success rate of the therapy would increase, and the number of failing CA procedures minimized. This strategy would help avoiding unnecessary procedures, and reducing hospitalization costs and duration, and potential complications to patients who would not actually benefit from this therapy.

3.6 PREDICTING CA OUTCOME FROM ECG ANALYSIS

Remarks made in Sec. 3.3.2 about the important role played by the ECG in AF management justify the attempt of identifying any potential ECG-based descriptors, whose value can discriminate between successful and failing CA procedures, thus helping selection of patients who can be effectively treated by cardioversion or CA and experience durable SR restoration.

Recent research led in [52] demonstrates that some clinical factors, such as right atrial dimension, AF duration and patient's weight, can predict AF recurrence after CEE. Some attempts have also been made in [2, 3], based on sample entropy measures determined on surface ECG, whose tuning parameter values have been attentively set. The study carried out in [154] reveals that tracking AA frequency and its harmonics on certain precordial ECG leads can help prediction of CEE procedural failure in persistent AF.

In [124] the predictive power of some clinical features is corroborated. More precisely, AF termination by CA is more easily achieved in patients with a shorter history of AF, a smaller LA dimension, and a longer baseline AF cycle length (AFCL), measured in the left atrial appendage (LAA). Similar findings are confirmed by [98]. The same study also confirmed that AFCL measured on surface ECG is not only correlated with the endocardial measure, but it is also predictive of CA success. In [165] the decrease in AF dominant frequency between the baseline and instant of procedural AF termination is proved to be predictive of SR maintenance after CA in the follow-up. Even though no links with procedural success are proved, the study in [19] demonstrates that the impact of CA on heart substrate can be assessed in terms on AF spatio-temporal complexity, regardless of the outcome reported. The concept of AF organization and its characterization in a multivariate framework represents one of the main contributions of this doctoral thesis, and it will be developed in detail in Sec. 5.2. In [121], the value of the peak-to-peak f-wave amplitude measured in leads II and V_1 seems to predict CA outcome: the higher its value, the more likely AF termination by CA. Furthermore, the amplitude measured in lead II and V_1 was correlated with younger age and shorter AF history, and in lead II only it was correlated with a smaller LA.

Despite this evidence, all these features are affected by several shortcomings. First, some parameters, such as f-wave amplitude and AFCL [98, 121], are manually acquired, therefore their measure is quite subjective and is operator-dependent, thus more prone to errors. This could significantly affect prediction performance, due to the low values

of the parameters cited (the order of mV for amplitude, ms for AFCL). Secondly, all these parameters are merely computed in one ECG lead, while neglecting other leads. Even though it is widely known that lead V_1 exhibits the highest atrial-to-ventricular activity ratio [129], lead selection is not driven by any systematic criteria, and clinicians generally choose leads in which it is easier to inspect wave properties. However, standard ECG is characterized by a high degree of spatial variability, i.e., AA signal features may vary considerably from a lead to another, thus affecting prediction performance derived thereof. Furthermore, due to its location, lead V_1 may represent RA activity predominantly, therefore lacking sufficient information to describe LA activity. Accordingly, a parameter value could sensitively vary from one electrode to another one. Finally, this kind of approach lacks robustness, since the measure obtained could not be reliable, e.g., if an ECG lead gets loose or disconnected.

Such background motivates our research, which intends to avoid the shortcomings linked to the intrinsic spatial variability of the atrial signal on surface recordings. To this end, we aim at determining multivariate measures which combine contributions from all leads and exploit ECG spatial diversity to predict CA outcome.

3.7 Summary and conclusions

This chapter has provided a global description of AF. In particular, we defined this arrhythmia and its main causes. Several theories about its generation and maintenance mechanisms have been proposed in the literature, and they have been summarized herein. The long-term effects and the electromechanical remodeling performed by AF have been discussed as well. Subsequently, the therapeutic scenario has been characterized. We first focused on cardioversion, both pharmacological and electrical, whose long-term effectiveness rate is quite low in persistent and permanent AF. Particular attention has been paid to CA, whose performance has yielded more promising results, but whose effect assessment is currently an open challenge, due to the disparate protocols and techniques, as well as the difficulty in giving a procedural success definition. With the intent to achieve a trade-off between invasivity and risks on the one hand, and therapeutic efficiency on the other hand, clinical centers are increasingly involved in exploring the predictive power of surface ECG. This would allow for an a priori selection of positive responders to CA, and the reduction in the number of failing procedures. Since most of the measures obtained on the standard ECG are either manually computed or determined in only one ECG lead, our research aims at determining novel parameters which are able to condense contributions from all ECG leads and discriminate between successful and failing CAs at each follow-up moment. The next chapter begins to summarize the main contributions of this thesis.

Part II

Contributions

4 F-wave amplitude as a predictor of CA outcome in a multi-lead framework

4.1 Introduction

It is widely known that AF effects on the cardiac cycle are reflected on ECG pattern. As explained in Sec. 3.3.2, one of the main alterations is represented by the absence of the physiological P wave, which is replaced by small, irregular, rapid deflections in the ECG waveform, varying in amplitude, shape, and timing. Such oscillations from ECG baseline are referred to as fibrillatory waves (f-waves) and they are displayed in Fig. 4.1. This visual evidence serves as a powerful clinical tool for straightforward AF

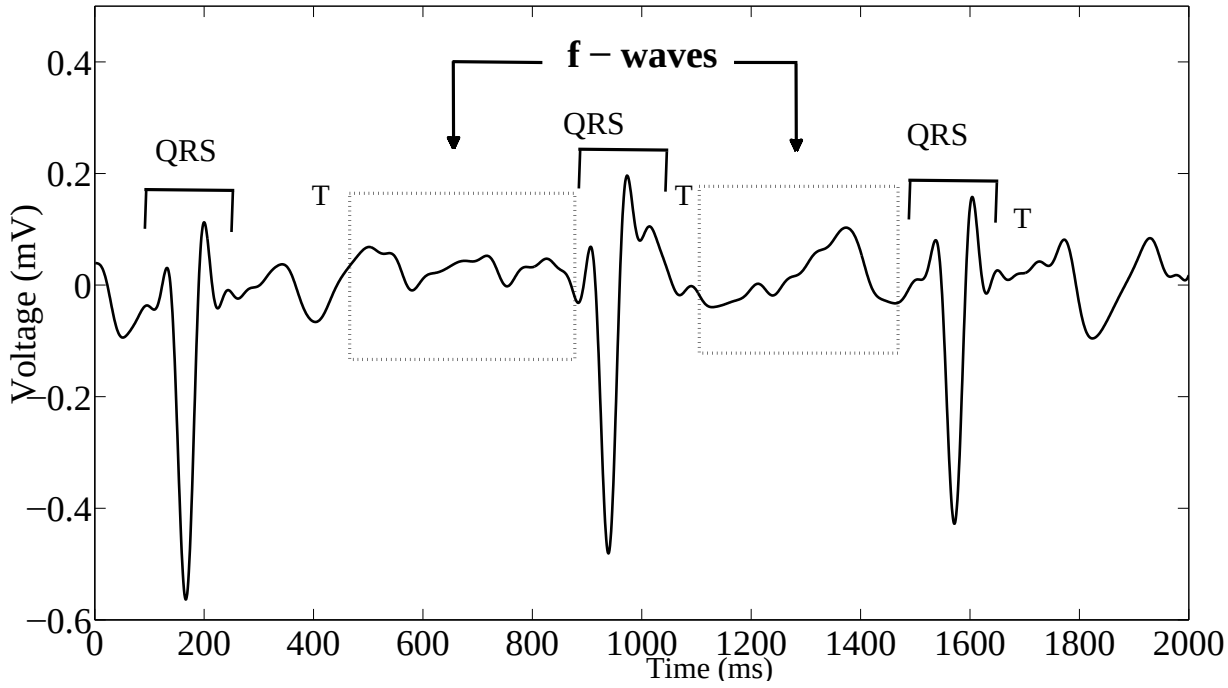


Figure 4.1: Example of ECG recording during AF and its characteristic waves. Boxes highlight TQ intervals where f-waves can be observed.

detection. In addition, its content has been so far exploited in the framework of CA description. Indeed, several works have demonstrated its correlation with procedural outcome. However, f-wave amplitude measure assessment is still operator-dependent and lacks a unique, standard definition. As a consequence, multilead ECG content is not

adequately exploited. Moreover, standard signal processing approaches for f-wave amplitude characterization do not entirely exploit ECG content, in particular components expressing its interlead spatial variability [121]. Our work aims at extracting information about f-wave amplitude in an automatic and quantitative framework taking into account all ECG leads. Spatial variability of standard ECG is properly exploited to enhance f-wave predictive power in the noninvasive assessment of CA outcome in persistent AF. The main results of this chapter have been published in [102–104, 106] and investigated in more detail in this doctoral thesis. The chapter is structured as follows. In Sec. 4.2 the concept of f-wave peak-to-peak amplitude and its role in AF analysis is illustrated. Multivariate characterization of this feature is then explained in Sec. 4.3. The method proposed is based on an interpolation algorithm which is able to automatically compute mean f-wave amplitude on a certain lead. Such algorithm represents the starting point for a multilead extension based on principal component analysis (PCA), as it can be applied to each lead of the AA signal low-rank approximation, detailed in the next sections. At the final step, contributions to f-wave amplitude description from all ECG leads are properly combined in a single parameter and applied in different contexts. Such an index can act as a binary classifier of CA outcome prediction, thus distinguishing between successful and failing CA procedures immediately before their performance at different follow-ups. The techniques developed are first applied to prediction of acute AF termination by CA in Sec. 4.4. Variations of this parameter are also able to quantify CA impact over AF activity within the ablation procedure, which is highly correlated with the procedural outcome; details are provided in Sec. 4.6. The main conclusions of this chapter are finally summarized in Sec. 4.7.

4.2 Clinical assessment of f-wave amplitude

4.2.1 Etiology and clinical interpretation

As stated in Sec. 3.3.2, the P wave observed on ECG under SR conditions reflects atrial depolarization. The depolarization wavefront propagates in a regular and organized fashion from the SA node toward the AV node, thus resulting in a coordinated atrial contraction and pumping of blood into the ventricles.

By contrast, during AF atrial contraction is irregular and chaotic, due to the multiple fibrillatory impulses propagating and colliding throughout the heart. These random phenomena of wavefront sum and cancellation result in the generation of f-waves, whose amplitude, repetition rate and shape vary according to the degree of evolution of the disease and other patient's conditions. More specifically, f-wave amplitude on ECG is function of the magnitude of the underlying cell voltage, which in turn renders the degree of conduction viability of the atrial myocardial tissue mass. In addition, it is also influenced by impedance between the electrode and the atria, as well as the directionality and cancellation of wavefronts. Typically in early stages of the disease (e.g., paroxysmal forms), the AF pattern can resemble atrial flutter (AFL), when it exhibits regular f-waves with high amplitude, while in other cases, especially more chronic forms of AF (e.g., long-standing persistent AF), the opposite characteristics can be observed. Both patterns can be also found in the same subject at different moments.

AF is generally referred to as coarse if f-waves peak-to-peak amplitude in lead V_1 is

higher than 0.1 mV, fine otherwise [129]. This distinction is usually not strict, as both patterns can be found in the same patient and multiple factors influence this parameter. Yet, most of the medical community agrees with the correlation between AF coarseness and LA function, especially when dealing with certain forms of AF (e.g., rheumatic, arteriosclerotic). More specifically, AF coarseness could derive from the progressive LA enlargement caused by atrial remodeling, and the consequent decrease in tissue compliance induces atrial contractile dysfunction [128].

Richness of f-wave amplitude content has spurred the development of different analysis approaches in the context of AF treatment, which take a step from the analysis of single-lead atrial amplitude led in [121].

4.2.2 Standard methods of f-wave analysis and their limitations

Valuable information can be extracted from the f-wave amplitude feature to explain CA effects on heart substrate and differentiate patients according to procedural outcome. Medical community widely recognizes the predictive power of f-wave amplitude, which is shown to be correlated with AF termination by CA. Indeed, high amplitude values result from multiple atrial cells depolarizing at the same instant, thus rendering a more organized and coordinated AF activity, which is easier to be treated by CA. This empirical observation is confirmed by several studies. In [31] the correlation between f-wave size and procedural success is demonstrated in lead V_1 and aV_F. Similar conclusions can be drawn in [121], where maximal and mean f-wave amplitude measured in leads V_1 and II are examined.

Different methods have been proposed to compute f-wave peak-to-peak amplitude. In [163] it is computed as the mean value of the 4 maximum-amplitude f-waves over the whole ECG recording. In [121] it is defined as the mean value over 10 (or 30) consecutive f-waves. In all these studies f-wave amplitude is manually determined on the surface ECG. Therefore, index accuracy is highly affected by operator's subjectivity and more prone to errors, due to the lower measure repeatability.

Moreover, these results seem to demonstrate f-wave size predictive value only in certain leads examined separately, thus disregarding potentially useful information from other leads. It has been demonstrated that lead V_1 exhibits the maximum atrial-to-ventricular amplitude ratio [129]. Yet, due to its proximity to the right atrial wall, valuable information about other areas responsible for AF triggering and maintenance (e.g., LA, PVs) may not be taken into account [62]. Therefore, not only these approaches do not consider contributions coming from multiple ECG leads, but selection of single electrodes is not driven by further systematic criteria. As we will see, our multilead approach not only avoids the drawbacks associated with the spatial variability of the atrial signal in surface recordings, but is able to effectively exploit this variability to improve prediction performance and robustness to electrode selection.

4.3 Multilead characterization of f-wave amplitude by means of principal component analysis

4.3.1 ECG preprocessing and atrial activity extraction

Before introducing some multivariate processing techniques of the AA signal, let us first illustrate how this signal is actually defined and extracted. Unless differently specified, this preprocessing stage will be accomplished throughout this work prior to ECG feature extraction.

ECG recordings are first processed by a fourth-order zero-phase type II Chebyshev bandpass filter with −3 dB attenuation at 0.5 Hz and 30 Hz cut-off frequencies. The filter selected is able to accurately reduce the influence of noisy components typically encountered in ECG analysis without deforming signal shape [143, 153]. The choice of this pass-band is consistent with the typical range of AF dominant frequency, between 3 and 12 Hz, and suppresses baseline wander and high frequency noise (e.g., myoelectric artifacts), besides 50 Hz power line interference.

In order to exclusively extract AA, removal of QRS complexes and segmentation of TQ intervals are carried out after automatically detecting ECG fiducial points. R waves are located on lead V_1 by means of the Pan-Tompkins' algorithm [127], whereas Q wave onset and T wave offset are detected with an improved version of Woody's method [24]. TQ intervals, which actually contain f-waves, are then mean-corrected and concatenated on each lead $\ell = 1, \ldots, L$, thereby representing AA in an $(L \times N)$ matrix $\mathbf{Y}_{\mathrm{AA}}$:

$$\mathbf{Y}_{\mathrm{AA}} = [\mathbf{y}_{\mathrm{AA}}(1) \cdots \mathbf{y}_{\mathrm{AA}}(N)] \in \mathbb{R}^{L \times N} \tag{4.1}$$

where vector $\mathbf{y}_{\mathrm{AA}}(n) = [y_1(n), \ldots, y_L(n)]^{\mathrm{T}}$ stands for the multilead AA signal at sample index n, L is the number of leads used, and N the number of samples of the AA signal $y_\ell(n)$ for each lead $\ell = 1, 2, \ldots, L$. All residual artifacts and spurious peaks due to concatenation have been automatically removed by means of signal first-derivative thresholding.

Depending on the application and the type of feature extracted, we chose either to process the full standard ECG, thus setting $L = 12$, or examine a subset of ECG leads. Indeed, as explained in Sec. 2.4.4, Einthoven's standard leads (or limb leads, I, II, III) and Golbderger's augmented leads (aV_R, aV_L, aV_F) are derived from the same 3 measurement points, and are thus redundant (linearly related, see Eq. (2.4)- (2.7)). Accordingly, lead III, aV_R, aV_L and aV_F can be discarded by our analysis, as I and II are sufficient to characterize heart electrical activity on the frontal plane. Finally, all precordial leads have been introduced too, in order to record the cardiac electric potential in a cross sectional plane, for a total of L=8 leads, that is, I, II, V_1-V_6. The number of ECG leads retained in our analysis will be clearly indicated in each section.

4.3.2 Automatic f-wave amplitude computation

According to previous studies, successful CA procedures can be predicted by higher values of f-wave peak-to-peak amplitude on the surface ECG [121]. Nevertheless, prediction accuracy is so far affected by amplitude manual computation, leading to higher error probability, especially in the presence of irregular and complex patterns. Similar shortcomings can occur when dealing with different operators performing the acquisition

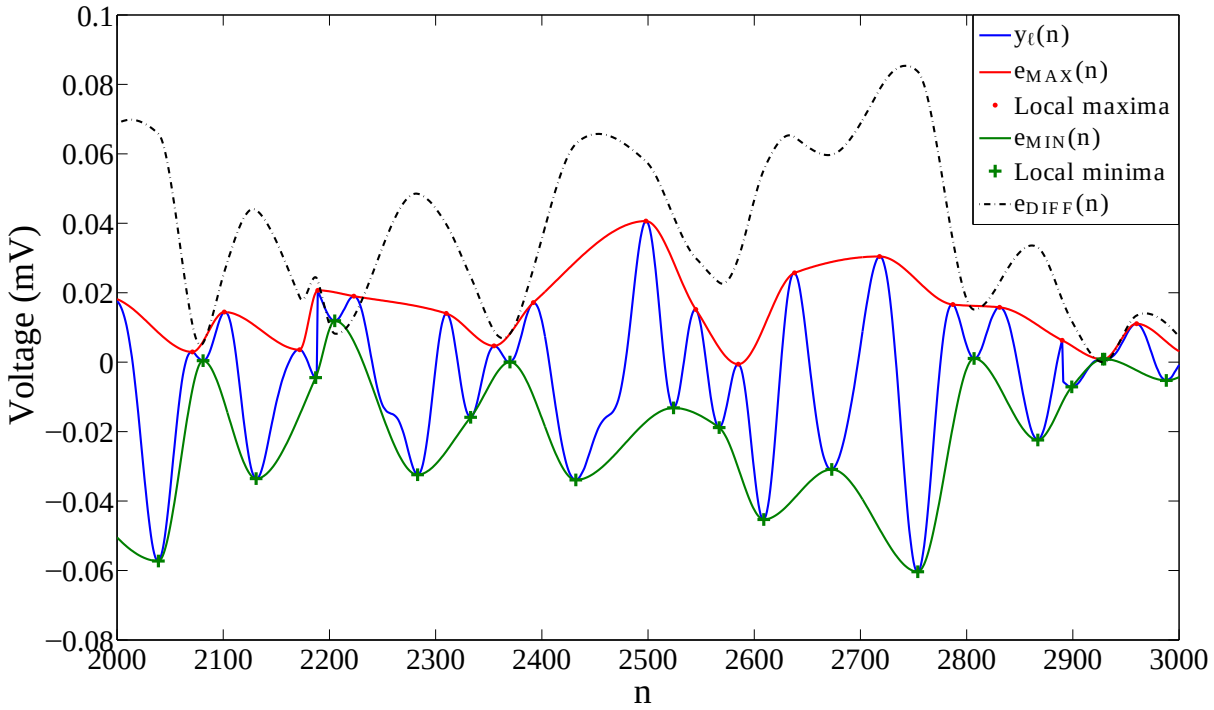


Figure 4.2: Single-lead atrial waveform interpolation algorithm. Upper and lower envelopes e_{MAX} and e_{MIN} pass through the local extrema of the input signal y_ℓ; their subtraction yields e_{DIFF}.

of such a parameter, so its measure is not uniquely defined. In this framework, we develop an automatic procedure for computing the mean amplitude value of the AA signal $y_\ell(n)$ on a specific lead $\ell = 1, 2, \ldots, L$. More precisely, its local maxima of $y_\ell(n)$ are detected so that an upper envelope $e_{\mathrm{MAX}}(n)$ passing through them can be determined by the shape-preserving piecewise cubic Hermite interpolating polynomial (PCHIP) [74]. Similarly, a lower envelope $e_{\mathrm{MIN}}(n)$ is computed as well, once detected the local minima of the signal. PCHIP interpolation reduces the negative effect of local spurious peaks and signal artifacts, and the global trend of the curve is exclusively taken into account. Peaks located near the edge between two consecutive TQ intervals are discarded from the computation. The difference $e_{\mathrm{DIFF}}(n) = |e_{\mathrm{MAX}}(n) - e_{\mathrm{MIN}}(n)|$ between the two curves outlines the general trend of the main oscillations of f-waves, and its temporal mean over the AA signal length N:

$$D(y) = \frac{1}{N} \sum_{n=1}^{N} e_{\mathrm{DIFF}}(n) \tag{4.2}$$

represents the final output of our algorithm. An example is shown in Fig. 4.2. The operator $D(\cdot)$ is characterized by an offset-invariance property:

$$D(ky + \alpha) = |k| D(y), \quad \forall k, \alpha \in \mathbb{R}. \tag{4.3}$$

Index D condenses the information about f-wave over the whole recording and its peak-to-peak amplitude pattern in a single objective parameter computed in a fully automated

manner.

4.3.3 Principal component analysis: definition and derivation of principal components

The rationale of our approach is the intrinsic variability of the surface ECG across leads, as they are all measured from different points of the patient's body. Assuming that the AA signal extracted from the standard ECG $\mathbf{Y}_{\mathrm{AA}}$ can be considered as a surface mixture of a certain number of unknown sources supports the application of PCA. This decomposition can express multivariate data as a linear combination of these uncorrelated, orthogonal, most descriptive sources, the so-called principal components (PCs) [29], with the highest percentage of input data information as explained by their energy. Other techniques are also employed in blind source separation for orthogonal component extraction. For instance, independent component analysis (ICA) allows the computation of such sources by taking into account their statistical independence constraint, and it has been widely employed for several biomedical applications, such as fetal ECG separation [41, 167, 169] and electro-magnetic brain signal analysis [71]. ICA requires that the components are not only orthogonal, but also statistically independent. This stronger assumption weakens the orthogonality constraint of mixing matrix columns. However, we aim at searching for any signal components which are not only common to all observations, but exhibit also the highest energy content. This goal motivates PCA application, since linear filtering highlights information shared by all the AA observations. Owing to the relation between energy and amplitude, we aim at investigating whether dominant PCs can retain the information necessary for an accurate characterization of f-wave on surface ECG. Most of the PCA theoretical description that follows is inspired by [168].

Observation model

The key idea of PCA is to reduce the dimensionality of input multivariate data in a few components, while retaining most of the information as measured by variance [73]. It is worth introducing the general concept of spatial filtering, as an optimal tool for recovering a certain signal of interest from the ensemble of observations [152]. Indeed, a multivariate set of observations $\mathbf{Y}_{\mathrm{AA}}$ with L components can be represented at each time instant by applying a generic linear transformation $\mathbf{M}$, formed by projection column vectors $\mathbf{m}_k$:

$$\mathbf{X} = \mathbf{M}^{\mathrm{T}}\mathbf{Y}_{\mathrm{AA}} \tag{4.4}$$

yielding a set of transformed variables $\mathbf{X}$. According to PCA rationale, large variances have important structure, therefore PCs with larger associated variances represent interesting structure, while those with lower variances are typically associated with noise [139].

Computational model

The core of PCA is searching for a linear combination of the observations, whose variance is maximized. Let us consider a generic one-dimensional signal or component $x \in \Re$ derived as a linear combination of the observations $\mathbf{y}_{\mathrm{AA}} \in \Re^L$ [168]:

$$x = \mathbf{m}^T\mathbf{y}_{\mathrm{AA}} \tag{4.5}$$

According to the PCA rationale, the first principal direction $\mathbf{m}_1$ is the unit-norm vector maximizing the variance of Eq. (4.5) as measured by the function:

$$E[x^2] = \mathbf{m}^T E[\mathbf{y}\mathbf{y}^T]\mathbf{m} = \mathbf{m}^T \mathbf{R}_y \mathbf{m} \tag{4.6}$$

where $\{\cdot\}^T$ represents the transpose operator and $\mathbf{R}_y = E[\mathbf{y}_{\mathrm{AA}}\mathbf{y}_{\mathrm{AA}}^T]$ stands for the covariance matrix of input data. In order to determine the first dominant direction $\mathbf{m}_1$, maximization of Eq. (4.6) can be accomplished by means of the Lagrange's multipliers' technique, consisting in working on the criterion:

$$J = \mathbf{m}_1^{\mathrm{T}} \mathbf{R}_y \mathbf{m}_1 - \lambda(\mathbf{m}_1^{\mathrm{T}} \mathbf{m}_1 - 1) \tag{4.7}$$

where λ represents the Lagrangian multiplier and the constraint $\mathbf{m}_1\mathbf{m}_1^T = 1$ is introduced to guarantee a unique solution. J is the Lagrange's function; its gradient is zero at the optimal solution, corresponding with local stationary points. To this end, we derive J with respect to $\mathbf{m}_1$ and we impose it is equal to zero.

$$\nabla_{\mathbf{m}_1} J = 2\mathbf{R}_y \mathbf{m}_1 - 2\lambda \mathbf{m}_1 = 2(\mathbf{R}_y - \lambda \mathbf{I}_L)\mathbf{m}_1 = 0 \tag{4.8}$$

where $\mathbf{I}_L$ is the identity matrix of order L. Eq. (4.8) highlights that λ is actually an eigenvalue of $\mathbf{R}_y$ and $\mathbf{m}_1$ the corresponding eigenvector:

$$\mathbf{R}_y \mathbf{m}_1 = \lambda \mathbf{m}_1 \tag{4.9}$$

By multiplying both sides of Eq. (4.9) by $\mathbf{m}_1^T$ we obtain:

$$\mathbf{m}_1^T \mathbf{R}_y \mathbf{m}_1 = \lambda \mathbf{m}_1^T \mathbf{m}_1 = \lambda \tag{4.10}$$

since $\mathbf{m}_1^T\mathbf{m}_1 = 1$. Substituting Eq. (4.10) into Eq. (4.7) yields $J = \lambda$. It turns out that the selection of the eigenvector maximizing variance must be performed by taking λ as large as possible. This condition is fulfilled when $\mathbf{m}_1$ is the normalized dominant eigenvector of $\mathbf{R}_{\mathrm{y}}$, and λ the corresponding eigenvalue. The second principal direction $\mathbf{m}_2$ is the unit-norm maximizer of criterion in Eq. (4.6), lying orthogonal to the first principal direction $\mathbf{m}_1$, i.e., $\mathbf{m}_2^T\mathbf{m}_1 = 0$. At the generic kth step, the kth principal direction $\mathbf{m}_k$ is the unit-norm maximizer of Eq. (4.6) lying orthogonal to the previous principal directions $\{\mathbf{m}_i\}_{i=1}^{k-1}$, i.e., $\mathbf{m}_k^T\mathbf{m}_i = 0$, for $i < k$. The principal components $\{x_1, x_2, \ldots, x_k\}$, are obtained by replacing $\mathbf{m}$ with the corresponding principal directions in Eq. (4.5).

4.3.4 Algorithms for computing PCA

PCA performance requires an eigenvalue decomposition (EVD) of the data covariance matrix $\mathbf{R}_{\mathrm{y}}$, which yields:

$$\mathbf{R}_{\mathrm{y}} = \mathbf{\Gamma}\mathbf{\Lambda}\mathbf{\Gamma}^T \tag{4.11}$$

where $\mathbf{\Gamma}$ is a $(L \times L)$ orthonormal matrix containing the eigenvectors of $\mathbf{R}_{\mathrm{y}}$, whereas $\mathbf{\Lambda}$ is a diagonal matrix containing the corresponding eigenvalues. With reference to the PCA definition introduced in Eq. (4.4), knowing that $\mathbf{\Gamma}\mathbf{\Gamma}^T = \mathbf{\Gamma}^T\mathbf{\Gamma} = \mathbf{I}_L$ for the orthonormality property, we can compute the PCA factors as:

$$\mathbf{M} = \mathbf{\Gamma} \tag{4.12}$$

Uniqueness of the solution is guaranteed only if additional constraints are introduced, as orthonormality of the columns of $\mathbf{M}$ in PCA. Sources' variance is normalized to 1 by means of the factor $\mathbf{\Lambda}^{-\frac{1}{2}}$.

The main issues of this algorithm is that processing $\mathbf{R}_{\mathrm{y}}$ can induce a loss of precision and lead to numerical instability. As a consequence, it is generally preferred avoiding the explicit computation of this matrix and running the singular value decomposition (SVD) of the input matrix $\mathbf{Y}$, which yields:

$$\mathbf{Y} = \mathbf{U}\mathbf{S}\mathbf{V}^T \tag{4.13}$$

where $\mathbf{U}$ is an $(L \times L)$ orthonormal matrix whose columns represent the left singular values of $\mathbf{Y}$, $\mathbf{V}$ is a $(N \times L)$ matrix containing the right singular values, and $\mathbf{S}$ is a L-sized diagonal matrix whose elements represent the corresponding rank-ordered, nonnegative singular values. By plugging these factors into $\mathbf{R}_{\mathrm{y}}$ expression, we obtain:

$$\mathbf{R}_{\mathrm{y}} \approx \frac{1}{T}\mathbf{Y}\mathbf{Y}^T = \frac{1}{T}\mathbf{U}\mathbf{S}\mathbf{V}^T\mathbf{V}\mathbf{S}^T\mathbf{U}^T = \frac{1}{T}\mathbf{U}\mathbf{S}^2\mathbf{U}^T \tag{4.14}$$

By keeping in mind the EVD of $\mathbf{R}_{\mathrm{y}}$ given in Eq.(4.11), we can verify the following identities:

$$\mathbf{U} = \mathbf{\Gamma} \tag{4.15}$$

$$\frac{1}{T}\mathbf{S}^2 = \mathbf{\Lambda} \tag{4.16}$$

It turns out that the PCA factors can also be directly determined from the SVD of the data matrix $\mathbf{Y}$ as:

$$\mathbf{M} = \mathbf{U} \tag{4.17}$$

The last equation in (4.16) clarifies the relation between eigenvalues of the covariance matrix $\mathbf{R}_{\mathrm{y}}$ and the singular values of input data $\mathbf{Y}$.

4.3.5 Reduced-rank PCA for AA approximation

Knowing that the first source retains most of the AA signal variance, we investigate whether it is possible to exploit this property to characterize f-wave spatial distribution. Consequently, we search for a linear function of the maximum-variance elements of $\mathbf{y} = \mathbf{y}_{\mathrm{AA}}$. The PCA algorithm yields the dominant source as:

$$x_1 = \mathbf{m}_1^{\mathrm{T}}\mathbf{y}_{\mathrm{AA}}, \tag{4.18}$$

thus isolating the contribution of x_1 to $\mathbf{y}_{\mathrm{AA}}$ from that coming from other sources. As explained in Sec. 4.3.3, the first principal direction $\mathbf{m}_1$ maximizes the variance of x_1, achieved when $\mathbf{m}_1$ is the normalized dominant eigenvector (related to the highest eigenvalue) of $\mathbf{R}_{\mathrm{y}}$. We find $\mathbf{m}_1$ such that x_1 is the most descriptive source, i.e., each lead $\mathbf{y}_i$ is represented by the term $m_{i1}x_1$ with the minimal global error, where $m_{i1} = [\mathbf{M}]_{i1}$. The output function in Eq. (4.18) can clearly be seen as a weighted average of the observed variables. As a result, contributions from all leads are taken into account in the computation of x_1.

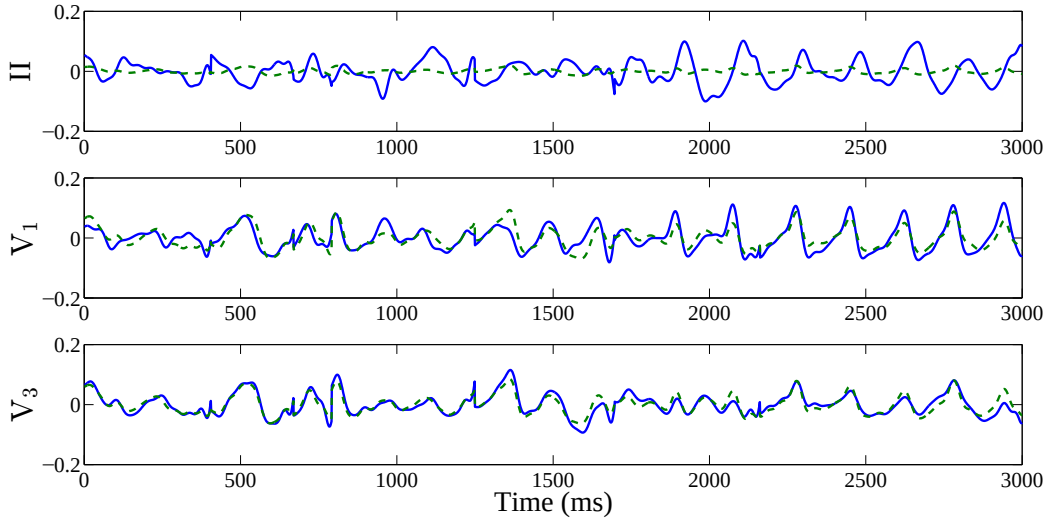


Figure 4.3: The multilead AA signal $\mathbf{Y}_{\mathrm{AA}}$ (continuous line) and its rank-1 estimation by PCA (dashed line). Top: lead II. Middle: lead V_1. Bottom: lead V_3.

More generally, the truncation of the model $\mathbf{Y}_{\mathrm{AA}} = \mathbf{MX}$ yields the rank-R approximation:

$$\widehat{\mathbf{y}}_{\mathrm{AA}}(n) = \sum_{k=1}^{R} \mathbf{m}_k x_k(n) \tag{4.19}$$

with $R < L$. Note that $\widehat{\mathbf{y}}_{\mathrm{AA}}$ has the same size as $\mathbf{y}_{\mathrm{AA}}$. In Fig. 4.3 an example of AA signal reconstruction through PCA iss reported in some ECG leads.

4.3.6 Multilead f-wave amplitude descriptor

Once AA signal approximation is carried out, f-wave amplitude in each ECG lead is computed as explained in Sec. 4.3.2. This results in an L-component vector D_L, whose entries represent the temporal mean of the f-wave amplitude envelope values on every electrode:

$$\mathbf{D}_L = [d_1, d_2, \ldots, d_L]^{\mathrm{T}}. \tag{4.20}$$

Generally speaking, in a rank-R approximation $\widehat{\mathbf{Y}}_{\mathrm{AA}}$, we compute amplitude entries as $d_{\ell,r} = D(m_{\ell r} x_r) = |m_{\ell r}| D(x_r)$, $r = 1, \ldots, R$, according to the property in Eq. (4.3). The entries of $\mathbf{D}_L$ are then sorted in increasing order, so as to determine their median value $\widetilde{D}_L$ in the final step. The choice of the median is justified by its ability to describe overall data distribution without loss of generality, with a higher degree of robustness to outliers, compared to other statistical descriptors such as the mean value. The sequence of the algorithm steps is justified by the need for capturing as most of input signal energy as possible and effectively rendering f-wave amplitude properties. Experimental evidence shows that reversing signal interpolation and PCA decomposition does not provide comparable results in multi-lead f-wave characterization. Indeed, interpolation induces a considerable loss of energy, which can not be effectively captured by PCA, thus disregarding information essential to atrial amplitude description. Parameter $\widetilde{D}_L$ can be considered as a descriptor of the global spatial distribution of f-wave amplitudes over the observed

leads. Its clinical significance in the context of CA outcome prediction is assessed in the remaining of this chapter.

4.4 Prediction of acute AF termination by CA

4.4.1 ECG data and CA success criterion

AA signal $\mathbf{Y}_{\mathrm{AA}}$ is processed by our algorithm once selected a reduced subset of 8 leads of the standard ECG, consisting of the precordial ECG leads and the Einthoven's leads I and II. This choice has been previously justified in Sec. 2.4.4. In order to describe the most representative components of AA signal for f-wave amplitude representation, input data are approximated by the dominant PC exclusively, that is to say, by setting $R = 1$ in Eq. (4.19). In the experimental section benefits from this technical choice are detailed. With reference to Sec. 4.3.6, it is worth noting that when $R = 1$, $m_{\ell 1} = [\mathbf{m}_1]_\ell$ is the ℓth component of the dominant direction $\mathbf{m}_1$. We examine the 31-procedure database employed for predicting acute AF termination by CA and previously presented in Sec. 3.5.5. It is worth to mention that the reduced number of failing CA procedures ($n_F = 5$) can limit the generalization power of experimental results. This issue mainly affects several parts of this thesis, especially the early stages, when the number of patients involved in the study is still quite limited and CA outcome sometimes is not known yet. The impact of such factor has been verified throughout this thesis by testing our predictors on new patients enrolled in the study.

4.4.2 Statistical Analysis

According to this protocol, categories under examination are referred to as "AF termination" and "non AF termination" by CA. All the ECG parameters defined in the sequel are expressed as mean ± standard deviation in Table 4.1. Data normal distribution is

Table 4.1: Interclass statistical analysis for AF procedural acute termination assessment.

	AF termination	Non AF termination	p value
$\widetilde{D}_8$	0.038 ± 0.019	0.015 ± 0.007	$\mathbf{9.56 \cdot 10^{-4}}$
$\widetilde{D}_{12}$	0.030 ± 0.012	0.015 ± 0.006	$\mathbf{8 \cdot 10^{-3}}$
$\overline{D}_8$	0.042 ± 0.023	0.022 ± 0.01	$6.4 \cdot 10^{-2}$
$\overline{D}_{12}$	0.049 ± 0.070	0.022 ± 0.01	$5.0 \cdot 10^{-2}$
$D(\mathrm{V}_1)$	0.068 ± 0.022	0.054 ± 0.017	$1.85 \cdot 10^{-1}$
$\mathrm{RMS}(\mathrm{V}_1)$	0.075 ± 0.110	0.027 ± 0.017	$1.55 \cdot 10^{-1}$
$\mathrm{SampEn}(L_s, r_s^{(1)})$	0.299 ± 0.063	0.218 ± 0.107	$2.67 \cdot 10^{-1}$
$\mathrm{SampEn}(L_s, r_s^{(2)})$	0.143 ± 0.029	0.106 ± 0.052	$3.25 \cdot 10^{-1}$
$\widetilde{\mathrm{RMS}}_8$	0.016 ± 0.009	0.009 ± 0.006	$1.40 \cdot 10^{-1}$
$\widetilde{\mathrm{RMS}}_{12}$	0.024 ± 0.015	0.016 ± 0.008	$1.40 \cdot 10^{-1}$
$\overline{\mathrm{RMS}}_8$	0.021 ± 0.016	0.021 ± 0.021	$3.76 \cdot 10^{-1}$
$\overline{\mathrm{RMS}}_{12}$	0.037 ± 0.048	0.026 ± 0.024	$2.48 \cdot 10^{-1}$

first verified through the Lilliefors' test. Interclass differences are then evaluated through an unpaired Student's t-test if data follow a normal distribution, a two-sample Wilcoxon

rank sum test otherwise, under a confidence level α=0.05; p values associated with each unpaired test are reported in Table 4.1 as well. The predictive power of our model is measured by the area under curve (AUC) of its receiver operating characteristic (ROC) curve, based on the maximization of sensitivity and specificity, i.e., the rate of true positives and true negatives, respectively. The generalization ability of our analysis to an independent dataset is assessed by a leave-one-out cross-validation (LOOCV) technique. More specifically, AUC values are computed several times by keeping a sample of 30 procedures out of 31 and thus discarding one case at each iteration, so as to compute their average value at the final step. AUC values of each descriptor are displayed in Table 4.2; in addition, we report the corresponding average of optimal cut-off values determined by LOOCV, associated with the maximization of the sum of true positive and true negative cases determined over the 31-procedure database.

Table 4.2: CA outcome prediction performance for AF procedural acute termination assessment.

	AUC	Best cut-off
$\widetilde{D_8}$	0.98	0.023
$\widetilde{D_{12}}$	0.91	0.022
$\overline{D_8}$	0.77	0.027
$\overline{D_{12}}$	0.78	0.027
$D(\mathrm{V_1})$	0.68	0.060
$\mathrm{RMS}(\mathrm{V_1})$	0.71	0.013
$\mathrm{SampEn}(L_s, r_s^{(1)})$	0.75	0.289
$\mathrm{SampEn}(L_s, r_s^{(2)})$	0.72	0.139
$\widetilde{\mathrm{RMS}_8}$	0.72	0.005
$\widetilde{\mathrm{RMS}_{12}}$	0.72	0.011
$\overline{\mathrm{RMS}_8}$	0.63	0.012
$\overline{\mathrm{RMS}_{12}}$	0.67	0.014

4.4.3 Results

Our multilead method is first compared with a classical single-lead descriptor of f-wave amplitude, namely, its mean value in lead $\mathrm{V_1}$ output by the algorithm previous proposed, denoted $D(\mathrm{V_1})$. Another classical single-lead method focusing on AA signal magnitude has been considered, namely, the root mean square value (RMS) on the lead $\mathrm{V_1}$, i.e., $\mathrm{RMS}(\mathrm{V_1})$. Finally, a non-linear complexity index, the sample entropy SampEn [130], is also examined on the same electrode. This feature depends on two parameters: L_s and r_s. Parameter L_s represents the length of the sequences the ECG recording is split in. Such sequences are then compared, and the tolerance for accepting matches is denoted by the parameter r_s. This threshold is chosen as a fraction of the AA input signal standard deviation in $\mathrm{V_1}$, denoted σ_{V_1}, so as to assure the translation and scale invariance of SampEn. Both parameters have been set according to the guidelines given in [80], yielding $L_s = 2$ besides two values of r_s, namely, $r_s^{(1)} = 0.1\sigma_{V_1}$ and $r_s^{(2)} = 0.2\sigma_{V_1}$.

In the multilead framework, the discriminative power of our descriptor $\widetilde{D_L}$ has been assessed both on the ensemble of 8 linearly independent ECG leads ($L = 8$), as defined

in Sec. 4.4.1, and on the full standard ECG ($L = 12$), yielding indices $\widetilde{D}_8$ and $\widetilde{D}_{12}$, respectively. The same comparison is carried out by replacing the median with the mean value when combining the entries of vector $\mathbf{D}_L$ in Eq. (4.20), thus giving $\overline{D}_8$ and $\overline{D}_{12}$ as output. More precisely, the index $\overline{D}_{12}$ has been already proposed in [102], but in this study PCHIP is applied instead of cubic spline interpolation. Accordingly, the ability of PCHIP interpolation to effectively render f-wave peak-to-peak amplitude is also examined and compared with the spline interpolation technique. For the sake of comparison with our algorithm, after PCA application and rank-1 approximation, the RMS value is computed on every row of the data matrix $\widehat{\mathbf{Y}}_{\mathrm{AA}}$ resulting from Eq. (4.19). This feature is computed both on 8 and 12 ECG leads, so as to compute the median ($\widetilde{\mathrm{RMS}}_8$, $\widetilde{\mathrm{RMS}}_{12}$) and mean values ($\overline{\mathrm{RMS}}_8$, $\overline{\mathrm{RMS}}_{12}$).

Robustness of our multilead predictor $\widetilde{D}_L$ to ECG lead selection has also been tested. For each value of lead-subset size L ranging from 1 up to 8, the proposed multilead predictor has been run on all $8!/((8-L)!L!)$ possible lead combinations. CA outcome prediction performance has then been assessed for each combination of ECG leads from the corresponding values of $\widetilde{D}_L$, using the LOOCV technique. In this manner, the minimum, maximum and mean AUC values over all L-lead subset combinations have been obtained as a function of the subset dimension L; their corresponding intervals are displayed in Fig. 4.4. The lead combinations providing the best prediction performance for

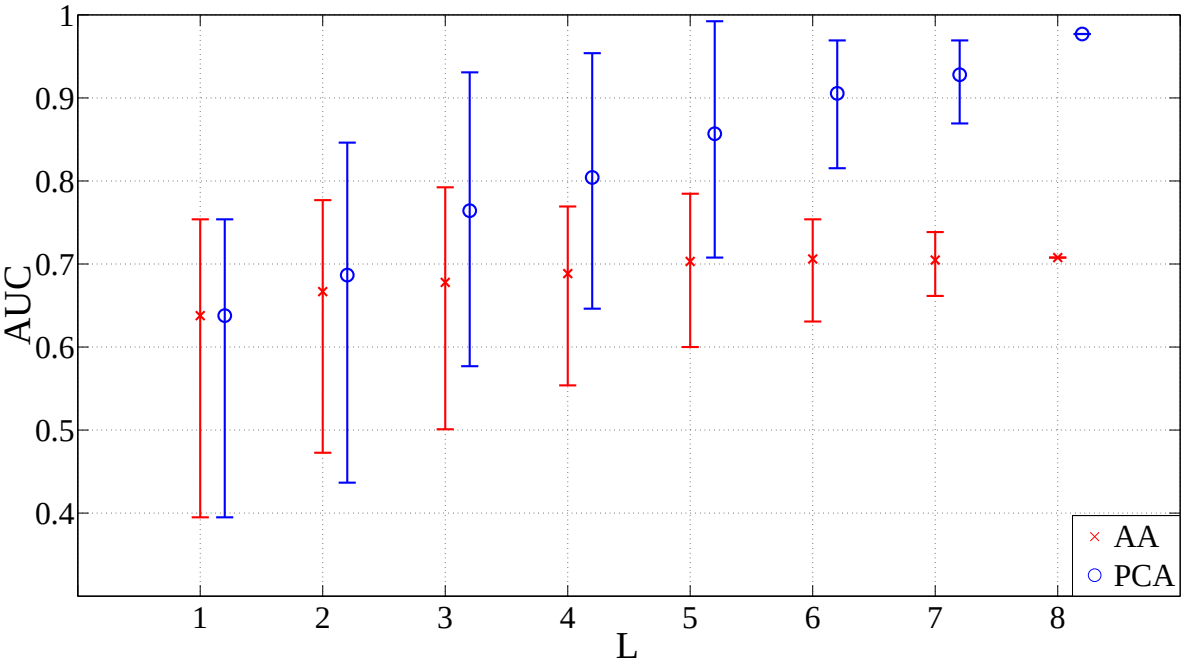


Figure 4.4: $\widetilde{D}_L$ prediction performance as a function of the size L of the subset of the 8 independent ECG leads. Vertical lines represent the range of AUC values between the minimum and the maximum obtained for each L; mean values are highlighted with markers. AA: measuring $\widetilde{D}_L$ directly from the observed AA signal. PCA: measuring $\widetilde{D}_L$ from approximation in Eq. (4.19) with $R = 1$.

each subset dimension are shown in Table 4.3. In order to demonstrate PCA effectiveness in filtering and enhancing content-bearing information from the AA signal, the same

Table 4.3: ECG lead subsets with optimal prediction performance based on parameter $\widetilde{D}_L$

Number of leads (L)	**Leads**
1	V_3
2	II, V_4
3	I, V_3, V_4
4	II, V_3, V_4, V_5
5	II, V_1, V_3, V_5, V_6
6	[I, II, V_1, V_3, V_5, V_6] [I, II, V_2, V_4, V_5, V_6] [II, V_1, V_2, V_4, V_5, V_6]
7	[I, II, V_1, V_2, V_4, V_5, V_6] [II, V_1, V_2, V_3, V_4, V_5, V_6]

analysis is repeated by combining all amplitude contributions from each of the leads of a L-sized subset directly computed on the AA signal, without previous PCA approximation. Benefits from PCA compression into the most descriptive PCs are demonstrated by results in Fig. 4.5, showing the AUC values assessing our algorithm performance for each value of the approximation rank R, ranging from 1 (the value adopted in our algorithm) to 8 (full-rank reconstruction of the input data). Each analysis based on AUC evaluation is further validated by the LOOCV technique.

4.4.4 Discussion

Benefits from automatic computation of f-wave amplitude

The predictive value of f-wave amplitude for CA of persistent AF has been scrutinized in previous studies [121]. However, not only it has been manually obtained, but only one ECG lead has been considered in its computation. By contrast, a method aiming at automatically computing f-wave peak-to-peak amplitude on a single lead is proposed in our study (Sec. 4.3.2). As in the study led in [121], the higher f-wave amplitude, the more likely AF termination by CA. Values of these parameters are very close to those obtained in [121] (0.08 ± 0.03 mV for successful CA procedures, 0.05 ± 0.03 mV for the failing ones, $p < 0.01$, AUC = 0.77) However, no significant interclass differences can be highlighted by $D(V_1)$, as reported in Table 4.1.

Comparison with other atrial signal parameters

Single-lead methods for computing f-wave amplitude do not prove to be adequate for CA outcome prediction. For instance, like $D(V_1)$, no significant differences are highlighted by the RMS value, whose prediction performance is rather inaccurate. Non-linear analysis is neither capable of distinguishing between successful and failing CA procedures. Indeed, not only sample entropy SampEn in V_1 does not prove to be an effective predictor of CA outcome, but our results show that this index exhibits lower values when dealing with failing CA procedures. By contrast, lower values of this index were associated with higher probability of CEE success in [5]. Indeed, these results contradict our hypothesis about a positive correlation between the sample entropy and AA signal spatio-temporal

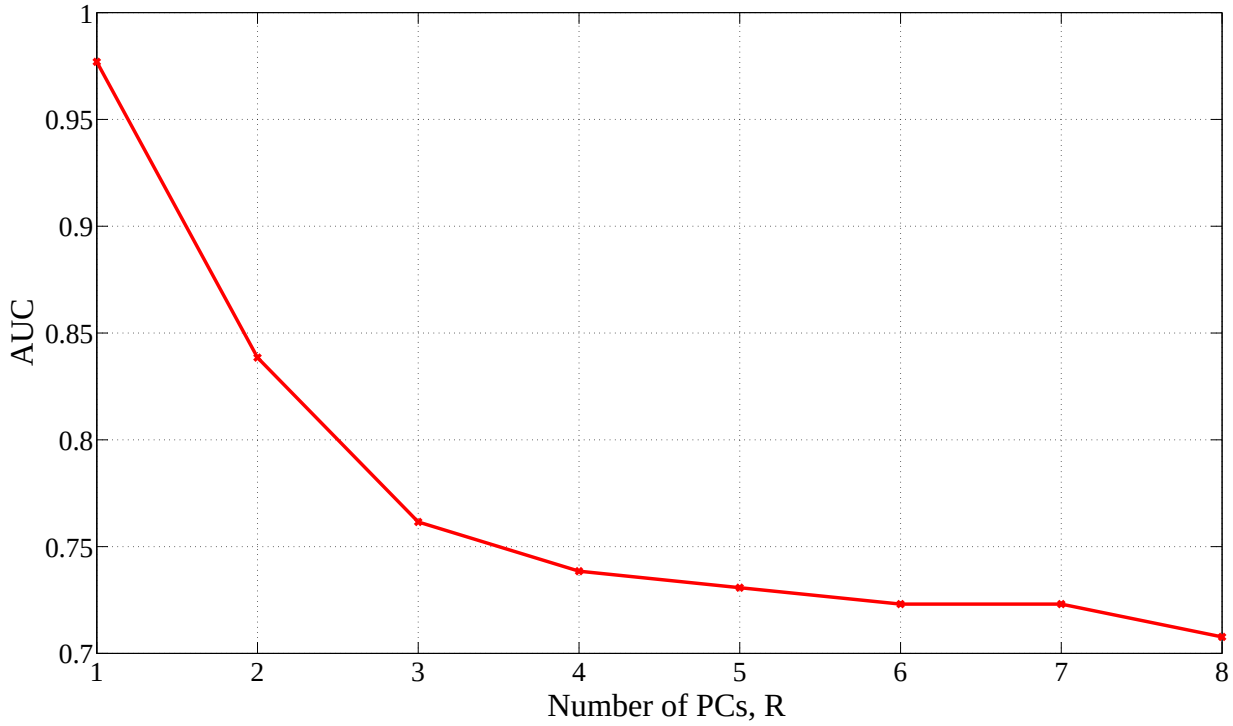


Figure 4.5: Classification performance for the 8 linearly independent ECG leads. AUC of $\widetilde{D}_8$ as a function of R, the number of PCs retained in approximation (4.19).

complexity. One would actually expect that more organized AA waveforms as measured by lower SampEn values render a less critical disease profile, easier to be treated by CA. Yet, this hypothesis is not verified in our study, regardless of the threshold r_s chosen. Finally, not only the computational load demanded by SampEn is notably higher than that of other predictors, but its parameters must be also tuned, which requires further assumptions on the AF model.

Multilead atrial signal amplitude measurement

The method presented is able to exploit spatial variability as a tool for f-wave amplitude characterization in CA outcome prediction framework. Regarding this multilead perspective, features based on RMS values computed on several leads do not seem to be able to quantify f-wave amplitude content. Indeed, no significant interclass differences are underlined by these descriptors, and AUC values in Table 4.2 are quite weak too, especially those related to the prediction performance of $\overline{\text{RMS}}_8$ and $\overline{\text{RMS}}_{12}$. By contrast, descriptors defined in our PCA-based multilead framework are more robust and reliable than their single-lead counterparts and than classical multilead approaches. The novel predictor $\widetilde{D}_8$ effectively discriminates between successful and failing CA procedures, as shown in Table 4.1, and its values are directly correlated with CA success, in conformity with results of previous studies [121]. We also confirmed the advantages derived from multilead analysis, as we can see in Fig. 4.4 that the mean AUC increases as the number of ECG leads do.

Benefits of PCA-based ECG signal approximation

A further advantage of our multilead approach over the direct examination of AA signal amplitude is proved in Fig. 4.4. Indeed, AUC mean values associated with our method are generally higher than those obtained without PCA preprocessing. In addition, the higher the number of leads, the larger the difference between the two methods, as AUC intervals partially or completely overlap only when L is sufficiently low. Moreover, additional benefits derive from PCA compression. As shown in Fig. 4.5, displaying the AUC index as a function of the PCA approximation rank R, the fewer PCs are retained, the higher the discriminative power of the predictor. Indeed, PCA ascribes noisy and/or spurious signal components to the least significant PCs, which seems to enable the extraction of the information about f-wave amplitude shared by observations when retaining the dominant PC of the atrial ECG data.

ECG-lead preselection

The use of all 12 leads of the ECG in standard clinical practice is justified by clinicians' necessity to compare the projections of heart electrical vectors in two orthogonal planes and at different angles, so as to increase pattern recognition accuracy [96]. However, as stated in the Introduction of the present thesis, linear relations between limb and augmented leads do not add further information which can be effectively exploited for CA outcome prediction. Conversely, it seems that selecting the 8 independent leads boosts PCA filtering action, as redundant elements are already partially removed before the decomposition, and the relevant components are put into evidence more easily. This may explain why $\widetilde{D}_8$ outperforms its 12-lead counterpart.

Table 4.3 shows leads helping discrimination between successful and failing CA procedures for a certain subset size L chosen. Note that some ECG lead combinations recur in each subset. In particular, the optimal L-lead subset typically includes leads of smaller optimal subsets, together with a new electrode. The presence of leads representing heart electrical activity on multiple planes confirms again the hypothesis that clinical information coming from multiple electrode locations can improve ablation outcome prediction.It is also worth noting that lead V_1 starts giving effective contribution when more than 4 leads are considered, in contrast with standard medical practice for AF analysis focusing on feature extraction in this electrode for single-lead analysis [129]. This result can be probably explained by the fact that this lead is not close enough to the PVs and the LA, therefore it is not able to sufficiently characterize information from these sites.

Combining contributions from multiple ECG leads

In this section further attention is paid to the computation modalities of the multilead descriptor of f-wave amplitude, i.e., how single-lead contributions coming are combined with each other. Such feature should provide a measure of central tendency of the dataset, namely, the value which is roughly equidistant from all the elements of the set considered. Experimental evidence reveals that the median value statistic $\widetilde{(\cdot)}$ performs better than the mean $\overline{(\cdot)}$ on our signal database, since it is less sensitive to outliers. Furthermore, the median is more suitable for skewed data distributions, this being often the case of f-wave amplitude, whose visibility and magnitude can depend on lead location as well as on AF characteristics in the patient examined. Hence, the low accuracy affecting CA

outcome predictors $\overline{D}_{12}$ and $\overline{D}_{8}$. These results do not seem to generalize evidence reported in [102]. This phenomenon can be probably explained by the fact that the mean value $\overline{D}_L$ indistinctly takes contributions from all leads into account. On the contrary, the median $\widetilde{D}_L$ exclusively highlights the role played by the middlemost elements in the sequence of contributions. In this manner, the global trend of f-wave amplitude is effectively depicted, while neglecting the extrema of $\mathbf{D}_L$, which are generally not representative enough to summarize the main characteristics of this spatial distribution.

Conclusions

The method put forth in this section is able to predict CA outcome in persistent AF by exploiting information about spatial distribution of f-wave amplitude. Such knowledge is effectively characterized on standard ECG by means of reduced-rank approximation to AA signal determined by PCA, which filters out the least significant components of the signal while enhancing the most discriminative contributions. An algorithm for f-wave amplitude computation based on PCHIP interpolation is also presented. This automatic approach yields results comparable with those reported in [121] and helps overcoming the shortcomings of manual measures. Combination of interpolation operations and PCA approximation, followed by the averaging of lead contributions, effectively improves CA outcome prediction quality. The proposed method overcomes traditional classification approaches and proves to be more robust to lead selection, which can be an advantage in practical settings where, e.g., electrodes may become loose or get disconnected from the patient's skin.

4.5 Measures of central tendency for long-term CA outcome prediction

The predictive power of the proposed descriptor of f-wave amplitude is now investigated so as to verify whether it can be extended to long-term CA outcome prediction. As explained in Sec. 3.5.5, changes in classification criterion do not only concern the duration of the follow-up, but also the evaluation of procedural success, merely defined as AF conversion to SR in the long-term follow-up, namely after 6 months [25]. In addition, we do not aim at evaluating the specific ablation intervention, but the patient's condition in a more general framework, which takes into account every factor of AF history and evolution after ablation. Accordingly, complementary cardioversion therapies (either electrical or pharmacological) and/or additional CA procedures can also contribute to the final outcome of ablation.

4.5.1 Methods and results

In this experimental section, we are going to test our method on the ECG database of $n_P = 36$ patients presented in Sec. 3.5.5. Freedom from AF recurrence is investigated in a long-term follow-up period of at least 6 months. As in the short-term analysis, also in this case we have to deal with unbalanced categories, since the database is characterized by a low number of failing CA procedures ($n_F = 7$). The influence of this factor on prediction performance needs to be more clearly elucidated. Accordingly, unpaired statistical

analysis is led as explained in Sec. 4.4.2; results are displayed in Table 4.4. Table 4.5 also

Table 4.4: Interclass statistical analysis: extension of amplitude measures to the long-term follow-up.

	AF termination	Non AF termination	p value
$\widetilde{D}_8$	0.033 ± 0.020	0.034 ± 0.016	$9.5 \cdot 10^{-1}$
$\widetilde{D}_{12}$	0.030 ± 0.013	0.031 ± 0.015	$7.8 \cdot 10^{-1}$
$\overline{D}_8$	0.035 ± 0.022	0.048 ± 0.026	$1.9 \cdot 10^{-1}$
$\overline{D}_{12}$	0.032 ± 0.017	0.042 ± 0.021	$2.0 \cdot 10^{-1}$

reports classification performance results.

Table 4.5: CA outcome prediction performance: extension of amplitude measures to the long-term assessment of AF termination by CA.

	AUC	Sensitivity	Specificity	Best cut-off
$\widetilde{D}_8$	0.49	0.59	0.57	0.033
$\widetilde{D}_{12}$	0.51	0.62	0.57	0.030
$\overline{D}_8$	0.63	0.21	0.86	0.045
$\overline{D}_{12}$	0.65	0.21	0.86	0.036

4.5.2 Discussion and conclusions

Our investigation demonstrates that each of the amplitude features previously proposed can not accurately discriminate the categories of interest and generalize our results to long-term prediction of CA outcome. This can be probably explained by the multiplicity of confounding factors (e.g. cardioversion, additional ablations), whose impact may be not adequately reflected on the atrial amplitude index. Owing to the risk of arrhythmic episodes and the application of complementary therapies after CA over the long-term follow up (namely, chemical or electrical cardioversion), these two criteria can return different results for the same patient.

By contrast, multivariate RMS-based parameters now seem to be able to effectively predict AF termination by CA in the long-term followup, in contrast with evidence related to prediction of acute procedural success. This can be probably explained by the impossibility for these parameters to capture certain effects immediately after CA performance, which may be hidden by inflammations and other postoperative reactions. The impact of such factors probably decreases after several months, whereas the role of other elements, such as atrial remodeling and auxiliary therapies, becomes more important.

As explained in Sec. 4.4.4, each ECG lead yields its own contribution to the characterization of the heart electrical vector in terms of magnitude and orientation, thus providing a different perspective of AF activity. As a consequence, such a specificity may be lost when simply averaging single-lead terms into a unique f-wave descriptor. This observation led us to explore other techniques which can selectively enhance the most content-bearing ECG leads so as to improve long-term CA outcome prediction. This line of investigation will be illustrated later in Chapter 6.

4.6 Assessment of therapy effects on AF dynamics during CA

4.6.1 Introduction

In this section we examine the ability of the f-wave amplitude index proposed in Sec. 4.4 to describe changes in AF pathophysiology during CA. We now investigate whether f-wave amplitude information can be used to quantify CA impact on AF by considering the evolution of heart electrical activity throughout the intervention. More precisely, we aim at assessing ablation effects by looking for a relation between the initial and the final part of the procedure and observing how f-wave amplitude varies within this temporal window.

This parameter highlights variations in f-wave amplitude for each patients' category, and allows the quantification of the ablation effects at different follow-up lengths. More specifically, we will demonstrate that a decline in f-wave amplitude between the beginning and the end of the procedure can be remarked in patients experiencing AF termination by CA, for the two follow-up windows considered in this study.

4.6.2 ECG data and CA outcome criteria assessment

According to the guidelines provided by HRS Expert Consensus Statement guidelines for CA trials [25] and introduced in Sec. 4.4.1, for each AF patient we can examine procedural success according to multiple criteria, which differ from each other, for instance, for the observation time and the endpoint of the procedure.

Following these guidelines, two different criteria of procedural success have been introduced into our study. Short-term CA outcome is verified on the dataset of 31 CA procedures defined in Sec. 3.5.5 . Long-term CA success is assessed on the 20-subject dataset described in the same section. Under this hypothesis, AF termination has been observed in 13 patients out of 20. The smaller size of the second dataset is due to the fact that some ablations were accomplished not long before this study, so long-term outcome is still unknown. For each sample of both datasets, one-minute surface 12-lead ECG signals acquired at the beginning and at the end of the CA procedure are examined.

4.6.3 Multilead descriptor of f-wave amplitude

The single-lead contributions to f-wave amplitude spatial distribution characterization are computed on the rank-1 AA signal PCA-approximation as explained in Sec. 4.3.6 by Eq. (4.20), and they are finally averaged so as to yield the index:

$$\overline{D}_L = \frac{\sum_{\ell=1}^{L} d_\ell}{L} = \frac{\sum_{\ell=1}^{L} |m_{\ell 1}| D(x_1)}{L} = \frac{\|\mathbf{m}_1\|_1}{L} D(x_1) \tag{4.21}$$

In [102], the role of $\overline{D}_L$ as a CA outcome predictor has been evidenced in a multivariate framework, as explained in Sec. 4.3.6: the higher its value, the more likely procedural AF termination. In this section, a further role is herein ascribed to $\overline{D}_L$ as a descriptor of AF evolution during CA, reflected on f-wave amplitude temporal variations which are negative for successful procedures, positive otherwise, regardless of the observation period during

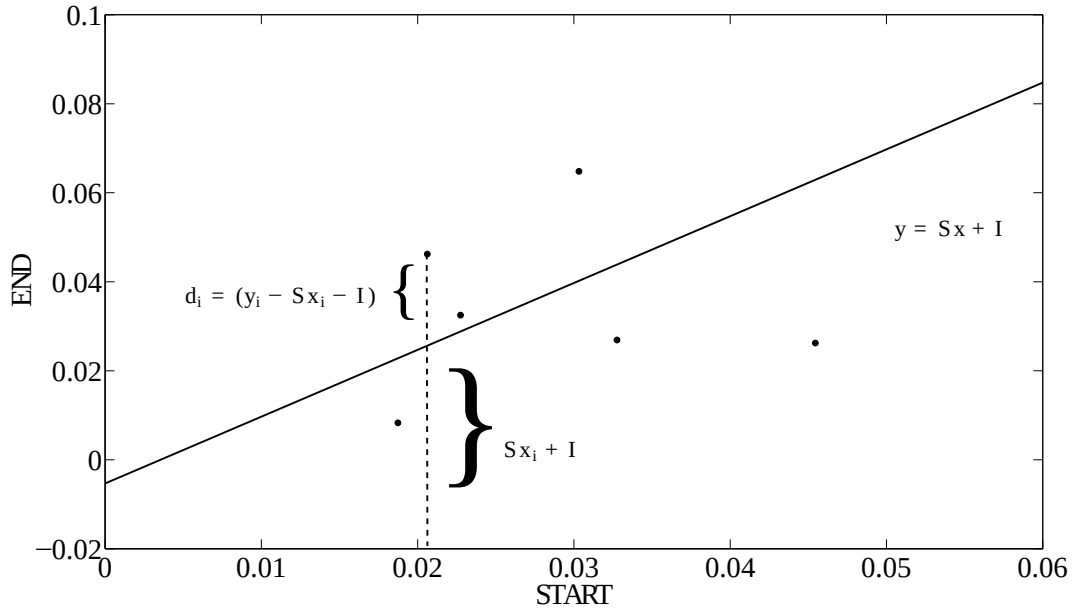


Figure 4.6: Example of a scatter plot of random data, the regression line $y = Sx + I$ and discrepancies d_i between estimated and real data

follow-up. Such variations are quantified by means of the linear regression analysis [14]. Generally speaking, given an observation i, this approach models the interaction between an independent (or control, or predictor) variable x_i and the effect (or response) variable y_i by means of the linear law:

$$y_i = Sx_i + I + e_i \tag{4.22}$$

where S stands for the slope of the straight-line relationship and I the intercept with the y axis, computed by the least squares (LS) method, which takes into account the discrepancies d_i between real observations y_i and their estimation $Sx_i + I$, as shown in Fig. 4.6. Mathematical demonstration is provided in Appendix A.1. The additional term e represents the unknown error component superimposed on the true linear relation, due to the measurement system or random disturbances. With reference to our application, we aim at modeling CA therapeutic impact as rendered by changes in f-wave amplitude measured between the beginning of CA (START) and its completion (END). Accordingly, in our application the index $\overline{D}_{L\text{START}}$ represents the regression independent variable, and we investigate whether any linear law can describe its relation with the dependent variable $\overline{D}_{L\text{END}}$.

4.6.4 Statistical analysis and results

Values of all parameters are expressed as mean ± standard deviation for each category in Table 4.6. Subscripts SUCC and FAIL refer to successful and failing CA procedures, respectively, according to the protocols above presented, whereas subscripts ST and LT are related to the length of the observation followup (short-term and long-term period, respectively); headings START and END are associated with the moment of the acquisition of the ECG recordings during the procedure. In this experimental session, in line

Table 4.6: Regression analysis of the parameters $\overline{D}_L$, $D(V_1)$, $\widetilde{D}_L$ (mV) and NMSE (n.u.: normalized units).

	START	END	R_P	S	P_S	P_I
$(\overline{D}_L)_{\text{SUCC,ST}}$	0.049 ± 0.070	0.046 ± 0.060	**0.982**	**0.836**	$\mathbf{1.52 \cdot 10^{-18}}$	$3.90 \cdot 10^{-11}$
$(\overline{D}_L)_{\text{FAIL,ST}}$	0.022 ± 0.010	0.033 ± 0.027	**0.900**	**2.422**		
$(\overline{D}_L)_{\text{SUCC,LT}}$	0.055 ± 0.100	0.051 ± 0.085	**0.998**	**0.849**	$\mathbf{8.52 \cdot 10^{-5}}$	$4.76 \cdot 10^{-5}$
$(\overline{D}_L)_{\text{FAIL,LT}}$	0.039 ± 0.020	0.036 ± 0.023	**0.894**	**1.008**		
$(\widetilde{D}_L)_{\text{SUCC,ST}}$	0.030 ± 0.012	0.029 ± 0.014	0.448	0.527	$1.88 \cdot 10^{-1}$	$2.93 \cdot 10^{-1}$
$(\widetilde{D}_L)_{\text{FAIL,ST}}$	0.015 ± 0.006	0.016 ± 0.010	0.788	1.381		
$(\widetilde{D}_L)_{\text{SUCC,LT}}$	0.026 ± 0.009	0.027 ± 0.010	0.725	0.791	$7.00 \cdot 10^{-1}$	$5.95 \cdot 10^{-1}$
$(\widetilde{D}_L)_{\text{FAIL,LT}}$	0.035 ± 0.013	0.031 ± 0.021	0.561	0.878		
$D(V_1)_{\text{SUCC,ST}}$	0.068 ± 0.022	0.067 ± 0.022	0.789	0.802	$1.68 \cdot 10^{-2}$	$4.01 \cdot 10^{-1}$
$D(V_1)_{\text{FAIL,ST}}$	0.054 ± 0.018	0.048 ± 0.012	0.665	0.446		
$D(V_1)_{\text{SUCC,LT}}$	0.076 ± 0.024	0.070 ± 0.023	0.883	0.834	$1.12 \cdot 10^{-4}$	$1.46 \cdot 10^{-1}$
$D(V_1)_{\text{FAIL,LT}}$	0.054 ± 0.012	0.062 ± 0.020	0.840	1.392		
$(\text{NMSE}_3)_{\text{SUCC,ST}}$	15.4 ± 15.9	14.0 ± 14.1	0.092	0.082	$2.40 \cdot 10^{-3}$	$6.72 \cdot 10^{-1}$
$(\text{NMSE}_3)_{\text{FAIL,ST}}$	18.7 ± 16.9	35.5 ± 29.7	0.813	1.428		
$(\text{NMSE}_3)_{\text{SUCC,LT}}$	9.80 ± 9.65	8.50 ± 7.80	0.476	0.384	$8.49 \cdot 10^{-1}$	$7.54 \cdot 10^{-2}$
$(\text{NMSE}_3)_{\text{FAIL,LT}}$	25.1 ± 24.7	26.5 ± 28.9	0.251	0.294		

with [103], we set $L = 12$ so as to take into account all lead contributions in regression analysis. For each patients' group (SUCC, FAIL) and follow-up window (ST, LT), the relation between $\overline{D}_L$ values computed at the beginning of the ablation (independent variable X) and those obtained at its completion (dependent variable Y) is assessed by the linear regression analysis. The value of Pearson's correlation coefficient R_P, defined in Appendix A.1, is computed so as to assess the validity of linearity hypothesis. We assume that the value of the slope S of each regression law $Y = SX + I$ can quantify CA effects over patients' heart substrate and their temporal dynamics, knowing that the intercept I has small values. In addition, statistical differences between slope values have been assessed through a parallelism test [156] for each couple of regression lines (SUCC, FAIL); p values output by such test are computed as explained in [156] and are referred to as P_S and P_I in Table 4.6. In first approximation, we assume that intercept value is close to zero and can be neglected. Then, in order to confirm the validity of our hypothesis, we perform a further test to assess statistical differences between the intercepts of each linear law, quantified by the p value P_I. If the slopes are significantly different, there is no point comparing intercepts. If the slopes are indistinguishable, the lines could be either parallel with distinct intercepts, or identical (i.e., same slopes and intercepts) [166].

The scatter plots in Fig. 4.7 display the distribution of $\overline{D}_L$ values acquired after the completion of the ablation ($(\overline{D}_L)_{\text{END}}$) as a function of those describing the beginning of the procedure ($(\overline{D}_L)_{\text{START}}$) for each criterion of procedural success (short-term success and long-term success, respectively); the regression laws related to each category are also represented. Statistical analysis has been carried out under a confidence level α equal to 0.05.

A comparison with previous works has been drawn as well. F-wave peak-to-peak amplitude $D(V_1)$ has been studied on lead V_1 [102, 121]. In addition, the NMSE_3 index defined in [19] as the NMSE between the AA signal and its rank-3 PCA-approximations on V_1 is examined as well. This index will be further studied in Chapter 5. It has also been computed for each CA step and analyzed according to the aforementioned protocol. Finally, in order to assess the ability of the mean value to properly condense ECG leads'

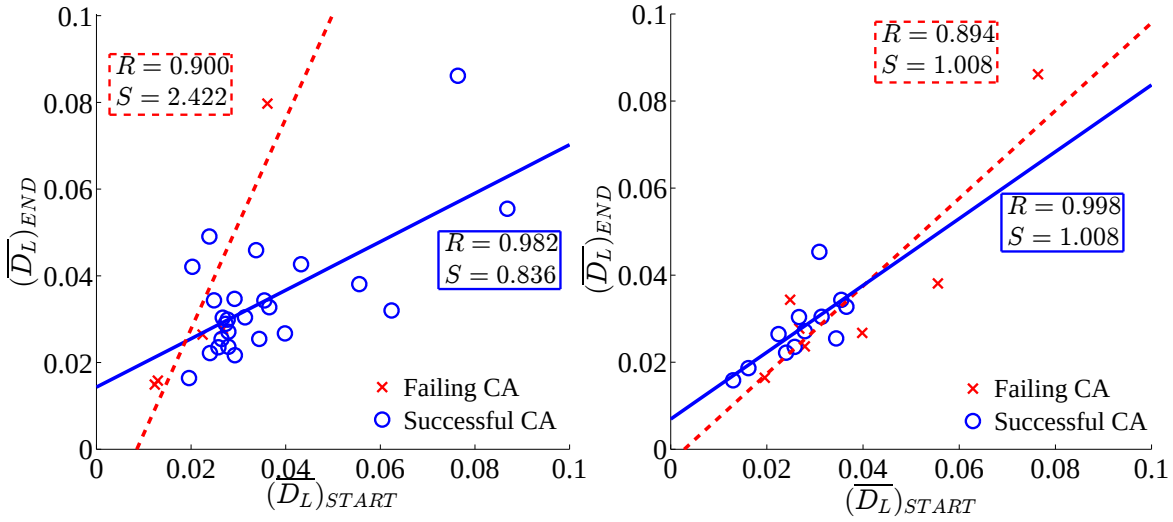


Figure 4.7: Scatter plot of $\overline{(D_L)}_{\text{END}}$ as a function of $\overline{(D_L)}_{\text{START}}$ and data regression lines associated with each category (successful CA: 'O', continuous line; failing CA: '×', dotted line.). (Left) Short-term follow-up; (Right) Long-term follow-up.

contributions in a unique measure, the proposed index $\overline{D}_L$ has been compared with the median f-wave amplitude as rendered by $\widetilde{D}_L$ and defined in [106].

4.6.5 Discussion and conclusions

Results of our analysis in Table 4.6 show highly linear correlation between $\overline{D}_L$ values acquired at the beginning of the procedure and those determined at the end. This result can be generalized for each class of subjects and CA outcome observation time. Experimental evidence also confirms our assumptions about reduction in f-wave amplitude within the observation temporal window chosen. Indeed, a significant reduction in f-wave amplitude is found to be associated with CA success, quantified by a value of the slope S lower than unity. By contrast, when CA procedures are ineffective, the index $\overline{D}_L$ increases or remains unchanged, which can be a clue of disease presence even after the ablation. Moreover, statistically significant differences can be observed for S values between the groups under examination (SUCC, FAIL) at each time of follow-up. Such results confirm the robustness of the ECG-based feature proposed even in presence of outliers. For example, even when we remove the point $(\overline{D}_L)_{\text{FAIL,ST}} = (0.036, 0.079)$ in the regression analysis, values obtained do not invalidate conclusions drawn by previous experiments ($R = 0.99$, $S = 1.34$, $P_S = 0.037$). This evidence shows the ability of our descriptor to evaluate CA impact over AF evolution, which are specific for each group of subjects. Mean f-wave amplitude on V_1 ($D(V_1)$) provides statistically significant inter-class differences, but its short-term value decreases after CA whether the procedure is effective or not. This outcome is not consistent with our initial assumption, as we expect a reduction in f-wave amplitude only when CA is successful. Moreover, the linearity assumption is not as reliable as for our descriptor. Single-lead amplitude seems to distinguish between the categories considered (SUCC, FAIL) more accurately in the long-term than in the short-term follow-up. However, its discrimination ability is clearly outperformed by that of our multilead descriptor, since interclass differences are quantified by lower P_S values. Regarding NMSE_3, even though significant differences are reported for the short-term CA outcome examination, the linearity hypothesis proves to be quite weak, especially when

dealing with successful procedures, as proved by the low R values in regression analysis. Similarly, analysis over longer periods shows no significant differences between regression line slopes. Moreover, our investigation merely focuses on V_1, the lead classically employed in clinical practice for AF analysis in surface ECG. Even if it is well known that this is the lead with the largest atrial-to-ventricular signal amplitude ration [129], contributions from other leads are not analyzed at all by this classical approach. Some pertinent information is neglected, thus leading to a partial comprehension of the disease. Concerning the median operator $\widetilde{D}_L$, despite the capability of effectively predicting of acute AF termination by CA [106], it seems not be able to differentiate successful and failing CA procedures when looking at f-wave amplitude dynamics, since the regression laws are not significantly different between each other. Moreover, data distribution is not accurately described by a linear law, as proved by the low regression coefficients values. This result could be explained by the fact that averaging single-lead atrial amplitude contributions better preserves information about CA dynamics. Indeed, it is more sensitive to amplitude variations, in particular those of extrema values (i.e., very low and/or very high amplitude values). By contrast, the median operator rejects outliers more easily, and this probably leads to discarding contributions describing amplitude dynamics.

To summarize, we corroborated the ability of the index $\overline{D}_L$ to quantitatively evaluate CA impact on AF dynamics during its performance through a multilead characterization of f-wave amplitude variations. A linear correlation between the beginning and the end of the procedure has been demonstrated. In particular, a reduction in $\overline{D}_L$ values can be associated with successful procedures, thus showing CA efficacy in progressively suppressing f-waves, regardless of the length of the postoperative followup. Experimental evidence proves that AF pathophysiology is deeply influenced by CA performance, and its modifications can be noninvasively quantified by f-wave amplitude variations in the standard ECG.

4.6.6 Further developments

In this section, we investigate whether these results can be extended over a larger database in a longer follow-up. Therefore, we repeat AF dynamics analysis on the 36-patient database introduced in Sec. 4.5.1 in the framework of long-term CA outcome prediction. Furthermore, we compare the measures of central tendency presented in this chapter, namely, mean value of the f-wave amplitude descriptor $\overline{D}_L$ and the median $\widetilde{D}_L$. Both the 8-lead subsets and the full standard ECG are examined. Finally, we examine the AA signal interpolation techniques presented in [103] and [106], i.e., the cubic spline method and the PCHIP algorithm, respectively.

In Table 4.7 we can generally remark that it is hard to generalize our initial assumptions over the database considered.

For instance, as in the previous analysis, despite the significant differences between the related linear laws, Table 4.7 underlines that mean amplitude $D(V_1)$ always decreases within CA performance time regardless of the procedural outcome. The NMSE index is also affected by several drawbacks, including the lack of linearity of the relation hypothesized. Generalization of previous results obtained on the parameter $\overline{D}_{12}$ cannot be effectively accomplished on this database. When applying the spline technique, not only linearity assumption seems not to be correct, but the hypothesis that f-wave amplitude decreases only when CA is effective is not verified anymore. Similar conclusions can be

Table 4.7: Linear regression of f-wave amplitude: statistical analysis and results over the 36-patient ECG database.

	START	END	R_P	S	P_S	P_I
$(\overline{D}_{12})_{\text{SUCC,SPLINE}}$	0.039 ± 0.028	0.0546 ± 0.071	0.676	1.726	$1.63 \cdot 10^{-2}$	$1.51 \cdot 10^{-1}$
$(\overline{D}_{12})_{\text{FAIL,SPLINE}}$	0.053 ± 0.029	0.060 ± 0.038	0.642	0.845		
$(\overline{D}_{8})_{\text{SUCC,SPLINE}}$	0.044 ± 0.039	0.049 ± 0.046	0.500	0.591	$1.47 \cdot 10^{-2}$	$4.01 \cdot 10^{-1}$
$(\overline{D}_{8})_{\text{FAIL,SPLINE}}$	0.061 ± 0.039	0.086 ± 0.055	0.882	1.241		
$(\widetilde{D}_{12})_{\text{SUCC,SPLINE}}$	0.036 ± 0.020	0.039 ± 0.026	0.735	0.913	$6.22 \cdot 10^{-1}$	$7.12 \cdot 10^{-1}$
$(\widetilde{D}_{12})_{\text{FAIL,SPLINE}}$	0.038 ± 0.018	0.042 ± 0.036	0.535	1.026		
$(\widetilde{D}_{8})_{\text{SUCC,SPLINE}}$	0.041 ± 0.030	0.046 ± 0.045	0.283	0.422	$1.24 \cdot 10^{-2}$	$1.08 \cdot 10^{-1}$
$(\widetilde{D}_{8})_{\text{FAIL,SPLINE}}$	0.040 ± 0.019	0.066 ± 0.056	0.759	2.295		
$(\overline{D}_{12})_{\text{SUCC,PCHIP}}$	0.032 ± 0.017	0.045 ± 0.062	0.538	1.971	$6.30 \cdot 10^{-2}$	$2.45 \cdot 10^{-1}$
$(\overline{D}_{12})_{\text{FAIL,PCHIP}}$	0.042 ± 0.021	0.048 ± 0.026	0.629	0.782		
$(\overline{D}_{8})_{\text{SUCC,PCHIP}}$	0.035 ± 0.022	0.034 ± 0.018	0.635	0.524	$1.25 \cdot 10^{-2}$	$7.28 \cdot 10^{-1}$
$(\overline{D}_{8})_{\text{FAIL,PCHIP}}$	0.048 ± 0.026	0.061 ± 0.036	0.663	0.907		
$(\widetilde{D}_{12})_{\text{SUCC,PCHIP}}$	0.029 ± 0.013	0.033 ± 0.030	0.330	0.740	$9.51 \cdot 10^{-1}$	$9.25 \cdot 10^{-1}$
$(\widetilde{D}_{12})_{\text{FAIL,PCHIP}}$	0.031 ± 0.015	0.033 ± 0.024	0.500	0.776		
$(\widetilde{D}_{8})_{\text{SUCC,PCHIP}}$	0.033 ± 0.019	0.032 ± 0.017	0.359	0.306	$2.30 \cdot 10^{-4}$	$2.16 \cdot 10^{-2}$
$(\widetilde{D}_{8})_{\text{FAIL,PCHIP}}$	0.034 ± 0.016	0.045 ± 0.034	0.726	1.502		
$D(V_1)_{\text{SUCC}}$	0.065 ± 0.028	0.064 ± 0.028	0.860	0.839	$9.04 \cdot 10^{-2}$	$5.50 \cdot 10^{-3}$
$D(V_1)_{\text{FAIL}}$	0.075 ± 0.040	0.078 ± 0.033	0.920	0.758		
$(\text{NMSE}_3)_{\text{SUCC}}$	10.2 ± 10.0	9.6 ± 10.6	0.362	0.382	$8.61 \cdot 10^{-1}$	$6.23 \cdot 10^{-2}$
$(\text{NMSE}_3)_{\text{FAIL}}$	21.2 ± 25.4	21.5 ± 30.7	0.274	0.332		

drawn when the PCHIP interpolation is introduced into the atrial amplitude algorithm. However, we can interestingly remark that the parameter $\widetilde{D_{8PCHIP}}$ presented in [106] and herein discussed in Sec. 4.3, is able to effectively quantify CA impact over AF dynamics as assessed in Sec. 4.6.4, since median f-wave amplitude descriptor decreases if CA is effective, otherwise it rises. The linear relationships computed are statistically different from each other, despite the lack of linearity of these features, which can be due to the limited number of sample (especially in the group of failing CA procedures) and the influence of certain outliers (among patients experiencing procedural AF termination), as shown in Fig. 4.8. For the sake of completeness, regression analysis of $\widetilde{D_{8PCHIP}}$ has been also performed in the short-term follow-up context. Indeed, in Fig. 4.8 we can remark that also in shorter follow-up windows actual amplitude data are not accurately fitted by a linear law. In addition, slope values are lower than 1 both when dealing with successful CA procedures (CA beginning: $(\widetilde{D}_8)_{\text{START,PCHIP}} = 0.038 \pm 0.019$; CA conclusion: $(\widetilde{D}_8)_{\text{END,PCHIP}} = 0.032 \pm 0.09$) and failing interventions ($(\widetilde{D}_8)_{\text{START,PCHIP}} = 0.015 \pm 0.007$, $(\widetilde{D}_8)_{\text{END,PCHIP}} = 0.019 \pm 0.009$), thus contradicting our hypothesis about the link between f-wave amplitude variations and procedural outcome. This experimental session also highlights how difficult it is to generalize AF dynamics during CA due to the wide variety of factors differentiating the short-term follow-up period (such as postoperative inflammations, edemas, anesthesia) from the long-term phase (complementary cardioversions therapies, atrial remodeling). In addition, similarly to classification tasks, regression analysis is hampered by the examination of unbalanced categories, thus the need to validate these results on larger databases, in particular with more data related to failing CA procedures.

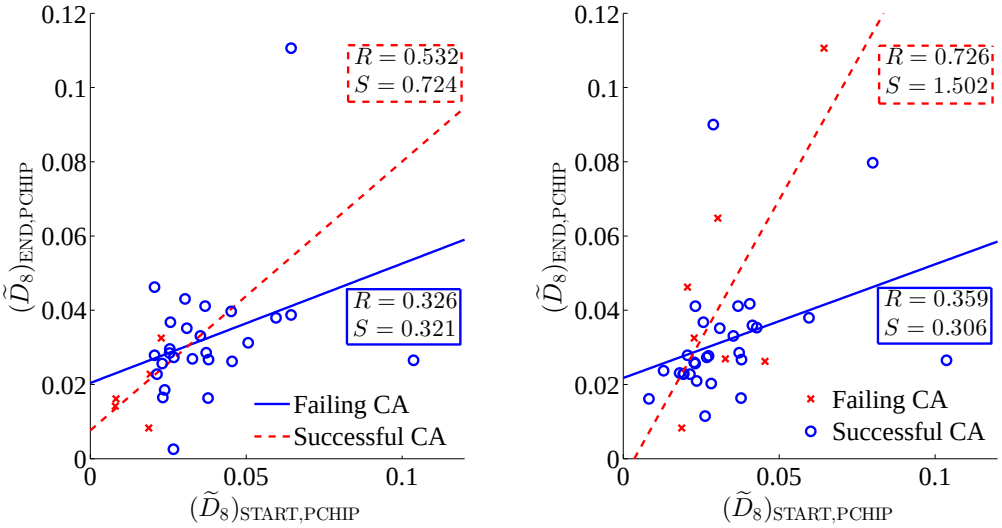


Figure 4.8: Scatter plot of $(\widetilde{D}_8)_{\text{START,PCHIP}}$ as a function of $(\widetilde{D}_8)_{\text{END,PCHIP}}$ and data regression lines associated with each category (successful CA: 'O', continuous line; failing CA: '×', dotted line). (Left) Short-term follow-up; (Right) Long-term follow-up.

4.7 SUMMARY AND CONCLUSIONS

In this chapter, the role of f-wave amplitude as a predictor of CA outcome in persistent AF has been investigated. In particular, its spatial distribution has been assessed on standard ECG, thus exploiting its multilead properties and overcoming the limited perspective of traditional single-lead methods. In addition, amplitude measures are uniquely determined and objective, since the algorithms proposed are fully automatic. Indeed, the introduction of signal interpolation techniques considerably improves amplitude computation accuracy, and f-wave global trend is effectively rendered. In addition, we demonstrated that reduced-rank approximations determined by PCA are able to capture the most descriptive components of the AA signal, which are relevant to f-wave amplitude characterization. Statistical measures of this ECG feature are found to be able to discriminate between successful and failing CA procedures, thus predicting acute AF termination, as illustrated in Sec. 4.3. The extension of such results to long-term CA outcome prediction is then carried out in Sec. 4.5. Finally, spatial diversity of f-wave peak-to-peak amplitude has been probed on standard ECG in combination with temporal dynamics within CA procedural time. Linear regression analysis allows for quantification of CA effects on heart substrate, which are found to be correlated with CA outcome, as demonstrated in Sec. 4.6.

Despite the effectiveness of our methods for f-wave amplitude characterization a CA outcome prediction, they merely extract an average information about f-wave amplitude without taking signal variability into account. To this goal, an attempt in this direction has been made in Sec. 4.6 by characterizing AF evolution between two distinct procedural moments. However, combining spatial information with knowledge about temporal AF variability could be of interest for our application, as we could expect a relation between signal variability and ablation results. In the next chapter, we investigate whether it is possible to assess AF temporal variability also within a specific moment of ablation (in

particular, the early beginning) and attempt to exploit such information to perform CA outcome prediction.

5 Multilead decompositions of ECG signal for STV feature definition in CA outcome prediction

5.1 Introduction

As we recalled in Sec. 3.3.3, the mechanisms underlying AF are not yet fully understood. Indeed, AF has a complex pathophysiology, with various substrates and mechanisms interacting in a complex fashion. This arrhythmia has long been described as a disorganized or "random" phenomenon [78, 111]. However, more recent works have highlighted the existence of an underlying structure behind the apparent chaos [22], depending on myocardium anatomy, electrophysiological properties, and autonomic innervation [94]. Several factors influence this activity, including age, simultaneous occurrence of other pathologies and effects of atrial remodeling due to disease chronification. Knowledge about AF organization has a crucial clinical value, as it can help clinicians determining the mechanisms triggering AF and choosing the most suitable therapy [47, 53]. Furthermore, spatiotemporal mapping of AF organization could enhance recognition of wave patterns and evaluate their correlation with atrial functional and structural properties [94].

Several attempts at quantifying AF organization have been made in previous studies. However, most of them focus on endocardial recordings, which are invasively acquired and mainly provide quite a local perspective of heart electrical activity [21, 48]. Other works [4, 18, 150] have rather explored surface recording properties so as to assess AF complexity noninvasively. Nevertheless, analysis is usually led in only one ECG lead, therefore potential clinical information from other leads could not be taken into account. Yet in [19] it has been demonstrated that atrial spatial variability manifests itself, and thus can be measured, on surface recordings. AF variability has been explained not only according to its temporal evolution, namely, in terms of the temporal repetitiveness of its pattern, but also by taking into account its spatial distribution over heart substrate, which can be easily observed on surface ECG signals, due to the different locations of recording electrodes.

So far, information about AF organization and its intrinsic variability has not been directly exploited for assessing AF therapy effects, in particular CA outcome. In fact, we could expect that CA treatment could influence the degree of pattern complexity when converting AF to SR or other more organized arrhythmia (for instance, AFL). Conversely, we could also suppose that more variable and irregular atrial waveforms hint more complex in-depth phenomena, which are more difficult to be treated by CA, whose effectiveness strongly depends on the correct detection of AF sources.

In the light of these considerations, this chapter tries to shed some light on spatio-

temporal variability (STV) of AF as assessed on the 12-lead ECG and investigate its links with AF therapy outcome. Henceforth, after an overview about classical methods for STV characterization in Sec. 5.2, we develop our multilead framework and their application to CA outcome prediction in persistent AF. Several multivariate techniques have been investigated for characterizing AF STV content in CA outcome prediction, with particular attention to PCA, weighted PCA (WPCA) and nonnegative matrix factorization (NMF) in Sec. 5.3, Sec. 5.4 and Sec. 5.5, respectively. Some general conclusions about AF STV investigation are drawn in Sec. 5.7.

5.2 Motivation and links with AF organization

Since a unified definition of AF organization has not been given yet, this concept has been widely employed to characterize different but complementary properties of heart electrical activity during AF, such as the repetition rate of atrial activations, correlation among atrial electrograms, and the level of morphology similarity of waveforms recorded at several atrial sites [94].

Measures of STV content have been mainly applied to classification of AF organization into different categories after visual inspection of waveform size, shape, polarity, amplitude, and beat-to-beat intervals, first observed on atrial electrograms (AEG). The degree of organization of AF wavefronts propagating inside the atria has been traditionally examined on intracardiac recordings. In [161] bipolar atrial electrogram signals have been classified on the basis of the AEG morphology and the nature of its baseline into 4 types, presented in Sec. 3.3.5. The same section also recalled another classification system widely employed in clinical centers and put forward in [78], based on the evaluation of AF frequency and irregularity by means of high resolution epicardial mapping of the RA free wall, as well as the incidence of continuous electrical activity and reentry.

As stated in Sec. 3.3.3, other models also tried to explain AF activity as the result of interactions between multiple wandering atrial wavelets [111]. Further studies have then confirmed the potential role of pulmonary veins (PVs) as an important source of spontaneous electrical activity initiating AF [62, 69].

The need for a systematic and quantitative evaluation of AF organization has prompted the development of several mathematical tools. As a consequence, different criteria and measures have so far been proposed for assessing this characteristic of AF pathology. The rationale is to investigate evidence of some underlying structure in atrial activity during AF. The wide variety of methods proposed in the literature makes it difficult to compare and interpret such indices.

In [21] the level of spatial correlation between multiple activation sequences is correlated with AF presence, and enables selection of antiarrhythmic drug therapy for SR maintenance. In [48], AF morphology characterization based on PCA and automatic clustering provides a quantitative tool for AF classification. The study described in [123] also proposes more advanced techniques for feature extraction and SVM-classification to perform the same task. Other approaches focus on temporal regularity of atrial activations and assess AF complexity according to the level of beat-to-beat variability [95]. More recently, time-frequency analysis has been applied to intracardiac recordings for paroxysmal AF analysis in [126]. Despite their effectiveness, such approaches are all invasive. Furthermore, even though information provided by endocardial recordings is local,

thus very accurate, in certain cases AF analysis could benefit from a wider perspective of heart electrical activity, accounting for multiple sites and their interaction. Noninvasive recordings can render a global vision of AF dynamics and noninvasively provide measures of heart electrical activity. Some nonlinear measures based on sample entropy [130] computed on surface ECG have also been exploited to predict spontaneous paroxysmal AF termination [4]. This study also claims that more organized AF patterns as quantified by this index predict AF termination by CEE. The main drawback of these indices is that they are computed in only one ECG lead, thus potential information about AF complexity provided by the remaining leads is not exploited.

Recent attempts to exploit ECG spatial properties have been made in [150] by combining frequency and complexity measures, in order to discriminate between persistent and long-standing AF. Also, in [57] wavefront propagation maps extracted on BSPM recordings have been used for visual classification of AF complexity types according to Konings' criteria [78]. This research prompted a quantitative multilead analysis in [18], and underlines that AA spatio-temporal organization can be effectively represented by the first few PCs determined by PCA, retaining most of the total variance, thus quantifying the similarity between the principal subspaces of the AA signal along consecutive time segments.

An attempt of assessment of AF therapy effects by means of complexity measures has been subsequently performed in [19], which demonstrated that AF complexity estimated in lead V_1 decreases after CA performance. Nevertheless, analysis is still limited by the single-lead perspective and therefore most of multilead ECG spatial content is not entirely exploited. Furthermore, no correlation with procedural outcome has been demonstrated.

In this chapter we take a step from past works focusing on AF complexity in order to outline this property in a multilead framework, thus stressing the descriptive power of spatial diversity typical of standard ECG. Indeed, it is widely known that measures of AF organization depict its level of chronification, which profoundly influences the choice of the therapy. On the other hand, the therapy itself modifies the heart substrate, and thus the degree of complexity of the arrhythmia, as confirmed by [60]. In this thesis we show that therapy-induced changes are reflected on STV content as measured by our noninvasive multilead indices. We also demonstrate that such indices, measured before CA, can predict its outcome, hence they can be a useful tool for an improved patient-tailored management of AF.

As stated in the previous section, PCA decomposition has already been applied both to endocardial [48] and surface recordings for AF analysis [19, 57]. In Sec. 4.3 PCA has been performed on standard ECG in order to describe f-wave amplitude spatial distribution. Similarly, PCA could help estimating how AF organization is distributed over heart substrate thanks to different lead locations. Such complexity can be rendered by its temporal evolution along ECG recording, namely, by evaluating the degree of temporal repetitiveness of signal patterns. To this end, we split the multilead AA signal $\mathbf{Y}_{\mathrm{AA}}$ in Eq. (4.1) in a fixed number S of equal-length segments (see Fig. 5.1), each containing $N_S = [N/S]$ samples, so that $\mathbf{Y}_{\mathrm{AA}} = [\mathbf{Y}^{(1)}, \mathbf{Y}^{(2)}, \ldots, \mathbf{Y}^{(S)}]$, with $\mathbf{Y}^{(s)} = [\mathbf{y}((s-1)N_S+1), \mathbf{y}((s-1)N_S+2), \ldots, \mathbf{y}(sN_S)], \quad s = 1, \ldots, S$. We can thus fix a reference segment $r \neq s$, so as to assess the persistence or repetitiveness of the components of the AA signal $\mathbf{Y}^{(r)}$ over the length of the whole recording.

In the next sections, some multivariate approaches for extracting STV content from the AA signal are illustrated. We explain how such information can be mathematically

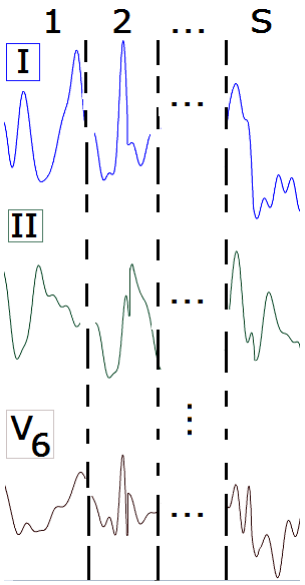


Figure 5.1: Repartition of the multilead AA signal in segments for STV content extraction.

assessed on the 12-lead ECG, and results of their application to CA outcome prediction in persistent AF are also provided and discussed.

5.3 Multilead STV predictors in the PCA framework

Taking a step from [18], we assume that components of the reference segment r in the ECG signal can be extracted by applying a linear transformation:

$$\mathbf{Y}^{(r)} = \mathbf{M}^{(r)}\mathbf{X}^{(r)} \tag{5.1}$$

Subsequently, a fixed number n of columns $\mathbf{M}_n^{(r)}$ is extracted from the mixing matrices $\mathbf{M}^{(r)}$ computed by PCA in this reference interval. Such columns, the so-called principal directions, weight the relative spatial contribution of the PCs to the ECG leads. After these steps, AA signal is estimated in all other segments $s \neq r$ by projecting $\mathbf{Y}^{(s)}$ on the subspace spanned by the columns of $\mathbf{M}_n^{(r)}$ computed in r, thus yielding:

$$\widehat{\mathbf{Y}}_n^{(s,r)} = \mathbf{M}_n^{(r)}[\mathbf{M}_n^{(r)^T}\mathbf{M}_n^{(r)}]^{-1}\mathbf{M}_n^{(r)^T}\mathbf{Y}^{(s)} \tag{5.2}$$

that is, the orthogonal projection of $\mathbf{Y}^{(s)}$ on the span of $\mathbf{M}_n^{(r)}$. In the light of these considerations, we expect that the closer the estimation as defined in Eq. (5.2) to the reference signal, the more persistent this atrial component throughout the recording, thus suggesting a sort of repetitiveness of the pattern, hence a higher level of organization. Therefore, the approximation quality can be generally evaluated by means of the normalized mean square error $\mathrm{NMSE}_\ell^{(s,r)}$ between the actual signal $y_\ell^{(s)}(t)$ on the ℓth lead and its

estimation $\widehat{y}_{\ell,n}^{(s,r)}(t)$:

$$\mathrm{NMSE}_{\ell,n}^{(s,r)} = \frac{\sum_{t=(s-1)N_S+1}^{sN_S} [y_\ell{}^{(s)}(t) - \widehat{y}_{\ell,n}^{(s,r)}(t)]^2}{\sum_{t=(s-1)N_S+1}^{sN_S} [y_\ell^{(s)}(t)]^2} \tag{5.3}$$

with $\ell = 1, \cdots, L$. In [18] it was shown that more organized AA waveforms needed fewer PCs to be approximated with an adequate level of accuracy. Consequently, for sufficiently low values of n, an inverse relationship between NMSE and AF organization was remarked, since the higher the NMSE value, the more disorganized AA. That study investigated the recurrence of the components related to the first segment, therefore the mean NMSE is computed by setting $r = 1$, and averaging Eq. (5.3) over the remaining segments ($s = 2, \ldots, S$). Nevertheless, this index has been computed in only one fixed ECG lead, V_1, which exhibits the largest atrial-to-ventricular amplitude ratio, as previously stated [129]. Yet its proximity to the right atrial free wall may neglect useful information about other sites, in particular the left atrium and the PVs, which play a crucial role in AF initiation and maintenance [62]. This observation prompts us to consider other leads in order to yield a global view of AA evolution.

5.3.1 COMBINATION OF NMSE INDICES IN A MULTILEAD FRAMEWORK

After PCA performance, we investigate how to properly combine NMSE values computed on each ECG lead so as to extract predictive information about AF therapy outcome. To overcome issues affecting previous studies, we propose computing the mean value $\mu_{\ell,n}$ and the standard deviation $\sigma_{\ell,n}$ of $\mathrm{NMSE}_{\ell,n}^{(s,r)}$ values over all possible combinations of estimated and reference segments (s, r), for each lead ℓ [101]. Index $\mu_{\ell,n}$ offers a global perspective of segment estimation performance, whereas $\sigma_{\ell,n}$ gives a measure of AF inter-segment variability along the recording. Contributions from the L leads analyzed are thereby combined into the interlead NMSE weighted sum:

$$\widetilde{\mu}_{\mathrm{PCA}_L} = \sum_{\ell=1}^{L} \frac{\mu_{\ell,n}}{\sigma_{\ell,n}^2} \Big/ \sum_{\ell=1}^{L} \frac{1}{\sigma_{\ell,n}^2} \tag{5.4}$$

whose weights are represented by NMSE inverse variance values $\frac{1}{\sigma_{\ell,n}^2}$ per lead; contributions coming from ECG leads rendering more regular and less dispersive patterns are thus considered to be more relevant. A further interpretation of $\sigma_{\ell,n}$ can be given in terms of uncertainty: low standard deviation values render a more stable reconstruction across time segments, whereas high values denote higher projection error uncertainty. Accordingly, leads guaranteeing a more robust AA content characterization have a stronger influence in the computation of the output descriptor. The choice of such weights can be further justified if we assume that the complexity information is reflected on the ensemble of ECG leads as a set of independent random variables. The best linear minimum-variance unbiased estimator of the complexity descriptor will thus be given by the weighted mean of Eq. (5.4) [75]. As a result, greater weight is given to values coming from lower-variance distributions. The flow chart in Fig. 5.2 summarizes the main processing stages of our method.

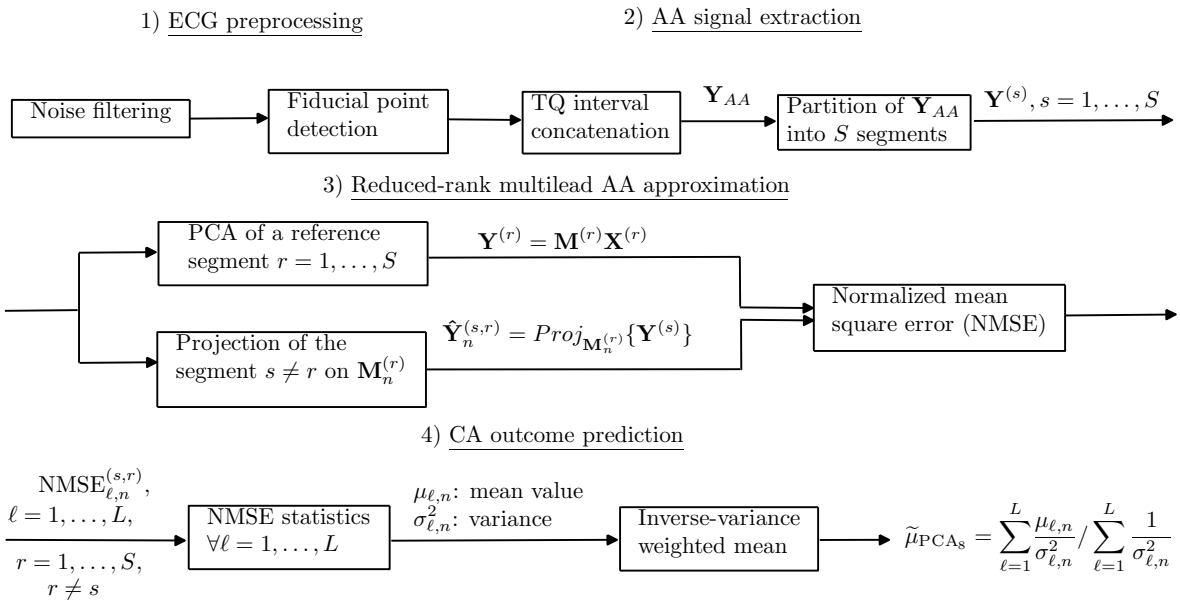


Figure 5.2: Diagram flow chart of the algorithm returning the inverse-variance weighted mean $\widetilde{\mu}_{\mathrm{PCA_8}}$ as a CA outcome predictor.

5.3.2 Setting the NMSE tuning parameters

Some parameters of the NMSE index need to be set prior to its computation, namely, the number S of AA segments which need to be processed, and the number of spatial topographies n retained for AA signal estimation. In particular, the choice of the adequate number of segments S must be accomplished by keeping their length N_S sufficiently high for AF pattern analysis. Accordingly, we investigated how the proposed NMSE index $\widetilde{\mu}_{\mathrm{PCA}_L}$ varies when changing S value. The number of samples per segment N_S is kept constant and equal to a specific value from the set $N_S = [1000200030004000]$. The corresponding evolution is displayed in Fig. 5.3. The feature keeps quite a constant value when S increases, thus proving its robustness to the choice of this parameter. In Fig. 5.3 we also examine how this measure varies as a function of N_S instead, once set the number S of segments. Also in this case the NMSE-based predictor proves its robustness to tuning parameters, since its variations are quite limited (below 10%) when S varies, regardless of the number of segments examined. In the light of this experimental evidence, a unique number of segments S has been set for all patients so as to generalize algorithm tuning.

Findings illustrated in Sec. 4.4.3 show that not only that the dominant PCA source retains the most of the AA global variance, but that it is also able to explain the most relevant components to CA outcome prediction as proved by the decreasing trend of the AUC index as a function of the truncation rank n shown in Fig. 4.5 in Sec. 4.4.3. Further experimental results are presented later in the chapter and support the choice of setting $n = 1$, so the corresponding subscript will be omitted in the sequel for convenience. Only the subscript PCA is kept as a reference to the type of decomposition applied (for further comparisons with other techniques in the following sections), as well as the one indicating the number of leads L employed (either $L = 8$ or $L = 12$).

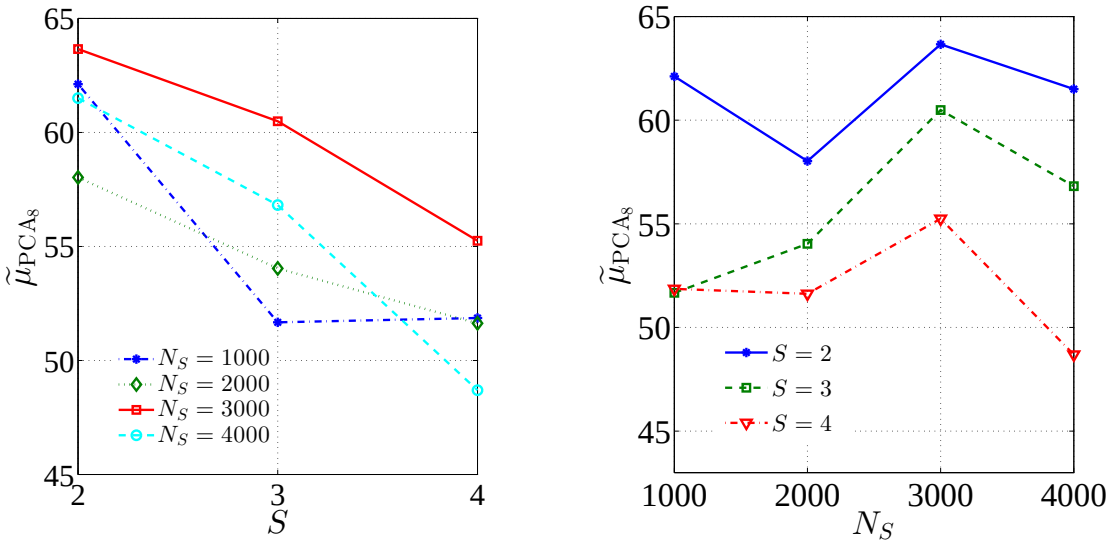


Figure 5.3: Evolution of the inverse-variance weighted mean $\widetilde{\mu}_{\mathrm{PCA}_L}$ as a function of NMSE tuning parameters. (Left): the number of segments S, for a fixed number N_S of samples per segment. (Right): the number N_S of samples per segment, for a fixed number S of segments. The index is determined on the rank-1 ($n = 1$) approximation to the 8-lead AA signal ($L = 8$).

Table 5.1: PCA characterization of STV content: interpatient statistical analysis and CA outcome prediction performance (n.u.: normalized units).

	AF termination	Non AF termination	p value	AUC	Sensitivity	Specificity	Best cutoff
$\widetilde{\mu}_{\mathrm{PCA}_8}$ [n.u.]	65.68 ± 19.27	37.59 ± 21.88	**0.0082**	0.84	0.77	0.86	45.57
$\widetilde{\mu}_{\mathrm{PCA}_{12}}$ [n.u.]	65.85 ± 28.41	44.09 ± 27.49	0.12	0.76	0.85	0.71	45.57
$\mathrm{NMSE}_{\mathrm{PCA}_8}$ [n.u.]	45.56 ± 26.93	30.35 ± 26.93	0.19	0.64	0.77	0.71	49.03
$\mathrm{NMSE}_{\mathrm{PCA}_{12}}$ [n.u.]	67.80 ± 22.11	80.73 ± 14.48	0.18	0.69	0.69	0.57	69.00
$D(V_1)$ [mV]	0.08 ± 0.03	0.06 ± 0.01	**0.03**	0.80	0.62	0.86	0.05
$\mathrm{SampEn}(L_s, r_s^{(A)})$ [n.u.]	2.82 ± 0.39	3.06 ± 0.43	0.21	0.70	0.62	0.86	3.12
$\mathrm{SampEn}(L_s, r_s^{(B)})$ [n.u.]	2.42 ± 0.38	2.66 ± 0.43	0.20	0.70	0.62	0.86	2.73
$\mathrm{SampEn}(L_s, r_s^{(C)})$ [n.u.]	2.14 ± 0.37	2.39 ± 0.42	0.20	0.70	0.62	0.86	2.44
AFCL_{V_1} [ms]	139.63 ± 19.66	121.75 ± 23.83	0.09	0.71	0.62	0.71	129.87

5.3.3 METHODS AND RESULTS

The 20-patient dataset described in Sec. 3.5.5 has been employed for assessing the prediction significance of our method. In our experimental framework, AF was successfully converted to SR or other arrhythmia in $n_S = 13$ out of $n_P = 20$ patients, whereas $n_F = 7$ procedures were not effective. As shown in Fig. 5.4, the spatial distribution of the single-lead mean error $\overline{NMSE}$, averaged over all patients on every ECG lead, underlines how irregular CA outcome prediction is and how strongly it depends on electrode selection. Hence, we demonstrate that a more robust and reliable prediction performance can be provided by a multi-lead approach. In Fig. 5.4 single-lead prediction performance is assessed by the AUC index as well. For the sake of comparison, the same setting parameter values as for $\widetilde{\mu}_{\mathrm{PCA}_8}$ are adopted. We also verified how CA outcome performance is affected by variations in the value of the PCA approximation rank n; results are displayed in Fig. 5.5.

As displayed in Table 5.1, categories under examination are referred to as "AF termination" and "Non AF termination". All parameters are expressed as mean $\pm$ standard

deviation. Once verified the kind of data distribution, differences between successful and failing CA procedures were statistically determined by a suitable unpaired test. The p values output by each unpaired test are obtained under a confidence level $\alpha = 0.05$, and are also reported in the same table. Binary classification accuracy of each feature is quantified by the AUC index. Furthermore, the optimal cutoff discriminating between the two groups of patients and the related values of sensitivity and specificity are indicated.

The proposed predictor $\widetilde{\mu}_{\mathrm{PCA}_8}$ is compared with its 12-lead counterpart $\widetilde{\mu}_{\mathrm{PCA}_{12}}$. With reference to Eq. (5.3), some single-lead NMSE measures are also determined in V_1 for both groups of ECG leads, namely, $\mathrm{NMSE}_{\mathrm{PCA}_8}$ and $\mathrm{NMSE}_{\mathrm{PCA}_{12}}$, as explained in [18]. The non-linear index of AF complexity based on sample entropy presented in [5] is also computed in the same ECG leads. The length L_s of the signal sequences to be compared is set to 2, whereas the threshold of sequence similarity is equal to a fraction of AA signal standard deviation in V_1, σ_{V_1} ($r_s^{(A)} = 0.1\sigma_{\mathrm{V}_1}$; $r_s^{(B)} = 0.15\sigma_{\mathrm{V}_1}$; $r_s^{(C)} = 0.2\sigma_{\mathrm{V}_1}$).

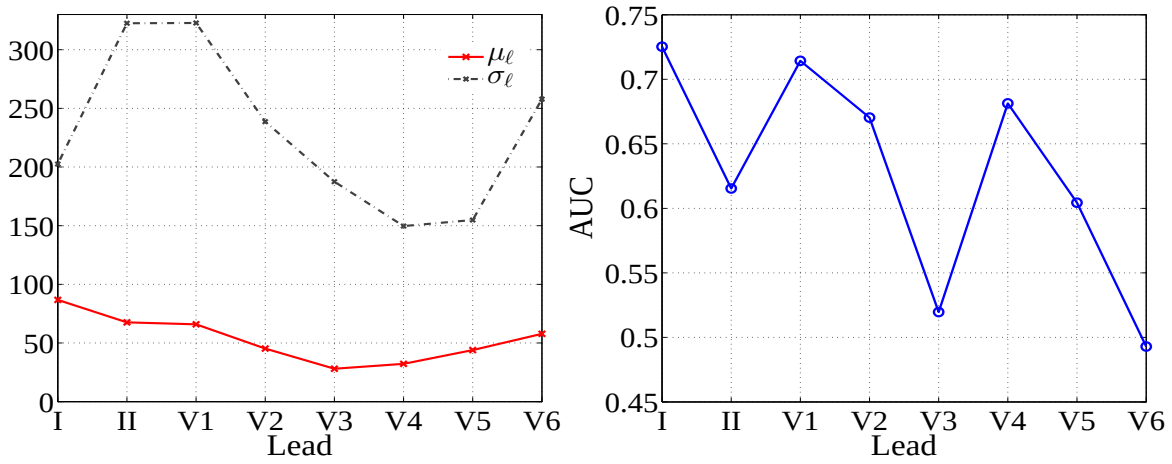


Figure 5.4: Single-lead mean NMSE as a predictor of CA outcome. (Left) Mean and standard deviation of the NMSE value $\mu\ell$, $\ell = 1, \ldots, L$ (averaged over the whole AF database) as a function of the ECG lead selected. (Right) AUC index describing the AA single-lead NMSE CA outcome prediction performance as a function of the ECG lead selected.

5.3.4 Results and discussion

The discriminative power of the NMSE-dependent parameters presented in the previous section is corroborated by experimental results. The most relevant contribution is to demonstrate the superiority of multilead strategy over standard single-lead NMSE: the inspection of NMSE spatial distribution can provide a more complete outlook of AF evolution on the heart substrate. Fig. 5.4 shows how the single-lead mean NMSE is strongly affected by the lead chosen. This variability is also confirmed by the spatial distribution of its variance, displayed in the same figure. Accordingly, CA outcome prediction performance is also affected by this choice, as highlighted by the AUC index trend in the same figure. This result supports the idea of combining all these contributions in a unique parameter offering a more global perspective of AF activity. In the weighted mean $\widetilde{\mu}_{\mathrm{PCA}_8}$ every single-lead contribution is weighed in terms of spatio-temporal dispersion.

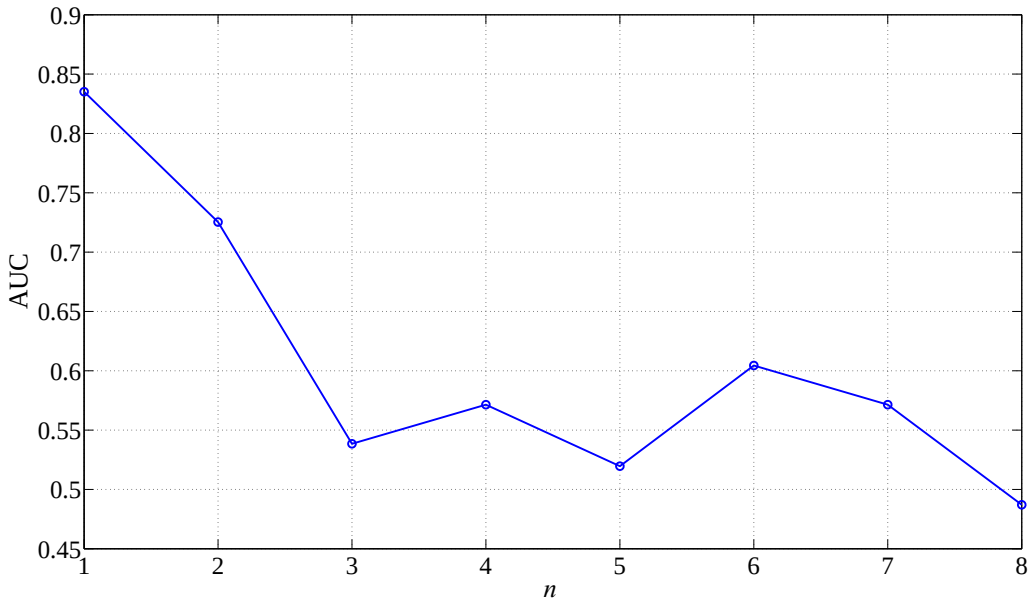


Figure 5.5: AUC values describing $\widetilde{\mu}_{\mathrm{PCA}_8}$ prediction performance as a function of the rank n of the WPCA decomposition.

Indeed, NMSE variance can be exploited as a lead selector: it detects the ECG lead providing the most stable and accurate signal reconstruction. It is worth noting that NMSE inter-segment variance can quantify the spatio-temporal degree of repetitiveness of the AA wavefront pattern: the higher NMSE dispersion among segments, the more complex and unpredictable AF pattern evolution.

PCA capability of representing AA by compressing its content into very few PCs is also confirmed by experimental evidence in Fig. 5.5, which supports our technical choice of n value. $\widetilde{\mu}_{\mathrm{PCA}_8}$ have been computed by varying the number of PCs n, which ranges from 1 (the value set for our algorithm) to 8 (full-rank decomposition, i.e., the original AA data without approximation). The quality of CA outcome prediction considerably worsens when increasing the truncation rank n. The fewer PCs employed in the decomposition, the better the classification performance, as if the dominant PCs preserved the discriminative power of the complexity index. Indeed, noisy and/or redundant elements are typically ascribed to the very last PCs, while preserving the most representative features of the AA signal. It it worth noting that this experiment has returned a similar result in Fig. 4.5 in Sec. 4.4 when characterizing f-wave amplitude, thus demonstrating once more that reduced-rank PCA approximations to AA signal can effectively retain the most discriminant components for CA outcome prediction.

Classification performance of multilead CA predictors proves to be more accurate when reduced-rank approximations are computed on the subset of 8 independent leads rather than the whole standard ECG. This is in line with results reported in Sec. 4.4. Hence, the higher predictive power of the index $\widetilde{\mu}_{\mathrm{PCA}_8}$, which outperforms its 12-lead counterpart $\widetilde{\mu}_{\mathrm{PCA}_{12}}$.

CA outcome prediction quality of our multilead descriptor of AF STV content is characterized by a higher degree of accuracy compared with traditional single-lead measures of AF complexity. Concerning single-lead AF complexity measures determined by PCA

on different sets of ECG leads, i.e., $\text{NMSE}_{\text{PCA}_8}$ and $\text{NMSE}_{\text{PCA}_{12}}$, not only statistically significant interpatient differences cannot be remarked, but AUC values related to their discrimination capability are also extremely low. These results could be explained by the limited outlook of single-lead complexity measures, which ignore interlead relationships. Relevant information from other electrodes is neglected, thus reducing discrimination capabilities. Furthermore, as lead V_1 is close to the right atrial free wall, there is the risk of ignoring useful information about other important anatomical areas, such as the left atrium and the PVs, which play a crucial role in AF initiation and maintenance [62], but do not reflect in V_1 with the same degree of significance as RA does. Also, concerning nonlinear AF complexity indices such as sample entropy, no statistically significant inter-class differences can be remarked, regardless of the values of tuning parameters. Not only sample entropy index is affected by the same shortcomings typical of the other single-lead features, but its parameters need to be fine-tuned prior to its computation.

Analysis of the AA amplitude as rendered by $D(V_1)$ arouses different remarks. Actually, we can notice the satisfactory ability to distinguish between successful and failing ablations, as well as the effective reproduction of results manually reported in previous works using a different persistent AF database [121]. Even though this descriptor can effectively capture AA signal amplitude characteristics if the pattern is sufficiently regular and f-waves are easily detectable, interpolation operations can be hampered by residual spurious peaks or very irregular patterns. What is more, no information about AF STV is provided by this feature. The study led in [98] assesses the predictive role of AFCL measured on surface ECG for CA of persistent AF. However, its measure is affected by a lack of reproducibility and prediction reliability of its measure, as it is usually manually acquired. Moreover, no significant differences are pointed out by this predictor in V_1, denoted AFCL_{V_1}. Finally, correlation between ECG-based parameters and intracardial measures of AFCL has not been confirmed in some studies [67].

One of the main shortcomings of our research is the impossibility to demonstrate the correlation between the NMSE-based predictor proposed and AF spatio-temporal organization, due to the lack of simultaneous invasive recordings. Such a connection can only be hinted at by the results presented in [18], which demonstrated such correlation in V_1. Accordingly, the potential connection with CA outcome and AF organization by means of our multilead characterization of the NMSE index should be further investigated.

5.4 Moving to the weighting perspective in the WPCA framework: weighted principal component analysis for STV quantification

As mentioned in the previous section, a possible strategy for processing multivariate standard ECG consists in searching for a reduced set of uncorrelated components retaining as much of its spatial variability as possible. To this goal, PCA has been widely applied to the ECG, due to its non-parametric nature, simplicity for implementation and versatility [29, 72, 131, 142]. Nevertheless, PCA is not always recommended in ECG processing. As it gives the same relevance to all observations, the low-rank approximation can be sensitive to outliers and become unstable. This issue affects every decomposition method based on the minimization of a criterion function in the ordinary least squares

(OLS) sense. Accordingly, in this section we explore another multivariate decomposition technique, referred to as weighted principal component analysis (WPCA), in order to improve the robustness of reduced-rank data representation and exploit its properties for CA outcome prediction [105].

5.4.1 WPCA DECOMPOSITION

The AA signal is processed as described in Sec. 5.2. Accordingly, we split the AA signal in S segments so as to quantify STV properties. Instead of classical PCA, the WPCA technique is thus applied to each reference segment $\mathbf{Y}^{(r)}$ by minimizing a weighted least squares (WLS) loss function [66] as described next. Hence, each entry of the input matrix $\mathbf{Y}^{(r)}$ is separately weighted with a fixed, nonnegative quantity. These leveraging factors can be collected in a matrix $\mathbf{W}^{(r)}$ having the same dimensions as $\mathbf{Y}^{(r)}$. The WLS loss function can be expressed as:

$$h(\widehat{\mathbf{Y}}^{(r)}|\mathbf{Y}^{(r)},\mathbf{W}^{(r)}) = \|(\mathbf{Y}^{(r)} - \widehat{\mathbf{Y}}^{(r)}) * \mathbf{W}^{(r)}\|_{\mathrm{F}}^2 = \sum_{\ell=1}^{L}\sum_{t=1}^{N}[w_\ell(t)^{(r)}(y_\ell(t)^{(r)} - \widehat{y}_\ell(t)^{(r)})]^2 \quad (5.5)$$

where $*$ stands for the Hadamard (or elementwise) product, whereas the operator $\|\cdot\|_{\mathrm{F}}$ represents the Frobenius norm. As in classical PCA, some orthogonality constraints are applied to $\mathbf{M}^{(r)}$ and $\mathbf{X}^{(r)}$ defined in Eq. (5.1) in order to reduce model ambiguities.

5.4.2 DEFINITION OF THE WEIGHT MATRIX

Special attention must be paid to the assignment of the weights collected in matrix $\mathbf{W}^{(r)}$. Indeed, an accurate choice of these values can give rise to a kind of filtering action which enhances not only the leads, but also the time samples giving the most meaningful contributions, while neglecting those that do not yield significant information or can pollute atrial observations. In the context of our application, temporal samples in each segment on the same lead are all equally treated, as we merely focus on intersegment and interlead variability. On the other hand, we aim to emphasize leads exhibiting a more stable and regular waveform while reducing the influence of those characterized by higher temporal dispersion, quantified in terms of energy. We assume that the input signal $\mathbf{Y}^{(r)}$ can be modeled as:

$$\mathbf{Y}^{(r)} = \mathbf{Y}_{\mathrm{S}}^{(r)} + \mathbf{Y}_{\mathrm{N}}^{(r)} \quad (5.6)$$

namely, as the sum of a content-bearing component $\mathbf{Y}_{\mathrm{S}}^{(r)}$ (describing AF activity in our application) and a noisy component $\mathbf{Y}_{\mathrm{N}}^{(r)}$, due not only to data acquisition noise, but also to elements discarded by the low-rank WPCA-approximation. We assume that the high dispersion level affecting the term $\mathbf{Y}_{\mathrm{N}}^{(r)} = (\mathbf{Y}^{(r)} - \mathbf{Y}_{\mathrm{S}}^{(r)})$ can alter or hide informative elements coming from $\mathbf{Y}_{\mathrm{S}}$ in each lead. This term can be regarded as the argument $\mathbf{Y}^{(r)} - \widehat{\mathbf{Y}}^{(r)}$ of the WLS criterion defined in Eq. (5.5) to be minimized according to the algorithm described afterward. To this end, each lead is weighted by the inverse of AA signal variance, thus reducing the influence of high-energy electrodes. More precisely, each row of $\mathbf{W}^{(r)}$ is weighed by the inverse of the standard deviation $\sigma_\ell^{(r)}$ associated with the corresponding lead $\ell = 1,\ldots,L$ in $\mathbf{Y}^{(r)}$ and computed on each segment $r = 1,\ldots,S$:

$$\mathbf{W}^{(r)} = [(\sigma_1^{(r)})^{-1}(\sigma_2^{(r)})^{-1}\ldots(\sigma_L^{(r)})^{-1}]^T\mathbf{1} \quad (5.7)$$

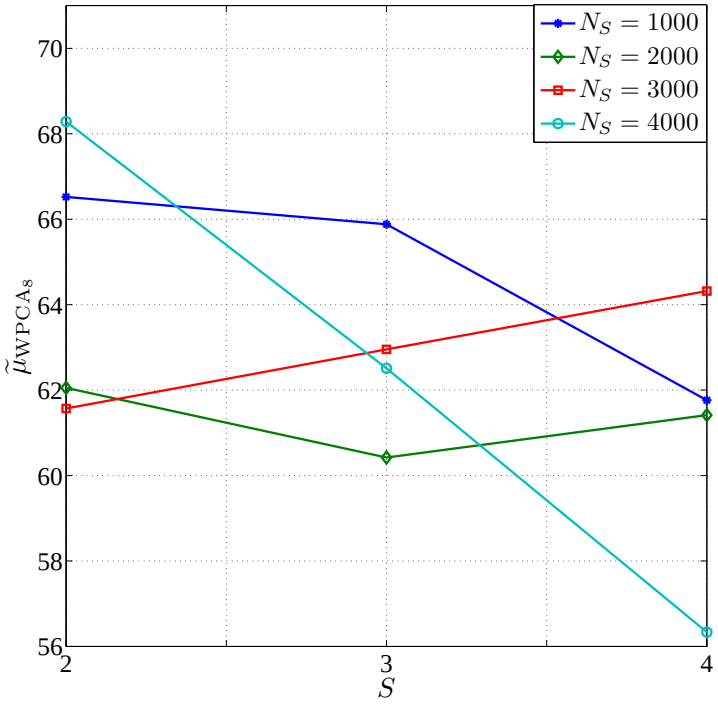


Figure 5.6: Evolution of $\widetilde{\mu}_{\mathrm{WPCA}_8}$ as a function of the number of segments S.

where $\mathbf{1}$ is a row vector with N unit entries. According to this definition, standard PCA is a special case of WPCA, where $\mathbf{W}^{(r)}$ is the unity matrix, i.e., a uniform weighting scheme. Once a weight matrix has been chosen, WPCA can be carried out by following the algorithm steps summarized in the Appendix A.2. Each reference segment r is thus processed in keeping with the WPCA model from Eq. (5.1). Then, STV feature extraction is accomplished as explained in Sec. 5.3, thus yielding the predictor $\widetilde{\mu}_{\mathrm{WPCA}_8}$ defined in Eq. (5.4) at the final step. It is worth noting that AA signal reconstruction is influenced by the choice of the weight matrix $\mathbf{W}^{(r)}$, thus the output value of the predictor will change in turn according to the weights selected. The predictive value of different forms of $\mathbf{W}^{(r)}$ will be tested in Sec. 5.4.5.

5.4.3 Choice of NMSE characteristic parameters

As in Sec. 5.3.2, NMSE requires an a priori tuning of algorithm parameters. In line with conclusions drawn for STV characterization through PCA in Sec. 4.4.1, an approximation of rank $n = 1$ has been applied to the AA signal, divided in $S = 4$ time intervals. This setting is motivated by results describing how the STV descriptor $\widetilde{\mu}_{\mathrm{WPCA}_8}$ is influenced by the values of S and N_s as for PCA, displayed in Fig. 5.6 and Fig. 5.7, respectively. Variations in this feature as a function of these parameters are quite limited, thus justifying application of our setting to the whole AF database.

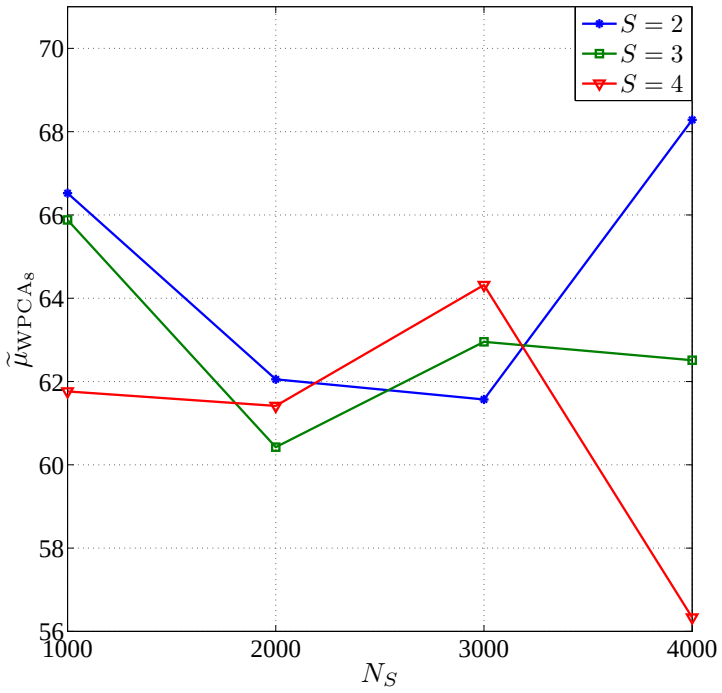


Figure 5.7: Evolution of $\widetilde{\mu}_{\mathrm{WPCA}_8}$ as a function of the number of samples per segment N_S.

5.4.4 WPCA COMPUTATIONAL LOAD

As WPCA is an iterative algorithm (described in Appendix A.2), a stopping criterion has been introduced, that is to say, the converge tolerance $\epsilon = 10^{-5}$. In order to assess WPCA computational load, the number of iterations for convergence and the final value of WLS convergence criterion C^* (defined in Eq. (7) in Appendix A.2) are determined for a fixed N_S value. These values are first computed on each segment $s = 1, \ldots, 4$ and then averaged over the 20-patient database presented in Sec. 3.5.5. Test results are reported in Table 5.2. We can remark that both parameters do not significantly vary when changing the segment to be processed, and that computational burden is relatively low in terms of iterations. A similar result is obtained when considering variations in the number of samples per segment N_S. This further evidence supports the robustness of our method to the choice of tuning parameters, and guarantees its convergence to solution.

5.4.5 ANALYSIS OF CA OUTCOME PREDICTION THROUGH WPCA AND RESULTS

The predictive power of the STV features determined by means of WPCA are tested on the 20-patient database aforementioned. Our 8-lead descriptor $\widetilde{\mu}_{\mathrm{WPCA}_8}$ is compared with its 12-lead counterpart $\widetilde{\mu}_{\mathrm{WPCA}_{12}}$. Results of the unpaired statistical test are reported in Table 5.3. AUC analysis results are validated by means of the LOOCV technique and are also herein indicated. Fig. 5.8 plots the AUC values describing the classification performance of $\widetilde{\mu}_{\mathrm{WPCA}_L}$ as a function of the number L of leads retained in the analysis. For each value of L ranging from 2 up to 8, $\widetilde{\mu}_{\mathrm{PCA}_L}$ value has been computed for all $8!/((8-L)!L!)$ possible ensembles of leads. CA outcome prediction performance has

Table 5.2: Assessment of WPCA convergence characteristics. (Top) Average number of iterations for convergence, with the stop threshold $\epsilon = 10^{-5}$. (Bottom) Average final value of WLS convergence criterion C^* (Eq. (7) after convergence, with $\epsilon = 10^{-5}$, [n.u.]). Criterion values normalized by a scaling factor equal to 10^{-6}.

N_S \ s	1	2	3	4
Average number of iterations				
1000	96	84	114	93
2000	92	100	92	96
3000	84	90	92	103
4000	85	98	101	112
C^*				
1000	9.0	8.8	9.1	8.9
2000	8.8	9.0	8.6	9.2
3000	8.6	9.1	9.1	8.7
4000	9.0	8.9	8.9	9.0

Table 5.3: Long-term CA outcome prediction through the WPCA decomposition: inter-patient statistical analysis and ROC assessment (n.u.: normalized units).

	AF termination	Non AF termination	p value	AUC	Sensitivity	Specificity	Best cutoff
$\widetilde{\mu}_{\mathrm{WPCA}_8}$ [n.u.]	70.76 ± 17.74	37.54 ± 20.01	**0.0013**	0.91	0.85	0.71	40.64
$\widetilde{\mu}_{\mathrm{WPCA}_{12}}$ [n.u.]	63.03 ± 18.12	61.64 ± 20.87	0.88	0.47	0.62	0.43	53.76

then been assessed for each lead combination from the corresponding values of $\widetilde{\mu}_{\mathrm{WPCA}_L}$, and validated by the LOOCV technique. As already done in Sec. 4.4.3, for each size L, the minimum, maximum and mean AUC values over all L-lead subsets are obtained as a function of the subset dimension L, and their related ranges of values are displayed in Fig. 5.8. The lead combinations with the best prediction performance for each subset dimension are shown in Table 5.4. The same type of analysis is performed on the descriptor $\widetilde{\mu}_{\mathrm{PCA}_L}$ obtained after PCA data approximation for sake of comparison. The case $L = 1$ has been excluded from this test, since in this case the method is equivalent to single-lead analysis.

In our application, we deal with multivariate decomposition techniques based on the maximization of the variance of the AA signal, conveying information about AF spatio-temporal distribution. Consequently, another crucial point of our investigation is understanding how these techniques act on AA signal energy content. More precisely, the input

Table 5.4: ECG lead subsets with optimal prediction performance of $\widetilde{\mu}_{\mathrm{PCA}_8}$ and $\widetilde{\mu}_{\mathrm{WPCA}_8}$.

Number of leads (L)	**Leads (PCA)**	**Leads (WPCA)**
2	I, V_1	I, V_1
3	V_3, V_4, V_6	I, II, V_2
4	V_1, V_3, V_4, V_6	I, V_2, V_3, V_5
5	[II, V_2, V_3, V_4, V_5] [V_2, V_3, V_4, V_5, V_6]	[I, II, V_2, V_4, V_5] [I, II, V_1, V_3, V_6]
6	I, V_2, V_3, V_4, V_5, V_6	I, II, V_2, V_3, V_4, V_6
7	[I, II, V_1, V_2, V_3, V_4, V_6] [I, II, V_1, V_2, V_3, V_5, V_6]	I, II, V_1, V_2, V_3, V_4, V_5

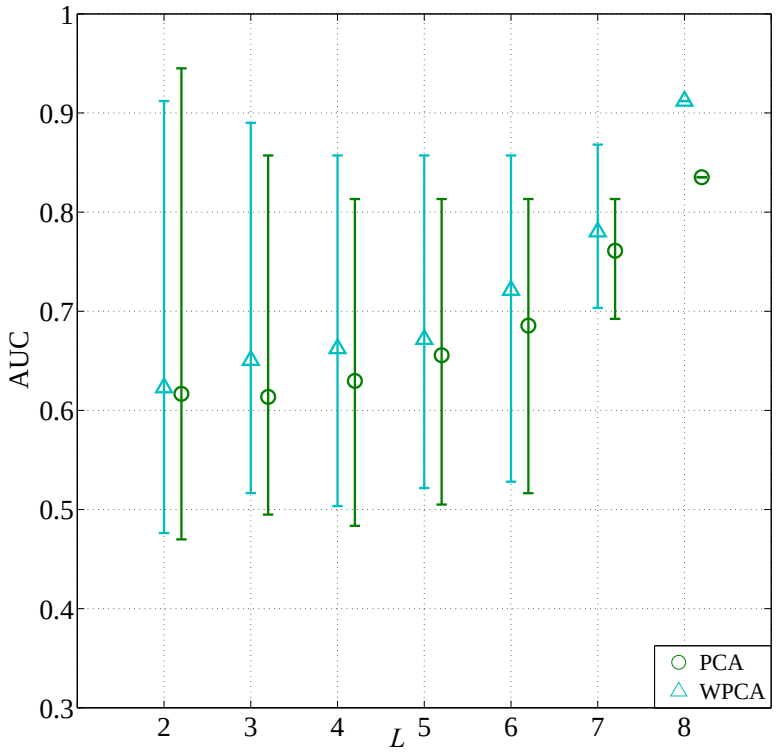


Figure 5.8: AUC values characterizing $\widetilde{\mu}_{\mathrm{WPCA}_L}$ prediction performance as a function of the size L of the subset of the 8 independent ECG leads ($S = 4$, $n = 1$). WPCA: rank-1 decomposition of the atrial signal in the ECG lead subsets according to the WPCA model; PCA: rank-1 decomposition of the atrial signal in the ECG lead subsets according to the PCA model.

AA signal variance has been computed on each ECG lead, thus obtaining the components of atrial power distribution forming the vector $\sigma^2_{\mathrm{AA}} = [\sigma_{AA_1}^2, \sigma_{AA_2}^2, \ldots, \sigma_{AA_L}^2]^T$, with $L = 8$. Effects of the multilead weighting scheme on the decompositions of AA observations are also compared to those obtained by standard PCA. The rank-1 approximations $\widehat{\mathbf{Y}}$ are computed by WPCA and PCA and averaged over all patients. The resulting power distribution vectors σ^2_{WPCA} and σ^2_{PCA} are plotted in Fig. 5.9. Following this line, this evaluation has been accomplished in the framework of CA outcome prediction as well. In particular, we tested whether AA signal energy σ^2_{AA} associated with each lead can effectively perform as a predictor of the ablation result; hence, the quantification of their classification accuracy on each ECG lead by means of the AUC criterion, whose values are displayed in Fig. 5.10. The same analysis is led on the energy values computed on the rank-1 approximations output by PCA and WPCA, σ^2_{PCA} and σ^2_{WPCA}, respectively, resulting in the AUC values also plotted in Fig. 5.10. Effects of WPCA truncation on CA outcome prediction are also assessed by the AUC criterion, whose evolution as a function of the decomposition rank n is plotted in 5.11. Finally, further tests confirm the validity of the model introduced in Eq. (5.6) by assessing CA outcome prediction performance on the basis of different definitions of the weight matrix $\mathbf{W}^{(r)}$ and comparing analysis results in Sec. 5.4.6.

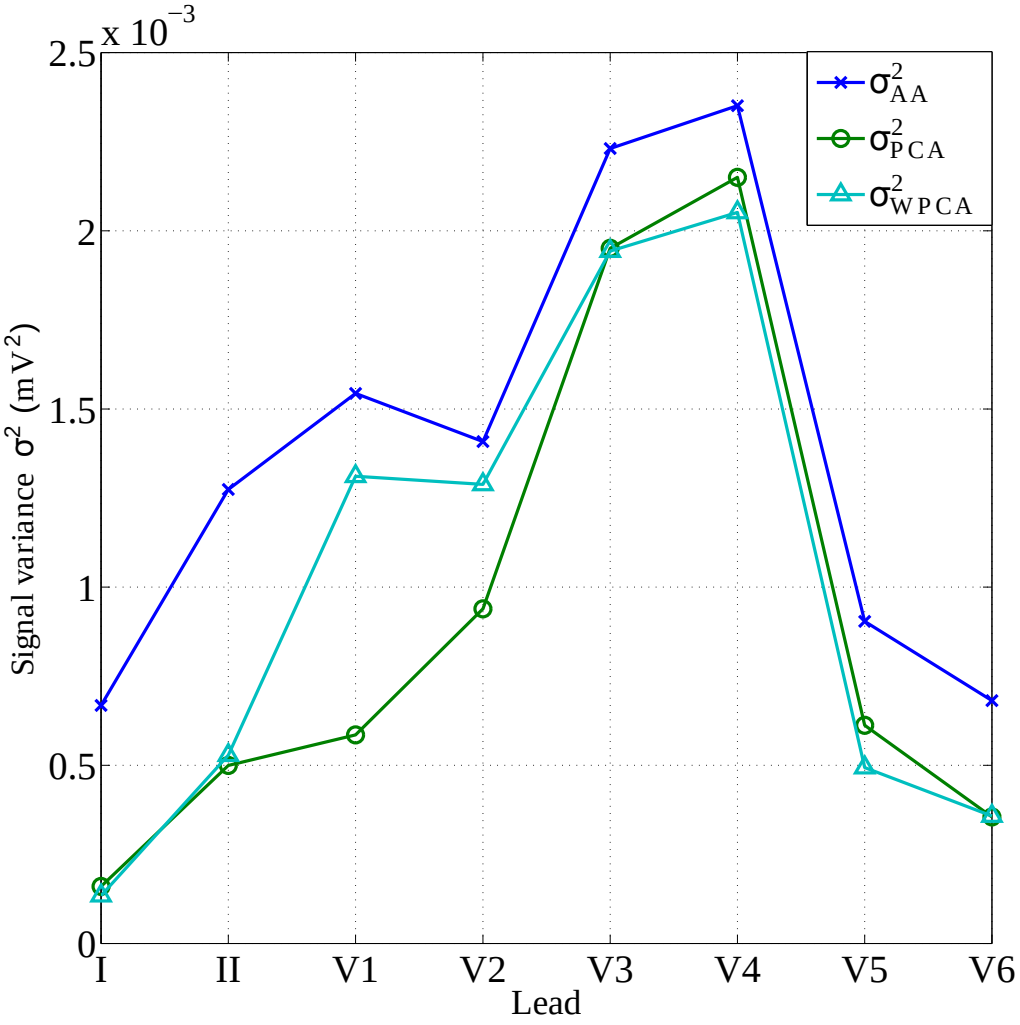


Figure 5.9: Effects of the multilead weighting scheme on AA reconstruction. σ^2_{AA}: variance of the input AA signal per lead; σ^2_{PCA}: variance per lead of the rank-1 AA signal approximation by PCA; σ^2_{WPCA}: variance per lead of the rank-1 AA signal approximation by WPCA.

5.4.6 Discussion

As for PCA, CA outcome prediction quality improves when the subset of 8 independent ECG leads is processed, in agreement with results in Table 5.3. The proposed index $\widetilde{\mu}_{\text{WPCA}_8}$ is able to discriminate between the groups of interest and outperform its PCA counterpart, thus proving the benefits of our a priori knowledge about atrial observations in the form of the weights used in WPCA. For both decomposition techniques, Table 5.4 displays the ensemble of leads which best help discriminating between successful and failing CA procedures based on the maximization of the AUC criterion. Except for the case $L = 2$, we can note that for a fixed subset size L the leads involved in the prediction change with respect to the method applied. As far as WPCA is concerned, lead V_1 does not generally provide the main contribution to CA outcome prediction. In fact, other leads, such as I, II, V_2, recur more frequently. This evidence is in contrast with standard

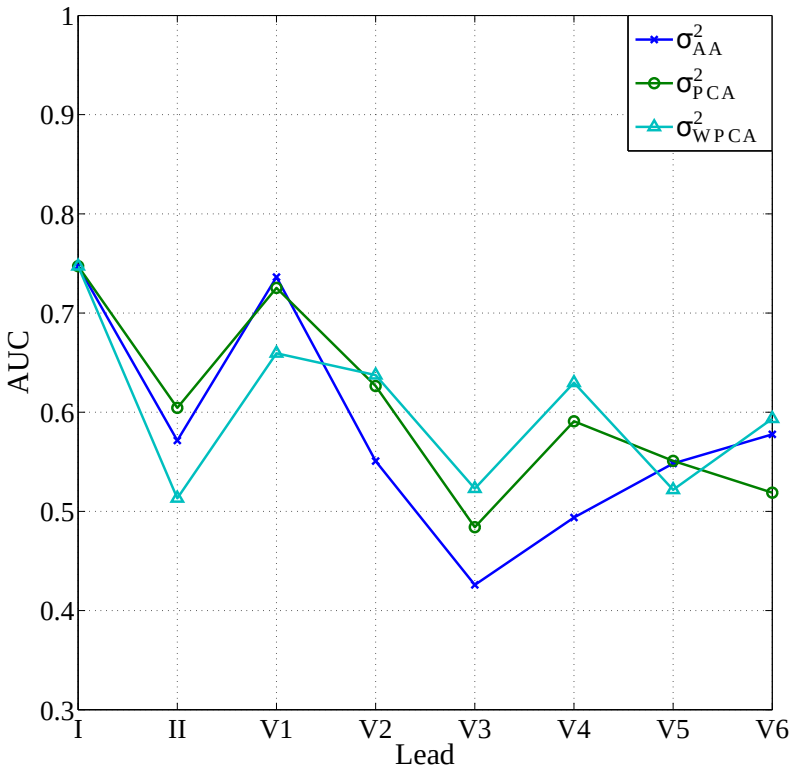


Figure 5.10: Assessment of CA outcome prediction performance of single-lead energy descriptors. σ^2_{AA}: energy per lead of the original AA signal; σ^2_{PCA}: energy per lead of the rank-1 AA signal approximation by PCA; σ^2_{WPCA}: energy per lead of the rank-1 AA signal approximation by WPCA.

medical practice, and it can be probably explained by the placement of lead V_1, not close enough to critical sites responsible for AF genesis and maintenance, such as the PVs and LA, commonly acknowledged as potential AF sources. This seems to be confirmed by the recurrence of at least one lead close to the left side of the heart in each L-size subset, for instance, V_5 and V_6. Moreover, we can note the simultaneous presence of at least one limb lead and one horizontal lead in each L-sized subset, in contrast with PCA, since some groups contain Wilson's leads exclusively. It turns out that the use of leads representing heart electrical activity on multiple planes improves prediction accuracy, which is further enhanced by the selective action of the WPCA weighting scheme.

On further analysis, AA standard deviation measured on each ECG electrode proves to be a reliable index, since it does not only weights AF temporal dispersion, but it is also a statistical measure of uncertainty. Indeed, if AA patterns on certain leads are excessively irregular and/or variable, the corresponding inverse standard deviation values automatically reduce their influence. This selective action seems to boost the compression power of the decomposition. More specifically, the effect of possible redundancies is already reduced before computing the iterative minimization algorithm by selecting the 8 linearly independent ECG leads, so that the most discriminant AA components are put into evidence more easily. In Fig. 5.8 the AUC criterion quantifies the classification performance of $\widetilde{\mu}_{\mathrm{WPCA}_L}$ and $\widetilde{\mu}_{\mathrm{PCA}_L}$ as a function of the number of ECG leads L exploited

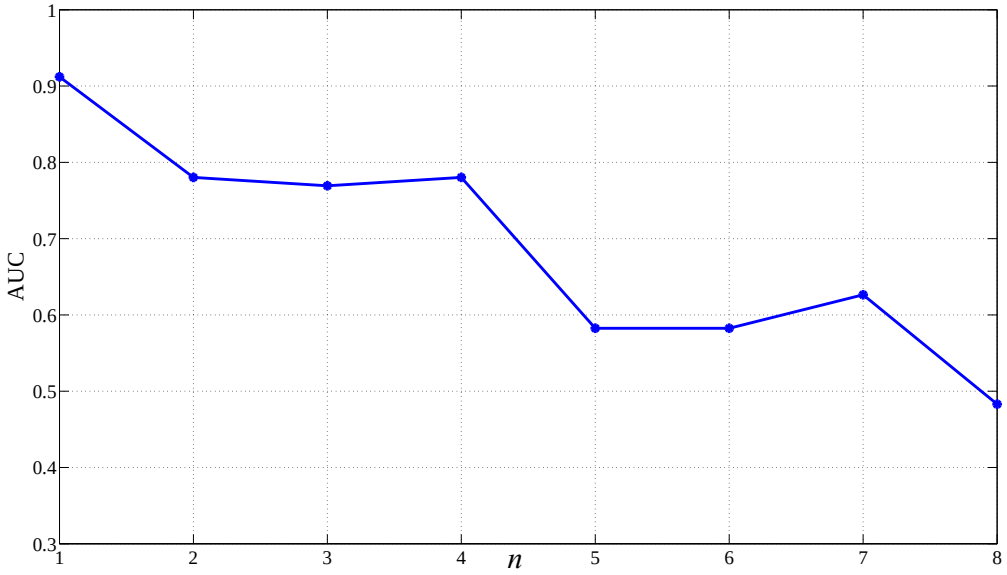


Figure 5.11: AUC values describing $\widetilde{\mu}_{\mathrm{WPCA}_8}$ prediction performance as a function of the rank n of the WPCA decomposition.

for the prediction selected among the 8 independent leads. Classification results obtained using WPCA in terms of mean AUC outperform those by PCA, especially as size L increases. This figure also confirms the benefits derived from the spatial variability of the standard ECG. The higher the number of leads employed, the more accurate CA result prediction, assessed by higher mean AUC values.

Further advantages derived from the weighting framework are displayed in Fig. 5.9. First of all, it can be noticed that the trend of σ^2_{WPCA} values is very similar to that of σ^2_{AA}. In addition, σ^2_{WPCA} values are closer to σ^2_{AA} than those obtained when performing classical PCA (σ^2_{PCA}), thereby quantifying a lower error of reconstruction of the original data for the same approximation rank. Energy values obtained after AA signal approximation, either by PCA or WPCA, are lower than those computed directly on input data because of the low-rank representation effect. It can be inferred that WPCA can better preserve energy content of the AA signal and condense it more efficiently in a single, maximum-variance PC than conventional PCA. Differences between these decompositions in terms of the amount of information retained by the rank-1 approximation are particularly evident in V_1 and V_2, which represent the reference leads for AF analysis in medical practice, owing to their proximity to the RA. Note how WPCA significantly enhances, in an automated fashion, the relevance of these leads in the AA signal decomposition. The use of these energy-descriptors in single-lead prediction does not provide satisfactory results, as shown in Fig. 5.10. Indeed, their prediction performance is poor, and also highly dependent on the lead considered. In general, these results confirm the need for an adequate combination of atrial signal contributions from different ECG leads in a more robust multilead framework, capable of filtering out uninformative AA signal features and exploiting ECG spatial variability. However, the importance of their contribution is significantly reduced when applying PCA, thus losing relevant information about AF energy content in the associated heart sites. By contrast, the WPCA scheme can effectively improve CA outcome prediction by reinforcing the most discriminative features of input data thanks to the a

priori knowledge about AA signal energy distribution.

In line with results presented in Sec. 5.3.3, Fig. 5.11 proves that ablation outcome prediction considerably benefits from low-rank representation of AA data. As for PCA, AUC values related to the index $\widetilde{\mu}_{\mathrm{WPCA_8}}$ have been computed by varying the number of PCs n retained in the WPCA truncation in Eq. (5.2) from 1 (the value set for our algorithm) to 8 (full-rank decomposition, i.e. original data). The lower n, the more accurate prediction performance, especially when retaining less than 5 PCs prior to WPCA application. The first dominant source seems to contain the most meaningful components of the AA signal, whereas the effect of noisy and/or redundant elements ascribed to the very last PCs is negligible. Also this evidence is consistent with results obtained on f-wave amplitude in Sec. 4.4.3.

Experimental results corroborate the validity of the weighting model adopted, assuming the inverse-standard deviation values as $\mathbf{W}^{(r)}$ weights as explained in Sec. 5.4.2. Conversely, other weighting schemes are not able to give comparable classification results. For instance, the weight matrix depending on AA standard deviation values per lead $\mathbf{W}^{(r)} = [\sigma_1^{(r)}, \sigma_2^{(r)}, \ldots, \sigma_L^{(r)}]^T\mathbf{1}$ does not manage to properly emphasize ECG lead contributions, thus showing a weak predictive power (AUC= 0.53, p value= 0.98). These results corroborate our AF model, as AA maximum-power components seem to selectively enhance the most informative contributions by means of the weighting structure. Another strategy consists in giving more weight to leads better explained by a reduced-rank PCA approximation, thus defining $\mathbf{W}^{(r)}$ elements as a function of the inverse value of standard deviation of the error between original data and rank-1 PCA approximation per lead ($\mathbf{W}^{(r)} = [(\sigma_{1_N}^{(r)})^{-1}, (\sigma_{2_N}^{(r)})^{-1}, \ldots, (\sigma_{L_N}^{(r)})^{-1}]^T\mathbf{1}$). However, no significant differences between effective and failing CA procedures have been found (AUC= 0.67, p value= 0.69). In other tests, we hypothesize that $\mathbf{W}^{(r)}$ components depend on the value of the standard deviation itself ($\mathbf{W}^{(r)} = [\sigma_{1_N}^{(r)}, \sigma_{2_N}^{(r)}, \ldots, \sigma_{L_N}^{(r)}]^T\mathbf{1}$), although, similar results are obtained (AUC= 0.63, p value= 0.37). This leads us to conclude that focusing on noisy components that may be present in the AA signal does not actually improve the selective action of the weighting scheme, whereas considering variance of the whole signal gives more emphasis to its most informative components, thus improving prediction accuracy.

5.4.7 CONCLUSIONS

Similarly to the PCA-based method, STV characterization in the presence of AF by means of the WPCA technique is affected by the lack of knowledge about AF spatio-temporal organization as claimed by standard clinical criteria, for instance those defined by Wells' and Konings [78, 161]. As a consequence, in this dissertation STV discriminative power in CA outcome prediction can be effectively assessed, but its link with clinical significance of AF spatio-temporal complexity needs to be more deeply explored. Further attention should also be paid to the implementation modalities of the WPCA weight matrix $\mathbf{W}$. Roughly speaking, even though this approach proves to be robust and appropriate for the application of interest, alternative computational strategies could be conceived for a deeper comprehension of AF electrophysiology. Despite these shortcomings, the methodology illustrated is able not only to effectively quantify STV of AF pattern by exploiting the multivariate character of standard ECG, but also to exploit such diversity as a tool for predicting CA outcome in persistent AF in the long-term follow-up. Compared with conventional PCA, WPCA is able to better capture the spatial variabil-

ity typical of multilead recordings by automatically enhancing the most bearing-content ECG leads from an appropriate subset of standard ECG while reducing the influence of not significant or highly dispersive contributions, thus remarkably improving prediction accuracy.

5.5 Multilead STV measures on standard ECG in the nonnegative matrix factorization framework

In the applications described until present, STV information has been extracted from standard ECG and quantified in terms on NMSE between the original AA signal and its rank-1 approximation determined by means of a suitable multivariate decomposition strategy. Temporal variability of AF components is explored by dividing the input AA signal in a fixed number of segments. ECG leads' contributions are adequately combined in a unique score acting as a predictor of procedural AF termination. Such contributions are represented by the single-lead intersegment mean NMSE value $\mu_{\ell,n}$ and the intersegment variance $\sigma^2_{\ell,n}$, rendering an outlook of global accuracy of AA signal estimation.

In this section we explore further strategies to represent NMSE indices and characterize STV content. In particular, we provide an alternative form of arrangement of NMSE data and compute their low-rank approximation by a nonnegative matrix factorization (NMF). NMF application implies non-negativity constraints of processed data and has extensively been used in areas as diverse as text processing, data mining and image processing, among other application domains [84]. To our knowledge, this technique is applied for the first time to ECG signal processing. Our aim is for predicting short-term AF termination by CA. After an overview of the NMF technique, its application to real ECG data for acute CA outcome prediction is presented, and an extension to long-term assessment is also put forward. These results were first producted in [107].

5.5.1 NMF decomposition of the NMSE matrix and feature extraction

Under these assumptions, we attempt an alternative characterization of the NMSE values computed on the AA signal. Most of the theoretical contributions to NMF definition take the study led in [12] as a reference. Indeed, as they are computed on multiple ECG leads, we expect that they share some common underlying factors that may be estimated by suitable signal decomposition techniques. Furthermore, in keeping with its definition in Eq. (5.3), the NMSE index can never have negative values. Therefore, by exploiting this property as a decomposition constraint, we can process NMSE data adequately arranged by means of the NMF technique and then compute the reconstruction error between the original NMSE data and their reconstruction as a STV measure of the AA signal across the standard ECG. More specifically, the NMSE values can be arranged so as to form a nonnegative matrix $\mathbf{A}$ with size $\Big(L \times \beta\Big)$, where $\beta = S(S-1)$. Indeed, for each reference segment r , $r = 1, \ldots, S$, we can estimate all the remaining $(S-1)$ time intervals. Each element $\mathrm{NMSE}^{(s,r)}_{\ell,n}$ is assigned to entry $[\mathbf{A}]_{\ell,(r-1)(S-1)+(s-1)}$ if $r < s$, otherwise in entry $[\mathbf{A}]_{\ell,(r-1)S+(s-1)}$, for $r, s = 1, 2, \ldots, S$, $s < r$. Therefore, matrix $\mathbf{A}$ contains the NMSE for all leads for all the possible pairs of reference-estimated segments (r, s). Once set this

input matrix, we can apply NMF, which yields the approximate rank-R factorization:

$$\mathbf{A} \approx \mathbf{WH} \tag{5.8}$$

where $\mathbf{W}$ and $\mathbf{H}$ with size $(L \times R)$ and $\Big(R \times \beta\Big)$, respectively, are the nonnegative factors, i.e., matrices with nonnegative entries, computed as the minimizers of the objective function:

$$\Psi(\mathbf{W}, \mathbf{H}) = \|\mathbf{A} - \mathbf{WH}\|_{\mathrm{F}}^2 \tag{5.9}$$

where $\|\cdot\|_{\mathrm{F}}$ stands for the Frobenius norm. This formulation may allow for a more attentive examination of the spatial distribution of the reconstruction error in each segment.

Several algorithms can be run to obtain NMF factors. Concerning our application, we employ an alternating least squares (ALS) minimization algorithm. Accordingly, given one of the 2 factors, the other one can be found with a simple LS computation. As reported in the Appendix A.3, nonnegativity is insured by the projection step, which sets all negative elements output from the least squares computation to 0. Not only this strategy is quite fast, but it also enhances sparsity and allows for some additional flexibility, which helps to avoid attraction basins of suboptimal spurious solutions.

Criterion (5.9) is also a measure of approximation quality. Thus, we can express the root mean square residual (RMSR) between $\mathbf{A}$ and its reduced-rank representation defined in (5.8) as:

$$\mathrm{RMSR} = \sqrt{\frac{\Psi(\mathbf{WH})}{L\beta}} \tag{5.10}$$

can naturally be exploited as a multilead AA STV measure as reflected on the NMSE array.

5.5.2 SETTING THE NMF APPROXIMATION RANK

One of the main critical points related to NMF performance is represented by the choice on the approximation rank R, which is generally application-specific. Accordingly, since we can regard the product $\mathbf{WH}$ as a compressed form of $\mathbf{A}$, we decided to process NMSE matrix my means of a rank-2 ($R = 2$) NMF approximation, since only this setting highlighted statistically significant differences between the categories of interest among all values ranging from 1 to $(L - 1)$.

5.5.3 NMF INITIALIZATION

Another issue that must be taken into account is the iterative nature of the NMF algorithm, which is therefore sensitive to initialization of factors $\mathbf{W}$ and $\mathbf{H}$. Nearly all NMF algorithms use random initializations that are simple to be implemented but often provide unsatisfactory performance. A good initialization can improve decomposition speed and accuracy, as it can sidestep some of the problems coming from convergence to spurious local minima [84].

In our research we examined two initialization methods returning the matrices $\mathbf{W}_0$ and $\mathbf{H}_0$ as outputs. The first algorithm searches for the 2 leads (i.e., rows of the NMSE matrix) presenting the maximum mean square value (MSV) of the NMSE index in $\mathbf{A}$, in line with the maximum-variance formulation of PCA. Just as PCA achieves the best rank-R subspace approximation by maximizing the components' variance, one could expect

that the rows of $\mathbf{A}$ with maximal MSV may lie not too far from the NMF components in $\mathbf{H}$ minimizing the objective (5.9). As a consequence, rows fulfilling these criteria form $\mathbf{H}_0$. Concerning the other NMF factor, the initial value $\mathbf{W}_0$ is determined by the ALS algorithm under the positivity constraint as:

$$\mathbf{W}_0 = \mathbf{A}\mathbf{H}_0^{\mathrm{T}}(\mathbf{H}_0\mathbf{H}_0^{\mathrm{T}})^{-1} \tag{5.11}$$

and then setting all its nonnegative elements to 0.

The second initialization strategy stems from the "concept vector" notion proposed in [43]. This approach basically aims at partitioning input data into clusters, whose centroids will form the unknown matrices. This strategy can be quite time-consuming when processing high-dimensional data, which has led to several clustering variants looking for a trade-off between compression and data content preservation. In line with [83], the SVD output can be used to form cheap centroid basis vectors. Accordingly, we exploit the singular value decomposition (SVD) of $\mathbf{A}$, given by $\mathbf{A} = \mathbf{U}\mathbf{S}\mathbf{V}^{\mathrm{T}}$, to form the R-component centroid basis vectors. These clusters can thus obtained by taking into account the low dimension $\mathbf{V}^{\mathrm{T}}$. Accordingly,

1) A clustering algorithm is run on the first $\beta = S(S-1)$ orthogonal right-singular vectors in $\mathbf{V}$ and we identify R clusters through the Euclidean k-means method, as in [83]. We remind that the input matrix $\mathbf{A}$ has size $L \times \beta$.

2) We locate columns of $\mathbf{A}$ corresponding to clusters of $\mathbf{V}$.

3) We compute the centroids of such clusters, so as to form the columns of $\mathbf{W}_0$.

4) Matrix $\mathbf{H}_0$ is finally given by the ALS update:

$$\mathbf{H}_0 = (\mathbf{W}_0^{\mathrm{T}}\mathbf{W}_0)^{-1}\mathbf{W}_0^{\mathrm{T}}\mathbf{A}. \tag{5.12}$$

The choice of the input matrix for the clustering algorithm notably helps reducing initialization computational load, as a lower dimensional matrix is processed and successive operations are computationally less complex. Thanks to this grouping action, a sort of temporal quantization of AF information carried by every segment is fulfilled, unlike the first initialization proposed above, in which a spatial selection of ECG leads is rather accomplished.

5.5.4 NMF application to prediction of acute AF termination by CA

In [107] it has been demonstrated that NMF feature extraction can be successfully applied to prediction of acute AF termination by CA. This evidence has been corroborated by results obtained on an ECG dataset acquired in relation with 21 CA procedures. In this experimental session we aim at investigating whether this result can be extended to a larger database, consisting of 31 ECG signals, already introduced in Sec. 3.5.5. The goal is predicting acute AF termination by CA in line with the criteria explained in the same section. According to this short-term criterion, 26 CA procedures were successfully accomplished.

In keeping with remarks made in previous sections, NMSE indices assess estimation quality of the PCA approximation of rank $n = 1$ of the AA signal split into $S = 4$

Table 5.5: Short-term CA outcome assessment: interclass statistical analysis.

	AF termination	Non AF termination	p value
$\mathrm{RMSR}_{\mathrm{SVD8,1}}$ (mV)	10.79 ± 9.62	15.24 ± 7.80	$\mathbf{1.71 \cdot 10^{-1}}$
$\mathrm{RMSR}_{\mathrm{MSV8,1}}$ (mV)	10.79 ± 9.62	15.24 ± 7.80	$\mathbf{1.71 \cdot 10^{-1}}$
$\mathrm{RMSR}_{\mathrm{SVD8,2}}$ (mV)	5.97 ± 6.22	5.60 ± 3.24	$\mathbf{4.05 \cdot 10^{-1}}$
$\mathrm{RMSR}_{\mathrm{MSV8,2}}$ (mV)	6.09 ± 6.21	6.00 ± 3.24	$\mathbf{4.68 \cdot 10^{-1}}$
$\mathrm{RMSR}_{\mathrm{PCA8,1}}$ (mV)	0.006 ± 0.001	0.007 ± 0.001	$\mathbf{2.49 \cdot 10^{-1}}$
$\mathrm{RMSR}_{\mathrm{PCA8,2}}$ (mV)	0.005 ± 0.001	0.006 ± 0.001	$\mathbf{1.70 \cdot 10^{-1}}$
$\widetilde{\mu}_{\mathrm{PCA}}$ [n.u.]	44.22 ± 26.40	65.50 ± 37.47	$1.7 \cdot 10^{-1}$
$(\mathrm{NMSE})_{\mathrm{V_1}}$ [n.u.]	22.54 ± 17.25	24.00 ± 20.68	$\mathbf{8.51 \cdot 10^{-1}}$
$\widetilde{D}_8$ (mV)	0.038 ± 0.019	0.015 ± 0.007	$\mathbf{9.56 \cdot 10^{-4}}$
$D(\mathrm{V_1})$ (mV)	0.068 ± 0.022	0.054 ± 0.017	$1.85 \cdot 10^{-1}$

segments. As in previous experimental sessions, once verified the type of data distribution, differences between the groups examined ("AF termination" and "Non AF termination" by CA) are assessed by an unpaired test under a confidence level $\alpha = 0.05$ (see Table 5.5).

Classification performance ROC curve parameters, namely, the AUC index and the optimal cutoff, as well as the related values of sensitivity and specificity, are reported in Table 5.6. Once set the NMF approximation rank R, evaluation indices are computed

Table 5.6: ROC analysis of the NMF decomposition for short-term CA outcome prediction. All the parameters are expressed in normalized units [n.u.], except of $\widetilde{D}_8$ and $D(V_1)$ (mV).

	AUC	Sensitivity	Specificity	Best cutoff
$\mathrm{RMSR}_{\mathrm{SVD8,1}}$ [n.u.]	0.70	0.54	0.85	8.34
$\mathrm{RMSR}_{\mathrm{MSV8,1}}$ [n.u.]	0.70	0.54	0.85	8.34
$\mathrm{RMSR}_{\mathrm{SVD8,2}}$ [n.u.]	0.50	0.46	0.85	4.35
$\mathrm{RMSR}_{\mathrm{MSV8,2}}$ [n.u.]	0.50	0.46	0.85	4.02
$\mathrm{RMSR}_{\mathrm{PCA8,1}}$ (mV)	0.66	0.73	0.60	0.008
$\mathrm{RMSR}_{\mathrm{PCA8,2}}$ (mV)	0.68	0.62	0.80	0.005
$\widetilde{\mu}_{\mathrm{PCA}}$ [n.u.]	0.71	0.62	0.80	65.62
$(\mathrm{NMSE})_{\mathrm{V_1}}$ (mV)	0.54	0.46	0.80	16.09
$\widetilde{D}_8$ (mV)	0.98	0.92	0.80	0.023
$D(V_1)$	0.68 (mV)	0.50	0.80	0.06

for both NMF initialization methods described in Sec. 5.5.3 on a subset of L ECG leads, yielding $\mathrm{RMSR}_{\mathrm{MSV}L,R}$ and $\mathrm{RMSR}_{\mathrm{SVD}L,R}$, respectively. Subscripts MSV and SVD refer to the NMF initialization methods proposed. For sake of comparison with investigation results presented in [107], we set $R = 2$. In the unpaired statistical analysis we also take into account minimum-rank NMF approximation of the NMSE data, i.e., $R = 1$. Dependence of CA outcome prediction performance on the NMF approximation rank R has been investigated by means of the ROC analysis. Accordingly, the AUC index has been determined as a function of the rank R (Fig. 5.12), ranging between 1 and $S = 4$ (the minimum dimension of input data $\mathbf{A}$). Our analysis is performed on the 8-lead subset previously presented, thus $L = 8$. The RMSR criterion is also computed by replacing NMF processing of the input matrix with the PCA decomposition, and the same rank values R have been adopted as well. Special attention is also paid to the multilead STV descriptor $\widetilde{\mu}_{\mathrm{PCA}}$ defined in Sec. 5.3, averaging single-lead contributions of AF organization,

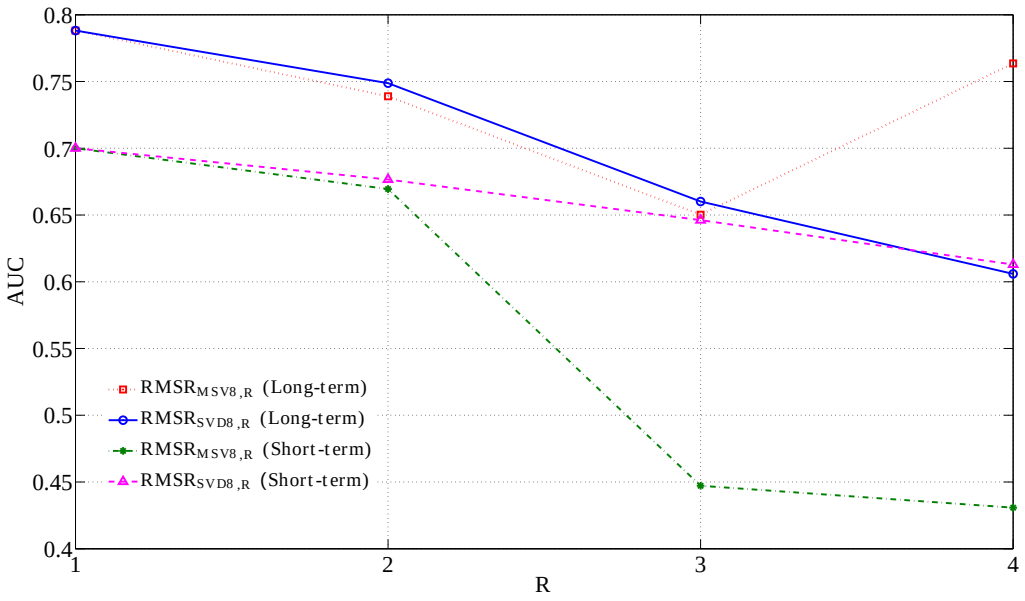


Figure 5.12: Evolution of the AUC index describing prediction performance of the RMSR criterion. CA outcome is observed at two follow-up moments (short-term and long-term prediction, and both NMF initialization methods are examined).

weighted by their temporal variance in a unique index [101, 105]. Moving to the single-lead perspective, the AF complexity descriptor based on the mean NMSE and presented in Sec. 5.3 has also been computed in V_1. This parameter, denoted $(\text{NMSE})_{V_1}$, has been averaged over $S = 4$ segments; for the sake of comparison with the other predictors, we set PCA rank $R = 2$. Moreover, the f-wave amplitude, originally proposed as a CA-outcome predicting feature but obtained manually in [121], is herein automatically computed. The single-lead parameter $D(V_1)$ and the multilead index $\widetilde{D}_8$ are determined in V_1 and in multiple leads ($L = 8$), respectively, as in Sec. 4.3.

5.5.5 Discussion and conclusions

Even though the NMF-based RMSR measures seem to be able to accurately distinguish between effective and failing CA procedures in [107], from experimental evidence in Table 5.5 we deduce the impossibility to confirm such significance on the ECG database under examination. As a consequence, low RMSR values are not significantly associated with acute AF termination by CA, and the index is not able to convey STV information estimated by the multilead NMSE-based classifiers put forth in 5.3. Assessment of procedural AF termination seems to be globally more accurate when lower rank values R are selected prior to NMF performance, as we can see in Fig. 5.12.

Despite the lower reconstruction errors compared with NMF, neither PCA performance can underline intergroup significant differences, regardless of the rank chosen. Similar conclusions can be drawn for the weighted NMSE mean $\widetilde{\mu}_{\text{PCA}}$, exhibiting low predictive accuracy. These results seem to underline that STV content may not be the most adequate ECG feature for depicting CA effects in the first followup, since probably some postoperative factors (such as edemas, inflammations, cardioversion, etc.) do not

allow for accurately capturing STV of AF content.

The single-lead analysis is neither able to effectively discriminate between successful and failing CA procedures. Despite its ability to assess AF organization as demonstrated in [18], the NMSE index assessed in V_1 seems to be characterized by a weak predictive power in CA outcome evaluation. As far as atrial amplitude measures are concerned, it seems that the median descriptor $\widetilde{D}_8$ is characterized by the most accurate prediction performance, and it significantly correlates higher amplitude values with procedural success. By contrast, limitations of the single-lead perspective are confirmed by experimental evidence related to $D(V_1)$, whose prediction performance is quite poor. Despite the predictive role of f-wave amplitude, there is no evidence of its ability to characterize STV properties of AF by exploiting f-waves properties. In addition, prediction could be less reliable when dealing with very complex or irregular patterns, which can hamper interpolation performance and atrial amplitude characterization accuracy.

To conclude, we can state that the reconstruction error of the low-rank NMF approximation can not effectively predict CA outcome before ablation, therefore the clinical value of this STV measure as a therapy outcome predictor can not be assessed in the immediate postoperative phase. Interesting open questions concern the rank selection for the NMF decomposition and the links of the proposed predictor with recent indices exploiting the ECG multilead character, as well as the application of the algorithm to other features extracted from standard ECG (e.g., f-wave amplitude).

5.6 STV predictors of CA outcome: extension to long-term CA outcome prediction and classification test on a larger ECG database

As done in Chapter 4, results discussed until present are obtained on a subset of our persistent AF database, due to constraints imposed by the follow-up duration in each subject. In this section we investigate whether it is possible to confirm the conclusions about AF STV quantification drawn in previous sections by validating these findings on the ECG database consisting of 36 patients, presented in Sec. 3.5.5. In particular, we inspect the role of each of the features introduced as a predictor of AF termination by CA in the long-term follow-up (mean duration: 8 ± 4 months). It is worth mentioning once again that changes in the ECG database alter not only its size, but can also concern CA clinical outcome, thus modifying data labels employed in our classification session. This factor represents one of the main difficulties encountered in this doctoral thesis, as it makes harder to generalize the methods proposed to different follow-up lengths.

In the light of these considerations, we examine the inverse-variance weighted mean NMSE indices obtained subsequently to PCA and WPCA approximation, $\widetilde{\mu}_{\mathrm{PCA}_L}$ and $\widetilde{\mu}_{\mathrm{WPCA}_L}$, which have been respectively introduced in Sec. 5.3 and Sec. 5.4. Moreover, NMF estimation error defined in Sec. 5.5 is evaluated. Both types of decomposition initializations are tested, for 2 rank values ($R = 1, 2$), thus yielding $\mathrm{RMSR}_{\mathrm{SVD}L,R}$ and $\mathrm{RMSR}_{\mathrm{MSV}L,R}$ as output. All parameters are computed both on the proposed reduced 8-lead ensemble and the whole standard ECG ($L = 8$ and $L = 12$). In order to verify whether of the aforementioned STV measures are able to predict long-term freedom from AF recurrence. Results of the statistical analysis and the ROC indices assessment are

Table 5.7: Interpatient statistical analysis and CA outcome prediction performance assessment on the 36-patient database in the long-term follow-up.

	AF termination	Non AF termination	p value	AUC	Sensitivity	Specificity	Best cutoff
$\widetilde{\mu}_{\mathrm{PCA}_8}$ [n.u.]	41.74 ± 30.41	34.66 ± 29.66	$5.82 \cdot 10^{-1}$	0.57	0.24	0.86	30.85
$\widetilde{\mu}_{\mathrm{PCA}_{12}}$ [n.u.]	46.85 ± 32.18	49.40 ± 29.44	$8.50 \cdot 10^{-1}$	0.53	0.76	0.29	74.33
$\widetilde{\mu}_{\mathrm{WPCA}_8}$ [n.u.]	50.16 ± 27.73	66.47 ± 26.01	$1.67 \cdot 10^{-1}$	0.66	0.72	0.43	69.60
$\widetilde{\mu}_{\mathrm{WPCA}_{12}}$ [n.u.]	56.11 ± 23.94	76.92 ± 13.77	$\mathbf{3.48 \cdot 10^{-2}}$	0.76	0.69	0.71	70.52
$\mathrm{RMSR}_{\mathrm{SVD8,1}}$ (mV)	7.86 ± 5.98	15.32 ± 9.70	$\mathbf{1.33 \cdot 10^{-2}}$	0.76	0.72	0.57	8.70
$\mathrm{RMSR}_{\mathrm{SVD12,1}}$ (mV)	9.21 ± 7.59	17.95 ± 10.18	$\mathbf{1.51 \cdot 10^{-2}}$	0.79	0.62	0.71	10.01
$\mathrm{RMSR}_{\mathrm{MSV8,1}}$ (mV)	7.86 ± 5.98	15.32 ± 9.70	$\mathbf{1.33 \cdot 10^{-2}}$	0.76	0.72	0.57	8.70
$\mathrm{RMSR}_{\mathrm{MSV12,1}}$ (mV)	9.21 ± 7.59	17.95 ± 10.18	$\mathbf{1.51 \cdot 10^{-2}}$	0.79	0.62	0.71	10.01
$\mathrm{RMSR}_{\mathrm{SVD8,2}}$ (mV)	3.86 ± 3.00	7.37 ± 4.32	$\mathbf{1.55 \cdot 10^{-2}}$	0.78	0.76	0.71	5.27
$\mathrm{RMSR}_{\mathrm{SVD12,2}}$ (mV)	4.39 ± 3.30	7.34 ± 4.24	$\mathbf{5.21 \cdot 10^{-2}}$	0.75	0.76	0.57	5.98
$\mathrm{RMSR}_{\mathrm{MSV8,2}}$ (mV)	4.21 ± 3.44	7.76 ± 4.15	$\mathbf{2.44 \cdot 10^{-2}}$	0.79	0.72	0.86	4.89
$\mathrm{RMSR}_{\mathrm{MSV12,2}}$ (mV)	4.64 ± 3.55	7.34 ± 4.23	$9.07 \cdot 10^{-2}$	0.74	0.76	0.71	6.00

reported in Table. 5.7.

We can remark that STV descriptors determined by PCA are not able to point out significant differences between the groups of patients, regardless of the ECG leads considered. The p values are high, and prediction quality assessed by the AUC criterion seems poor. Similar conclusions can be drawn for the WPCA parameter $\widetilde{\mu}_{\mathrm{WPCA}_8}$ described in Section 5.4. Conversely, concerning the index $\widetilde{\mu}_{\mathrm{WPCA}_{12}}$, even though the unpaired test yields significant results and prediction is quite satisfactory, it seems that successful CA procedures are predicted by low values of this parameter, which apparently contradicts our deductions about STV content assessed by NMSE. By contrast, parameters assessing NMF observation reconstruction accuracy seem to improve results obtained on smaller datasets. AUC values are generally satisfactory and categories of interest are well distinguished, as confirmed by the low p values. We can interestingly note that predictive information about CA outcome can be extracted by a reduced number of ECG leads ($L = 8$), and both $\mathrm{RMSR}_{\mathrm{SVD8,2}}$ and $\mathrm{RMSR}_{\mathrm{MSV8,2}}$ outperform their 12-lead counterparts $\mathrm{RMSR}_{\mathrm{SVD12,2}}$ and $\mathrm{RMSR}_{\mathrm{MSV12,2}}$, whole corresponding p values slightly exceed the significance level $\alpha = 0.05$. Prediction accuracy of this index seems to be globally more accurate when low approximation rank values R are chosen, as confirmed by Fig. 5.12. Consequently, such evidence corroborates the descriptive power of observation reduced-rank approximations, and their ability to emphasize the AA components which are more discriminant and relevant to CA outcome prediction.

5.7 Summary and conclusions

This chapter has investigated STV properties characterizing AF on surface ECG. Taking a step from classical parameters describing AF complexity, AF STV content is characterized in a multilead framework by applying suitable multivariate decomposition techniques underlining the most descriptive AA signal components. Regardless of the decomposition applied, we showed that reduced-rank approximations to AA signal effectively enhance significant contributions to CA outcome prediction. Contributions coming from each ECG lead are selectively emphasized by exploiting AA signal intersegment temporal variability, providing a measure of dispersion and statistical uncertainty at the same time. AA observation reconstruction error proves to be a reliable index able to discriminate between successful and failing CA procedures at several followup lengths.

Correlation with AF complexity according to classical medical criteria [78, 161] has still to be demonstrated, due to the lack of this clinical information in our AF database. In the next chapter we attempt to merge ECG features illustrated until present and we investigate whether AF characterization can benefit from such a combined approach in a multivariate framework.

6 Combination of multiple features assessed on standard ECG

6.1 Introduction

In previous chapters we have introduced some ECG features and we have characterized their descriptive role in CA outcome evaluation in a multivariate context. In Chapter 4 we have looked at f-wave amplitude spatial diversity as measured on surface ECG recordings; in Chapter 5 AF variability has been explored both in time (in terms of AA signal component repetitiveness) and space (in terms of complexity distribution over ECG leads). In this chapter we investigate whether it is possible to combine such heterogeneous ECG properties and which technique can help merging our multilead features so as to improve AF therapy outcome assessment. As it will be explained in the next section, the solution to this problem comes from the logistic regression (LR) analysis, which will prove to be a suitable tool for processing contributions from all electrodes at the same time and selectively enhance the most content-bearing ECG leads according to a leveraging scheme. In Sec. 6.2 we first illustrate the theoretical background of the LR analysis. In Sec. 6.3 this model is applied to multivariate f-wave amplitude characterization and some application to CA outcome prediction are illustrated. In Sec. 6.4 LR analysis of AF STV content is accomplished for the same kind of application. In Sec. 6.5 we finally merge such features and we characterize their predictive content through the LR model. General comments and remarks about this topic are summarized in Sec. 6.6.

6.2 Definition of the logistic regression model

The goal in any data analysis is to extract from raw observations the accurate estimation of the information of interest. One of the most important and common question concerning if there is statistical relationship between a response variable and explanatory variables $\mathbf{z}$ of a certain phenomenon [6]. More specifically, we would like to investigate whether the probability of getting a particular value of the nominal variable is associated with the measurement variable. The second goal is to predict the probability of obtaining a particular value of the nominal variable, given the measurement variable [100].

One possible solution to model such relationship is to employ regression analysis. There are various types of regression analysis, depending on the type of distribution of the nominal variable.

The LR model assesses the impact of multiple independent variables presented simul-

taneously to predict membership to one of the two categories of the dependent or response variable, with mutually exclusive membership probabilities θ and $(1-\theta)$ [87]. LR model is generally defined as:

$$LR = \log \frac{\theta}{1-\theta} = \mathbf{b}^{\mathrm{T}}\mathbf{z} \tag{6.1}$$

where $(\cdot)^{\mathrm{T}}$ denotes transposition. The LR score is defined as the ratio of the probability of occurrence of an event θ to that of non-occurrence with level $(1-\theta)$, i.e. the odds of that event. In our problem, θ represents the probability of procedural AF termination. LR forms a best fitting equation using maximum likelihood (ML), which finds the values of the parameters most likely to have produced the observed results. Indeed, it aims at maximizing the probability of assigning observations $\mathbf{z}$ to the correct category given the fitted regression coefficients $\mathbf{b} = [b_1, b_2, \ldots, b_L]^T$. Unlike linear regression, there is no closed-form expression for the estimates of model coefficients, but they need to be computed by means of an iterative algorithm.

6.3 LR modeling of multivariate f-wave amplitude

In our application, $\mathbf{z}_{\mathrm{A}} = \mathbf{d} = [d_1, d_2, \ldots, d_L]$, whose entries d_ℓ are the single-lead atrial amplitude features from Eq. (4.2), determined in each lead of the PCA-approximated AA signal defined in Eq. (4.19). Such coefficients quantify the contribution of each independent variable (i.e., ECG leads $\ell = 1, \ldots, L$ regarded as linearly independent as aforesaid in Sec. 2.4.4) to the response variable (i.e., CA outcome). It is worth to note that interlead independence is not strictly true in the LR context, but it seems to be a good approximation for the subset of ECG leads considered. It turns out that the higher the score (6.1), the more likely AF freedom in the long-term follow-up. Given these considerations, the score output by the LR linear combination of $\mathbf{z}_{\mathrm{A}}$ components acts as a classifier which has to discriminate between successful and failing CA procedures:

$$LR_{\mathrm{A}} = \mathbf{b}_{\mathrm{A}}^{\mathrm{T}}\mathbf{z}_{\mathrm{A}}. \tag{6.2}$$

6.3.1 Statistical analysis and prediction performance assessment

Groups of patients under examination are referred to as "Non AF recurrence" and "AF recurrence", and LR scores related to each class are expressed as mean ± standard deviation. The level of separability of the two groups and statistical significance are quantified by the p value output by the unpaired test under a confidence level $\alpha = 0.05$. Statistical analysis results are reported in Table 6.1.

Prediction accuracy is quantified by the AUC criterion. The optimal cutoff value guaranteeing the maximum discrimination level between the two classes is reported as well. In addition, the related maximum rates of positive and negative detections, namely, sensitivity and specificity, are indicated. Classification results are then validated by the LOOCV technique as in Sec. 4.4.2 and displayed in Table 6.2.

6.3.2 Results

ROC assessment and statistical analysis are led according to the modalities explained in Sec. 4.4.2. Advantages of multilead analysis are demonstrated in Fig. 6.1. More specif-

Table 6.1: Statistical analysis of the LR modeling of f-wave amplitude in long-term CA outcome prediction.

	AF termination	Non AF termination	p-value
LR_A	0.90 ± 0.11	0.42 ± 0.41	$\mathbf{1.95 \cdot 10^{-6}}$
$LR_{D(V_1)}$	0.81 ± 0.04	0.79 ± 0.07	$1.45 \cdot 10^{-1}$
$\overline{D}_8$	0.035 ± 0.022	0.048 ± 0.026	$1.9 \cdot 10^{-1}$
$\mathrm{RMS(V_1)}$	0.036 ± 0.011	0.507 ± 0.024	$1.11 \cdot 10^{-1}$
$\widetilde{\mathrm{RMS}}_8$	0.030 ± 0.012	0.041 ± 0.011	$\mathbf{3.92 \cdot 10^{-2}}$
$\widetilde{\mathrm{RMS}}_{12}$	0.027 ± 0.010	0.042 ± 0.012	$\mathbf{2.20 \cdot 10^{-3}}$
$\overline{\mathrm{RMS}}_8$	0.032 ± 0.020	0.054 ± 0.027	$\mathbf{2.19 \cdot 10^{-2}}$
$\overline{\mathrm{RMS}}_{12}$	0.030 ± 0.016	0.049 ± 0.022	$\mathbf{1.39 \cdot 10^{-2}}$
$\mathrm{SampEn}(L_s, r_s^{(1)})$	0.310 ± 0.057	0.255 ± 0.773	$\mathbf{3.88 \cdot 10^{-2}}$
$\mathrm{SampEn}(L_s, r_s^{(2)})$	0.148 ± 0.028	0.126 ± 0.041	$9.30 \cdot 10^{-2}$

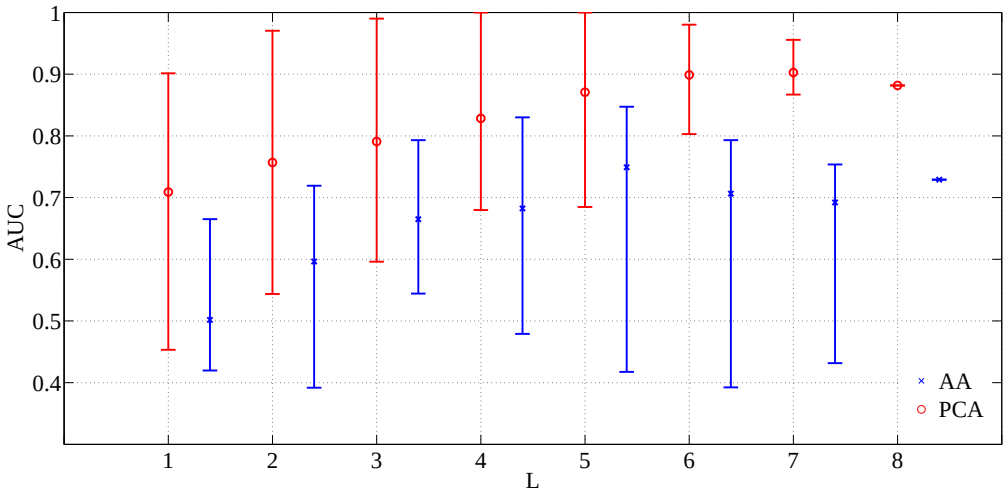


Figure 6.1: Analysis of the LR score prediction performance: AUC index as a function of the size L of the subset of the 8 independent ECG leads. Mean values are highlighted with markers; the vertical bars represent the range of AUC values between the minimum and the maximum obtained for each L. AA: direct computation of the LR score on the observed AA signal. PCA: LR score computation on the truncated AA signal in Eq.(4.19) with $R = 1$.

Table 6.2: ROC analysis of the LR modeling of f-wave amplitude in long-term CA outcome prediction.

	AUC	Sensitivity	Specificity	Best cut-off
LR_A	0.88	0.93	0.71	0.69
$LR_{D(V_1)}$	0.56	0.52	0.71	0.82
$\overline{D}_8$	0.63	0.21	0.86	0.045
$\mathrm{RMS}(\mathrm{V}_1)$	0.65	0.72	0.71	0.040
$\widetilde{\mathrm{RMS}}_8$	0.80	0.55	0.86	0.035
$\widetilde{\mathrm{RMS}}_{12}$	0.88	0.66	0.86	0.031
$\overline{\mathrm{RMS}}_8$	0.86	0.62	0.86	0.036
$\overline{\mathrm{RMS}}_{12}$	0.84	0.59	0.86	0.030
$\mathrm{SampEn}(L_s, r_s^{(1)})$	0.82	0.48	0.86	0.291
$\mathrm{SampEn}(L_s, r_s^{(2)})$	0.79	0.45	0.86	0.138

ically, the AUC index is determined for each value of lead-subset size L ranging from 1 up to 8 and validated by the LOOCV technique as in Sec. 4.4.2 as well. The minimum, maximum, and mean AUC values over all L-lead subset combinations have been obtained as a function of the subset dimension L. Furthermore, the subsets of ECG leads providing the most relevant contributions to CA outcome prediction are indicated in Table 6.3. The

Table 6.3: ECG lead subsets with optimal prediction performance based on the LR score LR_A

Number of leads (L)	**Leads**
1	I
2	I, V_6
3	I,II, V_5
4	[I, II, V_2, V_5] [I, II, V_3, V_5] [I, II, V_2, V_5] [I, II, V_3, V_6] [I, II, V_4, V_6]
5	[I, II, V_2, V_4, V_6] [I, II, V_2, V_5, V_6]
6	[I, II, V_1, V_4, V_5, V_6] [I, II, V_3, V_4, V_5, V_6]
7	[I, II, V_1, V_2, V_4, V_5, V_6]

LR descriptor of f-wave amplitude is then compared with some conventional predictors of CA outcome. The same parameters examined in Sec. 4.4.3 are herein applied to long-term CA outcome prediction. It is worth noting that the feature $\overline{D}_8$ is a particular case of LR, i.e. uniform weighting of all contributions from ECG leads ($\mathbf{b}_A = \mathbf{1}$). All numerical results are reported in Table 6.2. For the sake of completeness, f-wave amplitude in V_1 is also processed through the LR model, thus yielding the index $LR_{D(V_1)}$, even though numerical results are equal to those obtained in absence of LR processing (the single-

lead LR predictor is just scaled by a multiplicative constant). The RMS-based measures of atrial amplitude introduced in Sec. 4.4.3 have also been taken into account in this experimental section. Finally, a further comparison is drawn with the non-linear sample entropy index, which has been already presented in the same section. Some comments about LR generalization over the short-term prediction of CA outcome are also made in the final part of the experimental session.

6.3.3 Discussion and conclusions

The results obtained demonstrate that prediction of CA outcome in persistent AF benefits from multivariate LR of f-wave amplitude content. In particular, in Fig. 6.1 we can remark that the mean AUC value increases as the size of the set of ECG leads does, thus confirming the relevance of information coming from multiple leads. This plot also points out that PCA considerably improves classification performance relative to the raw multilead ECG. In particular, mean AUC index for a fixed subset size L is higher when PCA is applied to AA signal. Moreover, starting from $L = 5$, AUC ranges become narrower when PCA is performed. This proves the filtering effect of this decomposition, which underlines the most descriptive components of AA signal, which help discriminating between effective and failing CA procedures. Analysis of lead subsets in Table 6.3 highlights that prediction accuracy is due to contributions coming from multiple planes at different orientations. Indeed, when $L > 1$, we always find a combination of limb and precordial leads, thus supporting our assumptions about the role of ECG spatial variability. Furthermore, we can interestingly find some combinations of leads already presented in Table 4.3 for predicting acute AF termination by CA (for instance, I, II, V_2, V_5 for $L = 4$; I, II, V_2, V_4, V_6 for $L = 5$; I, II, V_1, V_2, V_4, V_5, V_6 for $L = 7$), thus they can effectively contribute to CA outcome prediction at different moments in the follow-up.

Experimental evidence shows the superiority of LR-based scores over conventional AF descriptors in CA outcome prediction. Such a multilead strategy provides a more accurate prediction than classical single-lead parameters, for instance, f-wave mean amplitude $D(V_1)$, whose prediction performance is quite poor and no significant differences between the groups of interest can be remarked. By contrast, prediction performance of the sample entropy index is quite satisfactory. Setting $r_s = r_s^{(1)}$ points out statistically significant interpatient differences (just below $p = 0.04$), whereas $r_s = r_s^{(2)}$ does not. This evidence makes us realize how sensitive to tuning parameter values this feature is, thus highlighting the difficulty in searching for the most suitable setting. What is more, regardless of setting parameter values, results obtained do not match basic assumptions made in previous studies [5], namely, correlation between low entropy values and CA success due to a higher degree of AF organization, as failing procedures are predicted by lower entropy values. Concerning the mean value of the PCA-descriptor of f-wave amplitude $\overline{D}_8$, note that attributing the same weight to all ECG leads by simply averaging their contributions does not improve prediction, as no significant differences can be observed between the groups examined. It turns out that CA outcome prediction takes benefit from multivariate data processing and classification, provided that independent variables (i.e., ECG leads) are properly combined, as when LR is applied. Similar conclusions can be drawn for $\widetilde{D}_8$ and the 12-lead counterparts $\overline{D}_{12}$ and $\widetilde{D}_{12}$. By contrast, it seems that central tendency measures of the RMS of f-wave amplitude effectively predict procedural AF termination, as proved by the high AUC values and by the significant statistical

tests. However, all the RMS-descriptors are affected by quite low sensitivity rates, thus increasing the risk of not treating AF patients who could actually benefit from CA. In addition, our investigation points out that procedural success is predicted by low values of RMS-based parameters, which is in contradiction with the clinical evidence about f-wave amplitude, which is directly correlated with CA outcome.

It seems that some ensembles of electrodes are able to perfectly distinguish between the categories of interest, in particular for $L = 4$ and $L = 5$, as proved by the unity AUC values. Indeed, LR distinguishes the groups of interest, to the extent that they are perfectly separated by a threshold value. This is a common issue with logistic models. In certain cases, it can be due to the low number of observations with respect to the number of parameters to be estimated. Another possible explanation can be also found in the high degree of correlation between the variables examined, which can lead to inaccurate inferences about the model parameters. Accordingly, input data require an a priori analysis in order to assess the feasibility of the LR application to AA signal.

6.3.4 Some comments about f-wave amplitude LR analysis for prediction of acute AF termination by CA

We aim now at investigating whether LR analysis can also effectively contribute acute AF termination immediately after CA, thus generalizing prediction outcomes observed at different follow-up periods. Therefore, we employed the LR coefficients determined in Sec. 6.3 to compute the new scores on the 31-procedure database presented in Sec. 3.5.5, and then we assessed results significance. Empirical evidence shows the impossibility to validate amplitude LR measures on shorter follow-ups, due to the lack of significance of the results obtained (successful CA: 1.34 ± 2.60; unsuccessful CA: 1.18 ± 1.81; p value$= 9.0 \cdot 10^{-1}$). Weak prediction performance is also confirmed by the ROC analysis and the extremely low values of the performance indices (AUC$= 0.53$, sensitivity$= 0.58$, specificity$= 0.60$, best cutoff$= 0.86$). Similar results are obtained even when LR coefficients are computed again and optimized on the 31-procedure database, as no significant differences between the categories of interest are highlighted by the LR amplitude descriptor (successful CA: 0.84 ± 0.01; unsuccessful CA: 0.84 ± 0.01; p value$= 9.2 \cdot 10^{-1}$) and its predictive power seems to be considerably low (AUC$= 0.53$, sensitivity$= 0.81$, specificity$= 0.40$, best cutoff$= 0.84$).

6.4 LR modeling of AF STV multilead measures

In line with previous section, we apply the LR technique so as to weight contributions provided by each ECG lead to spatio-temporal variability (STV) characterization in the presence of AF and enhance those which are most relevant to CA outcome prediction. Accordingly, the mean NMSE value over AA segments μ_ℓ, $\ell = 1, \ldots, L$ as defined in Section 5.3 is computed in each of the 8 ECG leads examined, so as to form the L-component vector $\boldsymbol{\mu} = [\mu_1, \mu_2, \ldots, \mu_L]^T$, rendering the estimation error of PCA approximation to the AA signal in each ECG lead. Therefore, LR modeling of AF STV data $\mathbf{z}_{\mathrm{STV}} = \boldsymbol{\mu}$ results in:

$$LR_{\mathrm{STV}} = \mathbf{b}_{\mathrm{STV}}^{\mathrm{T}} \mathbf{z}_{\mathrm{STV}}. \tag{6.3}$$

STV content examination is carried out on the 36-subject database described in Sec. 3.5.5. However, unlike LR measures of f-wave amplitude, it seems that this model overfits input NMSE data, thus yielding the score LR_{STV}, whose elements are equal either to 0 or 1. This results in a perfect clustering of patients' categories, and so AUC= 1.

In order to verify the correct assessment of this STV measure, we move to an unsupervised classification framework. More precisely, LOOCV technique is applied by splitting the original 36-patient ECG database into 2 parts, i.e., a training ensemble, including 35 ECGs, for learning classifier's features, and one sample test set for validation. Test feature is computed as a function of the LR coefficients estimated on the training set. This procedure is repeated 36 times by discarding one sample at each iteration. The AUC criterion quantifies the classification performance of the LR predictor. Such a validation method highlights the ability of the proposed STV measure to effectively predict long-term AF termination by CA, as corroborated by the ROC analysis (AUC= 0.89, sensitivity= 0.83, specificity= 0.86, best cutoff= 106.65). It turns out that higher LR score values are significantly associated with AF termination by CA (AF termination: 315.30 ± 238.30; non AF termination: -33.91 ± 208.47; p value= $1.1 \cdot 10^{-3}$).

For the sake of completeness, we also cite classification results related to the short-term CA outcome prediction. In this case, the LR method does not seem to underline any significant results (AF termination: 0.84 ± 0.01, Non AF termination: 0.84 ± 0.01, p value: $9.3 \cdot 10^{-1}$, AUC: 0.55, Sensitivity: 0.81, Specificity: 0.40, Best cutoff: 0.84). This could be due to postoperative events (for instance, inflammations, edemas, cardioversion therapies) which may hide some information about AF organization. A possible explanation can also come from the phenomena of reorganization of heart electrical activity subsequently to ablation-induced modifications, which may need a certain amount of time before definitive stabilization.

6.5 LR modeling of combined measures of f-wave amplitude and STV content

Previous sections have underlined the versatility of the LR model and its ability to properly weight contributions coming from each ECG lead in a multivariate perspective. The flexibility of this technique derives from the possibility of not only examining multiple indices at the same time, but also combining heterogeneous ECG features, due to the definition of the LR score as a ratio of probabilities in Eq. (6.1). Consequently, in this session we attempt to analyze f-wave amplitude STV measures simultaneously and characterize their content by means of the LR model.

6.5.1 Assessment of CA outcome based on the LR analysis of combined ECG features at several follow-ups

In this section we investigate whether LR combination of AF STV measures can yield predictive information about CA procedural outcome. Accordingly, we first examine the 31-procedure dataset used for assessing acute AF termination by CA and previously presented in Sec. 3.5.5. Subsequently, we switch to the long-term follow-up and we look at the procedural outcome on the 36-patient database introduced in the same section. Clinical endpoints evaluated on each dataset are explained in the same section.

As in Sec. 6.4, the ROC analysis yields AUC= 1, regardless of the temporal window examined, thus the categories of interest are perfectly separated, probably due to data overfitting phenomena of the LR model. Accordingly, we tested the prediction performance of the bi-feature LR score in a supervised classification framework, in line with the methodology presented in the same section.

Similarly to the STV-based LR score defined in Sec. 6.3, the LR score output by ECG feature combination does not seem to effectively discriminate between successful and failing CA procedures in the short-term postoperative period, and acute effectiveness of ablation can not be accurately estimated (Successful CA: 0.85 ± 0.37. Failing CA: 0.56 ± 0.52. p value: $1.42 \cdot 10^{-1}$. AUC: 0.68. Sensitivity: 0.73. Specificity: 0.60. Best cutoff: 0.76).

By contrast, therapy outcome analysis in longer follow-ups seems to benefit from the LR modeling of the combined ECG features, and higher LR scores effectively predict durable freedom from AF recurrence (AF termination: 0.83 ± 0.38. Non AF termination: 0.43 ± 0.53. p value: $3.86 \cdot 10^{-2}$. AUC: 0.70. Sensitivity: 0.85. Specificity 0.60. Best cutoff: $2.22 \cdot 10^{-16}$).

In keeping with remark made in Sec. 5.6, this section highlights once again that generalizing the predictive power of a certain ECG measure over different kinds of analysis is not a trivial task, since multiple factors have to be taken into account in our investigation model when switching to a different dataset, e.g., the therapy evaluation criteria and patient's clinical history.

6.5.2 Selection of candidates for CEE based on the LR analysis of combined ECG features

We move now to another clinical application, related to the selection of candidates for CEE after ablation. We demonstrate that merging the ECG measures previously introduced enhance the prediction of procedural acute AF termination by identifying patients who need to be treated by CEE immediately after CA, which can be regarded as a criterion of procedural failure according to certain medical protocols.

All therapies for AF treatment generally aim at either SR restoration or AF transformation into an intermediate arrhythmia, for instance, AFL. In this framework, AF termination is sometimes not exclusively obtained by CA. Different theories about therapy combination have been proposed. One of the most adopted curative strategies to restore SR and stabilize CA effects is performing CEE immediately after CA. In this context, we developed a method for individuating candidates to CEE after CA, i.e., those for whom CA did not terminate AF during the procedure. This tool combines information about f-wave amplitude and AF STV content extracted from the rank-1 approximation to the multilead AA signal and subsequently processed by LR. The proposed method enables a more efficient prediction of acute CA success, as well as a more detailed design of patient's treatment protocol.

6.5.3 LR of multivariate ECG descriptors

In this experimental section we examine the database consisting of 54 signals described in Sec. 3.5.5. As disclosed in Sec. 6.1, the main objective of this chapter is to verify whether combining heterogeneous features, i.e., f-wave amplitude and STV content as measured on

surface ECG, can improve AF therapy outcome evaluation. As a consequence, we examine the 8 linearly independent ECG leads defined in Sec. 2.4.4 and we determine the f-wave peak-to-peak amplitude feature vector defined in Sec. 6.3 $\mathbf{z}_{\mathrm{A}} = \mathbf{d} = [d_1, d_2, \ldots, d_L]^T$, and the intersegment mean NMSE value per lead $\mathbf{z}_{\mathrm{STV}} = \boldsymbol{\mu} = [\mu_1, \mu_2, \ldots, \mu_L]^T$ introduced in Sec. 6.4. LR analysis has been previously applied on each multilead feature separately. Simultaneous processing of these AF descriptors is achieved by concatenating them in a unique variable $\mathbf{z}_{(\mathrm{A;STV})} = [\mathbf{z}_{\mathrm{A}}^T; \mathbf{z}_{\mathrm{STV}}^T]^T$, giving the score $LR_{(\mathrm{A;STV})}$ as output. Accordingly, the LR score will be represented by a $2L$-component vector.

$$LR_{(\mathrm{A;STV})} = \mathbf{b}_{(\mathrm{A;STV})}^{\mathrm{T}} \mathbf{z}_{(\mathrm{A;STV})}. \tag{6.4}$$

6.5.4 Unpaired statistical analysis and prediction accuracy assessment

The categories of interest are referred to as "CEE" and "No CEE", and LR scores related to each class are expressed as mean ± standard deviation. The unpaired Student's t-test assesses interclass statistical differences under a confidence level $\alpha = 0.05$. Prediction quality is evaluated according to the AUC criterion, accompanied by the optimal cutoff separating the 2 categories and the related rates of sensitivity and specificity. These results are validated by the LOOCV technique described in Sec. 4.4.2. All the aforementioned values are reported in Table 6.4; values corresponding to the best prediction performance are shown in bold. Finally, advantages of multilead analysis are demonstrated in Fig. 6.2 and quantified by the AUC index over all possible L-sized lead combinations as explained in previous experimental sections. The minimum, maximum, and mean AUC values over all L-lead subset combinations have been obtained as a function of the subset dimension L. Such analysis is performed on all scores LR_{A}, LR_{STV} and $LR_{(\mathrm{A;STV})}$.

6.5.5 Results

The combined LR measure $LR_{(\mathrm{A;STV})}$ is first compared with LR scores of f-wave amplitude and STV features analyzed separately, LR_{A} and LR_{STV}, respectively. Some comparisons with some classical AF descriptors are drawn as well. In particular, we mention mean peak-to-peak amplitude on lead V_1 $D(V_1)$ is taken into account, as several studies demonstrated that it is predictive of CA outcome [121]. In addition, sample entropy $\mathrm{SampEn}(L_s, r_s)$, widely regarded as a predictor of AF termination by CEE [5], is considered. Tuning parameters are set as in the previous experimental sections. A normalized version of the sample entropy, i.e., the squared sample entropy (QSE), recently proposed in [79], is also tested here under the same conditions. The computational load of each algorithm is also reported in terms of execution time T_C in Table 6.4.

The proposed method required on average no more than 3.4 seconds for processing the whole ECG database on 2 leads through an Intel® Core™ 2 Quad 2.66 GHz Processor running MATLAB2012a (The MathWorks Inc.) when combining ECG features. Its execution on the whole 8-lead ensemble provides a satisfactory trade-off between computational load and classification accuracy compared with other methods. Influence of weighting coefficients over prediction has been investigated as well. Accordingly, for each procedure, f-wave amplitude computed on $\widehat{\mathbf{Y}}_{\mathrm{AA}}$ has been averaged over the ECG leads examined, thus giving $\overline{D}_8$ as output, already defined in Sed. 4.3. The same procedure has been repeated for STV indices obtained on each ECG lead, whose mean value is represented by $\overline{\mu}_8$. This is equal to attributing the same importance to all leads, according to

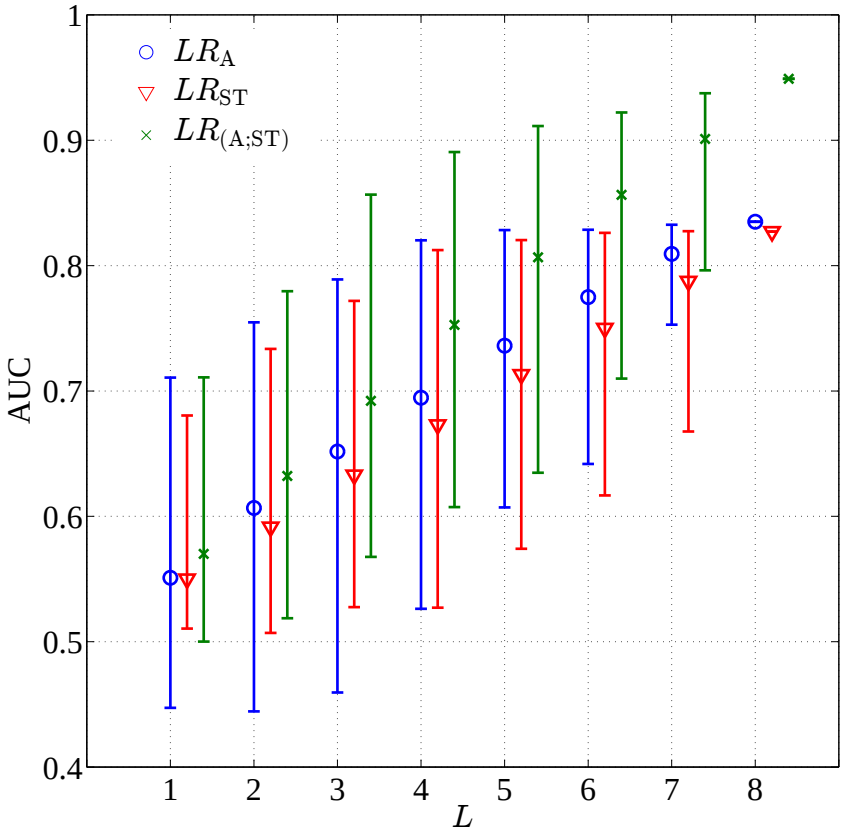


Figure 6.2: Evolution of the AUC index of the proposed LR scores LR_{A}, LR_{STV} and $LR_{(\mathrm{A;STV})}$ as function of the number of ECG leads L.

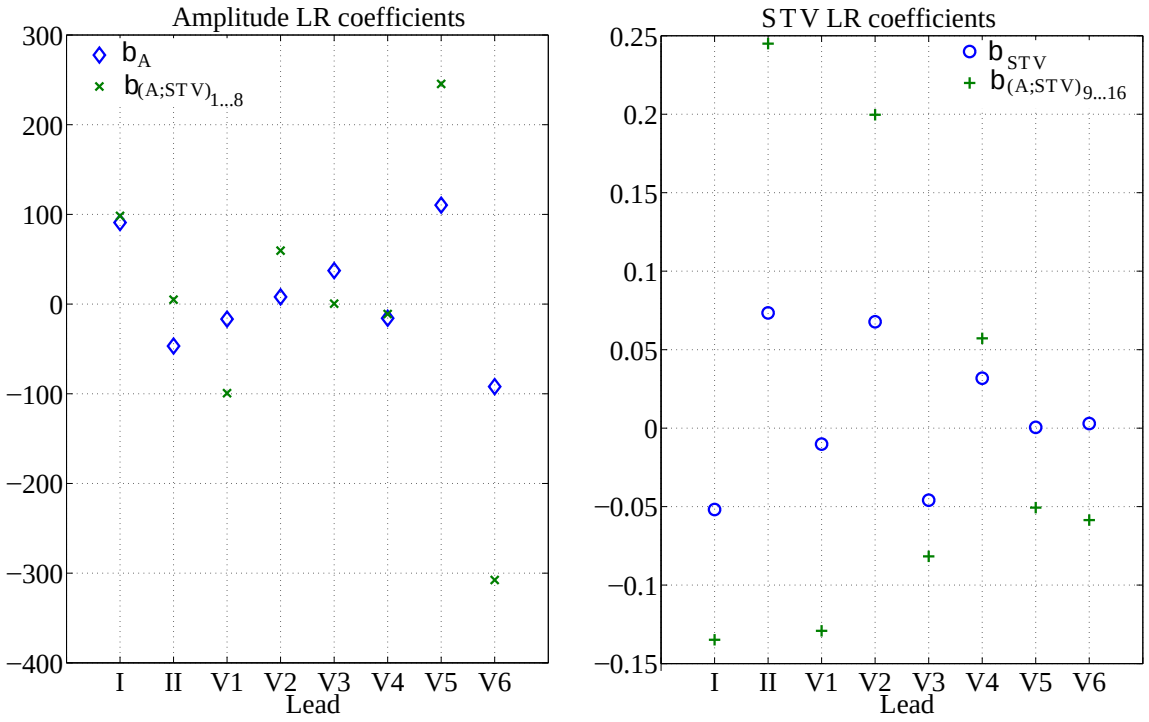


Figure 6.3: LR regression coefficients of ECG multivariate features, both in separate and combined analysis. Left: multivariate f-wave amplitude ($\mathbf{b}_{\mathrm{A}}$ and first 8 coefficients of $\mathbf{b}_{(\mathrm{A;STV})}$). Right: multivariate AF STV ($\mathbf{b}_{\mathrm{STV}}$ and last 8 coefficients of $\mathbf{b}_{(\mathrm{A;STV})}$).

a uniform weighting scheme ($\mathbf{b} = \mathbf{1}$). Furthermore, the regression coefficients' weighting action has been investigated. More precisely, values of LR coefficients $\mathbf{b}_{\mathrm{A}}$ computed on f-wave amplitude data only are compared with the corresponding atrial amplitude kept in the first L entries of vector $\mathbf{b}_{(\mathrm{A;STV})}$, obtained when amplitude and AF complexity are processed together. The same analysis is repeated for coefficients $\mathbf{b}_{\mathrm{STV}}$ and the last L entries of $\mathbf{b}_{(\mathrm{A;STV})}$, referring to STV content so as to verify how such information provided by every ECG lead influences prediction scores in both cases. Results of our examination are plotted in Fig. 6.3, providing spatial distribution of regression coefficients over ECG leads.

6.5.6 Discussion and conclusions

Our results show that amplitude and STV features seem to enhance prediction performance when contributions computed on each lead are combined into the LR linear combination and properly weighted by LR coefficients. This approach remarkably improves acute CA outcome prediction and helps assessing procedural success, which is associated with CEE performance right after the procedure.

Table 6.4 shows the advantages brought by LR measures to CA outcome prediction, as proved by the high AUC values and the presence of significant differences between the classes examined. Feature combination further enhances the degree of clustering of such groups, therefore notably improving prediction. Such a multilead strategy provides a more accurate prediction than classical single-lead parameters, for instance, f-wave mean amplitude $D(V_1)$, which is not able to underline significant interclass differences. Similar

remarks can be made for the sample entropy and the QSE index, as its discriminative power is considerably weak. What is more, results obtained do not match basic assumptions made in previous studies [5], namely, correlation between low entropy values and CEE success due to a higher degree of AF organization, independently from the setting adopted.

Concerning mean values of f-wave amplitude and NMSE, ($\overline{D}_8$ and $\overline{\mu}_8$, respectively), note that attributing the same weight to all ECG leads by simply averaging their contributions does not improve prediction, as no significant differences can be observed between the groups of interest. It turns out that CA outcome prediction benefits from multivariate data processing and classification, provided that input variables (i.e., ECG leads) are properly combined, as when LR is applied.

Fig. 6.3 highlights that LR coefficient dispersion is considerably lower when analyzing each set of features separately, as quantified by standard deviation ($\sigma_{\mathbf{b}_\mathrm{A}} = 68.00$ vs. $\sigma_{\mathbf{b}_{(\mathrm{A;STV})_{1\ldots8}}} = 159.51$, and $\sigma_{\mathbf{b}_\mathrm{STV}} = 0.05$ vs. $\sigma_{\mathbf{b}_{(\mathrm{A;STV})_{9\ldots16}}} = 0.15$). It could depict a lower degree of variability, which hides significant information coming from certain electrodes. However, it is important to keep in mind that such variability could also be due to model estimation errors, which tend to increase with the problem's dimensionality for a given sample size. Benefits from feature combination are confirmed by Fig. 6.2 as well. First, it shows that CA outcome prediction is improved by multilead processing, as the higher the number of leads L examined, the higher the AUC, in keeping with results shown in Sec. 4.4.4. Secondly, regardless of the number of electrodes L exploited, examining such ECG properties together probably provides a more complete overview of AF activity, which enhances classification quality. On one hand, f-wave amplitude is predictive of CA outcome and it is strictly correlated with AA signal energy; on the other hand, STV quantifies the degree of regularity and temporal repetitiveness of AF patterns, besides their spatial distribution over ECG leads. These characteristics are quite complementary with each other. Indeed, f-wave amplitude can effectively depict very regular signals; conversely, sharp patterns can hamper signal interpolation and do not render AF temporal evolution. In contrast, STV indices are more suitable for capturing signal diversity and characterizing its temporal dynamics. However, their descriptive power is reduced when dealing with very regular waveforms, where it is harder to extract information about their variability; hence the advantage of merging knowledge about these two aspects, so as to enrich AF characterization and overcome their respective limitations. The tool proposed can be effectively exploited for selecting positive responders to CEE after ablation, thus helping short-term CA outcome assessment in persistent AF.

6.6 Summary and conclusions

In this chapter we shed some light about the LR model ability to properly combine amplitude and STV measures derived from different ECG leads. Simultaneous examination of heterogeneous ECG features enrich AF characterization, thus making the prediction of procedural AF termination more accurate. This technique highlights ECG leads exhibiting components which are more relevant to CA outcome prediction, while reducing the influence of the remaining ones. Further investigation should be performed on LR coefficients and their interpretation. In addition, the algorithm should be tested on other features determined on standard ECG (e.g., frequency domain parameters). Despite these

shortcomings, the present multiple-feature framework notably improves CA outcome prediction and helps AF characterization.

In the next chapter we define a further strategy for assessing AF content over surface ECG, exploring the degree of spatial correlation and the amount of information shared between ECG leads by means of approaches derived from information theory

Table 6.4: LR analysis of combined ECG features for selection of CEE candidates: inter-class statistical difference assessment and ROC analysis. ([n.u.]: normalized units).

	CEE	No CEE	p-value	AUC	Sensitivity	Specificity	Best cutoff	T_C
LR_{A} [n.u.]	0.78 ± 0.20	0.48 ± 0.27	$1.98 \cdot 10^{-5}$	0.83	0.78	0.82	0.71	5.88
LR_{STV} [n.u.]	0.78 ± 0.20	0.48 ± 0.25	$2.32 \cdot 10^{-5}$	0.83	0.81	0.71	0.59	22.17
$LR_{(\mathrm{A;STV})}$ [n.u.]	0.88 ± 0.20	0.26 ± 0.26	$\mathbf{9.19 \cdot 10^{-13}}$	**0.95**	**0.95**	**0.88**	0.46	27.36
$D(V_1)$	0.06 ± 0.02 [mV]	0.07 ± 0.03	0.18	0.61	0.62	0.65	0.06	1.20
$\mathrm{SampEn}(L_s, r_1)$	2.78 ± 0.18 [n.u.]	2.77 ± 0.26	0.82	0.49	0.35	0.82	2.87	$2.96 \cdot 10^3$
$\mathrm{SampEn}(L_s, r_2)$ [n.u.]	2.09 ± 0.18	2.08 ± 0.25	0.83	0.49	0.35	0.76	2.18	$3.89 \cdot 10^3$
$QSE(L_s, r_1)$ [n.u.]	5.21 ± 0.38	5.19 ± 0.46	0.88	0.51	0.22	0.76	5.00	$2.21 \cdot 10^3$
$QSE(L_s, r_2)$ [n.u.]	4.37 ± 0.36	4.34 ± 0.42	0.77	0.52	0.46	0.53	4.36	$2.22 \cdot 10^3$
$\overline{D}_8$ [mV]	0.04 ± 0.02	0.03 ± 0.02	0.41	0.62	0.51	0.71	0.03	6.63
$\overline{\mu}_8$ [n.u.]	51.45 ± 12.18	49.36 ± 12.31	0.56	0.53	0.40	0.71	49.46	22.13

7 Contributions from information theory to CA outcome prediction

7.1 Introduction

As stated in Chapter 5, the concept of AF organization is not uniquely defined and it can be interpreted from multiple perspectives. In Chapter 5 we studied how AF content explains its variability over ECG leads (thus in terms of interlead spatial distribution) and how its components recur along the ECG recording (therefore characterizing signal repetitiveness). In the next sections we deal with a further strategy to assess AF regularity from a different perspective, aiming at quantifying the degree of mutual correlation between 2 or more ECG leads. Accordingly, we neglect signal temporal evolution, thus exclusively focusing on interlead spatial correlation assessed on the whole ECG recording. This approach is inspired by information theory (IT), the so-called "mathematical theory of communication" founded by Claude E. Shannon in 1948 [136]. The techniques presented in this chapter have been so far usually applied to telecommunication systems so as to quantify the amount of information exchanged by two systems and carrying out several signal processing operations (for instance, compressing data), as well as reliably storing and communicating data. Subsequently, such methods have been widely employed in other fields, for instance, statistical inference, natural language processing and neurobiology [164].

We organize this chapter in two main sections. The first part briefly sketches the key ideas of IT in Sec. 7.2 and provides an overview of the mathematical background at the basis of its development. These concepts then find a clinical application in the second part, which outlines the main experimental results obtained in a single ECG lead in CA outcome prediction and AF characterization in Sec. 7.3. Our analysis is then extended to multiple electrodes in Sec. 7.4. Final conclusions are summarized in Sec. 7.5.

7.1.1 Overview of IT

In a communication system, the main goal is conveying information from one point to another. This task arises from this question: what is the maximum amount of meaningful information which can be conveyed between two systems [164]? As explained in [136], the term "information" deals with a measurable quantity, assessing the ability of the receiving system to interpret data flows coming from the transmitter, namely, decoding the sequence of symbols it consists of. This explains the use of logarithmic measures (as explained in the next sections) typical of IT, since every kind of data is codified into

bits, the minimal units of information [136]. This assertion implies an idea of uncertainty around information conveyed, which is expressed as the minimal number of bits required for transferring data. These assumptions lead us to regard its sources as random variables, and probability theory is therefore employed to model the efficacy of this information transfer.

7.1.2 Some clinical applications of information theory tools

In [135] IT has been applied to molecular biology for understanding how proteins interact with DNA at specific sequences called binding sites. In [146] a clustering method based on mutual information (MI) enables co-expressing gene classification. Some applications to EEG analysis have also been put forward to investigate ischemic episode effects on human brain [13]. In addition, a spectral analysis through IT measures has been performed for analyzing EEG seizures on EEG [13]. The study led in [1] puts forward a classification system for myocardial information based on the maximization of entropy criteria on ECG. In [134] a method based on MI has been implemented for selecting electrodes for the noninvasive extraction of fetal cardiac signals from maternal abdominal recordings. Cardiac arrhythmia detection has been also envisaged in [88] by computing MI on the heartbeat interval series. To our knowledge, no correlation between IT background and AF therapy has been established until present. Accordingly, in the sequel we attempt at quantifying AF regularity in the IT framework and investigate its predictive power for CA characterization.

7.2 Basic theoretic definitions

7.2.1 Shannon's information measures: the 2-variable case

Before illustrating some clinical applications to persistent AF analysis, we first provide some definitions of the main concepts at the basis of IT mathematical background [37]. Accordingly, let us define a generic continuous random variable (r.v.) X that can take on any value from a domain $\mathcal{X}$ and that is characterized by a probability mass function $p(x) = Pr\{X = x\}, x \in \mathcal{X}$. However, every function defined in the sequel can be applied also to continuous variables, provided that sums are replaced by integrals.

We first introduce the marginal entropy $H(X)$, which quantifies the degree of uncertainty of the r.v. X:

$$H(X) = -E\{\log p(x)\} = -\int_{x\in\mathcal{X}} p(x)\log p(x) \tag{7.1}$$

Entropy is always a positive quantity ($0 \leq H(X) \leq 1$), so that $\log p(x) \leq 0$. The higher its value, the higher the degree of uncertainty of the variable considered. Entropy and all the IT measures are conventionally expressed in bits, thus logarithm function is computed in base 2. Moreover, note that $H(X)$ is a functional of the distribution $p(x)$, therefore it does not depend on the actual values taken by X, but only on their probabilities.

Just as with probabilities, we can compute joint and conditional entropies. Therefore, let us extend entropy definition to two r.v., and explore their mutual dependency. To this end, we introduce another r.v. Y taking values in $\mathcal{Y}$ with probability density $p(y)$

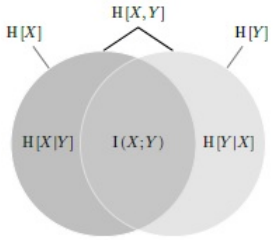


Figure 7.1: Graphical representation of the relationships between the IT parameters defined in Sec. 7.2.

and we attempt to quantify the degree of coupling with X, assuming $p(x, y)$ as their joint probability distribution. Accordingly, we present the joint entropy (JE):

$$JE = H(X;Y) = -E_X\{E_Y\{\log p(x,y)\}\} = -\int_{x\in\mathcal{X}}\int_{y\in\mathcal{Y}} p(x,y)\log p(x,y) \tag{7.2}$$

This index quantifies the degree of randomness shared between the pair of variables examined, thus we expect high values if the r.v. are independent. We also mention the conditional entropy $H(Y|X)$, which expresses the degree of uncertainty of Y conditioned to the value of X:

$$H(Y|X) = -E_X\{E_Y\{\log p(y|x)\}\} = -\int_{x\in\mathcal{X}}\int_{y\in\mathcal{Y}} p(x,y)\log p(y|x) \tag{7.3}$$

This definition allows for enunciating the chain rule, which puts the aforementioned parameters in functional relation with each other:

$$H(X,Y) = H(X) + H(Y|X) \tag{7.4}$$

Proof of Eq. (7.4) is provided in Appendix A.4.

Another feature already mentioned in Sec. 7.1.2, i.e., the MI index $I(X;Y)$, measures the amount of information that one r.v. X contains about another one Y, thus expressing the level of interdependence.

$$MI = I(X,Y) = -\int_{x\in\mathcal{X}}\int_{y\in\mathcal{Y}} p(x,y)\log\frac{p(x,y)}{p(x)p(y)} \tag{7.5}$$

Note that if X and Y are independent $p(x, y)$ can be factorized into the product $p(x, y) = p(x)p(y), \forall x \in \mathcal{X}, \forall\dagger \in \mathcal{Y}$, thereby $I(X, Y) = 0$. As a consequence, JE defined in Eq.(7.2) will be equal to the sum of the marginal entropies of each variable according to the expression in Eq. (7.1). MI relation with entropy can be expressed as:

$$I(X,Y) = H(X) - H(X|Y) = H(X) + H(Y) - H(X,Y) = H(X,Y) - H(Y|X) - H(X|Y), \tag{7.6}$$

which is also graphically explained in Fig. 7.1. MI is nonnegative ($I(X;Y) \geq 0$) and symmetric ($I(X;Y) = I(Y;X)$). Additionally, it is characterized by the property $I(X;X) = H(X)$.

7.2.2 IT extension to multiple variables: the chain rule

Definitions of entropy functions provided in Sec. 7.2.1 can be extended so as to evaluate interactions between L variables $X_1, X_2, \ldots, X_L$, whose probability density is denoted as $p(x_1, x_2, \ldots, x_L)$. Generalization of the 2-variable chain rule results in:

$$H(X_1, X_2, \ldots, X_L) = \sum_{i=1}^{L} H(X_i|X_{i-1}, \ldots, X_1) \tag{7.7}$$

Proof of Eq. (7.7) is detailed in Appendix A.4. This rule can be also applied to MI, also referred to as multivariate mutual information (MMI), thus yielding:

$$I(X_1, X_2, \ldots, X_\ell) = I(X_1; X_2; \ldots; X_{\ell-1}) - I(X_1; X_2; \ldots X_{\ell-1}|X_\ell) \tag{7.8}$$

with $\ell = 1, \ldots, L$. It can be interpreted as the gain (or loss) in the information transmitted between a set of variables due additional knowledge of an extra variable [144]. According to the formulation proposed by [64], Eq. (7.8) can be also expressed in terms of entropies :

$$\begin{aligned} I(X_1, X_2, \ldots, X_\ell) &= \sum_{i=1}^{L} H(X_i) - H(X_1, \ldots, X_{\ell-1}|X_\ell) = \\ &= -\sum_{i=1}^{\ell-1}(-1)^i H(X_i) + \sum_{i=1}^{\ell-1}(-1)^i H(X_1, \ldots, X_{i-1}|X_i) \end{aligned} \tag{7.9}$$

with $\ell = 1, \ldots, L$. According to this definition, the MMI index can be expressed as a function of L variables, depending on the ℓth conditional variable selected. In contrast with bivariate MI, it is worth noting that MMI can also take nonnegative values, owing to variations (either positive or negative) of dependence between variables when holding one of them, therefore interpretation of its value is not always straightforward. Note that the MMI measure is quantitatively different from the joint entropy computed on 2 leads, as suggested by the definition in Eq. (7.9).

After this overview of the IT theoretical background, we illustrate in next sections some applications to ECG analysis and CA outcome prediction for persistent AF characterization.

7.3 Single-lead assessment of AF regularity on surface ECG for CA analysis

7.3.1 Methods and results

As aforementioned in Sec. 7.2.1, the marginal entropy of a r.v. X as defined in Eq. (7.1) expresses the degree of uncertainty about a certain event to occur. In our application, as we deal with AA signal probability distribution functions (PDFs), entropy quantifies the amount of information about atrial amplitude values, which occur with a certain probability. The higher the uncertainty, the larger the amount of information conveyed by AA signal on average.

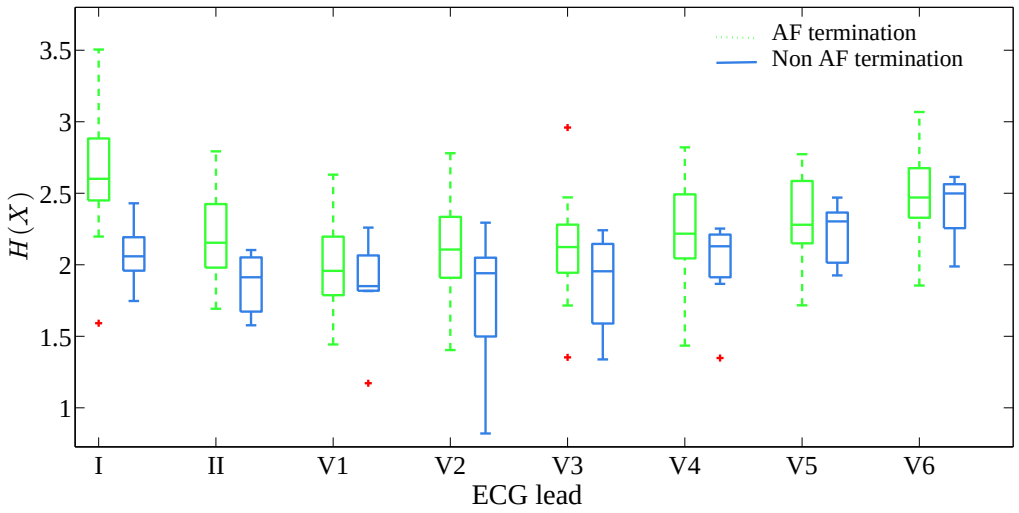


Figure 7.2: Box-and-whisker plot of the single-lead entropy $H(X)$ in the long-term CA outcome prediction. Outliers are marked with the symbol ×.

In the light of these considerations, we first computed this index for each patient of the 36-subject database presented in Sec. 3.5.5. Marginal entropy values have been determined in each of the 8 ECG leads of the subset introduced in Sec. 2.4.4. Entropy index requires computation of the AA signal PDF. Accordingly, for a given T-sample AA signal $\mathbf{y}_\ell$, ℓ, $\ell = 1, \ldots, L$, $L = 8$, its histogram has been computed in the range of values $[X_{\text{MIN}} - \frac{\delta}{2}, X_{\text{MAX}} + \frac{\delta}{2}]$, where $\delta = (T)^{\frac{1}{2}}$ is the bin width of the histogram. Interclass statistical differences are graphically represented by a box-and-whisker plot in Fig 7.2. Moreover, ROC analysis has been carried out, and the AUC index determined on each ECG lead has been plotted in Fig. 7.3. Dependence on signal amplitude has been finally verified by computing marginal entropy of the AA signal after normalization by its variance. This measures is then compared with that assessed on the non-normalized signal by means of an index named negentropy [37] and defined as:

$$Neg(X) = H(G) - H(X) \tag{7.10}$$

where $H(G)$ is the marginal entropy of a Gaussian distribution having the same mean and variance as the PDF of the r.v. X. The lower this index, the more input data PDF resembles a normal distribution. We hypothesize that if negentropy does not vary significantly from one electrode to another when AA signal variance is normalized to 1, it means that the entropy measures depends on input signal amplitude. In Fig. 7.4 we plot the spatial distribution of negentropy of the AA signal before and after normalization of variance to 1, and they are denoted $Neg(X)$ and $Neg(X)_{\text{NORM}}$ respectively. Values of this parameter are averaged over the whole AF-database in each ECG lead and normalized between 0 and 1.

In this section we do not include results concerning prediction of acute termination by CA since we observed that entropy measures do not significantly contribute to this clinical task, as confirmed by the poor prediction performance (AUC$<$ 0.65 in each ECG lead).

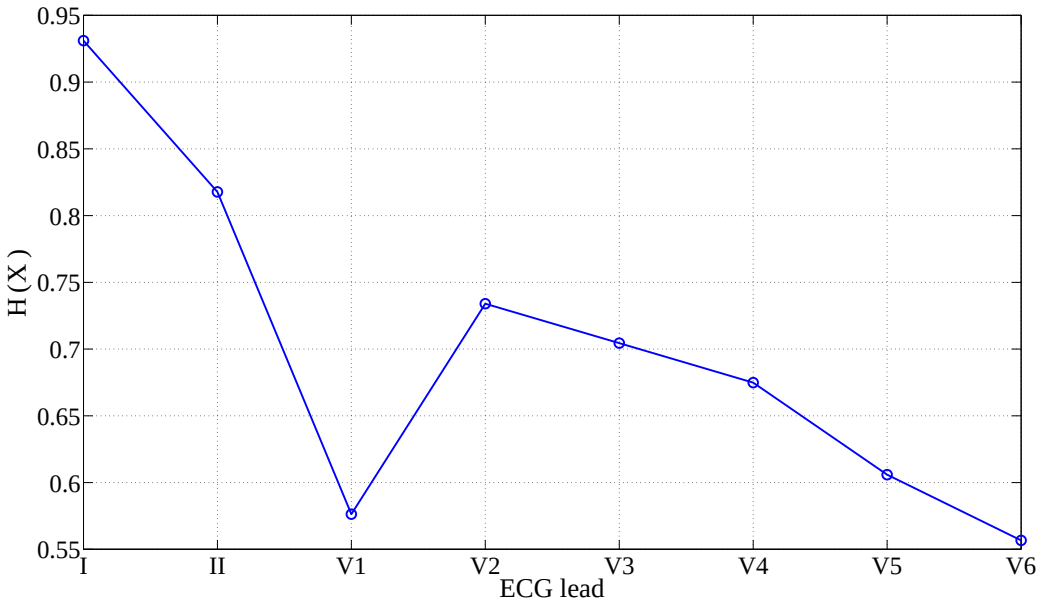


Figure 7.3: AUC index related to $H(X)$ long-term CA outcome prediction quality on each ECG lead.

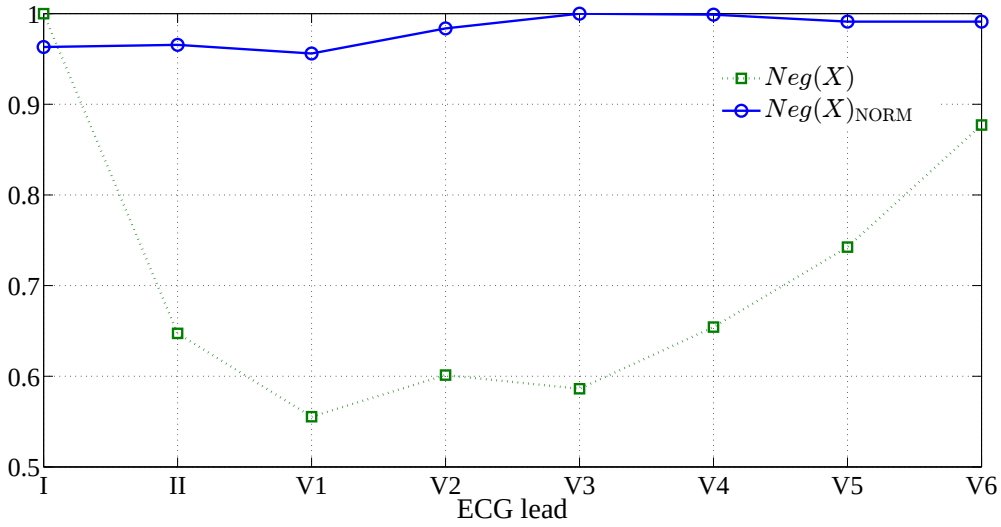


Figure 7.4: Spatial distribution of the negentropy index determined on each ECG lead of the AA signal before and after variance normalization.

7.3.2 Results and discussion

The marginal entropy measure seems to be quite sensitive the ECG lead chosen, as confirmed by Fig. 7.2. Significant interclass differences are obtained only in lead I (p value: $4.0 \cdot 10^{-4}$), II (p-value:$7.4 \cdot 10^{-3}$) and V_2 (p value: $1.8 \cdot 10^{-2}$), whereas the groups examined can not be significantly distinguished in the other leads. The ROC analysis corroborates the accurate prediction performance in the aforementioned leads in Fig. 7.3. Note the high degree of variability of the AUC index over the ECG leads. However, regardless of the electrode examined, we can generally remark that higher entropy values are always associated with procedural AF termination and freedom from the arrhythmia in the long-term follow-up. These results do not merely depend on signal PDF, but rather on its amplitude. Indeed, Fig. 7.4 shows that not only the negentropy measure varies when AA signal is normalized by its variance, but also that its values do not significantly change when switching from one lead to another. In fact, negentropy standard deviation σ computed on all leads is lower when AA signal is normalized ($\sigma(Neg(X_{\mathrm{NORM}})) = 0.02$; $\sigma(Neg(X)) = 0.16$). This experimental evidence confirm the relationship between marginal entropy and atrial amplitude, which is correlated with AF therapy outcome, as demonstrated in Sec. 4.4.4. In keeping with those results, the higher $H(X)$, the more likely AF termination by CA. In the next sections our investigation will focus on the assessment of the IT measures in a multivariate framework by taking into account more than one ECG lead.

7.4 Multilead assessment of AF regularity on surface ECG for CA analysis

7.4.1 Extension of IT measures to 2 ECG leads

The high degree of variability affecting CA outcome prediction performance in the single-lead perspective of entropy measures lead us to explore further strategies for assessing procedural AF termination in a more robust framework. This objective motivates the exploitation of ECG spatial diversity and the investigation of IT indices defined on more than one ECG lead.

CA outcome prediction based on IT indices has been carried out by taking into account two distinct follow-up windows, since we aim at predict both acute procedural success and long-term AF termination by CA. More precisely, short-term prediction performance of the IT parameters has been first evaluated on the 31-procedure dataset introduced in Sec. 3.5.5, whereas long-term procedural outcome has been assessed on the 36- patients' database mentioned in the same section. Our analysis aims at investigating whether any particular AF properties can be enhanced by this feature with respect to CA procedural success, and how relevant to AF investigation the choice of couple of electrodes is. The same histogram setting as that presented in Sec. 7.3.1 has been applied to both variables involved into JE computation. Accordingly, the JE index defined in Eq. (7.2) is computed for all the possible $\frac{L!}{2!(L-2!)} = 28$ combinations of the 8-lead subset under examination ($L = 8$), and CA outcome prediction performance is then assessed by the AUC index, whose values are reported for each combination of leads in Table 7.1 and Table 7.2 for the short-term and the long-term therapeutic outcome assessment, respectively. Entropy

Table 7.1: ROC analysis of the short-term CA outcome for each pair of ECG leads by means of the JE index directly computed on the AA signal (without PCA preprocessing). ECG leads examined are underline by the symbol ×.

Leads	AUC	I	II	V_1	V_2	V_3	V_4	V_5	V_6
[V_2 V_3]	0.68				X	X			
[V_1 V_5]	0.65			X				X	
[V_1 V_3]	0.65			X		X			
[V_2 V_4]	0.61				X		X		
[V_3 V_6]	0.61					X			X
[V_4 V_6]	0.60						X		X
[V_3 V_5]	0.60					X		X	
[II V_1]	0.60		X	X					
[V_1 V_6]	0.59			X					X
[I V_2]	0.57	X			X				
[V_1 V_4]	0.57			X			X		
[V_3 V_4]	0.56					X	X		
[II V_5]	0.56		X					X	
[II V_3]	0.56		X			X			
[V_5 V_6]	0.56							X	X
[V_4 V_5]	0.56						X	X	
[II V_6]	0.54		X						X
[I V_6]	0.53	X							X
[V_2 V_5]	0.53				X			X	
[I V_1]	0.52	X		X					
[II V_2]	0.52		X		X				
[I V_5]	0.52	X						X	
[I V_4]	0.52	X					X		
[I V_3]	0.52	X				X			
[I II]	0.51	X	X						
[V_2 V_3]	0.50				X	X			
[V_1 V_2]	0.50			X	X				
[V_2 V_6]	0.46				X				X

Table 7.2: ROC analysis of the long-term CA outcome for each pair of ECG leads by means of the JE index directly computed on the AA signal (without PCA preprocessing). ECG leads examined are underline by the symbol ×.

Leads	AUC	I	II	V_1	V_2	V_3	V_4	V_5	V_6
[I V_3]	0.95	X				X			
[I V_4]	0.94	X					X		
[I V_2]	0.93	X			X				
[II V_4]	0.93		X				X		
[II V_3]	0.91		X			X			
[I V_5]	0.91	X						X	
[II V_6]	0.89		X						X
[I V_6]	0.89	X							X
[I V_1]	0.89	X		X					
[II V_2]	0.89		X		X				
[II V_5]	0.89		X					X	
[V_3 V_4]	0.79					X	X		
[V_2 V_6]	0.79				X				X
[V_4 V_6]	0.78						X		X
[II V_1]	0.76		X	X					
[V_2 V_4]	0.76				X		X		
[V_4 V_5]	0.74						X	X	
[V_3 V_6]	0.74					X			X
[V_2 V_3]	0.74				X	X			
[V_3 V_5]	0.72					X		X	
[V_1 V_3]	0.72			X		X			
[V_2 V_5]	0.72				X			X	
[I II]	0.71	X	X						
[V_1 V_4]	0.71			X			X		
[V_1 V_2]	0.70			X	X				
[V_5 V_6]	0.70							X	X
[V_1 V_6]	0.70			X					X
[V_1 V_5]	0.63			X				X	

Table 7.3: AUC criterion assessment of long-term AF termination prediction performance of the MMI index directly computed on the AA signal for a fixed conditioned variable Y_c. In the 8-lead subset, the symbol − means that the lead has not been considered in the analysis.

Y_c	I	II	III	aV_R	aV_L	aV_F	V_1	V_2	V_3	V_4	V_5	V_6
MMI_8	0.79	0.64	−	−	−	−	0.66	0.58	0.66	0.56	0.66	0.62
MMI_{12}	0.76	0.61	0.55	0.73	0.80	0.70	0.66	0.58	0.56	0.64	0.71	0.74

value independence from atrial amplitude has also been investigated as in Sec. 7.3, and the dispersion of negentropy values over the 28 pairs of ECG leads (X, Y) has been quantified; it is denoted $\sigma(Neg(X,Y))$ and $\sigma(Neg(X,Y)_{\text{NORM}})$ for non-normalized and normalized AA data, respectively. Also in this case negentropy has been averaged over the whole database and normalized between 0 and 1.

7.4.2 Extension of IT measures to L ECG leads

Subsequently, we have investigated whether bivariate IT analysis can be generalized over a higher number of ECG leads so as to underline further properties of AF electrophysiology. Accordingly, we have attempted to combine ECG spatial variability and IT regularity measures by looking at a higher number of ECG leads. To this goal, MMI is computed as in Eq. 7.8 on the 8 linearly independent leads of the AA signal. In keeping with the MMI definition given in Eq. 7.8, a conditional variable has to be fixed for computing the conditional entropy term as defined in (7.3), and MMI value depends on the variable chosen. Accordingly, MMI has been computed for each of the L possible combinations by fixing an electrode Y_c at a time, and prediction quality has been then assessed by the AUC criterion, both for $L = 8$ and $L = 12$, as indicated in Table 7.3.

7.4.3 Discussion

Our investigation underlines that direct extraction of the JE feature from the AA signal does not significantly provide to CA outcome prediction performance right after ablation performance, as confirmed by the poor ROC analysis results in Table 7.1. Moving to the long-term perspective, one of the main results put forward by the JE index computation is the different relevance of ECG leads in characterizing AF with respect to therapy outcome. In particular, we can remark that the most discriminative signal components are properly emphasized when information about AF components is provided by different planes and orientations of heart electrical vector. Indeed, as shown in Table 7.2, the most accurate prediction performance is guaranteed by the combination of a frontal lead with a limb lead, as proved by the related high AUC values. By contrast, contributions coming from the same planes are not equally meaningful, or they poorly cluster the groups of interest. A similar result has been demonstrated by the LR analysis of f-wave amplitude in Sec. 6.4, in which CA outcome prediction performance of atrial amplitude descriptors determined on small ECG subsets proves to be more accurate when leads belonging to different heart planes are taken into account. On the other hand, we can remark that such method does not benefit from PCA preprocessing of raw AA data. Joint analysis of entropy on subsets of ECG leads confirms its robustness and efficacy in characterizing AF at a higher degree of accuracy than single-lead methods, due to their strong prediction

performance dependence on electrode selection, as confirmed by Fig. 7.3 The higher JE, the more likely procedural AF termination, e.g., in leads I and V_3, AUC= 0.95, AF termination: 7.17 ± 0.82, Non AF termination: 5.43 ± 1.69, p value: $3.45 \cdot 10^{-5}$. As in Sec. 7.3, negentropy analysis reveals a relation between bivariate IT measures and AA signal amplitude. Indeed, standard deviation of negentropy values computed on the AA signal normalized by its variance is globally lower ($\sigma(Neg(X,Y)_{\text{NORM}}) = 3.2 \cdot 10^{-4}$) than that determined on data in absence of normalization ($\sigma(Neg(X,Y)) = 0.10$). As a consequence, also in this case the higher JE values denote a more organized AF activity, which is reflected by higher atrial amplitude values, ans are significantly correlated with procedural AF termination by CA.

As far as the MMI multilead perspective is concerned, MMI does not seem to be able to effectively predict freedom from AF recurrence in the long-term follow-up. One of the main drawbacks is represented by the choice of the conditional variable prior to its computation, which is not guided by any quantitative criteria. In Table 7.3 we can note how variable and irregular classification performance is with respect to the electrodes examined, and how the MMI discriminative power can remarkably decrease if the conditional variable is not adequately selected. No significant differences between the groups of interest when increasing the number of variables and examining the whole standard ECG, thus confirming the redundancy exhibited by the electrodes removed by the reduced 8-lead subset under examination. Prediction of candidates to CEE after CA has been investigated as well. However, no significant results have been reported, thus they are not included in this dissertation, and we exclusively focus on clinical tasks in which IT measures demonstrate to provide relevant contribution. We did not report experimental details concerning prediction of acute AF termination by CA, since the discriminative power of the MMI index proves to be quite low in this context.

In the light of these considerations, given the relationship between IT measures and f-wave amplitude demonstrated in Sec. 7.4.3, we now investigate whether this property can be properly enhanced by PCA reduced-rank approximations of the AA signal, in keeping with Sec. 4.3, so as to improve AF characterization and therapy outcome assessment.

7.4.4 What happens if we apply PCA?

In order to explore the potential PCA combination with IT feature extraction, features defined in the IT scenario are computed on the rank-1 truncation of AA signal introduced in Eq. (4.19).

In the bivariate framework, the same type of analysis explained in Sec. 7.4.1 is repeated by computing IT features on the AA signal approximated by CA, and results are shown in Table 7.4 and Table 7.5.

Acute AF termination by CA seems to be considerably improved by PCA-based AA signal reduced-rank approximation in certain pairs of ECG leads, in particular those including lead V_5, as displayed in Table 7.5. This lead is located close to the left anterior axillary line, yet our analysis is limited by the lack of a relevant clinical interpretation of its role in AF characterization. In most of the ECG leads' combinations examined, higher values of this bivariate index significantly predict AF termination by CA in the long-term follow-up, whereas recurrence of this arrhythmia seems to be depicted by lower JE values, in line with remarks made about links between marginal entropy and atrial amplitude in Sec. 7.3.2.

Table 7.4: ROC analysis of the long-term CA outcome for each pair of ECG leads by means of the JE index after PCA preprocessing of the AA signal. ECG leads examined are underline by the symbol ×.

Leads	AUC	I	II	V_1	V_2	V_3	V_4	V_5	V_6
[V_2 V_3]	0.95				X	X			
[V_2 V_4]	0.92				X		X		
[I V_2]	0.88	X			X				
[I V_3]	0.87	X				X			
[V_3 V_4]	0.84					X	X		
[V_1 V_3]	0.84			X		X			
[V_1 V_2]	0.82			X	X				
[II V_2]	0.82		X		X				
[V_1 V_4]	0.81			X			X		
[I V_4]	0.74	X					X		
[V_2 V_5]	0.73				X			X	
[II V_3]	0.73		X			X			
[I V_1]	0.71	X		X					
[V_2 V_6]	0.71				X				X
[II V_1]	0.67		X	X					
[I II]	0.64	X	X						
[II V_4]	0.62		X				X		
[II V_6]	0.62		X						X
[V_3 V_5]	0.61					X		X	
[V_3 V_6]	0.61					X			X
[V_5 V_6]	0.59							X	X
[II V_5]	0.56		X					X	
[V_4 V_6]	0.54						X		X
[I V_5]	0.51	X						X	
[V_4 V_5]	0.51						X	X	
[I V_6]	0.50	X							X
[V_1 V_6]	0.50			X					X
[V_1 V_5]	0.47			X				X	

Table 7.5: ROC analysis of the short-term CA outcome for each pair of ECG leads by means of the JE index after PCA preprocessing of the AA signal. ECG leads examined are underline by the symbol ×.

Leads	AUC	I	II	V_1	V_2	V_3	V_4	V_5	V_6
[V_4 V_5]	0.92						X	X	
[V_3 V_5]	0.90					X		X	
[V_5 V_6]	0.89							X	X
[V_4 V_6]	0.86						X		X
[II V_5]	0.85		X					X	
[V_2 V_5]	0.78				X			X	
[I V_5]	0.78	X						X	
[V_1 V_2]	0.78			X	X				
[II V_6]	0.76		X						X
[V_3 V_6]	0.76					X			X
[V_3 V_4]	0.70					X	X		
[II V_4]	0.69		X				X		
[V_1 V_5]	0.69			X				X	
[I V_1]	0.68	X		X					
[II V_1]	0.68		X	X					
[I V_2]	0.67	X			X				
[I V_6]	0.65	X							X
[II V_3]	0.61		X			X			
[V_2 V_6]	0.60				X				X
[I V_4]	0.58	X					X		
[V_1 V_3]	0.57			X		X			
[V_2 V_4]	0.56				X		X		
[II V_2]	0.56		X		X				
[I V_3]	0.54	X				X			
[I II]	0.53	X	X						
[V_1 V_6]	0.52			X					X
[V_1 V_4]	0.52			X			X		
[V_2 V_3]	0.43				X	X			

Table 7.6: Unpaired statistical analysis and long-term CA outcome prediction performance of MMI measures.

	AF termination	Non AF termination	p-value	AUC	$Sensitivity$	$Specificity$	Best cut-off
MMI_8	2.52 ± 0.54	1.55 ± 0.33	$\mathbf{7.2 \cdot 10^{-4}}$	0.93	0.93	0.86	1.56
MMI_{12}	2.53 ± 0.54	1.63 ± 0.36	$\mathbf{1.8 \cdot 10^{-3}}$	0.93	0.93	0.86	1.75
$H(V_1)$	1.99 ± 0.29	1.86 ± 0.34	$3.0 \cdot 10^{-1}$	0.58	0.69	0.43	1.87

On the other hand, when looking at longer follow-up periods, even though CA prediction performance is extremely accurate on most of the ECG lead pairs examined and comparable with that reported on AA data, we can remark that physiological interpretation about the descriptive power of orthogonal planes in AF electrical activity characterization is partially lost. Also the role played by the most recurrent leads in the most discriminative pairs, i.e., V_2 and V_3 (see Table 7.4), needs to be further elucidated. Generally speaking, PCA preprocessing does not seem to significantly improve IT feature extraction when processing pairs of ECG leads, since variables determined on PCA reduced-rank approximations are all the same up to scale.

PCA preprocessing of the AA signal has also been combined with MMI computation in a multilead framework. Accordingly, this index has been computed on the ensemble of 8 linearly independent ECG leads and expressed as mean $\pm$ standard deviation. Furthermore, its descriptive power is compared with that of the same index determined on the full 12-lead ECG. In this experimental section we have interestingly remarked that PCA decomposition of AA data makes the MMI parameter independent of the conditional variable selected, and its value remains unvaried. Accordingly, after PCA performance, we can consider only one MMI value instead of the 8 possible combinations obtained on raw data. This method is also compared with a single-lead descriptor of entropy in V_1, denoted $H(V_1)$. The ability to discriminate between the categories of interest ("AF termination" vs "Non AF termination") is quantified by the p value of the unpaired test, and AUC analysis is carried out as well. All results are reported in Table 7.6. Independence from the conditional variable chosen prior to MMI computation may be explained by the fact that single-lead signals are all equal between each other up to a scale factor after PCA rank-1 approximation. However, unlike JE, this phenomenon considerably increases MMI index reliability, as it makes its computation independent from ECG lead selection. It can be probably explained by the definition of the rank-1 approximation in Eq. (4.19), underlining that in the AA signal truncation the dominant PC is influenced by the dominant spatial topography $\mathbf{m}_1$ exclusively in each lead, and such modulation may not be captured by the ROC analysis. MMI feature extraction after running PCA notably improves prediction results, as demonstrated by the AUC analysis in Table 7.6, on both groups of leads considered in this section. Indeed, after PCA preprocessing, both parameters MMI_8 and MMI_{12} are able to highlight significant differences between the categories examined. AF termination by CA is predicted by higher values of such descriptors, thus corroborating the hypothesis of a more organized and regular AF pattern, which is easier to be predicted and treated by ablation therapy.

7.5 Summary and conclusions

This chapter gives an overview of the basic concepts in the IT framework and their main applications, with particular interest to clinical tasks. After providing some mathematical tools and definitions, our investigation demonstrates the ability of such indices to emphasize AA signal predictive features, as well as underlining several aspects of ECG spatial variability. Higher values of the IT indices significantly correlate with successful CA procedures in the long-term follow-up. Moreover, they enhance AF content at orthogonal angles and orientations of the heart electrical activity, thus enriching disease characterization. A more detailed analysis of some theoretical properties of IT indices should be carried out, in particular when the dimension of the problem is higher than 2. Moreover, physiological interpretation of multivariate measures needs to be more deeply investigated. Finally, further attention should be paid to some algorithm parameters, in particular those related to AA signal histogram computation. Results concerning this part of the our study are still preliminary and deserve further investigation. However, they corroborate the role of interlead spatial correlation as a descriptor of AF content on multilead ECG, without accounting for signal temporal characterization. In the next chapter, our research demonstrates that a further characterization of AF content can be provided by features describing the distribution of RR intervals (RRIs) in a parametric probabilistic approach.

8 Ventricular response characterization during AF in a point process framework

8.1 Introduction

It is widely known that the irregular electrical dynamics typical of AF strongly influence the ventricular activity. Indeed, several studies demonstrated that the electrophysiological properties of the AV junction are profoundly altered in presence of AF [20, 82]. More precisely, the irregular pattern of ventricular responses during AF are determined by effects of concealed conduction and modifications of the physiological refractory period of the AV junction, whose length is related to the duration of the preceding RR intervals (RRIs). The study led in [34] also showed that alterations in AV node function and its refractoriness during AF are reflected on RRI distribution irregularity on ECG. Indeed, in subjects affected by AF the AV node transmits the random, fibrillatory atrial pattern to the ventricles at a scaled-down rate, thus converting the rapid firing input into a slower ventricular response [76]. Given these considerations, if such mutual relationships are to determine the RRI behavior in AF, at least some correlation between the duration of a RRI and that of its successors can be expected. AF effects on ventricular responses make heart rate control one of the main strategies in its treatment [170] and ventricular response analysis. In addition, estimation of the effects of several pharmacological therapies has been performed [141]. Further clinical applications also concern ECG-based AF detection, which can help rapidly diagnosing ventricular arrhythmias [113]. The study in [33] demonstrates that populations of predominant RRIs, i.e., the most probable intervals, are multiple of the AV node refractory period, which are in turn related to AF cycle length. Research led in [32] established that ventricular response during AF is affected not only by AV node properties, but also by fibrillatory process irregularity. Similar remarks in [76] confirm that ventricular rhythm is profoundly altered by AF complexity. In [160] the presence of multiple electrical pathways in AV nodal tissue during AF has been correlated to the number of peaks of the RRI histogram. An attempt to characterize ventricular variability in the presence of AF has been made in [151], which assessed vagal tone control by means of heart rate variability (HRV) features. The predictive power of such features has also been employed in [158] to verify AF recurrence after electrical cardioversion. However, in most of the previous studies RRI distributions are visually inspected, and quantitative assessment of their features is not accomplished. An attempt in modeling probabilistic properties of RR length time series is then made in [65]. Nevertheless, such an approach provides significant results only if applied to stationary signals, and it is also highly dependent on histogram setting parameters (in particular the bin

width), thus making it hard to generalize analysis results. In [35] the refractory periods of the AV node dual pathways and other properties of electrical pattern propagation are determined by performing maximum likelihood (ML) estimation of the RRI series. In [36] some properties are also characterized on the Poincaré plot of the RRIs. Nevertheless, all these methods prove their efficacy on long ECG recordings (at least 10 minutes up to 24-hour Holter recordings), which are not always available in daily clinical practice.

In this doctoral thesis we assume that AF properties are reflected on ECG signals and are linked with therapy outcome. Indeed, electrical wavefronts spreading through the AV node are altered by AF, since their firing rate is higher and their propagation more chaotic and irregular. This induces a higher degree of refractoriness in the AV node, which delays atrial impulses, or even blocks some of them, thus leading to concealed conduction effects. All these events cause an irregular ventricular rhythm, and we hypothesize that they can be investigated on surface ECG. To this end, assessing RRI variability can help shed some light on alteration of ventricular response in presence of AF and that such complexity and unpredictability can somehow influence AF therapy outcome. In this chapter we illustrate a novel parametric method for characterizing the probability distribution of heartbeat interval series, regarded as a history-dependent inverse Gaussian (HDIG) point process, as opposed to standard non-parametric methods [11]. To our knowledge, this method has been applied for the first time to AF analysis. Point process theoretical framework is introduced in Sec. 8.2. The parameters involved in AF content characterization enable the computation of features on RRI distribution which have been first employed as predictors of CA outcome in Sec. 8.3. Then, we also describe an application to AF pattern recognition in Sec. 8.4, in which these indices can significantly distinguish patients affected by the disease from healthy SR subjects. Finally, the main conclusions about this methodology are summarized in Sec. 8.5. Most of the theoretical concepts presented in this chapter takes a step from the study in [11, 23].

8.2 Point process modeling of RRI distribution

8.2.1 Point process model assessment

Our model definition takes a step from the physiological process of R wave generation. Indeed, R wave occurrences can be represented as a sequence of discrete events in continuous time, namely, as a point process [11]. Every R wave event is correlated with the depolarization phenomenon starting in the SA node in the RA and then propagating to the LA and the ventricles. After each depolarization process, the transmembrane potentials of the conduction system cells return to their resting values, so that the spontaneous rise toward depolarization threshold can start again. The beginning of this rise also marks the beginning of the waiting time until the next ventricular contraction (i.e., the next R wave). Previous studies demonstrated that the time between 2 consecutive threshold crossings, i.e., the RRI length, is more accurately modeled by the inverse Gaussian (IG) distribution [145]. This length is not fixed, but it varies according to the sympathetic and parasympathetic dynamic inputs from the autonomic nervous system to the SA node, whose effects can persist on the following heartbeat for several seconds [11]. More specifically, an increase in the sympathetic input reduces RRI length, whereas an increase in parasympathetic action leads to the opposite effect. It turns out that RRIs cannot be

regarded as mutually independent, but it is reasonable to hypothesize their dependence on the previous history of these time-varying inputs. In addition, as previously stated, further contributions mechanisms contribute to modulate R wave temporization during AF because of the alterations in AV node conduction and the irregular propagation of the electrical wavefronts in the atria [36].

Let us consider an ECG interval $(0, T]$, where K consecutive R waves $0 < u_1 < u_2 < , \ldots, < u_k < , \ldots, < u_K \leq T$ at time $\{u_k\}_k = 1^K$ occur. We assume that the probability density of RRIs over the ECG recording can be modeled by a HDIG distribution $f(t, H_{u_k}, \boldsymbol{\theta})$ for each instant $t > u_k$. Each interval $w_k = u_k - u_{k-1}$ is considered as dependent on its previous history $H_{u_k} = (u_k, w_k, w_{k-1}, \ldots, w_{k-q+1})$, i,e., q the most recent RRIs. The probability density function (PDF) $f_{\mathrm{RR}}(t, H_{u_k}, \boldsymbol{\theta})$ of the waiting time before the next R wave event is defined as:

$$f_{\mathrm{RR}}(t, H_{u_k}, \boldsymbol{\theta}) = \left(\frac{\theta_{q+1}}{2\pi(t-u_k)^3})\right)^{\frac{1}{2}} \exp\{-\frac{1}{2}\frac{\theta_{q+1}[t-u_k-\mu(H_{u_k}, \boldsymbol{\theta})]^2}{\mu(H_{u_k}, \boldsymbol{\theta})^2(t-u_k)}\} \tag{8.1}$$

where $\boldsymbol{\theta} = \boldsymbol{\theta}(t) = [\theta_0, \theta_1, \ldots \theta_q]$ is a vector of model parameters and θ_{q+1} is the distribution shape factor. The PDF mean value $\mu(H_{u_k}, \boldsymbol{\theta}) = \mu_{\mathrm{RR}}$ can be mathematically expressed a linear combination of the most recent q intervals:

$$\mu_{\mathrm{RR}} = \mu(H_{u_k}, \boldsymbol{\theta}) = \theta_0 + \sum_{j=1}^{q} \theta_j w_{k-j+1} \tag{8.2}$$

thus summarizing the effects of the recent sympathetic and parasympathetic dynamic inputs to the SA node on the RRI duration, namely, we take into account the influence of RRI previous history on the successive R-wave occurrences.

In Fig. 8.1 we plot the HDIG distribution for some fixed values of the mean μ_{RR} and the scale factor θ_{q+1}. The former represents the barycenter of the PDF; the latter yields a measure of the shape of the distribution: the higher its value, the less peaked the PDF, the slower the decaying of the right tail, the more the model resembles a Gaussian PDF with the same mean value. We set $q = 0$ in these graphical examples, thus assuming RRI history independence, so as to give an idea of the shape of this kind of distribution.

The HDIG PDF defined in Eq. (8.1) depicts the stochastic properties of the RRIs, thus it can be employed to describe RRI variability by means of suitable statistical features. Since heart rate (HR) is generally defined as the reciprocal of the RRIs, for any $t > u_k$, for any RRI $t - u_k$, we can also introduce the HR random variable $r = c(t-u_k)^{-1}$, where $c = 60\, s/min$ is the factor of conversion from seconds to beats per minute (bpm) [11]. This is a one-to-one transformation, which allows for deriving the HR PDF from the RRI distribution in Eq. (8.1) by means of the transformation:

$$f_{\mathrm{HR}}(r|H_{u_k}, \boldsymbol{\theta}) = \left|\frac{dt}{dr}\right| f_{\mathrm{RR}}(t|H_{u_k}, \boldsymbol{\theta}) \tag{8.3}$$

thus rendering HR stochastic properties. This parametric modeling enables the assessment of HR and RR variability, whose dynamics can be tracked instant by instant with no need for interpolation between consecutive heartbeat intervals.

Several approaches for modeling RRI series PDF are examined in this section.

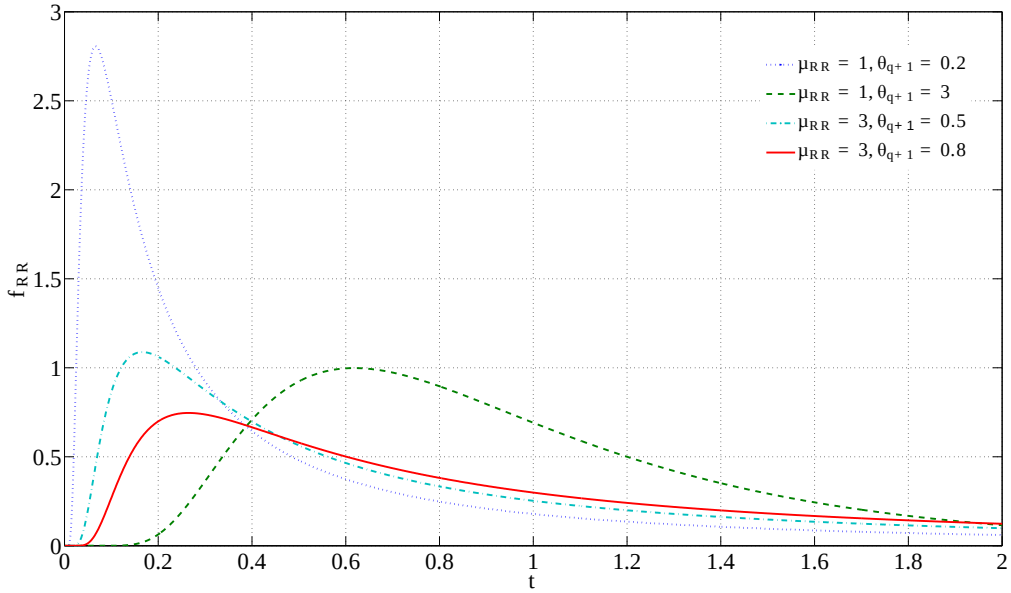


Figure 8.1: Some representative examples of HDIG PDF.

1) **Non-parametric analysis of RRI time series**: RRIs w_k are considered independent of each other. HR and HRV descriptors are computed under no assumptions on heartbeat interval PDF; their mathematical expresions are provided in Sec. 8.2.2.

2) **Point process analysis of a stationary RRI time series**: we assume that RRI series is a point process with time-invariant statistics and that its PDF obeys a HDIG law. We test two distinct hypotheses. To a first approximation, the first moment of the distribution is considered equal to the mean RRI length $\overline{\mathrm{RR}}$. In further analysis, all the parameters of interest are computed as a function of the actual HDIG mean value, which thus depends on the first q intervals of the series, as in Eq. (8.2). This comparison assesses the reliability of the RRI regression model, whose output values are supposed to be similar in those actually computed on the raw series.

3) **Point process analysis of a non stationary RRI time series**: RRI series is regarded as a non stationary point process. The HDIG model can be applied in this case as well, but its statistics are time-varying. Indeed, the series is split in multiple subintervals, and distribution parameters are determined by local ML of the IG distribution. Accordingly, each RRI w_k can be regarded as a linear function of the q previous ones $w_{k-j}, j = 1, \ldots, q$, and the first moment is defined at each time instant as in Eq. (8.2). The output value of distribution statistics equals the temporal average of their instantaneous estimates.

Going in more detail in the point process approach, under RRI series stationarity assumptions, ML estimation of PDF characteristic parameters, namely, μ_{RR} and θ_{q+1}, is globally performed on the whole length of the RRI series by taking into account the first q R-wave events, thus each of them takes only one value along the series itself. However, unless the series pattern is very regular and stable, it can be necessary to take

into account a higher level of variability in time, especially in subjects affected by AF. Accordingly, when series is assumed non stationary, ML estimation of instantaneous HR and HRV is locally carried out on observation time intervals with length L^* [11]. At each time instant t, we define an interval $(t - L^*, t]$ in which we observe n R waves $t - L^* < u_1 < u_2 < \cdots < u_{n_t} \leq t$ where distribution parameter θ can be instantaneously defined as θ_t. The parameter Δ is also set to indicate how much each interval must be shifted so as to compute the next parameter update. ML estimation performance requires the definition of the local joint PDF of the R waves $(u_1, \ldots, u_{n_t})$, where each occurrence is conditioned on the previous q events according to the law:

$$\begin{aligned} \log f_{\mathrm{RR}}((u_1, \ldots, u_{n_t})|\boldsymbol{\theta}_t) = \sum_{i=2}^{n_t} W(t-u_i) \log f_{\mathrm{RR}}(u_i - u_{i-1}|H_{u_{i-1}}, \boldsymbol{\theta}_t) \\ + W(t-u_{n_t}) \log \int_{t-u_{n_t}}^{\infty} f_{\mathrm{RR}}(\nu|H_{u_{n_t}}, \boldsymbol{\theta}_t) d\nu \end{aligned} \tag{8.4}$$

where $W(t-u) = \exp\{-\alpha(t-u)\}$ is a weighting function, characterized by a time constant α assessing the degree of influence of the previous observation u on the local likelihood at time t. Once the estimation $\widehat{\boldsymbol{\theta}}_t$ is determined, we move from interval $(t - L^*, t]$ to $(t - l + \Delta, t + \Delta]$, and local ML estimation is performed again. Prior to ML performance, we also need to set a time resolution parameter t_u for updating statistics. The procedure is continued until the end of the RRI time series.

8.2.2 HEART RATE AND RRI VARIABILITY FEATURE EXTRACTION

Extraction of HRV measures and analysis of RRI probability distribution is motivated by some empirical considerations. More precisely, we computed the RRI histogram in one of the AF patients of our database, so as to compare it with one determined in a SR healthy subject (see Fig. 8.2).

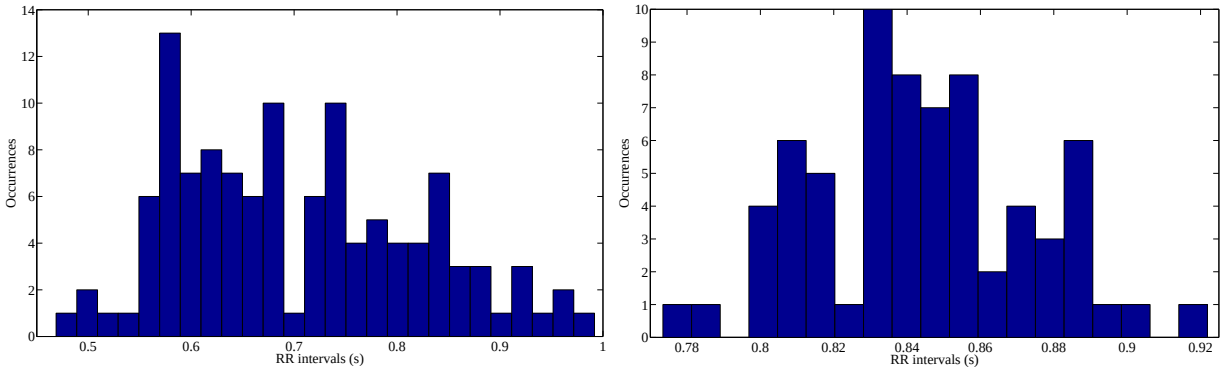


Figure 8.2: RRI histogram: Left: AF, subject 7; Right: SR, subject 8.

Their visual inspection in Fig. 8.2 highlights a certain level of asymmetry around the distribution mean in the histogram, which is rather tailing toward long RRIs, in contrast with the PDF in case of SR. Indeed, as stated above, during AF rapid atrial activations irregularly propagate throughout the AV node, leading to a correspondingly irregular ventricular activation, as reflected on RRIs on the ECG. These effects can be also observed in the RRI length time series plot in Fig. 8.3. During SR, not only RRIs

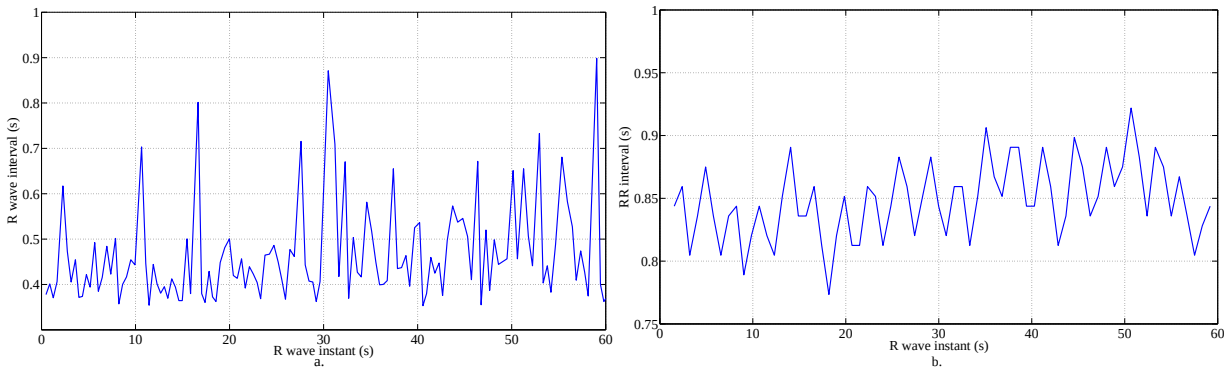


Figure 8.3: RRI time series as a function of R wave time instants: Left. AF, subject 7; Right. SR, subject 8.

are more evenly spaced, but their duration seems to be characterized by a low degree of variability. By contrast, during AF, repetition rate of RRIs seems considerably higher, and their length values are more irregularly distributed. These remarks lead us to investigate whether more elaborate descriptors of RRI variability can quantify such characteristics on the heartbeat interval series and overcome the limitations of traditional histogram-based methods.

We determined the following descriptors of RRI variability each heartbeat interval model proposed in Sec. 8.2.1.

- **Skewness**: it assesses the level of asymmetry of the RRI PDF, and it is defined as:

$$Skewness = \frac{E\{(w_k - \overline{\mathrm{RR}})^3\}}{E\{(w_k - \overline{RR})^2\}^{\frac{3}{2}}}. \tag{8.5}$$

  Positive skewness values are typical of distributions with a longer right tail (as for RRI histogram in the presence of AF); a negative skewness means a longer left tail. If the distribution is symmetric about its mean, its skewness is equal to zero. In the HDIG model, one of the main advantages is that skewness and all the HRV indices can be expressed exclusively as a function of the distribution parameters, i.e., the mean μ_{RR} and the factor shape θ_{q+1}, thus enabling results' generalization. As a consequence, Eq. (8.5) can be rewritten as:

$$Skew = 3\sqrt{\frac{\mu_{\mathrm{RR}}}{\theta_{q+1}}}. \tag{8.6}$$

  Such differences in symmetry between AF and SR subjects can be visually detected. However, no studies have so far quantitatively assessed such a dissimilarity, hence the interest in evaluating this feature in our ECG database.

- **RRI standard deviation**: RRI length irregularity typical of AF can be also detected by visual inspection and intuitively estimated by second-order statistics $SDNN = E\{(w_k - \overline{\mathrm{RR}})^2\}$ quantifying the degree of scattering of data distribution. In the point process framework, it can be identified with the second moment of the HDIG distribution:

$$\sigma_{\mathrm{RR}} = \sqrt{\frac{\mu_{\mathrm{RR}}^3}{\theta_{q+1}}}. \tag{8.7}$$

- **Mean RRI**: it is computed as the average value of all RR lengths ($\overline{\mathrm{RR}}$) in the non-parametric description. It is also an accurate approximation of the HDIG first moment as demonstrated in the experimental section. The point process characterization of this parameter underlines the dependence of RRI length on previous history according to the definition in Eq. (8.2).
- **HR mean value**: it is conventionally assumed as the reciprocal mean RRI ($\overline{\mathrm{HR}}$). For the HDIG model, it can be expressed as a function of μ_{RR}:

$$\mu_{\mathrm{HR}} = c(\mu_{\mathrm{RR}}^{-1} + \theta_{q+1}^{-1}). \tag{8.8}$$

- **HR standard deviation**: defined as the standard deviation of the reciprocal RRIs $SDHR$, adequately scaled by the conversion factor c. In the HDIG density function, it is expressed as:

$$\sigma_{\mathrm{HR}} = \frac{c}{\theta_{q+1}}\sqrt{2 + \frac{\theta_{q+1}}{\mu_{\mathrm{RR}}}} \tag{8.9}$$

In the following sections we illustrate some clinical applications in AF treatment and investigation based on the point process characterization of these HRV features.

8.3 Point process analysis of heart rate and heart rate variability in CA outcome prediction

8.3.1 Methods

The first task concern CA outcome prediction, and we attempt to discriminate between effective and failing CA procedures at different follow-up lengths. Accordingly, RRI time series have been extracted on each of the standard ECGs acquired in 36 patients before CA performance prior to evaluation of the long-term CA outcome. This database has been already introduced in Sec. 3.5.5.

Selection of the point process regression order

The choice of the optimal order q of the HDIG model is guided by the Akaike information criterion (AIC), defined as:

$$AIC = 2\frac{q+1}{N_{RR}} + 2\log E \tag{8.10}$$

where E stands for the final prediction error of the estimated q-order model of the RRI series with length N_{RR} computed by means of the Yule-Walker (or autocorrelation) method. In an autoregressive (AR) model of order q, the current output is linearly dependent on the past q outputs plus a white noise input. The AIC criterion measures the trade-off between the fitting quality of a model and the number of model parameters needed to achieve such level of accuracy. This method assumes that the system examined is driven by white noise and attempts to fit a q-th order AR model to the actual series, by minimizing the forward prediction error in the LS sense. This formulation leads to the Yule-Walker equations, which are solved by the Levinson-Durbin recursion [112]. In the light of these considerations, we compute the prediction error E once set AR regression order q, ranging from 1 up to 10, and for each subject we choose the order q minimizing the aforementioned criterion.

8.3.2 Goodness-of-fit evaluation

Once chosen the most appropriate regression order, we actually verified whether the HDIG model proposed effectively describes original data PDF. Evaluating model goodness-of-fit when attempting to fit spike train series data is not a straightforward extension of the continuous-valued process theory. As a consequence, standard measures of discrepancies between estimated model and raw data PDF (e.g., the NMSE index) cannot be directly used for the point processes [23]. Accordingly, several methods have been put forward in order to convert discrete processes to continuous-valued processes and perform this comparison by means of classical measures. In the point process framework, a widely accepted theory is represented by the general time-rescaling theorem [108]. It states that any point process may be rescaled into a Poisson process with a unit rate, provided that it has an integrable rate function $\lambda = \lambda(t, H_{u_k}, \boldsymbol{\theta})$, defined as:

$$\lambda = \frac{f_{\mathrm{RR}}(t, H_{u_k}, \boldsymbol{\theta})}{1 - \int_0^t f_{\mathrm{RR}}(\nu, H_\nu, \boldsymbol{\theta}) d\nu} \tag{8.11}$$

The rescaled heartbeat intervals can be generated by this model through the relation:

$$\tau_k = \int_{u_{k-1}}^{u-k} \lambda(\nu, H_\nu) d\nu \tag{8.12}$$

for $k = 1 \ldots, K$ consecutive R waves. The output variables are independent exponential variables with unity mean. Accordingly, if we apply the transformation:

$$z_k = 1 - \exp\{\tau_k\} \tag{8.13}$$

the new variables z_k are independent and uniform in the interval $[0, 1]$. Since the transformations in Eq. (8.12)- (8.13) are one-to-one, every comparison between the variables z_k and a uniform distribution directly refers to the relation between the model and the actual data.

In this framework, the Kolmogorov-Smirnov (KS) test allows us to quantify the degree of fitting precision in terms of distance between the point process model and the input RRI data. The lower the distance, the closer the model to the real RRI series. Constructing this test requires arranging z_k values in increasing order, thus yielding the sequence z_k^*. Subsequently, the cumulative distribution function (CDF) of the uniform density is computed as $b_k = \frac{k-0.5}{K}$, $k = 1, \ldots, K$, and it is plot against the z_k^* values. If the model is correct and fitting is accurate, the points of this plot should lie on the 45°-degree line. Confidence bounds are determined by the KS statistic, and they are expressed as $b_k \pm \frac{1.36}{\sqrt{K}}$. Some examples of KS plot are provided in Fig. 8.4.

In agreement with the time-rescaling theorem, the rescaled intervals τ_k must be independent, regardless of the level of independence of the actual RRIs, thus the model proposed is consistent with the input series. As independence is not easily quantifiable in a time series, we can simplify our analysis and assume that, if rescaled RRIs are at least uncorrelated, they are more likely to be independent as well. Accordingly, a further strategy to verify whether model properties are respected is computing the autocorrelation function of the rescaled τ_k values. For each patient we have taken into account 10 lags: the lower their values, the higher the degree of uncorrelation. Some examples are displayed in Fig. 8.5.

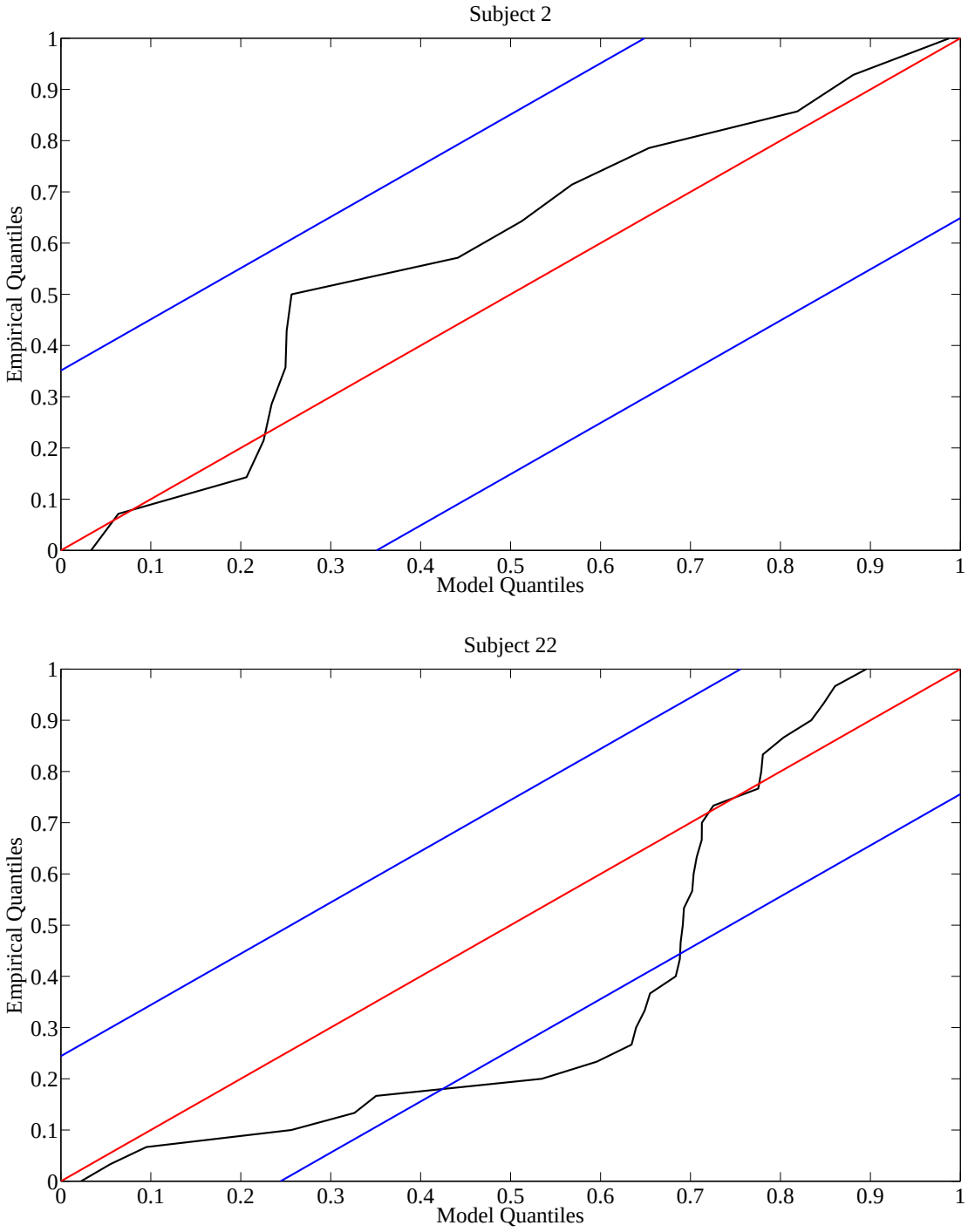


Figure 8.4: Representative examples of KS plots for testing HDIG model goodness-of-fit. Top: an example of accurate fit (patient 2). Bottom: an example of poor fit (patient 22).

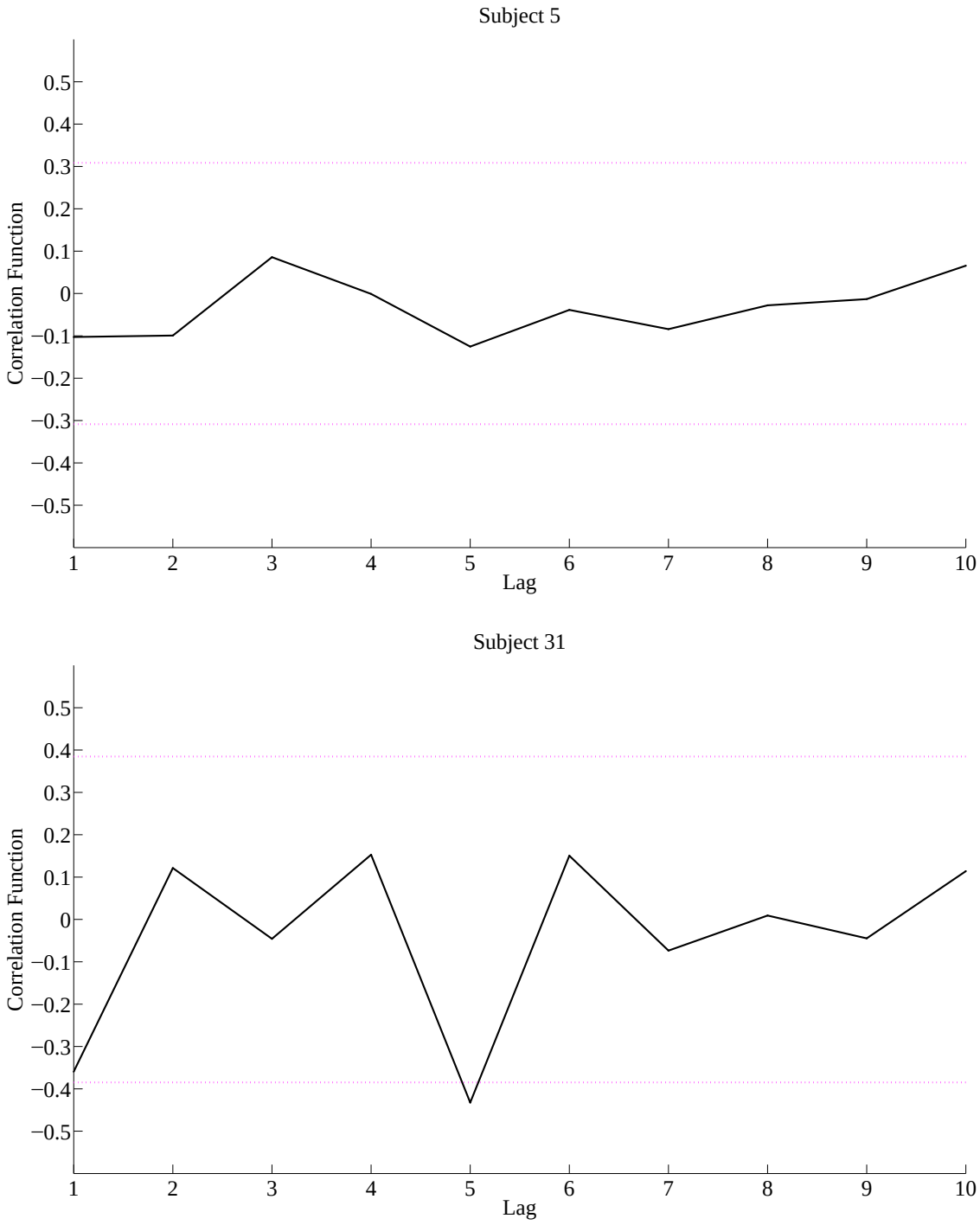


Figure 8.5: Representative examples of autocorrelation function of the rescaled RRIs and their related bounds of confidence. Top: good agreement with uncorrelation hypothesis (patient 5). Bottom: an example of low consistency with uncorrelation hypothesis (patient 31).

8.3.3 UNPAIRED STATISTICAL ANALYSIS

Algorithm parameters' setting is followed by the computation of the models explained in Sec. 8.2.1 and HRV indices defined in Sec. 8.2.2. The predictive power of each HRV measure in assessed by the ROC analysis, and statistical interclass differences are quantified by the p value on an unpaired test (t test in the presence of normal data distributions, Mann-Whitney U test otherwise) under the confidence level $\alpha = 0.05$.

In order to compute HRV indices and improve their accuracy, as far as the non-stationary RRI model in concerned, the window length Δ for local ML estimation is taken as large as possible, thus reducing the number of values involved in the final average of model statistics. In addition, employing shorter windows in certain subjects sometimes can give rises to isolated, spurious negative μ_{RR} values, which are not consistent with basic hypotheses about HDIG PDF definition. Therefore, for a RRI series with N_{RR} samples, the length of such window is assumed equal to $\Delta = N_{RR} - 1$, by keeping a resolution $t_u = 5$ ms.

The order of the HDIG model q has been chosen so as to minimize the AIC criterion as defined in (8.10), in a set of values ranging from 1 to 10. The overall number of subjects n_s for whom each order value q is optimal is reported in Table 8.1, as well as the rate of occurrences per category ("AF termination" vs "Non AF termination"). The analysis of these results led us to set $q = 1$ prior to estimation of each model.

Table 8.1: Number of subjects n_s for whom regression order q is optimal according to the AIC criterion.

n_s \ q	1	2	3	4	5	6	7	8	9	10
All patients	11	5	3	2	3	2	3	2	1	4

Goodness-of-fit of each model has been assessed by the KS test. Local ML estimation is performed on several intervals, whose width is equal to the 60% of the whole series length,so as to account for a sufficient number of samples for accuracy assessment, in agreement with series total length at the same time. The analysis of the KS plot in each subject allowed us to verify any possible deviations form the reference uniform distribution (represented by the 45°-degree line in the plot). Two representative examples are displayed in Fig. 8.4. The maximum KS distance provides us such a measure of model goodness-of-fit. The percentage of points in the KS plot N_{KS} exceeding the confidence bounds has been computed in each subject as well and averaged over the whole database. Such results are indicated for the two patients' groups of interest in Table 8.6. Further confirmation about model representation ability is also provided by the examination of the autocorrelation function of the rescaled RRIs; two examples are shown in Table 8.5.

After verifying HDIG model accuracy, CA outcome prediction performance has been assessed on the HRV features for each of the models aforementioned. Findings of the statistical analysis are summarized in Table 8.2- 8.5, besides the results of the ROC analysis, i.e., the AUC index and the related cutoff, and the rates of sensitivity and specificity.

Table 8.2: Long-term CA outcome prediction: HR and RRI variability parameters under the RRI independence assumption (non-parametric approach); n.u.: normalized units; bpm: beats per minute.

	AF termination	Non AF termination	p value	AUC	Optimal cutoff	Sensitivity	Specificity
Skewness [n.u.]	0.50 ± 1.15	0.75 ± 0.79	$5.8 \cdot 10^{-1}$	0.61	0.86	0.69	0.71
$SDNN$ [s]	0.16 ± 0.08	0.14 ± 0.04	$6.9 \cdot 10^{-1}$	0.52	0.14	0.45	0.57
$\overline{\text{RR}}$ [s]	0.74 ± 0.18	0.76 ± 0.11	$8.0 \cdot 10^{-1}$	0.56	0.69	0.45	0.71
$\overline{\text{HR}}$ [bpm]	90.79 ± 22.15	83.52 ± 12.12	$4.1 \cdot 10^{-1}$	0.57	89.79	0.62	0.43
$SDHR$ [bpm]	28.41 ± 61.43	15.33 ± 4.34	$5.8 \cdot 10^{-1}$	0.63	13.89	0.41	0.86

Table 8.3: Long-term CA outcome prediction: HR and RRI variability parameters; RRI time series is considered stationary and obeys a HDIG model. Approximation of the first moment to mean RRI ($\mu_{RR} = \text{RR}$); n.u.: normalized units; bpm: beats per minute.

	AF termination	Non AF termination	p value	AUC	Optimal cutoff	Sensitivity	Specificity
Skew	0.64 ± 0.33	0.55 ± 0.12	$4.0 \cdot 10^{-1}$	0.61	0.55	0.72	0.43
σ_{RR}	0.16 ± 0.11	0.14 ± 0.04	$5.4 \cdot 10^{-1}$	0.53	0.14	0.52	0.57
$\overline{\text{RR}}$ [s]	0.74 ± 0.18	0.76 ± 0.11	$8.0 \cdot 10^{-1}$	0.56	0.69	0.45	0.71
μ_{HR}	90.72 ± 22.12	83.45 ± 12.04	$4.1 \cdot 10^{-1}$	0.57	89.86	0.62	0.43
σ_{HR}	19.17 ± 11.29	15.26 ± 4.02	$3.4 \cdot 10^{-1}$	0.62	14.56	0.66	0.57

8.3.4 Results

In 1 patient out of 7 experiencing an ineffective CA procedure some points fall outside the confidence band of the KS plot. Similar remarks can be made for 4 patients out 29 among those who underwent a successful CA procedure. Nevertheless, the number of outliers is negligible with respect to the amount of KS plot points, as it can be inferred from Table 8.6. Accordingly, no patients have been discarded from our investigation. Examination of the autocorrelation function of the rescaled RRIs also underlines the agreement of the HDIG model with the uncorrelation hypothesis. Indeed, even though autocorrelation function values fall within the confidence interval in 31 patients out of 36, we can remark that only one outlier point can be detected outside the band for these subjects and that its deviation from confidence band is very limited. Therefore, the point process model is effectively capable of depicting RR series in AF patients and render its variability properties.

Despite modeling effectiveness, extraction of HRV features in patients affected by AF does not seem to highlight any potential predictive features from which CA outcome assessment can benefit from. Indeed, regardless of the methodology proposed, no HRV parameter is able to predict procedural AF termination, as results in Tables 8.2- 8.5 con-

Table 8.4: Long-term CA outcome prediction: HR and RRI variability parameters; RRI time series is considered stationary and obeys a HDIG model. The actual mean μ_{RR} of the distribution is herein employed for statistics' computation; n.u.: normalized units; bpm: beats per minute.

	AF termination	Non AF termination	p value	AUC	Optimal cutoff	Sensitivity	Specificity
Skew	0.64 ± 0.32	0.55 ± 0.12	$4.5 \cdot 10^{-1}$	0.60	0.56	0.56	0.71
σ_{RR}	0.16 ± 0.10	0.14 ± 0.04	$9.7 \cdot 10^{-1}$	0.51	0.13	0.56	0.57
μ_{RR}	0.74 ± 0.18	0.77 ± 0.10	$5.2 \cdot 10^{-1}$	0.58	0.68	0.59	0.57
μ_{HR}	91.34 ± 23.05	82.26 ± 11.15	$3.2 \cdot 10^{-1}$	0.60	97.11	0.62	0.57
σ_{HR}	19.28 ± 11.52	15.16 ± 4.03	$3.0 \cdot 10^{-1}$	0.63	14.10	0.45	0.71

Table 8.5: Long-term CA outcome prediction: HR and RRI variability parameters; RRI time series is assumed non-stationary and obeys a HDIG model. The temporal average of features' instantaneous values is examined in the statistical analysis; n.u.: normalized units; bpm: beats per minute.

	AF termination	Non AF termination	p-value	AUC	Optimal cutoff	Sensitivity	Specificity
$Skew$	0.67 ± 0.47	0.55 ± 0.11	$3.8 \cdot 10^{-1}$	0.61	0.56	0.66	0.57
σ_{RR}	0.17 ± 0.14	0.14 ± 0.03	$6.6 \cdot 10^{-1}$	0.56	0.13	0.45	0.86
μ_{RR}	0.74 ± 0.18	0.75 ± 0.10	$9.0 \cdot 10^{-1}$	0.55	0.68	0.41	0.86
μ_{HR}	91.49 ± 23.69	84.05 ± 10.83	$4.3 \cdot 10^{-1}$	0.57	91.48	0.62	0.43
σ_{HR}	20.87 ± 20.67	15.36 ± 3.78	$3.4 \cdot 10^{-1}$	0.62	14.00	0.62	0.43

Table 8.6: Evaluation of the goodness-of-fit of the HDIG model in CA outcome prediction: maximum KS distance and percentage of points inside the confidence bounds.

	AF termination	Non AF termination
KS distance	0.11 ± 0.03	0.14 ± 0.06
$N_{KS}[\%]$	98.55 ± 5.06	96.31 ± 9.76

firm. Indeed, no statistically significant differences between the categories examined are emphasized by such indices, and prediction accuracy as quantified by the ROC analysis seems to be rather poor as well. Even though we are not able to provide any clinical explanation of this phenomenon, we can hypothesize that the exclusive characterization of the ventricular response only does not prove sufficient to describe the complexity and the randomness of the AF pattern. Indeed, ventricular activity irregularity is a reflection of AA in the presence of AF, whose effects are not easily quantifiable. We should also to mention that not all patients are treated by exactly the same CA steps, thus making it harder to compare the groups of interest. Despite the agreement of a procedural protocol, consisting of a fixed number of specific steps, patient's conditions and physical reactions at the moment of the procedure profoundly influence some decisions, such as the number and the type of lesions actually performed, thus increasing the degree of variability and the complexity of ablation, which could be harder to be described by the ventricular response only. Finally, CA always implies modifications on one or more sites (for instance, PVs, LA, CS, etc.), whose contribution to AF dynamics is generally at least comparable to that coming from the SA, whose activity risks to be hidden. In the light of these considerations, we can deduce the inability of our analysis to shed some light about the effective potential of the point process modeling to predict AF termination by CA, which can be probably helped by adding some complementary features for patients' characterization and/or improving the HDIG model adopted (e.g., with AF non-linearities integration).

8.4 POINT PROCESS APPLICATION TO AF PATTERN RECOGNITION

8.4.1 INTRODUCTION

Despite the weak predictive performance of the point process modeling in CA outcome assessment, we demonstrate next that this approach can actually emphasize some properties of RRI series which are typical of AF and help its diagnosis and character-

ization. In clinical centers, AF is often visually investigated, either by detecting the absence/presence of the P wave (replaced by irregular fibrillatory waves) or alterations in the heartbeat distribution variability, more irregular in subjects affected by AF. RRIs analysis presents some advantages, such as the easier detection of the R peaks on the ECG and their robustness to artifacts and signal noise, which can alter waveform pattern, in particular the shape of the P wave. Furthermore, it is practically unaltered by the choice of a specific electrode on multilead ECG recordings, whereas most of the classical ECG characterization methods (especially those performed on a single lead) require an accurate ECG inspection prior to lead selection.

Particular attention has been paid to RRI histogram analysis, and we actually show that some characteristics of RRI PDF are exclusively encountered in AF patients, and not in healthy subjects. This assumption derives from investigation about RRI histograms acquired in AF patients, and then compared with those computed in SR control subjects. We include one example for each group of subjects in Fig. 8.2 for the sake of clarity. Visual inspection of RRIs histograms reveals a higher degree of asymmetry around PDF mean value in AF patients, tailing toward long RRIs. Concentration around short RRIs may reflect rapid ventricular contractions due to uncoordinated AA evolution. It is also worth noting the higher PDF dispersion around the mean, whereas in SR subjects probability distribution is narrower. Such differences can be also observed in the RRI length time series plot is Fig. 8.3. During AF, RRI repetition rate seems considerably higher than in SR subjects. By contrast, in healthy subjects, not only RRIs are more evenly spaced, but duration values seem also to be characterized by a lower degree of variability compared with the irregular RRI length distribution typical of AF patients. Our preliminary examination led us to investigate whether RRI histograms characteristics encountered in AF patients could be properly quantified by HRV measures presented in Sec. 8.2.2, with particular attention to skewness and dispersion indices of HR and RRI variability, in the point process framework, thus reintroducing the concept of RRI history-dependence.

8.4.2 ECG database

One-minute standard ECG was acquired in 47 male patients, aged 50 to 70, affected by persistent AF, at a sampling rate of $F_S = 977$ Hz. Seventy-one healthy subjects are assigned to the SR control group ($F_S = 128$ Hz) [56], 35 men (aged 26 to 76 years) and 37 women (aged 20 to 73). Long-term ECG recordings of 18 subjects from the Arrhythmia Laboratory at Boston's Beth Israel Hospital (now the Beth Israel Deaconess Medical Center) are added to the control group. Healthy subjects are not at rest conditions. Information about the remaining healthy subjects comes from the Normal Sinus Rhythm RR Interval Database [15], which includes beat annotation files obtained by automated analysis with manual review and correction.

8.4.3 Methods

Most of the methodological steps presented in Sec. 8.3 are herein applied again. More precisely, after assessing the optimal regression order q through the Akaike criterion, each of the models introduced in Sec. 8.2.1 is determined in each subject. Accordingly, KS test is carried out to verify whether the HDIG model fits the actual RRI series. Examination of the autocorrelation function of the rescaled RRIs is also accomplished so as to check

agreement with their mutual uncorrelation hypothesis. Subjects can be discarded from the analysis if their related RRI series do not fulfill these hypotheses.

Correctness of the HDIG model hypothesis is further validated by comparing this probability distribution with a history-dependent Gaussian (HGG) PDF. Discrepancies of the estimated models from actual RRI data are quantified by the maximum distances computed by the KS test.

We also examined a classical non-parametric method, the so-called kernel density estimation (KDE), and compared it with the point process method. According to this approach, PDF is estimated by applying a smooth kernel function (for instance, the normal function) $K(\cdot)$ to each data point $x(i)$ of a generic series x of n samples (in our application, heartbeat interval series samples). Therefore, PDF estimate is defined as:

$$\widehat{f}(x) = \frac{1}{n}\sum_{i=1}^{n} K\Big(\frac{x - x_i}{h}\Big) \tag{8.14}$$

where h is the kernel bandwidth, the most critical setting parameter in KDE application. Accordingly, we first chose the number of points N_{KDE} (related to the histogram bin width) in which PDF estimation is performed. Model fitting of each KDE distribution is evaluated by means of the KS test in Table 8.7. Effects of the tuning parameters' selection on HRV assessment are shown in Table 8.8 for the skewness index.

Table 8.7: Mean KS distance of transformed RRIs modeled by the KDE method for each value of N_{KDE}: comparison with the point process approach.

	$N_{KDE} = 50$	$N_{KDE} = 100$	$N_{KDE} = 300$	$N_{KDE} = 1000$	HDG ($q = 5$)	HDIG ($q = 5$)
AF	0.6583 ± 0.0703	0.6688 ± 0.0392	0.6925 ± 0.0158	0.2847 ± 0.0962	0.7023 ± 0.0049	0.1193 ± 0.0581
SR	0.6789 ± 0.0470	0.6833 ± 0.0454	0.6989 ± 0.0209	0.7035 ± 0.0086	0.2040 ± 0.0889	0.1225 ± 0.0492

Table 8.8: Analysis of the skewness index computed on RRI data modeled by the KDE method.

	AF	SR	p-value
$N_{KDE} = 50$	0.4740 ± 0.8067	0.8566 ± 3.3065	$9.0 \cdot 10^{-3}$
$N_{KDE} = 100$	0.4822 ± 0.8107	0.3455 ± 3.9585	$9.2 \cdot 10^{-3}$
$N_{KDE} = 300$	0.4877 ± 0.8133	2.4503 ± 9.9187	$4.9 \cdot 10^{-2}$
$N_{KDE} = 1000$	0.4905 ± 0.8143	1.0760 ± 2.8033	$4.7 \cdot 10^{-2}$

Once the model fitting accuracy has been verified, HR and RRI variability descriptors are computed and statistical analysis is accomplished as described in Sec. 8.3.1. Its outcome is quantified by the test p value. HRV indices underlining statistically significant differences between the two groups examined ("AF" vs "SR") are subsequently exploited for supervised classification of all subjects. More precisely, classification accuracy of statistically significant HR and HRV features in the non-stationary point process framework is tested. Therefore, linear discriminant analysis (LDA) is performed to classify each test sample into the correct category based on information provided by the training group. Each classifier (C_1 =Skewness, C_2 = RRI standard deviation and C_3 =HR standard deviation) is either tested separately or in combination with the other ones, thus yielding 2D ($C_{12} = (C_1, C_2), C_{13} = (C_1, C_3), C_{23} = (C_1, C_3)$) or 3D features ($C_{123} = (C_1, C_2, C_3)$). In this section, feature combination is not accomplished according to the logistic regression

(LR) analysis introduced in Sec. 6.2, since data risk to be overfitted due to the very low number of features (ranging from 1 to 3). By contrast, LDA seems a more suitable tool, since the database accounts a high number of samples (117 subjects). Indeed, classification can benefit from a supervised framework, in which predicting features can be properly learned by a sufficiently large training set and then applied to ascribe the new test samples to the correct category. LOOCV technique is applied for results' validation. Classification accuracy of each classifier *Acc* is the quantified by the ratio between the number of correct detections and the overall number of subjects. Let us consider AF patients as positive cases, and SR subjects as the negative ones. Under these assumptions, the number of correct detections per category (true positive TP and true negative TN) and the number of misclassifications is also computed (false positive FP and false negative FP). Classification performance of the point process approach is also compared with that of the same classifiers obtained with the non-parametric approach.

Influence of the model order q on the autoregressive structure of the RRI series has also been investigated. Accordingly, autocorrelation function has been computed for each subject by setting 2 different q values, the default $q = 5$ (explanations about this setting are provided is Sec. 8.4.4) and a lower one, $q = 2$. Differences in model representation accuracy as estimated by the autocorrelation function are shown in Fig.8.7. Structure of the autoregressive model has also been investigated by assessing the mean maximum log-likelihood MLL for each category.

Assuming dependence of each heartbeat interval on its previous history implies HDIG point process model agreement with the principle of causality. We verified this assumption by reversing the order of the RRI sequence and computing HRV statistics on the new series. If our hypothesis is correct, HRV parameters should take different values on the reversed series. For sake of example, in Fig. 8.6 we report results obtained on the reversed RRI series examined in the point process framework, under the hypothesis of series non-stationarity.

We finally focused on the influence of ECG sampling frequency F_S on RRI series modeling and feature extraction. As a matter of fact, as this parameter changes according to the group of subjects, we set the same value $F_S = 128$ Hz for all subjects (thus downsampling AF ECG signals), we computed HRV descriptors and performed statistical analysis again so as to verify whether interclass differences are exclusively due to RRI series properties and are not influenced by the sampling rate.

8.4.4 Results

The same tuning parameters adopted in Sec. 8.3.4 are set for this application as well, except for the regression order q, which is equal to 5, as demonstrated by Table 8.9, showing the number of occurrences of RRI database subjects for each q value. Also in this experimental session, we have taken into account the compromise between an accurate modeling of RRI series and their limited length (around one minute). More specifically, we set this order value so as to accurately describe RRI series in control subjects, exhibiting a more correlated structure. Concerning AF patients, even though q is generally quite low, we can note that increasing its value does not alter time series characterization accuracy, since higher order regression terms can be considered negligible. Hence, a satisfactory trade-off between such objectives is accomplished by setting $q = 5$.

The ability to fit the actual RRI series is expressed in terms of maximum KS distance

Table 8.9: Number of subjects n_s with optimal regression order q according to the AIC criterion. AF: number of subjects in AF group. SR: number of subjects in SR group.

q	1	2	3	4	5	6	7	8	9	10
$n_s(AF)/47$	15	6	3	2	3	2	6	5	1	4
$n_s(SR)/71$	8	10	7	9	11	4	4	6	6	6

(mean $\pm$ standard deviation) for each category (AF vs SR) and each model (HDIG, HDG and KDE for several values of N_{KDE}) in Table 8.7. As far as AF patients are concerned, model representation accuracy assessed by the KS test is globally quite high (more than 75% of KS plot points belong to the confidence band). Only in the healthy patient 62 the model fails to fit real data, and estimation quality is quite poor. As a consequence, this subject is discarded from the statistical analysis discussed in the following sections. RRI series PDF in healthy subject is also well fitted by the point process model, except in one subject, who has been removed from our analysis.

Statistical analysis outcome is reported in the box-and-whiskers plots in Fig. 8.6. The non-parametric approach is denoted by H_{MAN}. Notations $H_{\text{STAT,APP}}$ and H_{STAT} refers to the point process under RRI series stationarity hypothesis, with and without approximation of the HDIG first moment to the mean RRI interval $\overline{RR}$, respectively. When RRI series is assumed non-stationary, notation H_{NONSTAT} is employed. AF data downsampling effects on HRV parameters make reference to $H_{\text{MAN,DS}}$ and H_{DS} for the non-parametric and the point process approaches, respectively. Finally, experiments about RRI series time reversal are ascribed to H_{REV}. For the sake of clarity, in Fig. 8.6 we report statistical results obtained on downsampled AF data for the non-parametric approach and the point process analysis of RRI series regarded as non-stationary only, since similar results are obtained under the hypothesis of HRV statistics' time-invariance.

Classification outcomes output by the point process modeling are reported in Table 8.11 and they are compared with those displayed in Table 8.10, which are obtained by features directly determined on RRI series in a non-parametric framework. The ratios TP, TN, FP, FN and the classification rate Acc are indicated for each of the classifiers previously defined, either separate or combined. The 47 AF patients included in the classification task are regarded as positive cases, whereas the 71 SR control subjects form the group of negative cases.

8.4.5 Discussion

This part of our study demonstrates the ability of the point process method to properly enhance RRI series content in the presence of AF, applied to this arrhythmia for the first time [11].

Point process setting parameters of the proposed method have been adequately chosen by taking into account database characteristics as well as the type of features to be extracted. Regression order analysis in Table 8.9 underlines that RRI series in most of AF patients are better described by a lower number of terms for regression, whereas the more correlated structure of RRI series in healthy subjects requires a higher number of components in the linear combination. This is also corroborated by the inspection of the MLL measure, which takes higher values in healthy subjects, thus rendering a more correlated heartbeat interval series structure (AF: 66.43 ± 94.97, SR: 188.63 ± 94.17, p

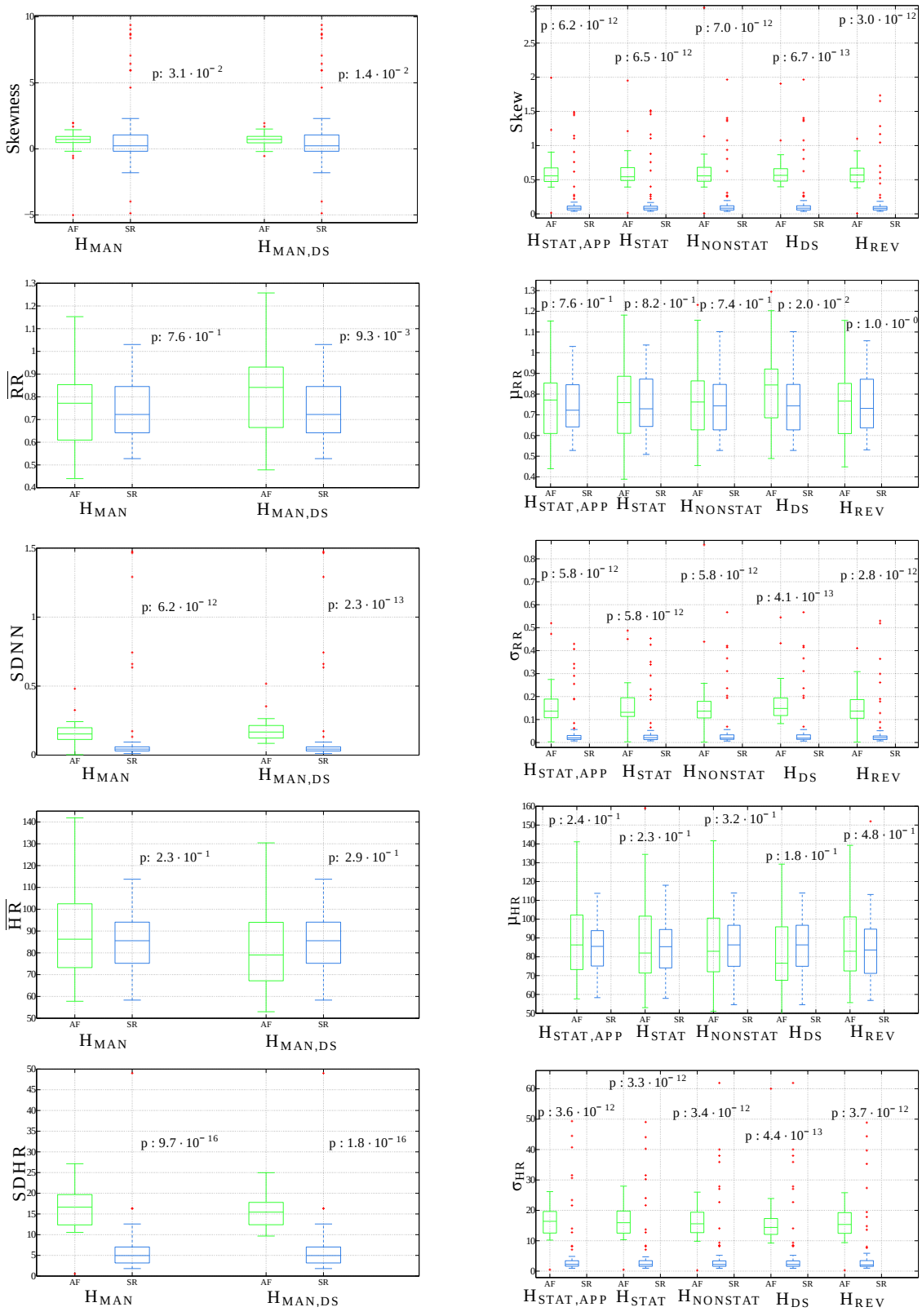


Figure 8.6: [
Box-and-whiskers plots of HR and RRI variability indices: non-parametric analysis vs point process]Box-and-whisker plot of HR and RRI variability parameters. Left: Non-parametric analysis. Right: Point process modeling according to different assumptions about RRI time series. In each plot, for each method examined, AF group is on the left (continuous line), SR group on the right (dotted line). Results concerning effects of AF data downsampling and time-reversed RRI series are also reported. Notations. H_{MAN}: non-parametric approach. $H_{\mathrm{STAT,APP}}$ and H_{STAT}: point process under RRI series stationarity hypothesis, with and without approximation of the HDIG first moment to the mean RRI interval $\overline{RR}$, respectively. H_{NONSTAT}: point process under RRI series non-stationarity hypothesis. H_{DS} and H_{REV}: AF data downsampling in

Table 8.10: LDA classification outcomes of features determined in 47 positive cases (AF) and 71 negative cases (SR) on the raw RRI series under no assumptions about their PDF (single-feature classifiers $C_1 = Skewness$, $C_2 = SDNN$ and $C_3 = SDHR$, and their multivariate combinations $C_{12}, C_{13}, C_{23}, C_{123}$).

	TP	TN	FP	FN	Acc
C_1	26	24	46	21	0.4274
C_2	25	63	7	22	0.7521
C_3	27	67	3	20	0.8034
C_{12}	32	44	26	15	0.6496
C_{13}	33	65	5	14	0.7607
C_{23}	27	62	8	20	0.8376
C_{123}	35	58	12	12	0.7949

Table 8.11: LDA classification outcomes of features determined in 47 positive cases (AF) and 71 negative cases (SR) on the non-stationary RRI series estimated by the point process HDIG model (single-feature classifiers $C_1 = Skew$, $C_2 = \sigma_{\mathrm{RR}}$ and $C_3 = \sigma_{\mathrm{HR}}$, and their multivariate combinations $C_{12}, C_{13}, C_{23}, C_{123}$).

	TP	TN	FP	FN	Acc
C_1	43	62	8	4	0.8974
C_2	34	62	8	13	0.8205
C_3	37	62	8	10	0.0.8462
C_{12}	35	62	8	12	0.8291
C_{13}	38	62	8	9	0.88034
C_{23}	41	62	8	6	0.8547
C_{123}	42	62	8	5	0.8889

value: $4.35 \cdot 10^{-10}$). This evidence hints a higher degree of irregularity in AF patients compared with SR and a lack of structure of RR series, thus implying a higher level of unpredictability, as we expect in AF patterns. This is also confirmed by the examination of the AIC values corresponding with the optimal order q of each subject, which are by average lower in SR control subjects (AF: -7.9341 ± 2.6794; SR: -13.8983 ± 4.8411; p value$= 2.3096 \cdot 10^{-12}$).

Visual inspection of KS plots generally reveals a good agreement between model and real data for most of subjects, as their values generally fall within the 95% confidence bounds. A pair of examples is displayed in Fig. 8.8. Indeed, even when HDIG model computation is not completely accurate, deviation from real data evolution is limited, and global fitting precision is generally quite high (80% by average).

To the same end, autocorrelation function computation has been performed for two different regression order values so as to inspect the correct assessment of the regressive structure properties. A representative example in Fig. 8.7. We can see that increasing the regression order notably improves model accuracy as series structure becomes more robust when more terms are taken into account. This is confirmed by the reduction, and in several cases the disappearance of autocorrelation function outliers.

Our investigation demonstrates the adequateness of the PDF chosen for fitting RRI

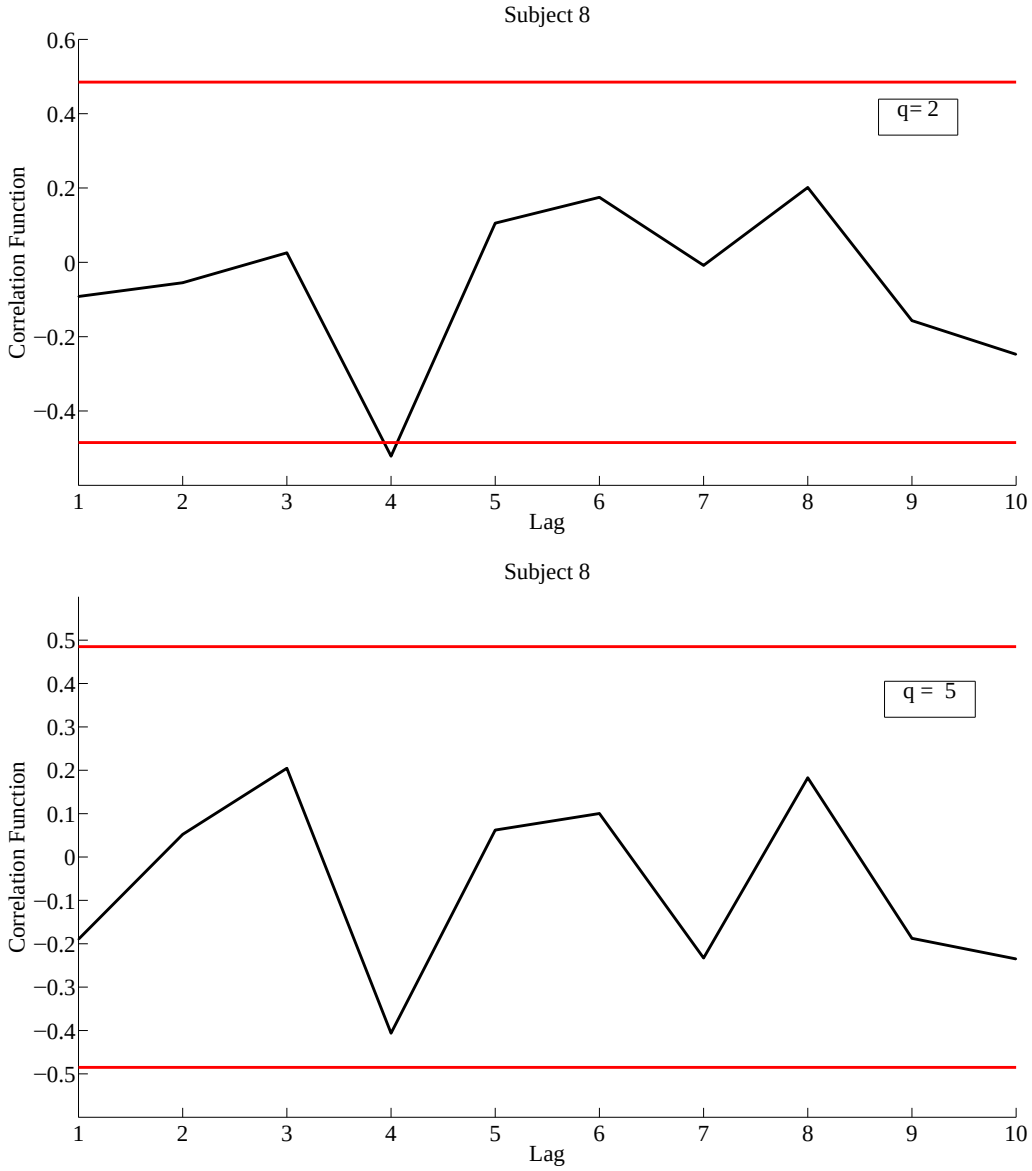


Figure 8.7: Autocorrelation function of the rescaled RRIs computed in AF patient 8 for 2 distinct regression order values q. Left: $q = 2$. Right: $q = 5$.

series probability distribution. Indeed, RRI series during AF are better fitted by the HDIG model than the HDG one, as confirmed by the lower KS distance values in Table 8.7 for 34 patients out of 47. Mean global accuracy as quantified by the number of points N_{KS} falling within the confidence bounds is equal to 97.23 ± 6.88. Even in patients whose KS plots of estimated RR series are not entirely bounded by the confidence limits, our results show that the HDIG model can better describe RR length distribution, as in subjects 7 and 30. The comparison with the HDG distribution also confirms the HDIG modeling is not biased by distribution variance values. Consequently, higher values of certain statistics observed in presence of AF (in particular, skewness and RRI standard deviation) are exclusively due to disease effects and not to assumptions about RRI PDF. Concerning the control group, lower KS distances can be by average found when we assume that RR length series obeys a HDIG distribution law as well ($N_{KS} = 97.14 \pm 7.96$).

Similar remarks arise from the comparison with the KDE estimation approach, as proved but the higher KS distances values in Table 8.7 obtained for each class, regardless of the number of points used for PDF estimation. In addition, such an analysis also shows how the method is dependent on setting parameters. Furthermore, in some subjects PDF can not be correctly estimated if the number of points N_{KDE} is too low, thus making it hard to properly assess HRV statistics. Such a variability is reflected on the computation of HRV features, as confirmed by the statistical analysis of the skewness index in Table 8.8, even though the method always underlines statistically significant differences between the categories of interest.

The point process modeling considerably enhances the descriptive power of RR length distribution statistics, and it overcomes the non-parametric approach, as there is no need for interpolating between consecutive heartbeat intervals for characterizing series dynamics and HRV measures are independent from histogram settings. The method we put forward is able to effectively discriminate between AF and SR conditions, despite the high level of RR variability encountered in healthy subjects. Indeed, it must be noticed once again that ECGs in control subjects are not acquired at rest conditions, whereas AF signals are recorded right before ablation performance. This experimental condition underscores the descriptive power of the point process methodology, which is able to correctly distinguish the two groups despite such complexity. HRV statistical assessment for the classical non-parametric modeling in Fig. 8.6 highlights that dispersion measures of RRI and HR variability are significantly higher in AF patients. Statistical significance of the index $SDHR$ is not altered by the presence of an outlier (AF patient 15), which is still valid even if it is removed from our analysis (AF: 16.70 ± 5.32, p value: $2.3 \cdot 10^{-15}$). Concerning PDF asymmetry quantification, we can remark that skewness does not seem a reliable index when it is directly computed on raw data. Indeed, it underlines more skewed distributions in healthy subject, which is in contradiction with conclusions drawn about our visual inspection in Fig. 8.2. The fist moment of the HDIG PDF proves to be a reliable estimation of the mean RRI directly computed on the input RRI series, as confirmed by results in Fig. 8.6, which are quite similar to each other. Results can also be generalized for non-stationary RRI series, as confirmed in the same figure, thus demonstrating the ability of this model to capture series dynamics, which are even more complex and variable.

Supervised classification outcome also corroborates the predictive power of HRV features characterized in the point process framework, which overcomes the classical non-parametric computation. In Table 8.10 we can clearly remark the low discriminative

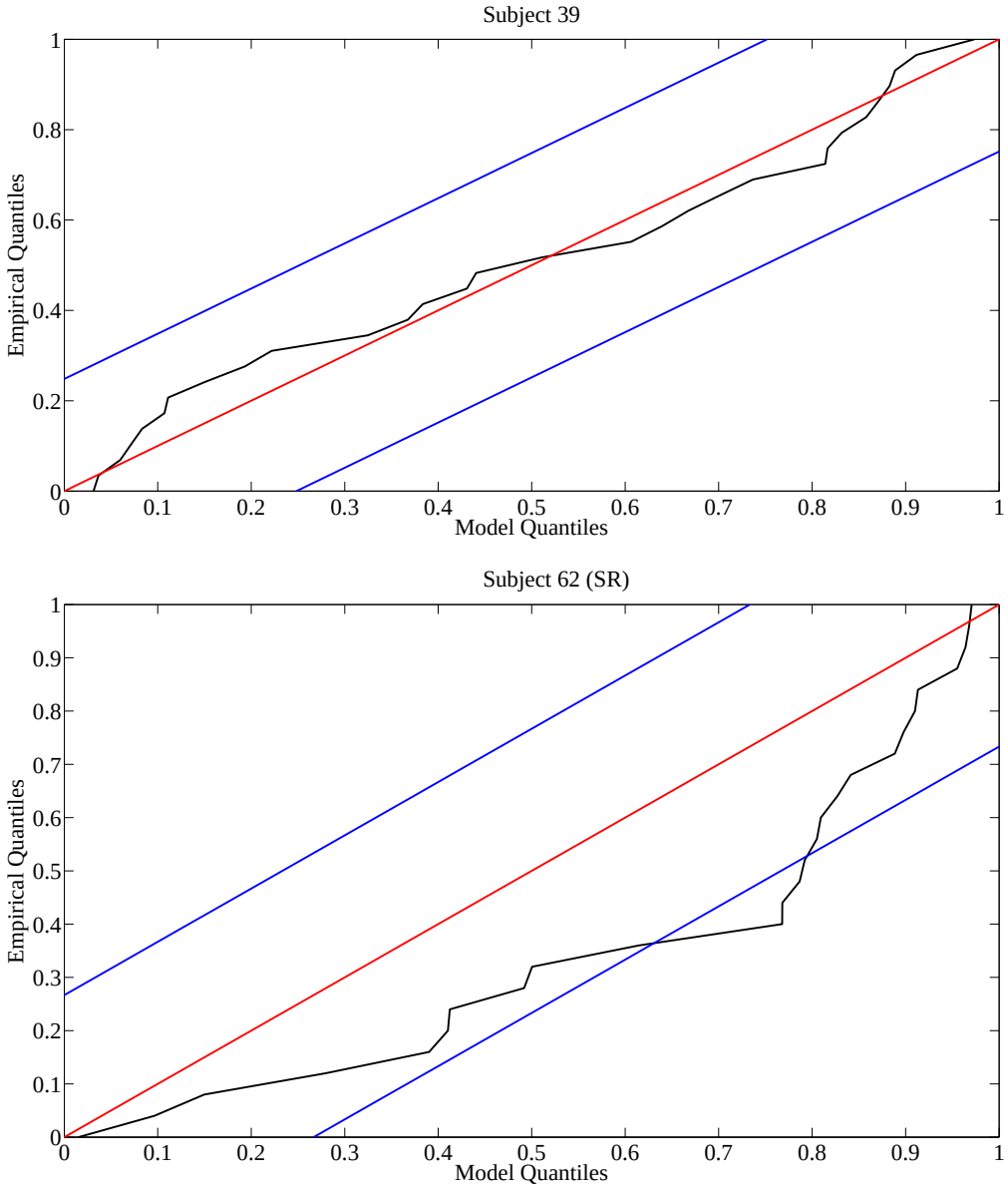


Figure 8.8: Two examples of KS plots for HRV characterization in AF patients and healthy subjects. Left: High modeling accuracy (AF, subject 39). Right: Low modeling accuracy (SR, subject 62).

power of the skewness index, which is rather improved by the combination with dispersion measures, in particular with $C_3 = SDHR$; multivariate features generally perform better than features considered separately. By contrast, all parameters estimated in the point process scenario can effectively distinguish between AF and SR, as confirmed by the high accuracy scores, and the number of incorrect detections is considerably low for both categories. The skewness index proves to be the most accurate classifier, even though classification performance of other parameters is equally satisfactory. Multidimensional predictors are also able to ascribe each sample to the correct category, as indicated in Table 8.11. This evidence shows the advantages of point process assumptions, making AF characterization more robust and reliable.

We also demonstrate the robustness of the point process method to the influence of ECG acquisition factors, in particular to ECG sampling frequency (see Table 8.6. Regardless of the approach considered, we can remark that features computed on the modified RRI series in AF patients sometimes take values which are slightly higher than those obtained at their typical sampling rate ($F_S = 977$ Hz). However, interpretation of statistical analysis results remains unchanged for most of the features considered, except of the mean RRI value for all the approaches ($\overline{RR}$ and μ_{RR}). More precisely, HR and RR dispersion indices are still significantly higher in AF patients than in healthy subjects, thus correctly depicting the higher level of RRI irregularity reflecting AF uncoordinated activity. Similarly, the higher values of skewness denote RRI PDF asymmetry in presence of AF. In contrast with results previously commented, it seems that mean RRI can significantly discriminate the groups, and it takes higher values in AF patients, regardless of the method applied.

Finally, we verified the ability of the point process approach to underline the most content-bearing components of the RRI series in presence of AF by modeling their temporal evolution and underlining the relation of each heartbeat interval with the previous ones, which is shown to be physiologically correlated with autonomous system activity [11]. The results of the statistical analysis in Fig. 8.6 demonstrate that altering such dynamics by reversing the order of RRI sequences influences the properties of the HDIG model computed and the numerical results of our statistical analysis. Accordingly, even though variations are quite limited and significance levels do not change, also the values HRV measures computed on the reversed series are affected by RRI sequence reversal, thus confirming the dynamical structure emphasized by the point process. Point process structural dependence on previous history provides a useful tool in terms of RRI series predictability and evolution characterization at each time instant.

8.5 SUMMARY AND CONCLUSIONS

This chapter has shed some light on the potential characterization of the ventricular response in the presence of AF by means of HRV measures obtained in a parametric probabilistic point process framework, which has been employed for the first time for the characterization of this arrhythmia. RRI PDF is shown to obey a HDIG law, and each heartbeat interval is modeled as a function of its previous history, thus rendering the influence of the autonomic inputs as reflected on RRI length variations. Our study represents the first application of the point process method to AF analysis and ventricular response modeling in the presence of this arrhythmia. It overcomes limitations of

traditional approaches, especially those related to dependence on histogram bin width and strict hypotheses about RRI series, and it leads to a more refined, instantaneous characterization of HRV features, even in short recordings. From the statistical model proposed we can derive a novel formulation of HR and HRV indices instant by instant, the capability of our model to describe real data and capture the dynamics of heartbeat interval temporal evolution is confirmed by the KS test and correlation analysis. Despite the inability to predict AF termination by CA, the method proposed here can on the other hand highlight and quantify some properties of RRI distribution encountered in the presence of AF. These results open new lines of investigation for enriching HDIG model so as to better render AF properties, e.g., by including non-linearities. Future research about other HR and RR features could be performed as well. The method could be potentially applied to further clinical applications, for instance, arrhythmia classification and prediction of AF episode onset.

Part III

Summary and conclusions

9 Conclusions and future work

In this doctoral thesis we have put forward several techniques and tools aiming at an improved, more robust noninvasive prediction of CA outcome in persistent AF. We illustrated the potential role of standard ECG for improving AF understanding and treatment. Particular attention has been paid to CA, since prediction of its outcome is still an open challenge in current medical practice. We have developed some mathematical tools aiming at extracting the most descriptive components of ECG signal, which are relevant to CA outcome prediction. In particular, we have exploited standard ECG spatial variability to highlight such predictive features, by combining contributions coming from multiple ECG leads and properly enhancing the most significant descriptive ones. In most of the applications introduced in our dissertation, PCA has proved to be suitable for representing the most meaningful characteristics of AA signal, thanks to its ability to compress its maximum-variance features into a few, representative components. In particular, we demonstrated that rank-1 approximations to AA signal can effectively render most of its structure without loss of significant information and represent a suitable basis for subsequent feature extraction. The introduction of further constraints (e.g., component non-negativity, ECG lead weighting schemes) has also allowed the application of other multivariate decomposition techniques (NMF, WPCA), which are equally able to emphasize the most discriminative components of the AA signal in CA outcome prediction. AA signal properties such as f-wave amplitude, regularity and STV content have been characterized in the presence of AF in a multivariate framework. The approaches developed thus overcome the limitations of traditional methods, which are manual or exclusively focus on only one ECG lead, thus neglecting the richness of multilead recordings and lacking of robustness to lead selection. Investigation of RR variability has also been envisaged for ventricular response characterization, and peculiarities of RRI distribution in AF patients have been assessed in a probabilistic point process framework. We next summarize the main contributions of this doctoral thesis

9.1 Summary and conclusions

9.1.1 Multivariate characterization of f-wave amplitude on standard ECG

One of the main objectives achieved in this work is represented by the assessment of f-wave amplitude in a multivariate framework. Moving from the empirical correlation between f-wave amplitude and CA outcome, widely acknowledged in clinical practice, we have developed an automatic method able to assess atrial peak-to-peak amplitude

distribution over multiple ECG leads. Single-lead measures obtained on reduced-ranks approximations to AA signal through PCA are properly combined in a unique parameter which can predict AF termination by CA. This approach allows us to extract the most significant components of f-wave amplitude by processing all the ECG leads at the same time, thus overcoming the limited perspective of single-lead methods. Results obtained are consistent with the clinical assumption that high values of f-wave amplitude predict AF termination by CA. By adequately combining contributions from each ECG lead, not only an extension to prediction in the long-term followup has been performed, but variations of this parameter within CA procedure have also been quantified. Our research corroborates the predictive value of atrial amplitude for CA outcome prediction and the improvement in performance accuracy and robustness provided by multilead processing.

9.1.2 Assessment of multivariate ECG measures of AF STV

Spatial diversity of the 12-lead ECG has also proved to be exploitable for quantifying the degree of STV of the AF pattern. Previous studies have noninvasively quantified AF organization on surface recordings. The extension of these works to a multilead framework has yielded novel measures of AF STV content, which quantify not only the degree of temporal repetitiveness of AF pattern between consecutive AA signal segments, but also its spatial distribution over ECG leads. PCA reduced-rank approximations to AA signal effectively retain its most content-bearing components, while rejecting noisy and/or redundant elements. Similar remarks can be made about WPCA application, which decomposes the AA signal based on a priori knowledge about contributions from each ECG lead in terms of temporal variance: the most stable and low-dispersion patterns effectively contribute to AA content characterization, whereas the most variable ones are automatically filtered out. The same rationale guides the choice of the multilead STV descriptor, once again underlining the advantages of correctly recognizing and emphasizing the most descriptive ECG leads for CA outcome prediction, at different follow-up lengths. An important line of research the application of the NMF technique to CA outcome prediction, which is, to our knowledge, employed for the first time in ECG signal processing in general, and in AF analysis in particular. Indeed, the NMF-compressed form of the multivariate information about AF STV proves to be still predictive of CA outcome, thus preserving its clinical meaning. Relation with AF organization according to classical clinical criteria, such as Wells' and Koning's, represent a future line of investigation.

9.1.3 Combination of multiple ECG features in a multivariate framework

The ECG descriptors aforementioned show to be reliable predictors of AF termination by CA and effectively render some properties which are visible on this type of heart electrical activity recording and are typical of persistent AF. In this dissertation, we have demonstrated that these measures of f-amplitude and AF STV can be properly examined at the same time by means of the LR analysis. This model linearly combines these multivariate measures extracted from PCA low-rank representations of the AA signal and selectively highlights ECG leads exhibiting the most content-bearing contributions. Components enhanced by this technique seem to be relevant to CA outcome prediction, and effectively assess AF therapy success. AF characterization seems to be enriched when these indices are simultaneously processed, thus opening promising perspectives for

the multivariate analysis of other heterogeneous ECG-based parameters, which can be potentially merged with further clinical data about the AF patient.

9.1.4 MULTIVARIATE PROCESSING OF IT MEASURES FROM CA OUTCOME PREDICTION

In this thesis, the concept of spatial variability of standard ECG has been investigated from multiple perspectives. A further way to explore such a diversity takes a step from the examination of the degree of mutual correlation between pairs of ECG leads, which has been subsequently extended to subsets of multiple electrodes. We demonstrated the existence of a relation between the degree of interlead uncorrelation and AF pattern regularity, assumed to be closely related to therapy outcome. This analysis provides a more accurate characterization of AF pattern distribution over ECG leads, and better enhances contributions coming from different orientations of the heart electrical axis. AF regularity content also proves to be correlated with CA outcome, and we actually verified the assumption that more uncorrelated and irregularly propagating patterns are linked to a lower probability of a successful CA procedure. To our knowledge, IT mathematical support has been employed for the first time not only for AF study on standard ECG in a multivariate framework, but also for establishing a relation between AF uncorrelation and CA clinical outcome.

9.1.5 PARAMETRIC APPROACHES FOR RR VARIABILITY CHARACTERIZATION DURING AF

For the sake of completeness, after characterizing information extracted for the AA signal, we also investigated the ventricular response as quantified by RRI analysis. RRI variability has been described in a probabilistic framework, by assuming that R wave occurrences represent a point process model. Accordingly, their probability distribution has been rendered through a HDIG model by taking into account the temporal variability of RRI length as induced by the sympathetic and the parasympathetic inputs to the SA node. This parametric description is free from tuning parameters of RRI histograms, in particular bin width, as RRI distribution parameters are estimated at each time instant, with no need for interpolation between consecutive R wave events. Moreover, the adequateness of the model proposed to depict RRI distribution can be mathematically assessed by means of the point process theory, relying on the time-rescaling theory and the goodness-of-fit analysis. This formulation allows for the extraction of HRV features which are exclusively function of HDIG distribution parameters estimated on the data themselves, and do not depend on histogram computation modalities. Despite the weak predictive power of the HRV measures in CA outcome assessment, such indices prove to be able to highlight some characteristics of RRI histograms, enhancing the differences between AF patients' and healthy subjects' RRI distribution, in particular concerning asymmetry and dispersion of the RRI PDF. These preliminary results hint new potential lines of research and clinical applications, in particular for instantaneous AF detection and arrhythmia classification.

9.2 Future work

9.2.1 Study challenges and limitations

The wide variety of AF aspects investigated in this work and the number of ECG features inspected can give rise to several questions about the best method which should be actually adopted to effectively predict CA outcome. The answer to such questions cannot come from just one methodology, since all the properties explored contribute to understand AF pathophysiology, whose complexity cannot be effectively rendered by examining just one property.

Consequently, we should rather wonder how to adequately exploit all these features. One potential strategy can come from proper combination of such ECG measures, in which only the most significant contributions are enhanced. This strategy resembles the approaches adopted throughout this dissertation for combining ECG leads' contributions, such as statistical measures of central tendency or LR analysis, but also multivariate decompositions, e.g., PCA. More sophisticated solutions come from the machine learning theory, which perform feature selection based on ranking criteria or distance measures. Different methods for variable subset selection can be actually taken into account. For instance, wrappers utilize the learning machine of interest as a black box to score subsets of variable according to their predictive power. Filters extract subsets of variables as a pre-processing step, independently of the chosen predictor. Finally, embedded methods perform variable selection in the process of training and are usually specific to given learning machines [59]. However, it must be mentioned that advanced approaches based on feature leaning generally need a large number of samples (i.e., AF patients or CA procedures in the applications of our interest), especially when a large set of variables is under examination. Roughly speaking, a higher number of subjects undergoing CA should be included in our study so as to confirm the predictive power of the ECG-based parameters introduced in this thesis.

In the same line, generalization of the results reported in this work is hampered not only by the variability of the ECG database size, but also by changes in criteria defining CA outcome. In certain groups, procedural success is obtained only if SR is restored, whereas other studies also admit conversion to intermediate, more organized arrhythmias (e.g., AFL). These changes have been frequently encountered throughout the present study, and make it harder to validate the ECG measures proposed. Furthermore, the application of complementary cardioversion therapies and/or additional ablations can also radically influence CA outcome evaluation in time, especially when switching to longer followup periods. Indeed, CA procedures regarded as failing in the immediate postoperative phase can turn into AF termination in the long-term followup because of one of the aforementioned therapies. Similarly, acute CA success can change into a procedural failure later in the follow-up because of clinical complications or atrial remodeling effects.

In this thesis, all the findings made on smaller groups of patients' have been validated on a bigger set, and links between acute procedural success and long-term AF termination have been established when possible. In future works, including a higher number of AF patients and applying machine learning techniques could help generalizing methods' validity and overcome issues related to dependence on followup length, since the most suitable features will be automatically determined and chosen by the algorithm.

9.2.2 CA OUTCOME PREDICTION IN PERSISTENT AF BY TENSOR DECOMPOSITIONS

The present doctoral thesis has explored in detail the potentialities of matricial representations of the 12-lead ECG as directly obtained in clinical centers. More precisely, in order to assess how AF pattern is distributed over leads and how it can be characterized from different planes and angles, we assumed to analyze signal variability throughout ECG leads at a fixed time instant. Therefore, ECG analysis has been performed both in terms of space and time. However, despite the suitability of this matrix representation, further potential information about AF content could be properly highlighted by this kind of approach. Indeed, it could be useful to include in the analysis other signal properties (for instance, frequency), or examine multivariate features on the same lead all at once, without decomposing their matrix structure (as we did, for example, in Chapter 5 when dealing with AF STV extraction and NMSE computation over AA segments). Hence, moving to tensorial analysis could help overcoming these issues and better enhancing AF properties. More precisely, the main purpose of this approach is the exploitation of tensorial forms to extract suitable features which are based on projections on data linear subspaces and are predictive of CA outcome in persistent AF.

A tensor is a multidimensional array. More formally, an N-way or Nth-order tensor is an element of the outer product of N vector spaces, each characterized by its own coordinate system [77]. As in the 2-D case, the core of our investigation is to which extent it is possible to transfer properties of matrix decompositions to higher tensor orders, and, when this transposition is not possible, which aspects and differences should be taken into account from a mathematical point of view. In fact, as compared to matrix techniques, tensor decompositions present some remarkable features such as essential uniqueness under mild conditions and rank possibly exceeding the data dimensions, but some computational constraints should be also taken into account, dealing with greater time and space complexity inherent in tensor algorithms. One of the main fields of application of tensor decompositions has been so far represented by telecommunications [40]. In particular, some techniques, such as the PARAFAC (Parallel factor analysis) decompositions, aim at representing the tensor as a sum of rank-1 tensors, and have been successfully applied to wireless communication [122, 140]. A higher order generalization of SVD , i.e. the HOSVD, has also been presented in [86]. Another line of research has attempted to perform an orthogonal decomposition of tensorial data in keeping with the bidimensional case of PCA in the variance-extraction sense, thus yielding the contribution presented by [149]. Some of its variants, i.e., the multinear PCA (MPCA) and the uncorrelated MPCA (UMPCA) have been applied to image classification [90, 91] and EEG feature selection [9]. A non-negative factorization (i.e., the tensorial counterpart of the equivalent NMF in the 2-D case) has also been implemented, with particular concern for sparse image coding [137].

In our application, one of the most crucial points is the correct identification of the structure of input data. We actually wonder not only how many dimensions (the so-called tensor modes) we can process by means of our algorithm (roughly speaking, the optimal order of tensorial data), but also which feature should be taken into account for each dimension. Intuitively, we could keep the spatial notion intrinsic to ECG leads' spatial distribution, besides the temporal evolution of signal samples. Choice of further ECG properties to be analyzed is not a trivial task, and it must take into account which global information we aim to extract. For instance, a possible experimental line could concern

the introduction of frequency-based features determined on each ECG lead, provided that ventricular activity is previously removed from the ECG recording. Another possible solution could aim at exploring AF STV content and considering the AA segment as a mode of the tensor, thus introducing the non-negativity constraint intrinsic to NMSE definition. In addition, the proper tensorial decomposition must be selected so as to extract potentially predictive features, whose interpretation must be consistent with AF pathophysiology.

Bibliography

[1] C. Abreu-Lima, D.M. Correia, J. Almeida, and et al. A new ECG classification system for myocardial infarction based on receiver operating characteristic curve analysis and information theory. *Circulation*, 67(6):1252–1257, 1998.

[2] R. Alcaraz, D. Abasolo, R. Hornero, and J. J. Rieta. Optimized assessment of atrial fibrillation organization through suitable parameters of sample entropy. In *Proceedings IEEE EMBC 2010*, pages 118–121, 2010, Aug 31 - Sept 4.

[3] R. Alcaraz, F. Hornero, and J. J. Rieta. Noninvasive time and frequency predictors of long-standing atrial fibrillation early recurrence after electrical cardioversion. *Pacing Clin Electrophysiol.*, 34(10):1241–1250, 2011.

[4] R. Alcaraz and J. J. Rieta. A review on sample entropy applications for the non-invasive analysis of atrial fibrillation electrocardiograms. *Biomed Signal Proces*, 5(1):1–14, 2010.

[5] R. Alcaraz and J.J. Rieta. A novel application of sample entropy to the electrocardiogram of atrial fibrillation. *Nonlinear Analysis: Real World Applications*, 11:1026–1035, 2010.

[6] E. C. Alexopoulos. Introduction to multivariate regression analysis. *Hippokratia*, 14(Suppl 1):23–28, 2010.

[7] M. Allessie, J. Ausma, and U. Schotten. Electrical, contractile and structural remodeling during atrial fibrillation. *Cardiovascular Research*, 54:230–246, 2002.

[8] M. Allessie, F. Bonke, and F. Schopman. Circus movement in rabbit atrial muscle as a mechanism of tachycardia. iii. the "leading circle" concept: a new model of circus movement in cardiac tissue without the involvement of an anatomical obstacle. *Circ Res*, 41:9–18, 1977.

[9] A. Althoff. *Online Tensor Factorization for Feature Selection in EEG*. PhD thesis, Honors Thesis, Department of Cognitive Science, University of California - San Diego, 2012.

[10] V. Barbaro, P. Bartolini, G. Calcagnini, and et al. An index of organization of the right atrium during atrial fibrilaltion: Effects of internal cardioversion. In *Proceedings of the Third International Symposium on Medical Data Analysis*, pages 127–133. Springer-Verlag, 2002.

[11] R. Barbieri, E. C. Matte, A. A. Alabi, and E. N. Brown. A point-process model of human heartbeat intervals: New definitions of heart rate and heart rate variability. *Am. J. Heart Circ. Physiol.*, 288(1):424–435, 2005.

[12] M. W. Berry, M. Browne, A. N. Langville, and et al. Algorithms and applications for approximate nonnegative matrix factorization. In *Computational Statistics and Data Analysis*, pages 155–173, 2006.

[13] A. Bezeranios, S. Tong, and N. Thakor. Time-dependent entropy estimation of EEG rhythm changes following brain ischemia. *Ann. Biomed. Eng.*, 31(2):221–232, 2003.

[14] G.K. Bhattacharyya and R.A. Johnson. *Statistical concepts and methods*. Wiley, 1977.

[15] J.T. Bigger, L.F. Fleiss, R.C. Steinman, and et al. RR variability in healthy, middle-age persons compared with patients with chronic coronary heart disease or recent acute myocardial infarction. *Circulation*, 91:1936–1943, 1995.

[16] C. Blomström-Lundqvist, M. Scheinman, E.M. Aliot, and et al. ACC/AHA/ESC guidelines for the management of patients with supraventricular arrhythmias: a report of the American College of Cardiology/American Heart Association Task Force on practice guidelines and the European Society of Cardiology Committee for practice guidelines (writing committee to develop guidelines for the management of patients with supraventricular arrhythmias. *Eur Heart J*, pages 1857–1897, 2003.

[17] A. Bollmann, D. Husser, L. Mainardi, and et al. Analysis of surface electrocardiograms in atrial fibrillation: techniques, research, and clinical applications. *Europace*, 8(11):911–926, Nov. 2006.

[18] P. Bonizzi, M. S. Guillem, A. M. Climent, J. Millet, V. Zarzoso, F. Castells, and O. Meste. Noninvasive assessment of the complexity and stationarity of the atrial wavefront patterns during atrial fibrillation. *IEEE Trans. Biomed. Eng.*, 57(9):2147–2157, 2010.

[19] P. Bonizzi, O. Meste, V. Zarzoso, D. G. Latcu, I. Popescu, P. Ricard, and N. Saoudi. Atrial fibrillation disorganization is reduced by catheter ablation: A standard ECG study. In *Proceedings IEEE EMBC 2010*, pages 5286–5289, 2010.

[20] B. K. Bootsma, A. J. Hoelen, J. Strackee, and F. L. Meijler. Analysis of R-R intervals in patients with atrial fibrillation at rest and during exercise. *Circulation*, 41:783–794, 1970.

[21] G. W. Botteron and J. M. Smith. A technique for measurement of the extent of spatial organization of atrial activation during atrial fibrillation in the intact human heart. *IEEE Transactions on Biomedical Engineering*, 42(6):579–586, June 1995.

[22] G.W. Botteron and J.M. Smith. Quantitative assessment of the spatial organization of atrial fibrillation in the intact human heart. *Circulation*, 93:513–518, 1996.

[23] E. N. Brown, R. Barbieri, U.T. Eden, and L.M. M. Frank. *Computational Neuroscience: A Comprehensive Approach*. Chapman & Hall/CRC Mathematical & Computational Biology, 2002.

[24] A. Cabasson and O. Meste. Time delay estimation: A new insight into the Woody's method. *IEEE Signal Processing Letters*, 15:573–576, 2008.

[25] H. Calkins, J. Brugada, D. L. Packer, and et al. HRS/EHRA/ECAS expert consensus statement on catheter and surgical ablation of atrial fibrillation: recommendations for personnel, policy, procedures and follow-up. *Heart Rhythm*, 4(6):816–861, 2007.

[26] H. Calkins, J. Brugada, and D.L. Packer. HRS/EHRA/ECAS expert consensus statement on catheter and surgical ablation of atrial fibrillation: recommendations for personnel, policy, procedures and follow-up. *Europace*, 9(6):335–379, 2007.

[27] H. Calkins, K. H. Kuck, R. Cappato, and et al. HRS/EHRA/ECAS expert consensus statement on catheter and surgical ablation of atrial fibrillation: Recommendations for patient selection, procedural techniques, patient management and follow-up, definitions, endpoints, and research trial design. *Europace*, 14(4):528–606, 2012.

[28] A. J. Camm, P. Kirchhof, and G. Y.H. Lip. Guidelines for the management of atrial fibrillation - the task force for the management of atrial fibrillation of the european society of cardiology (ESC). *European Heart Journal*, 31:2369–2429, 2010.

[29] F. Castells, P. Laguna, L. Sörnmo, and et al. Principal component analysis in ECG signal processing. *EURASIP Journal on Advances in Signal Processing*, 2007:1–21, 2007.

[30] J. Chen, R. Mandapati, O. Berenfeld, and et al. Dynamics of wavelets and their role in atrial fibrillation in the isolated sheep heart. *Cardiovasc Res*, 48(2):220–232, Nov. 2000.

[31] Z. Cheng, H. Deng, K. Cheng, T. Chen, P. Gao, M. Yu, and Q. Fang. The amplitude of fibrillatory waves on leads aV_F and V_1 predicting the recurrence of persistent atrial fibrillation patients who underwent catheter ablation. *Ann Noninvasive Electrocardiol.*, 18(4):352–358, 2013.

[32] F. J. Chorro, C. J. Kirchhof, J. Brugada, and et al. Ventricular response during irregular atrial pacing and atrial fibrillation. *Am. J. Physiol.*, 259:1015–1021, 1990.

[33] A. M. Climent, M. S. Guillem, D. Husser, and et al. Role of the atrial rate as a factor modulating ventricular response during atrial fibrillation. *Pacing Clin. Electrophysiol.*, 33:1510–1517, 2010.

[34] A.M. Climent, D. Husser, J. Millet, and et al. Non-invasive assessment of atrioventricular conduction properties and their effects on ventricular response in atrial fibrillation. In *Computers in Cardiology*, volume 33, pages 105–108, 2006.

[35] V. D. A. Corino and F. Sandberg. Statistical modeling of the atrioventricular node during atrial fibrillation: Data length and estimator performance. In *Proceedings IEEE EMBC 2013*, 2013.

[36] V. D. A. Corino, F. Sandberg, L.T. Mainardi, and et al. An atrioventricular node model for analysis of the ventricular response during atrial fibrillation. *IEEE Trans on Biomed Eng*, 58(12):3386–3395, 2011.

[37] T. M. Cover and J. A. Thomas. *Elements of Information Theory*. Wiley Series in Telecommunications and Signal Processing, 2nd ed., 2006.

[38] J.L. Cox, J.P. Boineau, R.B. Schuessler, and et al. Five year experience with the maze procedure for atrial fibrillation. *Ann Thorac Surg.*, 56:814–823, 1993.

[39] J.L. Cox, R.B. Schuessler, H.J. Jr D'Agostino, and et al. The surgical treatment of atrial fibrillation. III. development of a definitive surgical procedure. *J Thorac Cardiovasc Surg.*, 101(4):569–583, 1991.

[40] A.L.F. De Almeida, G. Favier, and J. C. M. Mota. A constrained factor decomposition with application to MIMO antenna systems. *IEEE Trans Sign Proc*, 56:2429–2442, 2008.

[41] L. De Lathauwer, B. De Moor, and J. Vandewalle. Fetal electrocardiogram extraction by blind source subspace separation. *IEEE Transactions on Biomedical Engineering*, 47(5):567–572, May 2000. Special Topic Section on Advances in Statistical Signal Processing for Biomedicine.

[42] J.T. Dell'Orfano, J.C. Luck, D.L. Wolbrette, and et al. Drugs for conversion of atrial fibrillation. *Am Fam Physician*, 2(58):471–480, Aug 1998.

[43] I.S. Dhillon and D.S. Modha. Concept decompositions for large sparse text data using clustering. *Machine Learning*, 42:143–175, 2001.

[44] T.J. Dresing and R. A. Schweikert. *Atrial Fibrillation: Current Clinical Medicine*. Elsevier, 2nd Edition, 2010.

[45] M. J. Earley and R. J. Schilling. Catheter and surgical ablation of atrial fibrillation. *Heart*, 92(2):266–274, 2006.

[46] C. S. Elayi, L. Di Biase, C. Barrett, and et al. Atrial fibrillation termination as a procedural endpoint during ablation in long-standing persistent atrial fibrillation. *Heart Rhythm*, 7:1216–1223, Sept. 2010.

[47] T.H. Everett, J. R. Moorman, L. C. Kok, and et al. Assessment of global atrial fibrillation organization to optimize timing of atrial defibrillation. *Circulation*, 103:2857–2861, 2001.

[48] L. Faes, G. Nollo, M. Kirchner, and et al. Principal component analysis and cluster analysis for measuring the local organisation of human atrial fibrillation. *Medical and Biological Engineering and Computing*, 39(6):656–663, 2006.

[49] C. Fisch. Centennial of the string galvanometer and the electrocardiogram. *Journal of the American College of Cardiology*, 36:1737–1745, 2000.

[50] R.N. Fogoros. Ablating atrial fibrillation. The pros and cons of ablation therapy for atrial fibrillation, available at http://heartdisease.about.com/cs/arrhythmias/a/ablateafib.htm, 2011.

[51] D. Foo, KS Ng, L. Qu, and A. Sutandar. Narrow complex tachycardia with alternating R-R intervals. What is the mechanism? *Indian Pacing Electrophysiol. J.*, 6(4):242–243, 2006.

[52] M. Frick, V. Frykman, M. Jensen-Urstad, and et al. Factors predicting success rate and recurrence of atrial fibrillation after first electrical cardioversion in patients with persistent atrial fibrillation. *Clin Cardiol.*, 24(3):238–244, Mar. 2001.

[53] V. Fuster, L. E. Rydén, D. S. Cannom, and et al. ACC/AHA/ESC 2006 guidelines for the management of patients with atrial fibrillation – executive summary. *Circulation*, 114:700–752, 2006.

[54] W. Garry. Auricular fibrillation. *Physiol Rev*, 4:215–250, 1924.

[55] A. L. Goldberger, Z.D. Goldberger, and A. Shvilkin. *Goldberger's Clinical Electrocardiography: A Simplified Approach*. Elsevier, 8th edtion, 2012.

[56] A.L. Goldberger, L.A.N Amaral, L. Glass, and et al. Physiobank, physiotoolkit, and physionet: Components of a new research resource for complex physiologic signals. *Circulation*, 101(23):215–220, 2000.

[57] M. S. Guillem, A. M. Climent, F. Castells, and et al. Noninvasive mapping of human atrial fibrillation. *J. Cardiovasc. Electrophysiol.*, 5:507–513, 2009.

[58] M.S. Guillem, A.M. Climent, J. Millet, and et al. Noninvasive localization of maximal frequency sites of atrial fibrillation by body surface potential mapping. *Circ Arrhythm Electrophysiol.*, 6(2):294–301, Apr 2013.

[59] I. Guyon and A. Elisseeff. An introduction to variable and feature selection. *Journal of Machine Learning Research*, 3:1157–1182, 2003.

[60] M. Haïssaguerre, M. Hocini, P. Sanders, and et al. Localized sources maintaining atrial fibrillation organized by prior ablation. *Circulation*, 113:616–625, 2006.

[61] M. Haïssaguerre, P. Jaïs, D. C. Shah, and et al. Electrophysiological end point for catheter ablation of atrial fibrillation initiated from multiple pulmonary venous foci. *Circulation*, 101:1409–1417, 2000.

[62] M. Haïssaguerre, P. Jaïs, D.C. Shah, and et al. Spontaneous initiation of atrial fibrillation by ectopic beats originating in the pulmonary veins. *N. Engl. J. Med.*, 339:659–65, 1998.

[63] M. Haïssaguerre, P. Sanders, M. Hocini, and et al. Catheter ablation of long-lasting persistent atrial fibrillation: critical structures for termination. *J Cardiovasc Electrophysiol*, 16(11):1125–1137, 2005.

[64] T. S. Han. Multiple mutual informations and multiple interactions in frequency data. *Information and Control*, 46(1):26–45, 1980.

[65] E. Hashida and T. Tasaki. Considerations of the nature of irregularity of the sequence of R-R intervals and the function of the atrioventricular node in atrial fibrillation in man based on time series analysis. *Jpn. Heart J.*, 25(5):669–687, Sept. 1984.

[66] A. Henk and L. Kiers. Weighted least squares fitting using ordinary least squares algorithms. *Psycometrika*, 62(2):251–266, 1997.

[67] M. Holm, S. Pehrson, M. Ingemansson, and et al. Non-invasive assessment of the atrial cycle length during atrial fibrillation in man: introducing, validating and illustrating a new ECG method. *Cardiovasc Res*, 38:69–81, 1998.

[68] J. M. Irvine, S. A. Israel, W. T. Scruggs, and W. J. Worek. Eigenpulse: Robust human identification from cardiovascular function. *Pattern Recognition*, 41(11):3427–3435, Nov. 2008.

[69] P. Jaïs, M. Haïssaguerre, and D. C. et al. Shah. A focal source of atrial fibrillation treated by discrete radiofrequency ablation. *Circulation*, 95:572–576, 1997.

[70] P. Jaïs, M. Hocini, P. Sanders, and et al. Long-term evaluation of atrial fibrillation ablation guided by noninducibility. *Heart Rhythm*, pages 140–145, 2006.

[71] C. J. James and C. W. Hesse. Independent component analysis for biomedical signals. *Physiol Meas.*, 26(1):R15–39, Feb 2005.

[72] J.J. Jansen, H.C.J. Hoefsloot, H. F. M. Boelens, and et al. Analysis of longitudinal metabolomics data. *Bioinformatics*, 20:2438–2446, 2004.

[73] I. T. Jolliffe. *Principal component analysis*. Springer, 2nd edition, 2002.

[74] D. Kahaner, C. Moler, and S. Nash. *Numerical Methods and Software*. Prentice Hall, 1998.

[75] S.M. Kay. *Fundamentals of Statistical Signal Processing: Estimation Theory, Volume I*. Prentice Hall Signal Processing Series, 1993.

[76] J.A. Kirsh, A.V. Sahakian, J.M. Baerman, and S. Swiryn. Ventricular response to atrial fibrillation: role of atrioventricular conduction pathways. *J. Am. Coll. Cardiol.*, 12:1265–1272, 1988.

[77] T. G. Kolda and B. W. Bader. Tensor decompositions and applications. *SIAM Review*, 51(3):455–500, 2009.

[78] K.T. Konings, C.J. Kirchhof, J.R. Smeets, and et al. High-density mapping of electrically induced atrial fibrillation in humans. *Circulation*, 89(4):1665–1680, Apr 1994.

[79] D. E. Lake and J. R. Moorman. Accurate estimation of entropy in very short physiological time series. *Am J Physiol Heart Circ Physiol*, 300(1):319–325, 2011.

[80] D.E. Lake, J.S. Richman, M.P. Griffin, and et al. Sample entropy analysis of neonatal heart rate variability. *Am. J. Physiol. Heart Circ Physiol.*, 283:789–797, 2002.

[81] V. Lane Price Rose. Significant body systems: pulmonary/respiratory system, available at http://webschoolsolutions.com/patts/systems/lungs.htm, 2000.

[82] R. Langendorf, A. Pick, and L. N. Katz. Ventricular response in atrial fibrillation: Role of concealed conduction in the AV junction. *Circulation*, 32:69–75, 1965.

[83] A.N. Langville and C. D. Meyer. Text mining using the nonnegative matrix factorization. In *Proceedings of the 29th annual SIAM Southeast Atlantic Section Conference*, March 2005.

[84] A.N. Langville, C. D. Meyer, and R. Albright. Initializations for the nonnegative matrix factorization. In *Proceedings of the 12th International Conference on Knowledge Discovery and Data Mining (KDD)*, 2006.

[85] R. Latchamsetty and A. Chugh. Catheter ablation of persistent atrial fibrillation. *The Journal of Innovations in Cardiac Rhythm Management*, 4:1187–1204, 2013.

[86] L. D. Lathauwer, B. D. Moor, and J. Vandewalle. A multilinear singular value decomposition. *Matrix Analysis and Application*, 21:1253–1278, 2000.

[87] M.P. LaValley. Statistical primer for cardiovascular research: Logistic regression. *Circulation*, 117:2395–2399, 2008.

[88] C.S. Lima and M.J. Cardoso. Cardiac arrhythmia detection by parameters sharing and MMIE training of hidden markov models. In *Proceedings IEEE EMBC 2007*, pages 3836–3839, 2007.

[89] B. Lown. Electrical reversion of cardiac arrhythmias. *Br Heart J.*, 29(4):469–489, 1967.

[90] H. Lu, K. N. Plataniotis, and A.N. Venetsanopoulos. MPCA: Multlinear principal component analysis of tensor objects. *IEEE Trans on Neural Net*, 19(1):18–39, Jan. 2008.

[91] H. Lu, K. N. Plataniotis, and A.N. Venetsanopoulos. Uncorrelated multilinear principal component analysis for unsupervised multilinear subspace learning. *IEEE Trans. Neural Netw.*, 20(11):1820–1836, 2009.

[92] S.A. Lubitz, A. Fischer, and V. Fuster. Catheter ablation for atrial fibrillation. *BMJ*, 336(7648):819–826, Apr 2008.

[93] R. MacLeod, , and B. Birchler. ECG measurement and analysis, available at http://www.sci.utah.edu/ macleod/bioen/be6000/labnotes/ecg/descrip.html, 2011.

[94] L. Mainardi, S. Cerutti, and L. Sörnmo. *Understanding Atrial Fibrillation, the Signal Processing Contribution: Part II.* Morgan and Claypool, 2007.

[95] L. T. Mainardi, A. Porta, G. Calcagnini, and et al. Linear and nonlinear analysis of atrial signals and local activation period series during atrial fibrillation episodes. *Med. Biol. Eng. Comput.*, 39:249–254, 2001.

[96] J. Malmivuo and R. Plonsey. *Bioelectromagnetism – Principles and Applications of Bioelectric and Biomagnetic Fields.* Oxford University Press, New York, 1995.

[97] V. Markides and R. J. Schilling. Atrial fibrilaltion: Classification, pathophysiology, mechanisms and drug treatment. *Heart*, pages 939–943, 2003.

[98] S. Matsuo, N. Lellouche, and M. et al. Wright. Clinical predictors of termination and clinical outcome of catheter ablation for persistent atrial fibrillation. *J Am Coll Cardiol*, 54(9):788–795, Aug. 2009.

[99] S. Matsuo, T. Yamane, T. Date, and et al. Substrate modification by pulmonary vein isolation and left atrial linear ablation in patients with persistent atrial fibrillation: its impact on complex-fractionated atrial electrograms. *J Cardiovasc Electrophysiol.*, 23(9):962–970, Sep. 2012.

[100] J. H. McDonald. *Handbook of Biological Statistics*. Sparky House Publishing, 2nd ed., 2009.

[101] M. Meo, V. Zarzoso, O. Meste, D. G. Latcu, and N. Saoudi. Catheter ablation outcome prediction in persistent atrial fibrillation based on spatio-temporal complexity measures of the surface ECG. In *Computing in Cardiology*, volume 38, pages 261–264., Hagzhou, China, Sept. 18-21, 2011 2011.

[102] M. Meo, V. Zarzoso, O. Meste, D. G. Latcu, and N. Saoudi. Non-invasive prediction of catheter ablation outcome in persistent atrial fibrillation by exploiting the spatial diversity of surface ECG. In *Proceedings IEEE EMBS 2011*, pages 5531–5534, 2011.

[103] M. Meo, V. Zarzoso, O. Meste, D. G. Latcu, and N. Saoudi. Multidimensional characterization of fibrillatory wave amplitude on surface ECG to describe catheter ablation impact on persistent atrial fibrillation. In *Proceedings IEEE EMBS 2012*, pages 617–620, Aug. 28 - Sep. 1, 2012 2012.

[104] M. Meo, V. Zarzoso, O. Meste, D. G. Latcu, and N. Saoudi. Automatic multilead characterization of f-wave amplitude enhances prediction of catheter ablation outcome in persistent atrial fibrillation. In *Europace*, 2013.

[105] M. Meo, V. Zarzoso, O. Meste, D. G. Latcu, and N. Saoudi. Catheter ablation outcome prediction in persistent atrial fibrillation using weighted principal component analysis. *Biomed Signal Proces and Control*, 8:958–968, 2013. Biomed. Sign. Proc. and Contro, 2013, in press.

[106] M. Meo, V. Zarzoso, O. Meste, D. G. Latcu, and N. Saoudi. Spatial variability of the 12-lead surface ECG as a tool for noninvasive prediction of catheter ablation outcome in persistent atrial fibrillation. *IEEE Trans. Biomed. Eng.*, 60(1):20–27, Jan. 2013.

[107] M. Meo, V. Zarzoso, O. Meste, D. G. Latcu, and N. Saoudi. Nonnegative matrix factorization for noninvasive prediction of catheter ablation outcome in persistent atrial fibrillation. *In: IEEE International Conference on Acoustics, Speech, and Signal Processing (ICASSP)*, pages 601–604, Kyoto, Japan, March 25-30, 2012.

[108] P. Meyer. *Démonstration Simplifiée d'un théorème de Knight*. In. Séminaire Probabilité. New York: Springer-Verlag, 1969.

[109] D.M. Mirvis and A. L. Goldberger. *Electrocardiography. In: Braunwald's Heart Disease: A Textbook of Cardiovascular Medicine*. Elsevier, 9th edition, 2011.

[110] G. Moe and J. Abildskov. Atrial fibrillation as a self-sustaining arrhythmia independent of focal discharge. *Am. Heart J.*, 58:59–70, 1959.

[111] G. K. Moe. On the multiple wavelet hypothesis of atrial fibrillation. *Arch Int Pharmacodyn Ther.*, 140:183–188, 1962.

[112] H. Monson. *Statistical Digital Signal Processing and Modeling.* John Wiley and Sons, 1996.

[113] G. B. Moody and R. G. Mark. A new method fro detecting atrial fibrillation using RR intervals. In *Computers in Cardiology*, pages 227–230, 1983.

[114] Z. Moussavi. Anatomy & physiology of the heart. *Heart Lecture, ECE4610*, pages 1–9, 2009.

[115] K. Nademanee, E. Lockwood, N. Oketani, and B. Gidney. Catheter ablation of atrial fibrillation guided by complex fractionated atrial electrogram mapping of atrial fibrillation substrate. *J Cardiol.*, 55(1):1–12, 2010.

[116] K. Nademanee, J. McKenzie, E. Kosar, and et al. A new approach for catheter ablation of atrial fibrillation: Mapping of the electrophysiologic substrate. *J Am Coll Cardiol*, 43:2044–2053, 2004.

[117] S. Narayan, C. Sehra, R.and Briggs, and D. E. Krummen. Rapid termination of human atrial fibrillation by ablation at localized sources: Focal impulse and rotor modulation (FIRM). *Circulation*, 124:Abstract 11104, 2011.

[118] S.M. Narayan, D. E. Krummen, K. Shivkumar, and et al. Treatment of atrial fibrillation by the ablation of localized sources. *Journ. Am. Coll. Card.*, 60(7):628–636, Aug. 2012.

[119] S. Nattel. New ideas about atrial fibrillation 50 years on. *Nature*, 415:219–226, 2002.

[120] S. Nattel, B. Burstein, and D. Dobrev. Atrial remodeling and atrial fibrillation: Mechanisms and implications. *Circulation: Arrhythmia and Electrophysiology.*, 1:62–73, 2008.

[121] I. Nault, N. Lellouche, S. Matsuo, and et al. Clinical value of fibrillatory wave amplitude on surface ECG in patients with persistent atrial fibrillation. *J. Interv. Card. Electrophysiol.*, 26(1):11–19, Oct. 2009.

[122] D. Nion and L. De Lathauwer. Line search computation of the block factor model for blind multi-user access in wireless communications. In *IEEE Workshop on Signal Processing Advances in Wireless Communications (SPAWC)*, July 2-5, 2006.

[123] G. Nollo, M. Marconcini, L. Faes, F. Bovolo, F. Ravelli, and L. Bruzzone. An automatic system for the analysis and classification of human atrial fibrillation patterns from intracardiac electrograms. *IEEE Trans on Biomed Eng*, 55(9):2275–2285, September 2008.

[124] M.D. O'Neill, M. Wright, S. Knecht, and et al. Long-term follow-up of persistent atrial fibrillation ablation using termination as a procedural endpoint. *European Heart Journal*, 30:1105–1112, 2009.

[125] F. Ouyang, R. Tilz, J. Chun, and et al. Long-term results of catheter ablation in paroxysmal atrial fibrillation: Lessons from a 5-year follow-up. *Circulation*, 122(23):2368–2377, 2010.

[126] G. Pagana, L. Galleani, S. Grossi, M. Ruo, E. Pastore, M. Poggio, and G. Quaranta. Time-frequency analysis of the endocavitarian signal in paroxysmal atrial fibrillation. *IEEE Transactions on Biomedical Engineering*, 59(10):2838–2844, October 2012.

[127] J. Pan and W. J. Tompkins. A real-time QRS detection algorithm. *IEEE Trans. Biomed. Eng.*, 3(3):230–236, 1985.

[128] S. Pehrson, M. Holm, C. Meurling, M. Ingemansson, B. Smideberg, L. Sörnmo, and S. B. Olsson. Non-invasive assessment of magnitude and dispersion of atrial cycle length during chronic atrial fibrillation in man. *Eur Heart J*, 19:1836–1844, 1998.

[129] S. Petrutiu, J. Ng, G. M. Nijm, H. Al-Angari, S. Swiryn, and A.V. Sahakian. Atrial fibrillation and waveform characterization. a time domain perspective in the surface ECG. *IEEE Eng Med Biol Mag*, 25:24–30, 2006.

[130] J. S. Richman and J.R. Moorman. Physiological time-series analysis using approximate entropy and sample entropy. *Am. J. Physiol. Heart Circ. Physiol.*, 278:2039–2049, 2000.

[131] J.L. Rodríguez-Sotelo, E. Delgado-Trejos, D. Peluffo-Ordóñez, and et al. Weighted-PCA for unsupervised classification of cardiac arrhythmias. In *Proceedings IEEE EMBC 2010*, pages 1906–1909, Buenos Aires, Argentina, 2010.

[132] M. Rousseau, R. J. Sargeant, C. Chow, and S. Park. Atrial fibrillation teaching file, available at http://afib.utorontoeit.com/, 2008.

[133] K. M. Ryder and E. J. Benjamin. Epidemiology and signficance of atrial fibrillation. *Am J Cardiol*, 84:131–138, 1999.

[134] R. Sameni, F. Vrins, F. Parmentier, and et al. Electrode selection for noninvasive fetal electrocardiogram extraction using mutual information criteria. In *26th International Workshop on Bayesian Inference and Maximum Entropy Methods in Science and Engineering, American Institute of Physics*, volume 872, pages 97–104, July 8-13, 2006.

[135] T. D. Schneider. Molecular information theory: From clinical applications to molecular machine efficiency. In *Proceedings IEEE EMBS 2003*, 2003.

[136] Claude E. Shannon. A mathematical theory of communication. *Bell System Technical Journal 2*, 7(3):379–423, 1948.

[137] A. Shashua and T. Hazan. Non-negative tensor factorization with applications to statistics and computer vision. In *Proceedings of the 22nd International Conference on Machine Learning*, 2005.

[138] J. B. Shea and W. H. Maisel. Cardioversion. *Circulation*, pages 176–178, 2002.

[139] J. Shlens. A tutorial on principal component analysis. Technical report, Salk Institute for Biological Sciences, 2009.

[140] N. D. Sidiropoulos, G.B. Giannakis, and R. Bro. Blind PARAFAC receivers for DS-CDMA systems. *Trans. Sign Proc.*, 48(3):810–823, 2000.

[141] D.W. Simborg, R. S. Ross, K. B. Lewis, and R.H. Shepard. The RR interval histogram. *JAMA*, 198(11):867–870, 1966.

[142] D. Skočaja, A. Leonardisa, and H. Bischofb. Weighted and robust learning of subspace representations. *Journal Pattern Recognition*, 40:1556–1569, 2007.

[143] L. Sörnmo and P. Laguna. *Bioelectrical Signal Processing in Cardiac and Neurological Applications*. Elsevier Academic Press, 2nd edition, 2005.

[144] S. Srinivasa. *A Review on Multivariate Mutual Information*. Notre Dame EE-80653 Information Theory Tutorials, 2005.

[145] G.B. Stanley, K. Poolla, and R.A. Siegel. Threshold modeling of autonomic control of heart rate variability. *IEEE Trans Biomed Eng*, 47:1147–1153, 2000.

[146] R. Steuer, J. Kurths, C. O. Daub, and et al. The mutual information: Detecting and evaluating dependencies between variables. *Bioinformatics*, 18(2):S231–S240, 2002.

[147] Y. Takahashi, M. D. O'Neill, M. Hocini, R. Dubois, S. Matsuo, et al. Characterization of electrograms associated with termination of chronic atrial fibrillation by catheter ablation. *Journal of the American College of Cardiology*, 51(10):1003–1010, 2008.

[148] E. G. Thompson and J. M. Miller. WebMD Heart Health Center, 2010.

[149] L. R. Tucker. Some mathematical notes of three-mode factor analysis. *Psychometrika*, 31:279–311, 1966.

[150] L. Uldry, J. Van Zaen, Y. Prudat, L. Kappenberger, and J.-M. Vesin. Measures of spatiotemporal organization differentiate persistent from long-standing atrial fibrillation. *Europace*, 14(8):1125–1131, 2012.

[151] M. P. Van den Berg, J. Haaksma, J. Brouwer, and et al. Heart rate variability in patients with atrial fibrillation is related to vagal tone. *Circulation*, 96:1209–1216, 1997.

[152] H. L. Van Trees. *Detection, Estimation, and Modulation Theory, Part IV: Optimum Array Processing*. John Wiley & Sons, New York, 2002.

[153] B. D. Van Veen and K. M. Buckley. Beamforming: a versatile approach to spatial filtering. *IEEE Acoustics, Speech and Signal Processing Magazine*, 5(2):4–24, April 1988.

[154] J. Van Zaen, U. Laurent, A. Buttu, and et al. Harmonic frequency tracking algorithm for predicting the success of pharmacological cardioversion of atrial fibrillation. In *Europace*, 2011.

[155] F. Vanheusden. Body surface potential mapping (bspm), available at http://www2.le.ac.uk/research/festival/meet/science/vanheusden/page-two, 2013.

[156] T. Verdel. Décision et prévision statistiques, lectures of statistics, 2007.

[157] A. Verma and A. Natale. Why atrial fibrillation ablation should be considered first-line therapy for some patients. *Circulation*, 112:1214–1230, 2005.

[158] T.H. Vikman, S.and Mäkikallio, S. Yli-Mäyry, and et al. Heart rate variability and recurrence of atrial fibrillation after electrical cardioversion. *Ann Med.*, 35(1):36–42, 2003.

[159] A. L. Waldo. Mechanisms of atrial fibrillation. *J Cardiovasc Electrophysiol*, 14:267–274, 2003.

[160] P. Weismüller, C. Kratz, B. Brandts, and et al. AV nodal pathways in the R-R interval histogram of the 24-hour monitoring ECG in patients with atrial fibrillation. *Ann Noninvasive Electrocardiol.*, 6(4):285–289, Oct. 2001.

[161] J. L. Wells, R. B. Karp, N. T. Kouchoukos, and et al. Characterization of atrial fibrillation in man: studies following open-heart surgery. *PACE*, 1:426–438, 1978.

[162] I. Wright. An introduction to electrograms, available at http://www.cardiologyhd.com/all-ep/an-introduction-to-electrograms.html, 2006.

[163] Q. Xi, AV. Sahakian, J. Ng, and S. Swiryn. Atrial fibrillatory wave characteristics on surface electrogram: ECG to ECG repeatability over twenty-four hours in clinically stable patients. *J Cardiovasc Electrophysiol.*, 15(8):911–917, 2004.

[164] R. W. Yeung. *Information Theory and Network Coding*. Springer, 2008.

[165] K. Yoshida, A. Chugh, E. Good, and et al. A critical decrease in dominant frequency and clinical outcome after catheter ablation of persistent atrial fibrillation. *Heart Rhythm*, 7(3):295–302, March 2010.

[166] J. Zar. *Biostatistical Analysis*. Prentice-Hall, 2nd edition, 1984.

[167] V. Zarzoso. Extraction of ECG characteristics using source separation techniques: exploiting statistical independence and beyond. In A. Naït-Ali, editor, *Advanced Biosignal Processing*, chapter 2, pages 15–47. Springer Verlag, Berlin, Heidelberg, 2009.

[168] V. Zarzoso, O. Meste, P. Comon, D. G. Latcu, and N. Saoudi. Noninvasive cardiac signal analysis using data decomposition techniques. In F. Cazals and P. Kornprobst, editors, *Modeling in Computational Biology and Biomedicine: A Multidisciplinary Endeavor*, Lecture Notes in Mathematical and Computational Biology, chapter 3, pages 83–116. Springer Verlag, Berlin, Heidelberg, 2013.

[169] V. Zarzoso and A. K. Nandi. Noninvasive fetal electrocardiogram extraction: blind separation versus adaptive noise cancellation. *IEEE Transactions on Biomedical Engineering*, 48(1):12–18, January 2001.

[170] Y. Zhang and T. Mazgalev. Ventricular rate control during atrial fibrillation and AV node modifications: past, present and future. *Pacing Clin. Electrophysiol.*, 27:382–393, 2004.

Appendix

Appendix

A.1 Derivation of the least squares estimates

The objective of the least squares (LS) method is computing the slope S and the intercept I of the linear law $y = Sx + I$ so that $E = \sum_{i=1}^{n} d_1^2$ introduced in Sec. 4.6.3 is minimized. We first introduce some definitions:

- $\overline{x}$: sample mean of the predictor variables;
- $\overline{y}$: sample mean of the response variables;
- σ_x^2: sum of squared deviations from $\overline{x}$;
- σ_y^2: sum of squared deviations from $\overline{y}$;
- σ_{xy}^2: sum of cross products of squared deviations.

For the generic sample i, we can write:

$$y_i - Sx_i - I = (y_i - \overline{y}) - S(x_i - \overline{x}) + (\overline{y} - I - S\overline{x}). \tag{1}$$

If we square both sides of Eq. (1) we obtain:

$$\begin{aligned}(y_i - Sx_i - I)^2 = \\ &= (y_i - \overline{y})^2 + S^2(x_i - \overline{x})^2 + (\overline{y} - I - S\overline{x})^2 \\ &- 2S(x_i - \overline{x})(y_i - \overline{y}) - 2S(x_i - \overline{x})(\overline{y} - I - S\overline{x}) + 2(y_i - \overline{y})(\overline{y} - I - S\overline{x}).\end{aligned} \tag{2}$$

By summing both sides of Eq. (2), it reduces to:

$$D = \sigma_y^2 + S^2\sigma_x^2 + n(\overline{y} - I - S\overline{x})^2 - 2S\sigma_{xy} = n(\overline{y} - I - S\overline{x})^2 + (S\sigma_x - \frac{\sigma_{xy}}{\sigma_x})^2 + (\sigma_y^2 - \frac{\sigma_{xy}^2}{\sigma_x^2}). \tag{3}$$

Minimization of this expression yields the estimates:

$$S = \frac{\sigma_{xy}}{\sigma_x^2}; I = \overline{y} - S\overline{x}. \tag{4}$$

The degree of linear correlation between the variables x and y can be quantified by Pearson's coefficient:

$$R_P = \frac{\sigma_{xy}}{\sigma_x \sigma_y}. \tag{5}$$

A.2 WPCA algorithm

WLS minimization is achieved by following the optimization algorithm proposed in [66]:

- Initialize $\widehat{\mathbf{Y}}_0$ and compute $h_0 = h(\widehat{\mathbf{Y}}_0 | \mathbf{Y}, \mathbf{W})$, where $h(\cdot)$ is the WLS cost function given by Eq. (5.5).

- for $i = 1, 2, \ldots$ until convergence
  1. Compute $\widetilde{\mathbf{Y}}_i = \widehat{\mathbf{Y}}_i + \beta \mathbf{W} * \mathbf{W} * (\mathbf{Y} - \widehat{\mathbf{Y}}_i)$, where $\beta = w_M^{-2}$, w_M is the maximum weight of $\mathbf{W}$. The update is based on a maximization-function approach.
  2. Compute $\widehat{\mathbf{Y}}_{i+1}$ as the reduced-rank model fitting the data $\widetilde{\mathbf{Y}}_i$:

$$\widehat{\mathbf{Y}}_{i+1} = \arg\min_{\widehat{\mathbf{Y}}} \|\widetilde{\mathbf{Y}}_i - \widehat{\mathbf{Y}}\|^2 \tag{6}$$

     subject to the orthogonality constraints on $\widehat{\mathbf{Y}}$. This is given by the best rank-r approximation (determined, e.g., via the SVD) of the matrix $\widetilde{\mathbf{Y}}_i$ obtained at the previous step.
  3. Compute $h_{i+1} = h(\widehat{\mathbf{Y}}_{i+1}|\mathbf{Y}, \mathbf{W})$. Given a fixed, small tolerance ϵ, if $C^* < \epsilon$, where:

$$C^* = (h_i - h_{i+1})/h_i \tag{7}$$

     the convergence is reached; otherwise set $i = i + 1$ and repeat the algorithm from Step 1 until convergence.

  end

More specifically, the criterion is monotonically minimized according to Eq. (6), knowing that $\widetilde{\mathbf{Y}}$ depends on the multivariate input signal $\mathbf{Y}$, the weight matrix $\mathbf{W}$ and the model $\widehat{\mathbf{Y}}$ at the current iteration.

Different procedures for initializing $\widehat{\mathbf{Y}}$ have been envisaged in earlier works. The implementation used in Sec. 5.4 assumes to assign the OLS solution obtained by the standard PCA, so that $\widehat{\mathbf{Y}}_0$ equals the best rank-r approximation determined without assigning loads to preferential leads.

A.3 NMF: ALS ALGORITHM

The basic ALS algorithm for NNMF consists in an alternation of LS steps and non-negativity (NN) constraint enforcing. Given the linear model $\mathbf{A} = \mathbf{WH}$, the main steps are herein introduced:

1. $\mathbf{W}$ initialization (as explained in Sec. 5.5)
2. for $i = 1, 2, \ldots$ until convergence
   1. LS: Solve for $\mathbf{H}$ in
$$\mathbf{W}^T\mathbf{WH} = \mathbf{W}^T\mathbf{A} \tag{8}$$
   2. NN: Set all negative elements in $\mathbf{H}$ to zero
   3. LS: Solve for $\mathbf{W}$ in
$$\mathbf{HH}^T\mathbf{W}^T = \mathbf{HA}^T \tag{9}$$
   4. NN: Set all negative elements in $\mathbf{W}$ to zero
3. end

As far as the stopping criterion is concerned, a convergence tolerance $\frac{\|w_k - w_{k-1}\|}{\|w_k\|}$ equal to 10^{-4} is set for our algorithm.

A.4 Chain rule in information theory

The chain rule cited in Chapter 7 can be demonstrated by starting from the definition of joint entropy. By applying Bayes' theorem, we can rewrite it as:

$$H(X,Y) = -\sum_{x\in\mathcal{X}}\sum_{y\in\mathcal{Y}} p(x,y)\log\left(p(x,y)\right) = -\sum_{x\in\mathcal{X}}\sum_{y\in\mathcal{Y}} p(x,y)\log\left(p(x)p(y|x)\right). \tag{10}$$

According to the linearity property, we can rewrite Eq. 10 as:

$$-\sum_{x\in\mathcal{X}}\sum_{y\in\mathcal{Y}}\left(p(x,y)\log\left(p(x)\right) - p(x,y)\log p(y|x)\right) = -\sum_{x\in\mathcal{X}} p(x)\log p(x) - p(x,y)\log p(y|x). \tag{11}$$

By applying the definition of marginal and conditional entropy put forth in Chapter 7:

$$-\sum_{x\in\mathcal{X}} p(x)\log p(x) - p(x,y)\log p(y|x) = H(X) + H(Y|X). \tag{12}$$

A.5 IT entropy extension to multiple variables

By iteratively applying the 2-variable expansion rule for entropies, we can write:

$$H(X_1; X_2) = H(X_1) + H(X_2|X_1). \tag{13}$$

In case of 3 variables we have:

$$H(X_1; X_2; X_3) = H(X_1) + H(X_3, X_2|X_1) = H(X_1) + H(X_2|X_1) + H(X_3|X_2, X_1). \tag{14}$$

Generalization to m variables yields:

$$\begin{aligned} H(X_1; X_2; \ldots; X_m) &= H(X_1) + H(X_2|X_1) + \cdots + H(X_n|X_{n-1}, \ldots, X_1) = \\ &= \sum_{i=1}^{m} H(X_i|X_{i-1}, \ldots, X_1). \end{aligned} \tag{15}$$